

**MARINE GRAVIMETRIC AND MAGNETIC INVESTIGATIONS
WITHIN THE AREA OF THE SOUTHEASTERN
MEDITERRANEAN SEA AND THE NORTHERN SECTION OF EGYPT**

A DISSERTATION
SUBMITTED TO THE GEOSCIENCE DEPARTMENT
OF THE UNIVERSITY OF HAMBURG
FOR THE DEGREE OF
DOCTOR OF NATURAL SCIENCES

Presented by
Hamdy A. M. Aboulela

Hamburg
December, 2003

**MARINE GRAVIMETRIC AND MAGNETIC INVESTIGATIONS
WITHIN THE AREA OF THE SOUTH EASTERN
MEDITERRANEAN SEA AND THE NORTHERN SECTION OF EGYPT**

DISSERATATION

Zur Erlangung des Doktorgrades
der Naturwissenschaften im Fachbereich
Geowissenschaften der Universität Hamburg

VORGELEGT VON

Hamdy A. M. Aboulela
aus ägypten

Hamburg

2003

Als Dissertation angenommen vom Fachbereich
Geowissenschaften der Universität Hamburg auf
Grund der Gutachten von Prof. Dr. Torsten Dahm
und Dr. G. Ali Dehghani

Hamburg, den 17.12.2003

Prof. Dr. U. Bismayer
Dekan
des Fachbereichs Geowissenschaften

	PAGE
CONTENTS	i
LIST OF FIGURES AND TABLES	iv
ABSTRACT	x

I. INTRODUCTION

I.1. Location of the study area and brief introduction.....	1
I.2. Scope of the study.....	1
I.3. Geophysical data sets.....	3
I.4. Objectives.....	6
I.5. Dissertation outline.....	7

II. GEOGRAPHIC SETTING AND GEOLOGY

II.1. Geographic setting of the area investigated.....	8
II.2. Geology.....	12
II.2.1. Regional geological features.....	12
II.2.2. Regional tectonic framework.....	14
II.2.3. Tectonic and structural setting.....	17
II.2.3.1. The Hellenic and Cyprean Arcs.....	19
II.2.3.2. The Levant Basin.....	22
II.2.4. Crustal structure of the southeastern Mediterranean Sea.....	22
II.3. Brief account of the geological history of the Mediterranean Sea.....	23

III. GRAVITY AND MAGNETIC INVESTIGATIONS AND QUALITATIVE INTERPRETATION

III.1. Gravity investigations.....	25
III.1.1. Evaluation processing of the Free-Air and Bouguer gravity field data.....	26
III.2. Magnetic investigations.....	28
III.3. A qualitative interpretation of the gravity and magnetic data.....	32
III.3.1. A qualitative interpretation of the Free-Air gravity data.....	32
III.3.2. A qualitative interpretation of the Bouguer gravity data.....	33

	PAGE
III.3.3. A qualitative interpretation of the total intensity magnetic data.....	34
III.4. Separation of the gravity and magnetic data.....	35
III.4.1. Separation acquisition and methods.....	36
III.4.2. Interpretation of the regional and residual gravity anomalies.....	37
III.4.3. Interpretation of the regional and residual magnetic anomalies.....	38
III.5. Satellite Gravity.....	44
III.5.1. The available satellite altimetry marine gravity field of the area investigated.....	46
III.5.2. Comparison with the shipboard marine Free-Air gravity and bathymetric data.....	50
III.5.3. The differences between the satellite and the shipboard gravity anomaly data.....	54

IV. RESULTS OF THE SEISMIC STUDIES

IV.1. Deep seismic sounding experiments (DSS).....	56
IV.1.1. Seismic profile of Cyprus-Israel.....	56
IV.1.2. Seismic profiles of Eratosthenes Seamount-Israel and Levant Basin-Israel.....	59
IV.1.3. Seismic profiles of Egypt-Rhodes and Egypt-Crete-Santorin.....	61
IV.1.4. Seismic profiles of Sidi Barani-Sidi Abdel Rahman.....	61
IV.2. Wide-angle reflection/refraction seismic profiles in and around the Cretan region.....	64
IV.3. Other deep seismic refraction profiles in the Eastern Mediterranean Sea.....	71

V. TWO AND THREE-DIMENSIONAL GRAVITY MODELLING

V.1. Two-dimensional gravity modelling.....	76
V.1.1. Theory of two-dimensional calculation according to Talwani et al., 1959.....	78
V.1.2. Results of the two-dimensional gravity models of the profiles A-A , B-B , C-C and D-D 	81
V.1.2.1. Two-dimensional gravity model along profile A-A (Cyprus-Israel).....	82
V.1.2.2. Two-dimensional gravity model along profile B-B (Eratosthenes Seamount-Israel).....	84
V.1.2.3. Two-dimensional gravity models along profile C-C (Egypt -Rhodes) and D-D (Egypt-Crete-Santorin).....	86
V.1.2.3.1. Two-dimensional gravity model along profile C-C (Egypt-Rhodes).....	86
V.1.2.3.2. Two-dimensional gravity model along profile D-D (Egypt-Crete-Santorin).....	88
V.2. Three-dimensional gravity modelling.....	91
V.2.1. Methodical aspects of the three-dimensional gravity modelling equations.....	91

	PAGE
V.2.2. Brief description of the preparation of the model input according to IGMAS.....	96
V.2.3. The area of three-dimensional gravity model.....	98
V.2.3.1. Accuracy and resolution of the modelled area.....	98
V.2.3.2. Results of the area of three-dimensional gravity model.....	102

VI. TECTONIC ACTIVITY AND REGIONAL STRESS PATTERN

VI.1. Tectonic activity and seismicity pattern.....	130
VI.2. Regional stress pattern.....	133

VII. DISCUSSION AND CONCLUSIONS.....138

VII.1. Discussion.....	138
VII.2. Conclusions.....	141

ACKNOWLEDGEMENTS.....147

REFERENCES.....148

APPENDIX [A].....174

APPENDIX [B].....181

APPENDIX [C].....183

LIST OF FIGURES AND TABLES

-LIST OF FIGURES

	PAGE
Figure 1.1: Location map of the area investigated.....	2
Figure 1.2: Location map showing the profiles computed on the area investigated.....	4
Figure 2.1: Bathymetric and topographic features pattern map of the southeastern Mediterranean Sea and the northern section of Egypt. “Contour interval is 500 m”	11
Figure 2.2: Simplified regional tectonic framework map of the study area and adjacent regions.....	16
Figure 2.3: Geodynamic framework of the Eastern Mediterranean Sea and surrounding areas, after Peter et al. (1998).....	18
Figure 2.4: Schematic configuration of the plates in the Eastern Mediterranean Sea and surrounding areas. Compiled from Mckenzie (1970, 1972).....	18
Figure 2.5: Models of active tectonic elements in the Eastern Mediterranean Sea, after Nur and Ben-Avraham (1978).....	20
Figure 2.6: Simplified models of active tectonic elements in the Eastern Mediterranean Sea, after Le Pichon and Angelier (1979).....	20
Figure 2.7: Simplified geotectonic setting of the Northeastern Mediterranean Sea. Compiled from Woodside et al. (1992).....	21
Figure 3.1: Free-Air gravity anomaly map of the southeastern Mediterranean Sea and the northern section of Egypt. “Contour interval is 10 mGal”	29
Figure 3.2: Bouguer gravity anomaly map of the southeastern Mediterranean Sea and the northern section of Egypt. “Contour interval is 10 mGal”	30
Figure 3.3: Total intensity magnetic anomaly map of the southeastern Mediterranean Sea and the northern section of Egypt. “Contour interval is 100 nT”	31
Figure 3.4: Regional Bouguer gravity anomaly map of the southeastern Mediterranean Sea and the northern section of Egypt. “Contour interval is 5 mGal”	39
Figure 3.5: Residual Bouguer gravity anomaly map of the southeastern Mediterranean Sea and the northern section of Egypt. “Contour interval is 10 mGal”	40

Figure 3.6: Regional magnetic anomaly map of the southeastern Mediterranean Sea and the northern section of Egypt. “Contour interval is 100 nT”	42
Figure 3.7: Residual magnetic anomaly map of the southeastern Mediterranean Sea and the northern section of Egypt. “Contour interval is 50 nT”	43
Figure 3.8: Free-Air gravity anomaly map based on the satellite data. Satellite data obtained from Sandwell et al., 1997.....	47
Figure 3.9: Free-Air gravity anomaly map based on the KMS99 satellite data. Satellite data obtained from Andersen and Knudsen, 1998.....	48
Figure 3.10: Free-Air gravity anomaly map based on the KMS02 satellite data. Satellite data obtained from Andersen and Knudsen, 1998.....	49
Figure 3.11: [A] A comparison of the shipboard gravity data with the satellite gravity data along profile B-B . [B] The difference between satellite and shipboard gravity data.....	51
Figure 3.12: [A] A comparison of the shipboard gravity data with the satellite gravity data along profile C-C . [B] The difference between satellite and shipboard gravity data.....	52
Figure 3.13: A comparison of the shipboard bathymetric data with the bathymetric data provided by satellite altimetry. [B] The difference between satellite and shipboard data.....	53
Figure 3.14: The differences between the KMS02 satellite and the shipboard gravity data. Satellite obtained from Andersen and Knudsen, 1998.....	55
Figure 4.1: Location map of the seismic profiles performed on the southeastern Mediterranean Sea and the northern section of Egypt.....	57
Figure 4.2: Sketch diagram shows velocity depth model of the profile Cyprus-Israel, shown as line A- A in Figure 4.1. Compiled from Makris et al. (1983).....	58
Figure 4.3: Velocity depth model from the Eratosthenes Seamount across the Levant Basin, based upon the Israel’ 89 seismic project, shown as line B-B in Figure 4.1. Compiled from Trey (1991).....	60
Figure 4.4: Sketch diagram shows geological cross-section between Egypt and Rhodes based on geological studies and borehole data. Compiled from Malovitskiy et al. (1975).....	62
Figure 4.5: The travel time plot of seismic recordings and velocity depth model of the crustal structure below Sidi Barani-Sidi Abdel Rahman profile, after Marzouk (1988).....	63
Figure 4.6: Sketch diagram shows velocity depth model along the Island of Crete, shown as line CR1 in Figure 4.1. Compiled from Makris (1978 a).....	65
Figure 4.7: Velocity depth model across Cretan Sea, shown as line CR3 in Figure 4.1, Interfaces	

controlled by the seismic data are marked by continuous lines, after Hartung (1987).....	66
Figure 4.8: 2D P-wave velocity depth model for northern shore profile on the Cretan region, based on Crete seismic experiment, shown as line PI in Figure 4.1, compiled from Bohnhoff (2000).....	68
Figure 4.9: 2D P-wave velocity depth model for southern shore profile on the Cretan region, based on Crete seismic experiment, shown as line PII in Figure 4.1, compiled from Bohnhoff (2000).....	69
Figure 4.10: 2D P-wave velocity depth model for north-south traverse profile on the Cretan region, based on Crete seismic experiment, shown as line PIII in Figure 4.1, compiled from Bohnhoff (2000).....	70
Figure 4.11: Velocity depth model along the central profile between Crete and Libyan margin-East Mediterranean Sea, based on Crete-Project 99, shown as line P#1 in Figure 4.1, after Helms (2001).....	72
Figure 4.12: Velocity depth model along the west profile between Crete and Libyan margin-East Mediterranean Sea, based on Crete-Project 99, shown as line P#2 in Figure 4.1, after Brönnner (2003).....	73
Figure 4.13: Velocity depth model along the east profile between Crete and Libyan margin-East Mediterranean Sea, based on Crete-Project 99, shown as line P#3 in Figure 4.1, after Planert, 2001.....	74
Figure 4.14: Schematic crustal sections in the Eastern Mediterranean Sea, based on deep seismic refraction profiles. Compiled from Morelli (1975).....	75
Figure 5.1: Free-Air gravity anomaly map of the southeastern Mediterranean Sea and the northern section of Egypt. The thick lines A-A , B-B , C-C and D-D are two-dimensional gravity modelling profiles, which coincide with the seismic lines (see Figure 4.1).....	77
Figure 5.2: Geometrical elements involved in the gravitational attraction of an n - sided polygon.....	78
Figure 5.3: The final results of two-dimensional gravity modelling along profile A-A (Cyprus-Israel).....	83
Figure 5.4: The final results of two-dimensional density gravity modelling along profile B-B (Eratosthenes Seamount-Israel).....	85
Figure 5.5: The final results of two-dimensional gravity modelling along profile C-C (Egypt-Rhodes).....	87

Figure 5.6: The final results of two-dimensional gravity modelling along profile D-D (Egypt-Crete-Santorin).....	89
Figure 5.7: Geometric layout of a polyhedron (after Götze, 1984).....	91
Figure 5.8: Geometric layout for the line integral (from Götze, 1984).....	94
Figure 5.9: Polyhedral assembly using triangulation as used in IGMAS (from Götze, 1984)....	97
Figure 5.10: The area of three-dimensional modelling.....	99
Figure 5.11: Interpretative 3D perspective sketch of the modelled area, based on the bathymetric and topographic features and seismic profiles.....	101
Figure 5.12: The final results of the vertical plane 2 through the three-dimensional gravity model and the related Free-Air anomaly.....	103
Figure 5.13: The final results of the vertical plane 3 through the three-dimensional gravity model and the related Free-Air anomaly.....	104
Figure 5.14: The final results of the vertical plane 4 through the three-dimensional gravity model and the related Free-Air anomaly.....	105
Figure 5.15: The final results of the vertical plane 5 through the three-dimensional gravity model and the related Free-Air anomaly.....	106
Figure 5.16: The final results of the vertical plane 6 through the three-dimensional gravity model and the related Free-Air anomaly.....	108
Figure 5.17: The final results of the vertical plane 7 through the three-dimensional gravity model and the related Free-Air anomaly.....	109
Figure 5.18: The final results of the vertical plane 8 through the three-dimensional gravity model and the related Free-Air anomaly.....	110
Figure 5.19: The final results of the vertical plane 9 through the three-dimensional gravity model and the related Free-Air anomaly.....	111
Figure 5.20: The final results of the vertical plane 10 through the three-dimensional gravity model and the related Free-Air anomaly.....	113
Figure 5.21: The final results of the vertical plane 11 through the three-dimensional gravity model and the related Free-Air anomaly.....	114
Figure 5.22: The final results of the vertical plane 12 through the three-dimensional gravity model and the related Free-Air anomaly.....	115
Figure 5.23: The final results of the vertical plane 13 through the three-dimensional gravity model and the related Free-Air anomaly.....	116
Figure 5.24: The final results of the vertical plane 14 through the three-dimensional gravity	

model and the related Free-Air anomaly.....	118
Figure 5.25: The final results of the vertical plane 15 through the three-dimensional gravity model and the related Free-Air anomaly.....	119
Figure 5.26: The final results of the vertical plane 16 through the three-dimensional gravity model and the related Free-Air anomaly.....	120
Figure 5.27: The final results of the vertical plane 17 through the three-dimensional gravity model and the related Free-Air anomaly.....	121
Figure 5.28: The modelled and the measured gravity fields without adaptation within the modelling area.....	123
Figure 5.29: The modelled and the measured gravity fields with adaptation within the modelling area.....	124
Figure 5.30: The differences between the modelled and the measured gravity anomalies within the modelling area.....	125
Figure 5.31: Isopach map displays the thickness of the oceanic crust on the modelling area...	126
Figure 5.32: Isopach map displays the thickness of the mantle layer on the modelling area.....	128
 Figure 6.1: Magnitude and depth distribution of earthquakes of the study area during the period of 1904-2002.....	 131
Figure 6.2: Focal mechanisms of some moderate to large earthquakes in the study area. Dilation quadrant are white 	135
Figure 6.3: The distribution and direction of the P-axes on a horizontal plane derived from focal mechanism solutions of moderate to large earthquakes in the study area.....	136
 Figure 7.1: Part [A]: Sketch map showing simplified regional tectonics and geodynamic framework in the study area. Based on Mckenzie (1972), Nur and Ben-Avraham (1978); Ben-Avraham et al. (1987); Courtillot et al. (19 87); Peter et al. (1998); Badawy and Horvath (1999 b), Mcklusky et al. (2000) and the principal results of this study. Part [B]: Structural model for the active EMTS at the base of the continental slope off the Egyptain coast.....	 139
 Figure Appendix [A1]: Tectonic setting of the eastern Mediterranean Sea and the Middle East. The black arrows indicate the left-lateral motion along the DST. Compiled from DESERT Group 2000, and Klinger et al. 2000.....	 175

Figure Appendix [A2]: Sketch diagram shows velocity depth models of profiles [IV], [V], and [VI]. Compiled from the Geological survey of Cyprus after Wang (1995).....	177
Figure Appendix [A3]: Sketch diagram shows velocity depth model of profile VI, southwest of Cyprus. Compiled from the Geological survey of Cyprus after Wang (1995).....	178
Figure Appendix [A4]: Location map of the Expanding spread profiles (ESP) recorded during the Pasiphae Cruise, black dots indicates ESP central points from where a velocity model is obtained. Compiled from De Voogd et al. (1992).....	179
Figure Appendix [A5]: Summary of ESP results from the Ionian Basin to the Herodotus Abyssal Plain. Vertical depth scale is in km. Compiled from De Voogd et al. (1992).....	180
Figure Appendix [C1]: Schematic diagram of a focal mechanisms solutions.....	184

- LIST OF TABLES

	PAGE
Table Appendix [B1]: Fault plane solutions data of some shocks, which occurred in the most seismically active zone of the area investigated (extracted from Harvard Seismology, CMT catalog search).....	181
Table Appendix [B2]: Fault plane solutions data of some shocks, which occurred in the most seismically active zone of the area investigated (extracted from WSM).....	182

ABSTRACT

The southeastern Mediterranean Sea and the northern section of Egypt constitutes one of the most complex tectonic areas in the Mediterranean. This study is an attempt to achieve a better understanding of tectonics, and geodynamical processes along a complex tectonization region. These include crustal structure, thickness of sediments, transition between oceanic and continental crust and regional integrated model of the gravity field observed. A wide range of field work from the geophysical data has been acquired and used in this study with respect to the gravity and magnetic data as well as the results of deep seismic soundings. A comparison between the marine gravity data and the gravity data derived from satellite altimetry was made to ensure that the marine gravity data compiled from different marine surveys were compatible. Furthermore, a successful attempt was made to understand the behaviour of the tectonic activity and regional stress pattern distribution within the area investigated by using the seismicity data.

◆ The geographic setting and geology of the study area show that the Eastern Mediterranean region includes a short segment of the convergence boundary between Africa and Eurasia. Subduction in this segment is along two very small Arcs, the Hellenic and Cyprean Arcs. Moreover, the study area has remarkably prominent morphogeologic features such as East Mediterranean Ridge, Herodotus Abyssal Plain, Levantine Basin, Eratosthenes Seamount, Nile Delta and Sinai Peninsula. At the base of the continental slope off Egyptain coast and eastern Libya, the shape and size of bathymetric depressions strongly suggested that they originated from an active eastern Mediterranean transcurrent fault system (EMTS). Additionally, there is a few major fault systems trending NE-SW and NW-SE, i.e. the Suez rift and faults from Arabian plate, extend into southeastern Mediterranean Sea. It reflects activation of the Dead Sea faults (DSF) and the Levant-Aqaba transform plate boundary.

◆ A qualitative interpretation of the observed potential anomalies revealed that the Free-Air anomalies are generally negative. The Bouguer anomalies are predominantly positive as might be expected for an oceanic area. A series of high magnetic anomalies around the Cyprean Arc, runs from the Antalya Basin across Cyprus to the coast of Arabian plate. It coincides with a large positive Bouguer gravity anomaly suggesting that the ophiolites in Cyprus, in southern Turkey and northwest Arabian plate have a common base, and that ophiolites probably exist around the whole Cyprean Arc.

The regional gravity anomaly field values in the study area generally decrease towards the E-W and SE directions. This behaviour trends reflect the effect of the transition from oceanic crust to the continental crust of the Eastern Mediterranean towards the Arabian plate. The re-

gional magnetic anomaly field in the study area on the other hand is dominant in NW- SE trends and increases towards the north, which may reflect the shallow depth of the basement rocks in this direction. The residual gravity and magnetic anomalies reflect the effect of the difference in density between the crystalline or igneous crust and the sediments, the variation of the basement geometry and also the effect of the bathymetric and topographic features.

The orientation of the Free-Air anomalies in the study area indicated that the isostatic equilibrium is far from being achieved. The absence of a large Bouguer anomaly associated with the extreme relief indicates that the area is, as could be expected, not isostatically compensated by local variations in the crustal or mantle structure.

The satellite data shows only minor deviations in some partial regions of the area investigated such as at Levant basin and nearest Rhodes basin, and differences between the satellite and the shipboard data are also small in some regions. These occurred mostly near to land. Furthermore, some strong deviations in some regions are spatially correlated with bathymetric depth and geological structures can be also obvious.

♦ Seismic profile results indicated that the thickness and velocity values of the crystalline unit under the Levant Basin are similar to the values determined for a normal oceanic crust. The seismic results of the Western Desert of Egypt showed that the Egyptian coast is underlain by a continental crust covered by 4-6 km thick sedimentary layer. The crust is about 26 km thick below the Mediterranean Sea.

♦ A quantitative interpretation of the Free-Air gravity field was undertaken by developing two and three-dimensional gravity modelling. The results show that the measured gravity field of the two and three-dimensional gravity models can be satisfied when using the structural layer boundaries of the given seismic studies. The transition of the oceanic-continental crust occurs near the coast of Israel, the Moho lies at a depth of about 32 km beneath Cyprus, and at a depth of about 27 km at the coast of Israel. The deep parts of the Levantine Basin is covered by about 13 km of thick sediments. The Moho depth varies from about 26 km beneath the Eratosthenes Seamount to about 23 km under the Levant Basin. The depth to the basement lies at about 6 km beneath the Egyptian coast. However, the thickness of the sedimentary layer increases towards the East Mediterranean Ridge. The basement depth varies from about 9 km at the Egyptian coast to about 13 km in the Herodotus Abyssal Plain and beneath the East Mediterranean Ridge.

The continental African plate extends to nearly 40 to 100 km offshore the Egyptian coast and has an abrupt transition to an oceanic crust. It seems that the proposed extends reflects the effect of an active EMTS and the main tectonic elements in this area, which are occurring on

the boundary between continental and oceanic crust units. Moreover, the crustal structure of the Levant Basin is significantly different from that of the adjacent land. The gravity modelling results identify the continental-oceanic crust transition at Levant Basin.

The average thickness of the mantle layer of the gravity model is 27 km towards the Egyptian coast. Moreover, there are strong lateral undulations in the average thickness of the mantle layer ranging from about 10 to 22 km towards Cretan Island Arc. This may reflect the effect of the main driving force for the opening of the Cretan Sea.

◆ The seismicity study of the area under investigation shows that most of the active seismicity is concentrated along and around the main tectonic and geological structural of the investigated area such as the Hellenic and Cyprean Arcs. There are also some activity areas along the trends of the Gulf of Aqaba- Dead Sea-Levant transform, and the Gulf of Suez-Cairo-Alexandria || northern Egypt ||. Additionally, the average P-axes orientations are in good agreement with plate tectonic framework and are broadly consistent with the absolute plate motion of African and its collision with Eurasian plates.

I. INTRODUCTION

I.1. Location of the study area and brief introduction

The area under investigation covers the northeastern margin of the African plate between Latitudes 29°:30'-37°:00' N and Longitudes 23°:30'-36°:00' E (Figure 1.1).

The southeastern Mediterranean Sea and the northern section of Egypt is a tectonically complicated area due to its location within the contact zone between the African and the Eurasian plates. Since the initiation of the plate tectonic theory, many geophysical and tectonic studies of the Eastern Mediterranean have been conducted in recent years (e.g. Allan and Morelli, 1971; Lort, 1971; Giermann, 1969, 1971; Ryan et al., 1971, 1982; Finetti and Morelli, 1973; Woodside, 1977; Makris et al., 1983; Makris and Stobbe, 1984; Ben-Avraham et al., 1987; Ben-Avraham, 1989; Kahle et al., 1988; Kastens, 1991; Rybakov et al., 2000). In particular, several parts of the region have been studied through a number of deep seismic sounding (DSS) and wide angle reflection/refraction seismic (WARRS) experiments and expanding spread profiles (ESP) in order to delineate the deep structures (e.g. Morelli, 1975; Makris et al., 1983; Makris, 1985; Makris et al., 1988; Hartung, 1987; De Voogd et al., 1992; Bohnhoff, 2000; Bohnhoff et al., 2001; El-Kelani et al., 2000; Ilinski et al., 2000; Vidal, 2000; Helms, 2001; Planert, 2001; Brönnner, 2003). Additional seismicity studies (e.g. Mckenzie, 1972; Ben-Menahem et al., 1976; Maamoun et al., 1980; Le Pichon et al., 1982 a; Le Pichon and Gaulier, 1988; Kebeasy, 1990; Kovachev et al., 1992; Delibasis et al., 1999; Rihm et al., 1999; Badawy and Horvath, 1999 a, and b, Papazachos and Papaioannou, 1999; Badawy and Abdel Fattah, 2001; Rische et al., 2003; Mahmoud, 2003), showed that the area investigated to be a tectonically very active region. It has the highest seismicity of the whole Mediterranean basin. This is also confirmed by seismicity studies all over Egypt which shows that most earthquakes took place at one of the main seismic trends in northern Egypt. These namely the Eastern Mediterranean-Cairo-Fayum Pelusiatic trend, the northern Red Sea-Gulf of Suez-Cairo-Alexandria Clysmic trend, and the Levant-Aqaba trend. Some small events were also observed in the Nile Delta as suggested by Kebeasy (1990).

I.2. Scope of the study

The southeastern Mediterranean Sea and the northern section of Egypt is characterized by high seismicity and a complex tectonization which is not yet fully understood. It has been the subject of extensive geophysical and geological studies in recent years. The southeastern

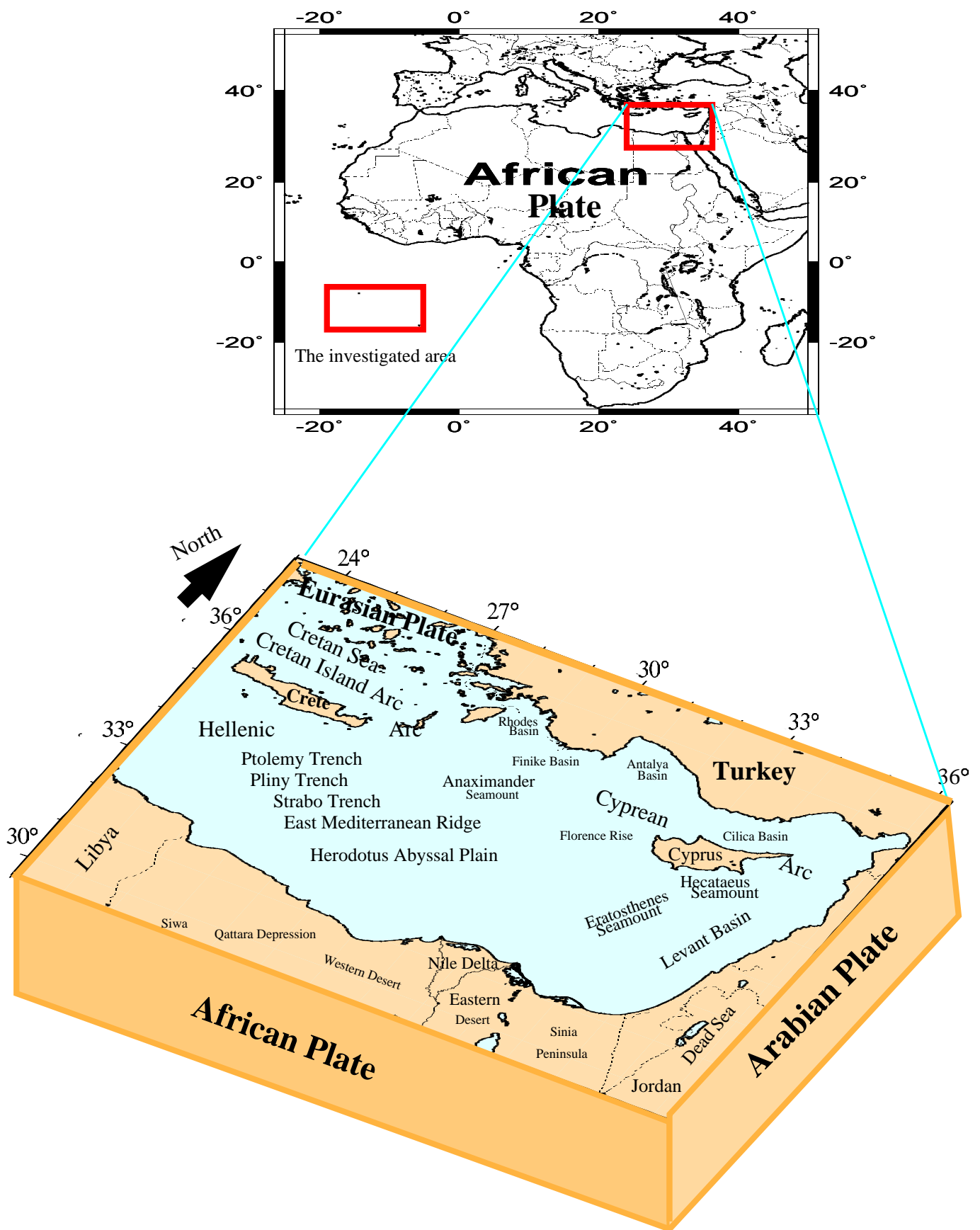


Figure 1.1: Location map of the area investigated

Mediterranean Sea includes a short segment of the convergence boundary between the African and the Eurasian plates. To date, the subduction processes along these segment, the crustal structure below a complex tectonization area and the deep structure of the north African passive continental margin remain poorly understood. However, there is only limited knowledge concerning tectonic and geodynamical processes along a complex tectonization region such as crustal structure, thickness of sediments, transition between oceanic and continental crust and regional integrated models of the potential field observed of the area investigated. This is not because of data deficiency, but rather due to problems in data interpretation. These problems are exacerbated by the apparent complexity of the geology and the interaction of tectonic effects. Additionally, a number of questions are still open, in particular:

- Few details are known about the morphotectonic situation, e.g. what is the absolute depth variation in the most elevated parts of the area investigated?
- Little is still known about the gravity and magnetic anomalies, e.g. what is the state of isostatic compensation on this tectonically complicated area?
- There is a variety of the tectonic activity interpretations concerning the boundaries between the various lithospheric plates-how do they fit together?
- Furthermore the question concerning crustal structures and geodynamical processes of the southeastern Mediterranean Sea remain controversially discussed.

I.3. Geophysical data sets

In order to investigate and provide some answers for the questions mentioned above and contribute to a better understanding of tectonics, complex structure, geodynamic features and tectonic activity within the area investigated, a wide range of field work from the marine potential field geophysical data (Figure 1.2) has been acquired and used in this study:

Gravity data

The focus of the study area will be on the gravity field. The main set of gravity data used in this study was acquired from the Meteor 25/4 expedition during July-August, 1993 and Meteor 40/1 expedition during November 1997. This data was combined with the available data obtained from the GEODAS data base (GEOphysical DAta System, provided by NOAA and NGDC). In addition, several gravity profiles were obtained from B. G. I. (Bureau Gravimétrique International). Furthermore, gravity anomaly data were obtained from the gravity map of a survey on Crete Island during 1997-1998 (Lange, 2000). All of these data were used in this study

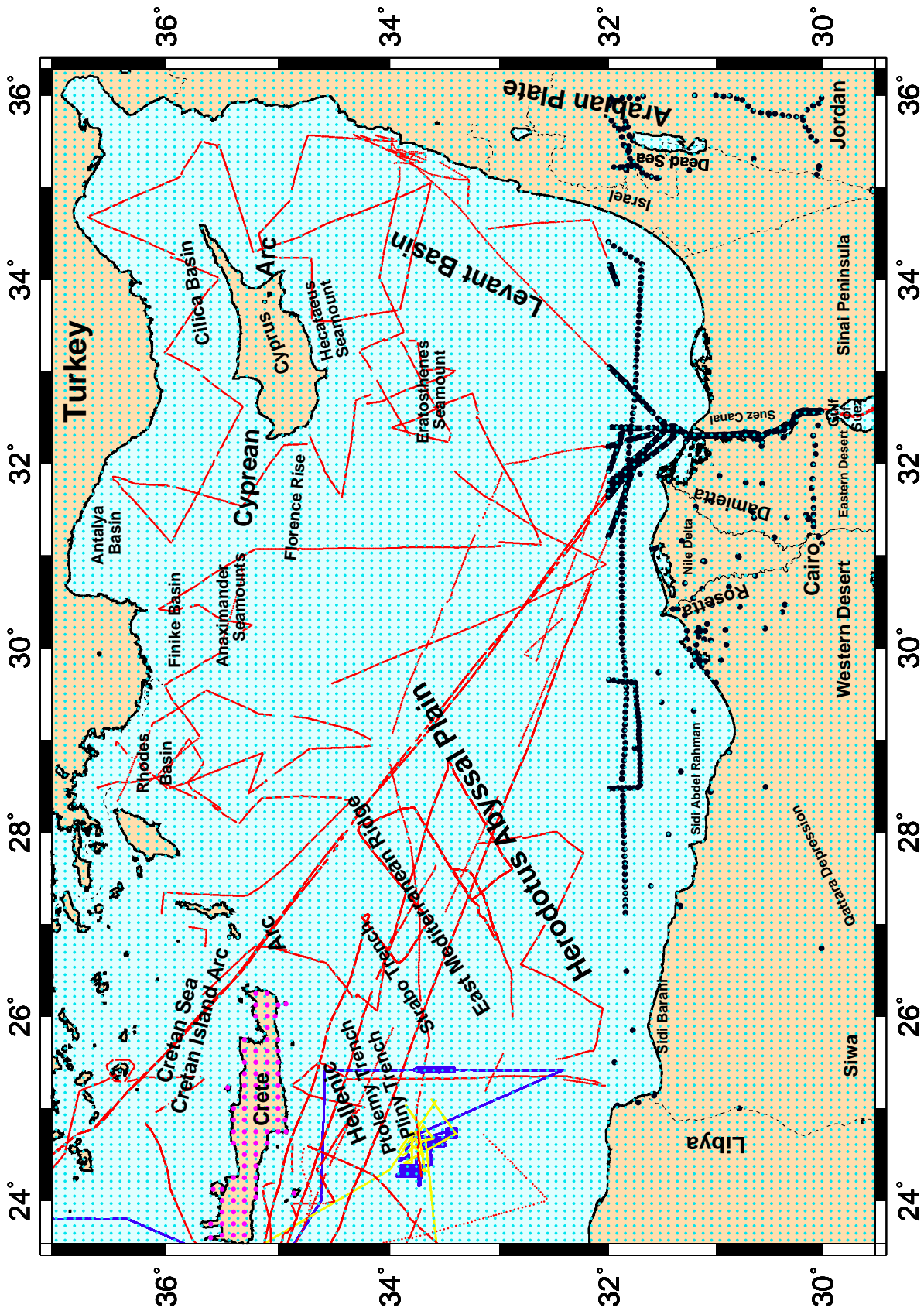


Figure 1.2: Location map showing the profiles computed on the area investigated

Data Sources: **GEODAS-Data**; **Meteor 25/4**; **Meteor 40/1**; **B.G.I**; **ETOPO** & some grid points represent gravity / topographic

data were obtained from map of a survey on Crete Island during 1997-98 (Iange, 2000).

to construct the new Bouguer and Free-Air gravity anomaly maps needed to carry out a qualitative and quantitative interpretation of the area investigated. Furthermore, the shipboard gravity data were compared with the gravity data derived from two most recent satellite altimetry sources: Sandwell's version 10.1 global grid (Sandwell et al., 1997); and KMS99, KMS02 (Andersen and Knudsen, 1998).

In general, from studying a qualitative interpretation of potential anomalies it is possible to trace conclusions about the state of isostatic compensation even on a tectonically complicated area like the one investigated. A quantitative interpretation of the potential field data alone does not provide a definite model geometry of geological structures. In addition to the potential field data, the results of reflection seismic, bathymetric and topographic data, geological investigations, and seismological data play a major role in generating the geometry of the structural models. Gravity modelling will assert whether the layer geometries and densities, required to reproduce the observed anomalies in most part favourably with the seismic velocity models.

Magnetic data

The available magnetic data used in this study were obtained from GEODAS data base. These data have been combined with data collected from the Meteor 25/4 expedition mentioned above. A new total magnetic intensity anomaly map was produced to carry out a qualitative interpretation of the area investigated.

Bathymetric and topographic data

In an attempt to learn more about the geographic setting of the area investigated and increase the knowledge of the relief of morphotectonic area, several profiles were acquired from Meteor 25/4 expedition and Meteor 40/1 expedition mentioned above, B.G.I., and GEODAS data base. Grid points representing topographic data were obtained from the topographic map of the survey mentioned above on Crete Island that was conducted during 1997-1998 (Lange, 2000). These data were combined with the available Etopo data (Eastern Topographics) to construct the Bathymetric and topographic map of the area investigated.

Seismic data

To estimate a tectonic model for the region, results from recent deep seismic sounding experiments in the Eastern Mediterranean Sea were obtained. These experiments were undertaken by the Institute of Geophysics, University of Hamburg, and the Department of Geophysics and

Planetary Sciences, Tel Aviv University. In addition, some results from recent deep seismic sounding experiments in the Cyprean region were obtained. These experiments were carried out by the Geological Survey Authorities of Cyprus to complement the information of deep sedimentary and crustal structures in the Eastern Mediterranean Sea.

Seismicity data

In order to gain an understanding of the tectonics of an area and to evaluate seismicity, it is important to extend our historical knowledge of earthquakes and the time of their occurrence. Based on historical records and documents of eyewitnesses on one the hand and instrumental records on the other hand, it is known that the southeastern Mediterranean Sea and north Egypt have been seismically active for a period of more than 2000 years.

The seismicity distribution in the whole southeastern Mediterranean Sea and the northern section of Egypt during the period of 1904-2002 has been obtained as revealed from the National Earthquake Information Center (NEIC) and the International Seismological Centre (ISC).

I.4. Objectives

The specific objective of this study is to achieve a better understanding of tectonics, and geodynamical processes along a complex tectonization region such as crustal structure, thickness of sediments, transition between oceanic and continental crust and regional integrated model of the potential field observed in the area investigated. In addition, a successful attempt was made to understanding of the behaviour of the tectonic activity within the area investigated by using the available geophysical data has been also achieved. In this study, a generalized review and interpretation of all the available geological and geophysical studies of the area investigated was made. This was performed by combining gravity and magnetic results to make a conjunctive geophysical study with particular emphasis on the following objectives:

- ◆ To construct gravity and magnetic anomaly maps of the region from recent marine gravity and magnetic data and existing land data to conclude on the state of isostatic compensation of the tectonically complicated area.
- ◆ To perform two and three-dimensional gravity tectonic models of the region within the regional tectonic concepts constrained by the seismic data and based on the results from the studies above.

- ◆ Shed light on the geographic setting of the area investigated to improve the knowledge of the absolute relief of morphotectonic area in the most elevated parts of the region.
- ◆ To achieve a better understanding of the tectonic activity and regional stress pattern distribution within the area investigated.

I.5. Dissertation outline

In chapter II the bathymetry and topography of the area investigated is shown. The regional geological features, regional tectonic framework, tectonic and structural setting, and crustal structure of the southeastern Mediterranean Sea are introduced. Furthermore, a brief account of the geological history of the Mediterranean Sea is presented.

Chapter III is devoted to the processing and compilation of the gravity and magnetic field data. A qualitative interpretation of gravity and magnetic anomaly maps as well as regional-residual gravity and magnetic anomaly maps are portrayed and presented. In addition, to ensure that the marine gravity data compiled from different marine surveys are compatible, a comparison between the marine gravity data and the gravity data derived from satellite altimetry was made.

A description of the main results from available recent seismic experiments in the area under investigation is described in chapter IV. The seismic results are used to constrain layer geometry and thickness. They provide initial estimates of the layers densities along four seismic profiles crossing the main tectonic elements in the investigation area which are used to estimate a tectonic model for this region.

Chapter V deals with a detailed description of a quantitative interpretation of the gravity field data. In this chapter two and three-dimensional gravity modelling methods will be described. The main results (e.g. variability in crustal structure, density and layer thickness) of these density models are presented and discussed.

The behaviour of the tectonic activity and regional stress pattern distribution within the area investigated are discussed in chapter VI. Finally, discussion and conclusions revealed from the geophysical data of the area investigated is given in chapter VII.

II. GEOGRAPHIC SETTING AND GEOLOGY

The geographic setting of the southeastern Mediterranean Sea and the northern section of Egypt are discussed below. In addition, geology and the geological history are also summarized.

II.1. Geographic setting of the area investigated

The area investigated extends from Latitudes 29°:30'-37°: 00' N and Longitudes 23°:30'-36°:00' E and covers the northeastern margin of the African plate. Figure 2.1 shows the bathymetric and topographic features of this region. This map and the other maps in this study were created by using the GMT software (Generic Mapping Tools, Wessel and Smith, 2001). The main bathymetric and topographic features such as Island arcs, bathymetric ridges, subduction trenches, basins or major Seamounts are briefly described below.

Cretan Sea and Cretan Island Arc

The Cretan Sea and the Island Arc lies in a prominent position in southern part of the Aegean Sea, the forearc of the Crete and the Hellenic Arc. The Cretan Sea is concave to the north and centred around 25° E and 36°N. It has a depth generally between 1000 and 2000 m, with a maximum of nearly 2500 m. Furthermore, the Cretan Island Arc is a submerged zone in the southern part of the Aegean Sea. It is associated also with a zone of inferred fault blocks submerged to different depths.

Hellenic and Cyprean Arcs

The Hellenic Arc is characterized by multiple, parallel ocean depths which follow the Arc. In addition, numerous short depths which are perpendicular to the trend of the Arc are also present. Several depths could probably qualify as subduction trenches. The Hellenic Arc consists of a number of rises and trenches, with the most prominent being the Ptolemy Trench and the Pliny Trench, both deeper than 4000 m, and the Strabo Trench, which cuts into the ridge province. The Cyprean Arc consists of the Anaximander Seamounts, the Florence Rise and the Island of Cyprus itself.

East Mediterranean Ridge

The East Mediterranean Ridge is the largest morphologically feature unit of the Eastern Mediterranean Sea which lies to the south of the trenches of the Hellenic Arc. Moreover, it is

an elongated bathymetric high in the Eastern Mediterranean Sea. It runs from Ionian Basin to the west, passing between Crete and Libya and curving sinuously northeastward to Cyprus to the east. It is about 150 km wide south of Crete, but narrows to about 110 km farther east with averages depth between 2000-2500m. In addition, the ridge is an accretionary complex that is largely composed of sediments that have been accreted from the African plate, which is subducted northeastwards beneath the Aegean. It is about a more than 1500 km long tectono-sedimentary-accretionary prism and characterized by numerous low hills, depressions and deformed sediments paralleling the plate margin between Africa and the Aegean as suggested by Ryan, et al. (1971) and Le Pichon et al. (1995) and (2002).

Herodotus Abyssal Plain

The Herodotus Abyssal Plain marks the southern boundary of the Mediterranean Ridge. It has very little topographic expression and emerges as a narrow Abyssal Plain to the northwest of the Nile Delta. It extends in a NE-SW direction and has a rather smooth bathymetry with a maximum water depth of about 3500 m.

The Levant Basin

The Levant Basin is located in the southeastern corner of the Eastern Mediterranean Sea. The seafloor slopes down gently in NE direction towards the Nile Delta. Its depth ranges from about 500 m to a maximum of about 2000 m southern of the Cyprean Arc.

Northeastern Levant

Most of the Northeastern Levant Sea is considerably shallower than the rest of the Eastern Mediterranean. The portion that lies between Cyprus and Turkey, the Cilica Basin, has a depth of about 1000 m. Southern of the Cyprus Arc, there are two submerged mountain complexes namely: The Hecataeus Seamount, which is a submerged part of the Island, and the Eratosthenes Seamount.

Eratosthenes Seamount

The Eratosthenes Seamount is one of the most prominent physiographic features of the southeastern Mediterranean Sea, situated southern of Cyprus between the Levant Basin, to the East, and the Herodotus Abyssal Plain, to the west. The Seamount has a massive rise with an oval shape, whose major axis is oriented to the NE-SW. The depth of the top of the Seamount

is about 500 m.

Several other physiographic observations of the southeastern Mediterranean Sea and the northern section of Egypt are interesting: the deep Finike and Rhodes Basins, Libyan and Egyptian coastlines, Nile Delta, Qattara Depression, and Sinai Peninsula.

Finike and Rhodes Basins

The Finike Basin, adjacent to the Antalya Basin trending E-W and is as deep as the Mediterranean abyssal plane. The Rhodes Basin is a deep basin, even deeper than the abyssal plane, which lies adjacent to the Antalya Basin.

Libyan and Egyptian coastlines

The gradient of the coastal line of the Libyan and Egyptian coastlines is very steep and the water depth falls rapidly to 2500 m. This continental margin is oriented ESE-WNW and seems to be tectonically controlled by a fault system which crosses Egypt near Cairo and terminates at the Gulf of Suez.

Nile Delta

The floor of the southern Levant Sea is dominated by the Nile Cone. The thick deltaic deposits exhibit only very gentle relief and an area of abyssal hills within the Rosetta and Damietta fans.

Qattara Depression

The Qattara Depression extends to about 15 square kilometres. It lies in the Western Desert in Egypt, and is largely below sea level. The lowest point of the Qattara Depression is 133 meters below sea level (Said, 1962). Badlands, salt marshes, and salt lakes cover the sparsely inhabited Qattara Depression. The Qattara Depression also contains some subsurface geological basins, like the Abu Gharadig Basin.

Sinai Peninsula

This area of triangular geometry lies in the northeastern part of Egypt. The elevation of Sinai's southern rim is more than 1000 meters. Moving northward, the elevation of the Sinai Peninsula decreases. The northern third of Sinai is a flat sandy coastal plain that extends from the Gulf of Suez and the Suez Canal into Israel (Said, 1962).

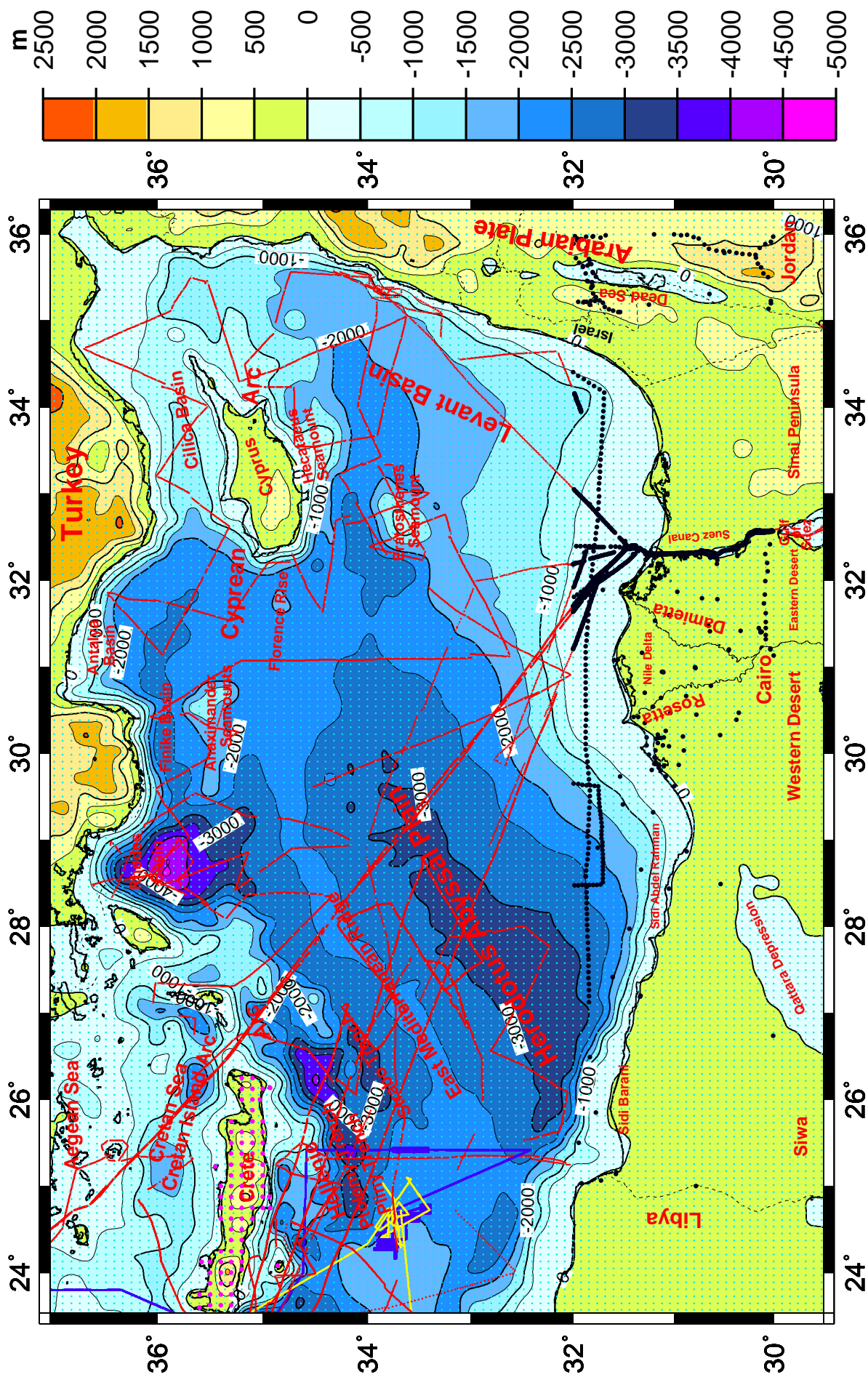


Figure 2.1: Bathymetric and topographic features pattern map of the southeastern Mediterranean Sea and the northern section of Egypt
"Contour interval is 500 m". Data Sources: **GEODAS - Data**; **Meteor 25/4**; **Meteor 40/1**; **B.G.I.**; **ETOPO** & some grid points represent topographic data were obtained from the topographic map of a survey on Crete Island during 1997-98 (lange, 2000).

II.2. Geology

The southeastern Mediterranean Sea and the northern section of Egypt is attracting considerable attention due to the complexities of its tectonic setting. Interpretation of the regional geological features, regional tectonic framework, tectonic and structural setting, and crustal structure allows a better understanding of the tectonic and geological evolution of this region. In the following section, an updated summary of the regional geological features and a brief review of the regional tectonic framework will be presented. The tectonic and structural setting, and the crustal structure of the area investigated are also summarized.

II.2.1. Regional geological features

In general, the southeastern Mediterranean Sea and surrounding regions comprise two distinct tectonic domains that were juxtaposed by subduction and plate collision: the first is the Alpine orogenic belt in the north and the second is the extra-orogenic domain south of it, on which this section focuses. This includes the part of the southeastern Mediterranean basin south of the Cyprus Arc and the bordering continental areas (Figure 2.2). Eastward from Cyprus the suture between these domains is marked by ophiolitic and related nappes that were emplaced in the late Cretaceous-the peri-Arabian ophiolite crescent (Ricou, 1971). Farther west, the suture continues beneath the seafloor, joining the Hellenic trenches. The currently active plate boundary approximately follows this suture, but details of the present plate configuration were established only in mid-Cenozoic times. Within the orogenic zone, much of Anatolia became an independent micro-plate that is extruded westward (Sengör et al., 1985). Now its junction with the African plate forms the active plate boundary along the southeastern Mediterranean Sea. In addition, mid-Cenozoic continental breakup separated the Arabian plate and the Sinai sub-plate from the African plate (e.g. Freund et al., 1970; Joffe and Garfunkel, 1987; Le Pichon and Gaulier, 1988).

The extra-orogenic southeastern Mediterranean Sea comprises several distinct geologic and morphologic units (Biju-Du val et al., 1978). The main regional geological features are outlined in Figure 2.2.

Most prominent is the division of the southeastern Mediterranean Sea into a shallower part east of about 32°E and a deeper region farther west. Most of the eastern part is occupied by the Levant Basin, up to 2 km deep. On its western side is the Eratosthenes Seamount whose top rises to about 0.8 km below the sea level (Figure 2.1). The transition to the deeper area farther west is obscured by the sediment pile of the Nile Delta and by a zone of diapirism and slumping

(Masclé et al., 2000 a). The deeper western part of the southeastern Mediterranean Sea comprises the Herodotus Basin, much of which is occupied by an about 3 km deep abyssal plain. North of it is the shallower East Mediterranean Ridge whose complex small-scale topography contrasts significantly with the smooth abyssal plain. On the northwest, the ridge is delineated by the Aegean trenches (Figure 2.2).

The southeastern Mediterranean Sea outside the orogenic domain has a thick sediment fill, but only its younger part is known in some details. The Pliocene to Recent sediments consists mostly of fine clastics carried by the River Nile. They are up to about 4 km thick under the Nile Delta, but thin to lower than one kilometre thin under the deeper parts of the basin (Ross and Uchupi, 1977). The Messinian evaporate-bearing series underlies much of the basin, being more than 2 km thick under a considerable area, but it thins and wedges out towards the basin margins and over high standing features such as the Eratosthenes block (Said, 1981).

In most of the study area, the fill is little deformed. However, in a large area Pliocene to Recent sediments are affected by considerable thin-skinned deformation as a result of instability and flow of the Messinian Series. Most conspicuous are large slumps and diapirs along the margins of the Levant Basin, south and west of the Eratosthenes block, and under parts of the Herodotus abyssal plain (Garfunkel, 1984; Robertson et al., 1995). The East Mediterranean Ridge consists of basinal sediments that were detached from their base as a result of compression in front of the Aegean subduction zone. They are being incorporated into the zone of Alpine deformation (e.g. Spakman et al., 1988; Chaumillon et al., 1996). This ridge was interpreted as an accretionary ridge or complex, because it is an elongated body of sediments deformed under compression, located above a subducting plate, and lying parallel to the oceanic trench associated with the subduction (Lallemant et al., 1994).

Despite its depth and thick sediment fill, the extra-orogenic part of the southeastern Mediterranean Sea is characterized by a strong positive Bouguer gravity anomaly that reaches 70-90 mGal in the Levant Basin and 150-190 mGal in the Herodotus abyssal plain (Chapter III gives more detailed description about this).

In view of the southeastern Mediterranean Sea depth and thick low-density sedimentary fill, this indicates the presence of thin crust under the southeastern Mediterranean Sea, which was confirmed by seismic studies (e.g. De Voogd et al., 1992). The crust under the adjacent part of Egypt is typically continental and more than 30 km thick (Makris et al., 1988). Detailed information from seismic studies in the southeastern Mediterranean Sea is given in Chapter IV.

II.2.2. Regional tectonic framework

Figure 2.2 is an outline of the regional tectonic map of the study area and adjacent regions compiled by Mckenzie (1972), Barka (1992), Jackson and Mckenzie (1984), Senögr et al. (1985), Ben-Avraham et al. (1976, 1987), Saroglu et al. (1987), Jarriage et al. (1990), Reuther et al (1993), Anastasakis and Kelling (1991), Hancock and Atiya (1979), Taymaz et al. (1991), Kempler and Garfunkel (1991), Barka (1992), Wong et al. (1995), Ten Veen and Meijer (1998), Cagatay et al. (1998), Peter et al. (1998), Glover and Robertson (1998), Yaltirak et al. (1998), Garfunkel (1998), Okay et al. (2000), Mascle et al. (2000 b), McClusky et al. (2000), and Piper and Perissoratis (2003). The area investigated and the adjacent areas are considered, world wide, an unique natural laboratory for studying the occurrence of extensional tectonics in a framework of continental convergence (e.g. Sengör and Yilmaz, 1981; Plag et al., 1998). This is because of the wide variety of tectonic processes encompasses, including various stages of continental collision (Zagros/ Black sea), subduction of oceanic lithosphere and associated back Arc spreading (Cyprean/ Hellenic Arcs and Aegean Sea), convergence between the seafloor and the Arc (Mediterranean Ridge), continental extension (e.g. Marmara Sea), major continental strike-slip faults (North and East Anatolian and Dead Sea faults) and a variety of smaller-scale processes associated with African-Arabian-Eurasian plate interactions (Figure 2.2). All of these processes are contained within the study area with distinct morphogeological features. The image of these prominent morphogeologic features in the bathymetric and topographic features map are shown in Figure 2.1 (e.g. Levantine Basin, Herodotus Abyssal Plain, Eratosthenes Seamount, and Nile Delta). Furthermore, the southeastern Mediterranean Sea and the northern section of Egypt has a remarkably long historical record of major earthquakes (e.g. Mckenzie, 1970; Udias, 1982; Kebeasy, 1990; Ambraseyes and Jackson, 1990) and has been the focus of intense geological and tectonical investigations (e.g. Ben-Avraham et al. 1976, 1988, and 1995; Perincek, 1991; Muller and Kahle, 1993; Kempler and Garfunkel, 1994; Le Pichon et al., 1995; Erwan et al., 1998; Kahle et al., 1998; Mantovani et al., 1997; Guiraud and Bosworth, 1999; Mascle et al., 2000 a; McClusky et al., 2000 and 2003; Huguen et al., 20001; Hübscher et al., 2002).

The regional tectonic framework of the study area is dominated by the collision of Arabian and the African plates with Eurasia (Mckenzie, 1970; Jackson and Mckenzie, 1984, 1988, Reuther, 1990; Reuther et al., 1993; Adam et al., 2000). Plate tectonic models (e.g. DeMets et al., 1990; Jestin et al., 1994; McClusky et al., 2000) based on analysis of global seafloor spreading, global positioning system (GPS), fault systems, and earthquake slip vectors indicate that

the Arabian plate is moving in a north-northwest direction relative to Eurasia at a rate of about 18-25mm/yr (Figure 2.2). Differential motion between Africa and Arabia (~ 10-15 mm/yr) is considered to be taken up predominantly by left-lateral motion along the Dead Sea Fault (DSF). This northward motion results in continental collision along the eastward extrusion of the Anatolian plate (Mckenzie, 1970; Noomen et al., 1996; Kahle et al., 1998).

The leading edge of the African plate is being subducted along the Hellenic Arc at a higher rate than the relative northward motion of the African plate itself, provided that the Arc moves southward relative to Eurasia (e.g. Royden, 1993). Subduction of the African plate is also thought to occur along the Cyprean Arc and/or the Florence Rise south of Turkey, although it is less well defined in these regions than along the Hellenic Arc (Figure 2.2).

A significant improvement to the simple three-plate model of the study area resulted from analysis of seismicity, global positioning system (GPS), tectonic and geologic information. Using such data, Mckenzie (1970), Jackson and Mckenzie (1984, 1988), Jackson (1992); McClusky et al. (2000) developed a regional tectonic framework, for understanding the deformation in the study area and examined the principles of controlling continental tectonics in the region. They suggested that continental lithosphere tends to move laterally away from zones of compression, presumably to minimize topographic relief and to avoid subduction of buoyant continental material. They further suggested that the Anatolian plate moves westward from the zone of intense convergence in eastern Turkey. They derive an Euler vector (i.e. rotation pole and rate) for Anatolia-Eurasia based on earthquake slip vectors along the North Anatolian fault (NAFZ). A few fault systems, the Suez rift and faults from Arabian plate, extend into southeastern Mediterranean Sea (Figure 2.2). These faults reflect activation of the Dead Sea faults and the Levant-Aqaba transform plate boundary. An active eastern Mediterranean transcurrent fault system (EMTS) runs through the Ionian Sea, the base of the continental margin of Eastern Libya and Western Egypt, into the land area through the apex of the Nile Delta and eventually into the Gulf of Suez (Ben-Avraham et al., 1987).

The regional geological features of the area investigated and adjacent areas, when integrated with the regional tectonic framework, provide much information about the geological history of the Mediterranean Sea.

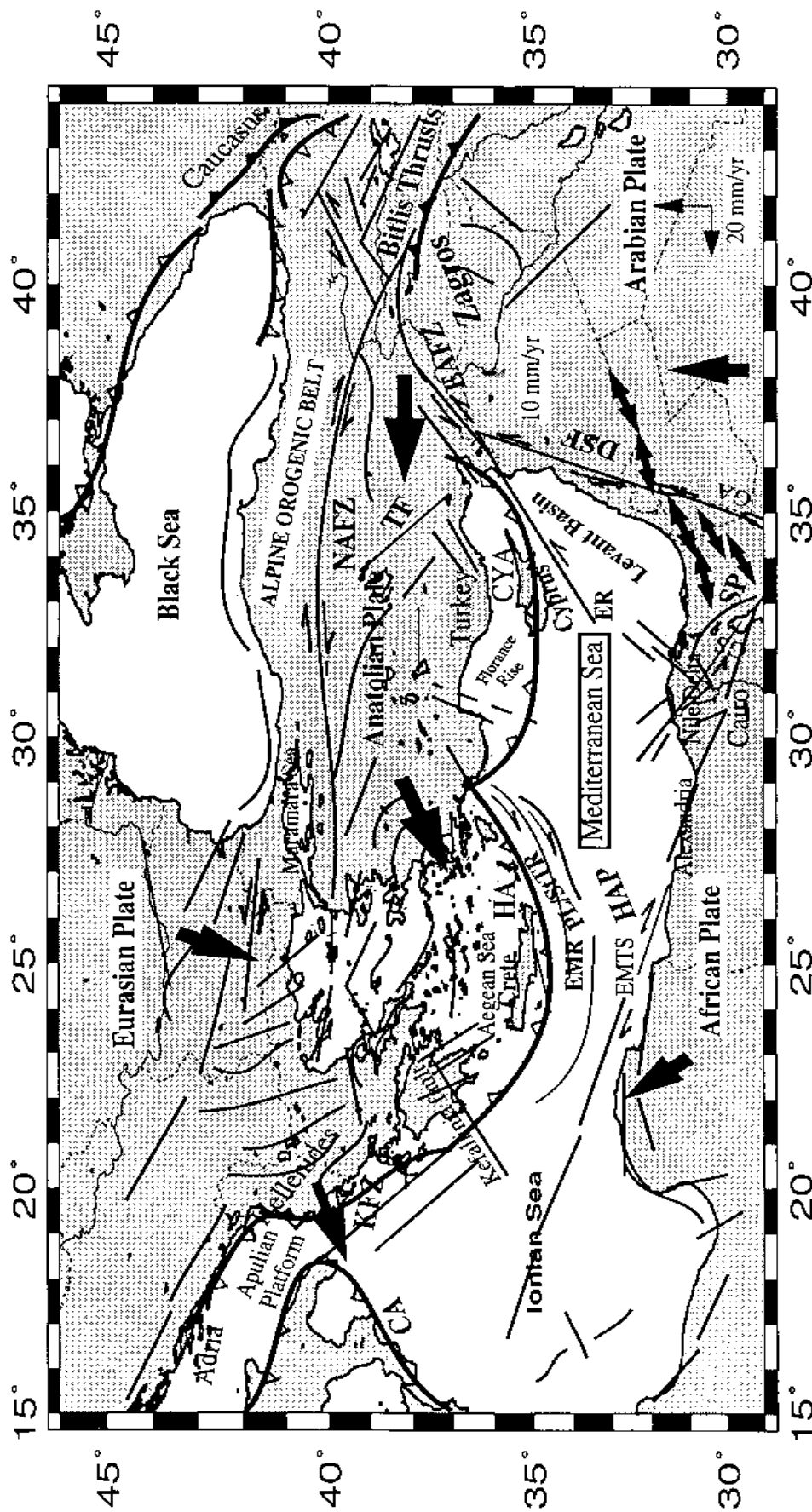


Figure 2.2: Simplified regional tectonic framework map of the study area and adjacent regions. Compiled from Mckenzie (1972), Barka (1992), Jackson and Mckenzie (1984), Senögr et al. (1985), Ben-Avraham et al. (1976,1987), Saroglu et al. (1987), Jarriage et al. (1990), Reuther et al. (1993), Anastakis and Kelling (1991), Hancock and Atiya (1979), Taymaz et al. (1991), Kempler and Garfunkel (1991), Barka (1992), Wong et al. (1995), TenVeen and Meijer (1998), Cagatay et al. (1998), Glover and Robertson (1998), Yalirak et al. (1998), Garfunkel (1998), Okay et al. (2000), Mascle et al. (2000 b), McClusky et al. (2000), Piper and Perissoratis (2003). The large solid arrows indicate the sense of motion of the lithospheric plates.

- Strike-slip fault ; — Normal fault ticks on downthrown side; — Reverse fault/ thrust, triangles on overriding block; — Subduction zone;
- Folds; CA =Calabrian Arc; CYA= Cyprean Arc; HA= Hellenic Arc; EMR= East Mediterranean Ridge; HAP= Herodotus Abyssal Plain; GS=Gulf of Suez;
- SP= Sinia Peninsula; GA= Gulf of Aqaba; ER= Eratosthenes Seamount; TF =Tuzgözü Fault ; PL/Sr TR= Pliny and Strabo Trench; DSF= Dead Sea Fault; NAFZ= North Anatolian Fault Zone; EAFZ= East Anatolian Fault Zone; EMTS = Eastern Mediterranean transcurent fault system.

II.2.3. Tectonic and structural setting

The specific area of this investigation lies in the contact zone between the African and the Eurasian plates. Along this zone, the Mediterranean lithosphere (African plate) underthrusts the Eurasian lithosphere (Eurasian plate) in an almost south-north direction. The convergence between the Eurasian and African lithospheric plates occurs in a north-south direction along the southern boundary of the Aegean area, along the arcuate zone of the Hellenic Arc, the Cyprean Arc, and its continental extension (Robertson, 1998).

Generally, the area under study lies on the northern margin of the African plate. This area is being actively subducted since the late Cretaceous along the destructive compressional plate boundary of Crete and Cyprus (Abdel Aal et al., 2000). Satellite Laser Ranging (SLR) has revealed that the kinematic field of the Eastern Mediterranean region is characterized by the westward motion of Anatolia and a southwest motion of the Aegean Sea area (Halsey and Grandner, 1975; Smith et al., 1994; Noomen et al., 1996).

The study area has always been a complicated puzzle for the geodynamic reconstructions. The main geodynamic factor controlling tectonics of the study area has usually been considered to be a relative motion of Africa and Europe as a consequence of different spreading rates along the Atlantic oceanic ridge (Erwan et al., 1998). The main tectonic elements in the area under investigation as well as the surrounding areas and their geodynamic relation are presented in Figure 2.3 according to Peter et al (1998). Various geodynamic frameworks have been proposed in the past to understand the tectonical and geological evolution of this region (e.g. Mckenzie, 1970, 1972; Ben-Avraham and Nur, 1976; Le Pichon and Angelier, 1979).

Mckenzie (1972) proposed convergence between the northward moving African and Arabian plates, which are separated by the Dead Sea transform fault system. The westward moving Turkish Anatolian subplate and the south westward moving the Aegean subplate (Figure 2.4). The Hellenic and Cyprean Arcs are formed where the African oceanic lithosphere is being consumed.

Papazachos (1973) and Rabinowitz and Ryan (1970), stated that the Eastern Mediterranean Sea is a small ocean basin known for its unusual tectonic complexity. The Eastern Mediterranean Sea includes a short segment of the convergence boundary between Africa and Eurasia. Subduction in this segment is present along two very small Arcs, the Hellenic and Cyprean Arcs. Both subduction Arcs have been documented using variations in bathymetry and magnitude of the earthquakes.

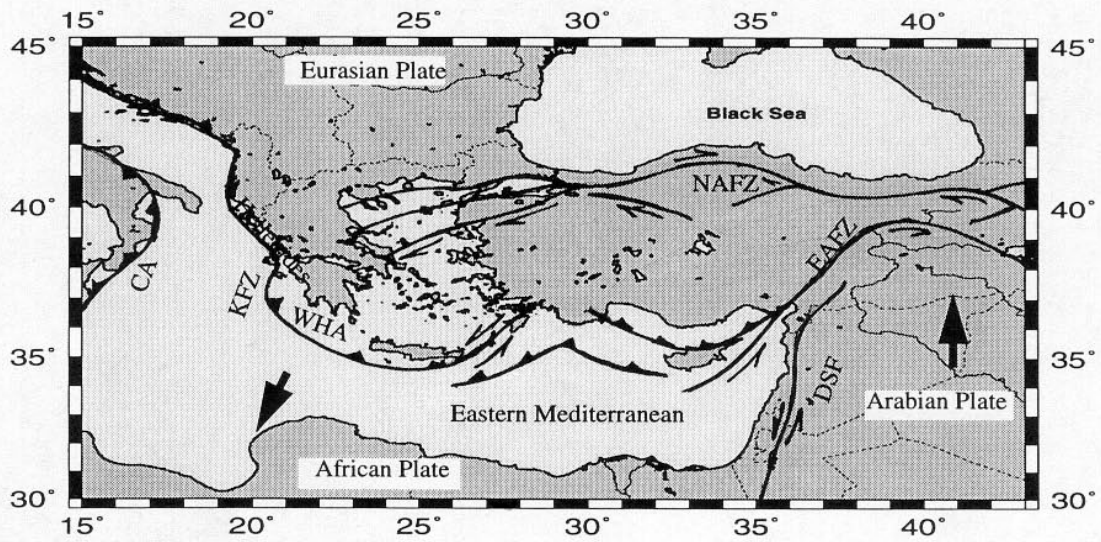
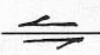

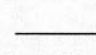


Figure 2.3: Geodynamic framework of the Eastern Mediterranean Sea and surrounding areas, after Peter et al. (1998).

 Strike Slip Fault ;
  Thrust Fault;
  Normal Fault;

CA=Calabrian Arc; DSF=Dead Sea Fault; EAFZ= East Anatolian Fault Zone;

KFZ=Kephallonia Fault Zone; NAFZ=North Anatolian Fault Zone; and WHA=West Hellenic Arc.

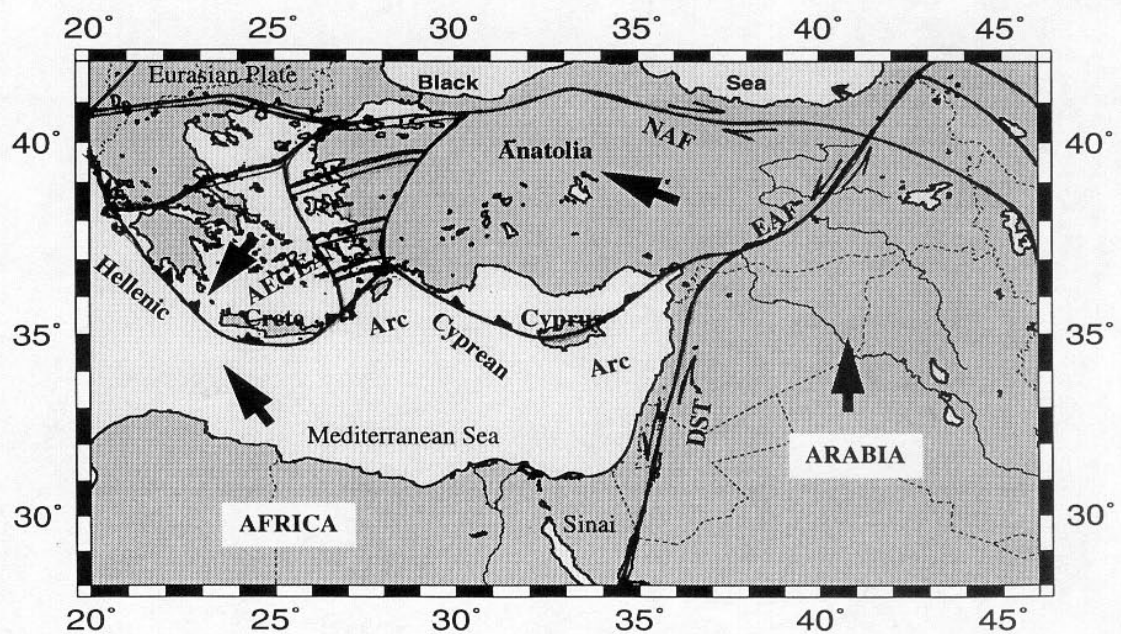


Figure 2.4: Schematic configuration of the plates in the Eastern Mediterranean Sea and surrounding areas. Compiled from McKenzie (1970, 1972).

DST=Dead Sea Transform; EAF=East Anatolian Fault; and NAF=North Anatolian Fault.

On the basis of these variations of the southeastern Mediterranean, the region is roughly subdivided into two parts: The Hellenic and Cyprean Arcs, and the Levant Basin.

II.2.3.1. The Hellenic and Cyprean Arcs

The southeastern Mediterranean Sea is characterized by subduction zones, the largest being the Hellenic and Cyprean Arcs (Figure 2.4). These subduction zones are the key areas of the seismotectonic activity which is caused by the collision of the African and Eurasian plates. The Hellenic Arc is associated with backarc basin and volcanism, while the Cyprean Arc is not. The Hellenic Arc is subjected to one of the largest tectonic motions in Europe (Peter et al., 1998).

The boundary between the plates and the relation between the Hellenic and Cyprean Arcs has been subject to a variety of tectonic interpretation (e.g. Gass and Masson-Smith, 1963; Vogt and Higgs, 1969; Mckenzie, 1970, 1972; Nur and Ben-Avraham, 1978).

Nur and Ben-Avraham (1978) proposed that the Hellenic and Cyprean Arcs are connected through a cusp. The Cyprean Arc forms a continuous plate boundary with the Hellenic Arc (Figure 2.5), but the plate boundary does not continue far East of Cyprus, where according to the model, the Arc is truncated by NNW trending faults.

Le Pichon et al. (1982 b) and Mercier (1981) stated that the Cyprean Arc is not continuous with the Hellenic Arc (Figure 2.6). Instead they are separated by a zone of external Alpine orogeny. However, the Cyprean Arc continues east of Cyprus into a zone of thrusting in Syria and Turkey.

Lort et al. (1974), Biju-Duval et al. (1978), Le Pichon and Angelier (1979), Dercour et al. (1986), Kempler and Ben-Avraham (1987) and Peter et al. (1998) considered a double boundary existing along the Cyprean Arc: the first branch crosses north Cyprus and the second passes south of the Island (Figure 2.6).

Another model was proposed by Woodside et al. (1992), who suggested that the south boundary of the Turkish subplate being a series of at least three or four extensive and curved shear belts (Figure 2.7).

An entirely different model was proposed by Dewey et al. (1973), who suggested that there is no single boundary between Africa and Europe, but rather a complex interacting set of microplates.

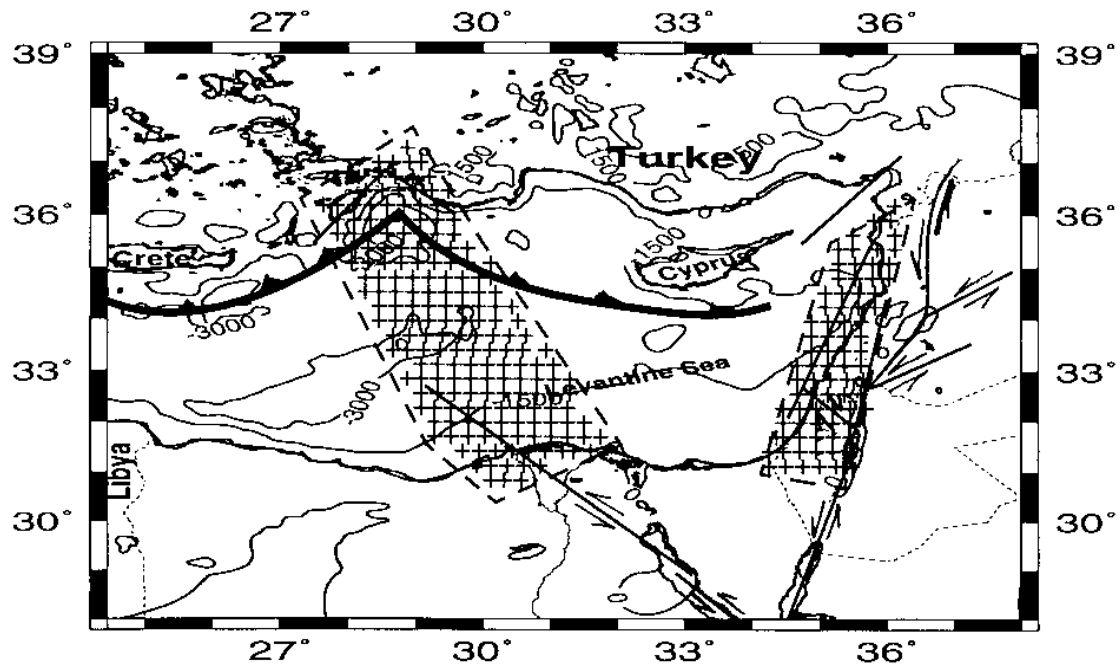


Figure 2.5: Models of active tectonic elements in the Eastern Mediterranean Sea, after Nur and Ben-Avraham (1978). Hatched areas indicates zones of transition.

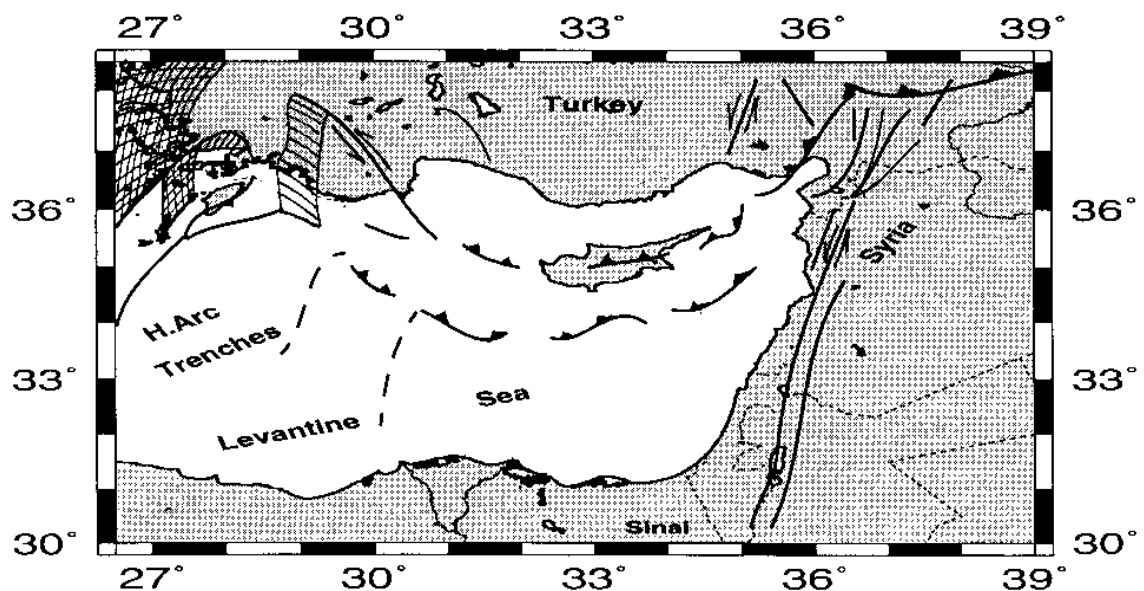
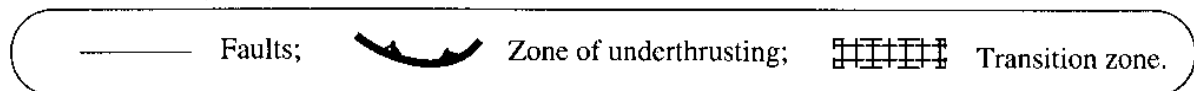


Figure 2.6: Simplified models of active tectonic elements in the Eastern Mediterranean Sea, after Le Pichon and Angelier (1979). Hatched areas indicate zone of external Alpine orogeny.

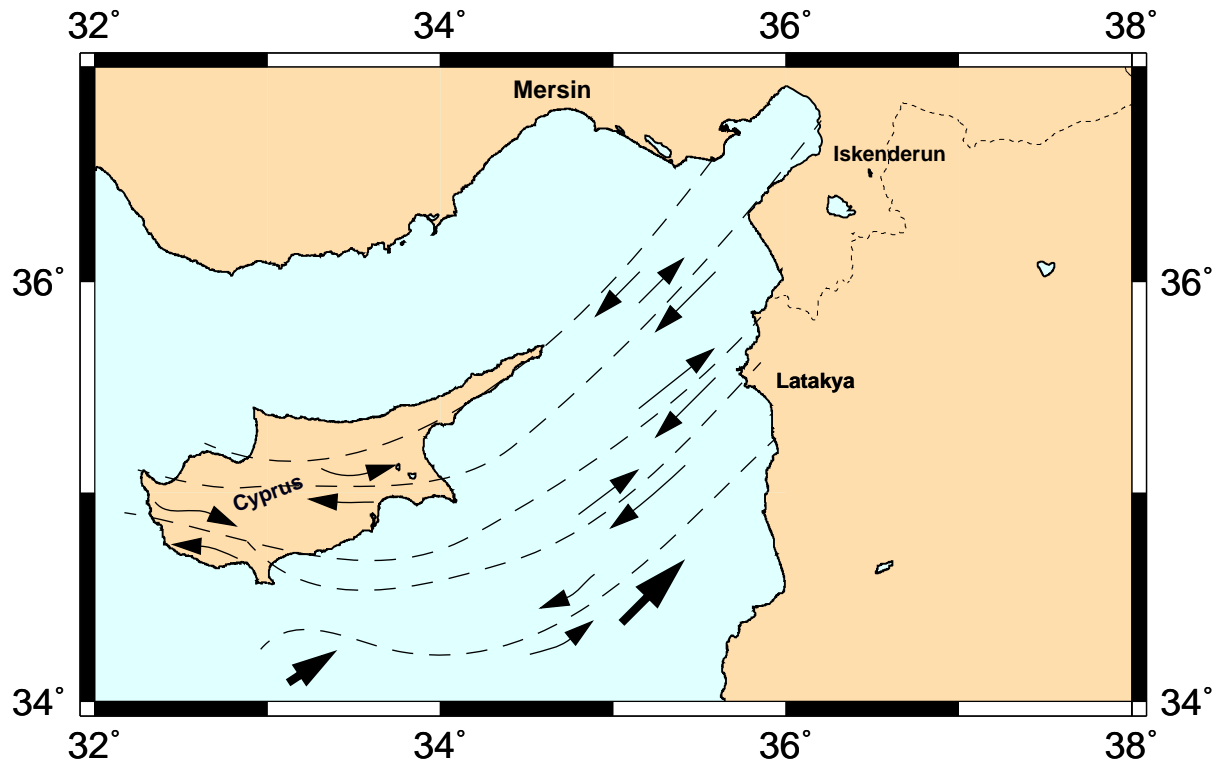
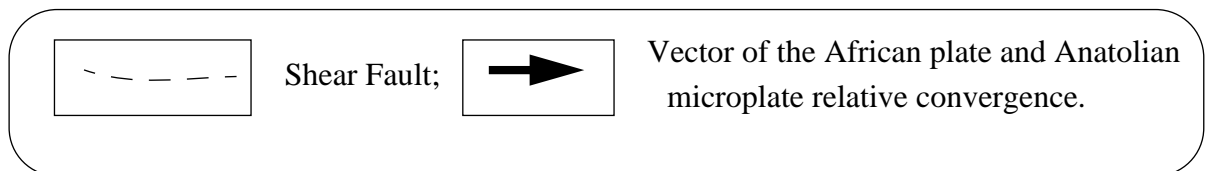


Figure 2.7: Simplified geotectonic setting of the Northeastern Mediterranean Sea. Compiled from Woodside et al. (1992).



II.2.3.2. The Levant Basin

The tectonic evolution of the Levant continental margin is governed by the evolution of the Levant Basin, and by the interaction of the Sinai plate with adjacent plates-mainly the Turkish plate. Several models have been proposed to explain the tectonic evolution of the Levant Basin. Some agreed that it was opened as a marginal basin (Freund et al., 1975), while others suggested that it was a small “Atlantic-type” ocean basin associated with a subduction zone (Dercourt et al., 1986).

Ben-Avraham et al. (2002) studied the crustal structure of the Levant Basin, eastern Mediterranean by a seismic refraction / wide-angle reflection experiment. Who showed that the basin is underlined by an oceanic crust. Its crustal structure is similar to other small ocean basins (Menard, 1967) and is characterized by an intermediate thickness. The crustal structure of the Levant Basin is significantly different from that of the adjacent land.

In addition, Ben-Avraham (1978) studied the continental slope and rise of a segment of the Levant continental margin by using seismic profiling. Who suggested that the Levant Basin was formed during the process in which the African lithospheric plate moved northward towards the Eurasian plate. The evolution of the basin passed through several phases from the early Mesozoic to the early Tertiary.

II.2.4. Crustal structure of the southeastern Mediterranean Sea

In general, the crustal structure of the southeastern Mediterranean Sea has been the subject of intensive discussions and has had various interpretations. Some authors have shown that the crust of the Eastern Mediterranean Sea is of continental character (e.g. Allan and Morelli, 1971; Woodside, 1977; and Morelli, 1978), while others suggested that the crust is characterized by an ancient oceanic crust (Rotstein and Ben-Avraham, 1985). Another model has shown that the crust consists of both oceanic and continental segments (Ryan et al., 1971).

Nur and Ben-Avraham (1978) suggested that an oceanic crust probably occurs only in the deep basin of the Eastern Mediterranean Sea, and is separated by crustal units of continental composition. Makris et al. (1983) and Makris and Stobbe (1984) showed that the crust under the Levant Basin is floored by oceanic crust, whereas the crustal type of the Cyprus and Eratosthenes Seamount are continental.

Papazachos (1969) suggested that the crustal structure of the Eastern Mediterranean Sea changes gradually from oceanic in the west to continental in the east. In southern Crete the crust is of more continental character with the depth to the mantle being about 21 km, whereas in the

Levantine Sea, the depth to the mantle is even greater 25 -27 km (Lort et al., 1974; Finetti and Morelli, 1973). The eastern most portion of the Levantine continental margin and the Levant Basin is characterized by the thickest crust, where along the Dead Sea transform the depth to the mantle is 35 km (Ben-Avraham et al., 1976).

A detailed description of the crustal structure and geodynamic relation between the various lithospheric plates of the investigated area, and its relation to the adjacent region, undertaken by developing two and three-dimensional density models are presented in Chapter V.

II.3. Brief account of the geological history of the Mediterranean Sea

To understand the geological history of the Mediterranean Sea, a knowledge of its geological evolution is essential. Several geological studies have been carried out extensively in and around the area investigated (e.g. Mckenzie, 1970; Ryan et al., 1971; Lort, 1971; Schembri, 1996). In the following, a brief summary of the geological history of the Mediterranean Sea elucidated by Schembri (1996) will be presented.

The origins of the present day Mediterranean can be traced to the Triassic (Ca.200 Ma, Ma = Million year ago). The first ancestor of the Mediterranean was the Tethys Sea consisting of an open shallow water basin in the supercontinent Panda.

Typical shallow water sediments of that age are still present in places around the Mediterranean Sea. In the Jurassic (Ca. 150 Ma) there was a period of intense ocean rifting in East-West direction along the Tethys, that produced the first outlines of Europe and Africa. Later in the Jurassic (Ca. 135 Ma) the initiation of rifting between Africa and south America produced the first south Atlantic Sea floor, and started the anticlockwise rotation of Africa towards Europe. This reversed the rifting process and converted the Palaeo-Mediterranean into a subduction zone. The original Tethys ocean floor gradually began to be consumed as it was subducted under the Eurasian plate. Much volcanism was produced and most of today's volcanic activity in the Mediterranean is associated with this subduction process.

By the Cretaceous (Ca. 65 Ma) tectonic movements progressively pushed the African landmass towards the Eurasian landmass until almost all the Tethys ocean crust had been consumed. A pocket of water was gradually pinched off. The forerunner of the Mediterranean, or Paleo Mediterranean became a zone of continent collision. The "collision front" between Africa and Europe followed roughly a line passing through the present north Africa coast, north Sicily, the Apennines, down through the Dinaric Alps, and the Hellenic Chain.

This collision initiated the main phase of Alpine orogeny (Mountain building) around the

Mediterranean, with great fold mountains composed of marine sediments and parts of African and European crust. The collision process continues to the present day and probably involves complex mechanisms of continent-continent interaction. Subduction of the African plate, under the European plate in the Eastern Mediterranean produced the Greek Volcanic Arc and the thinning of the crust on the European side and probably this led to subsidence of the Aegean plate, forming today's shallow Aegean Sea.

In the late Oligocene and Early to Middle Miocene (Ca. 28-10 Ma), there was a development of a new oceanic type basin in the Western Mediterranean-the Balearic and Tyrrhenian Basins. The opening of the Tyrrhenian Basin produced the anticlockwise rotation of the Italian Peninsula to its present position. Deposition of sediments, making up the Maltese Islands took place during this period. The Islands were uplifted above Sea level during Quaternary times coincidentally with the opening of the Pantelleria Rift.

During the late Miocene (Ca. 6-7 Ma), closure of the western portion of the Mediterranean basin led to an almost complete evaporation of the water in the Mediterranean basin (Messinian Salinity Event). This precipitated a layer of evaporitic sediments that is found at about 100 m below the surface of today's sediments. The increased salinity led to the extinction of marine biota in the Mediterranean at river mouths due to increased velocity of the river waters falling over the steep sides of the dry basin.

In the Pliocene (Ca. 5.5 Ma) a re-opening of the Straits of Gibraltar caused the re-flooding of the Mediterranean. A new population of marine biota from the Atlantic was introduced. Thus, the pre-evaporitic fossils (including Maltese fossils) are different from the post-evaporitic ones.

During the Pleistocene (Ca. 1.6 Ma to 10,000 y ago) the sea-level in the Mediterranean was affected by European glacial/ interglacial cycles. Glacials corresponded to lowering of the sea level (regression) probably resulting in the establishment of the connections between Malta and Sicily.

III. GRAVITY AND MAGNETIC INVESTIGATIONS AND QUALITATIVE INTERPRETATION

Over the last twenty years, many geophysical studies were carried out in and around the investigated area (e.g. Egeran, 1948; Harrison, 1955; Allan and Morelli, 1971; Finetti and Morelli, 1973; Woodside 1977; Makris and Stobbe, 1984; Peters and Huson, 1985; Tealeb, 1989; Makris and Wang, 1994; Makris et al., 1994; Wang, 1995). In this chapter, gravity and magnetic field data and their evaluation processing and transformation into new potential anomaly maps are discussed. A qualitative interpretation of these anomalies, which are related to major bathymetric and tectonic features are given. In addition, regional-residual separation processing of the potential field data is performed.

III.1. Gravity investigations

Gravity is an important geophysical tool in subsurface investigation to determine the differences in the existing earth's gravitational field at various locations and help to understand the structure of the earth's crust and mantle. In addition, the state of isostatic equilibrium can be determined by employing the gravity data.

Gravity field data in marine surveys must be collected in a grid or along a profile at stations with suitable spacing. The first step is to remove all predictable components of the earth's gravitational field in the acquired data set. The earth's gravitational field measured at the earth's surface is affected by topographic changes, the earth's shape and rotation. These factors must be removed before interpreting gravity data for subsurface features. The processed gravity data are known as Free-Air and Bouguer gravity anomalies, measured in mGal (milligal)^{*1}

The gravity field data can enhance geological mapping, locating boundaries between units of varying density. Large features (e.g. ridges, subduction trenches, and seafloor-spreading) produce anomalies, which are smooth over considerable distances. These large features are referred to as regional trends. The effect of these regional trends can be subtracted from the data to leave the small-scale variations or residual anomalies.

The location of the main set of gravity field data profiles used in this study are displayed and marked in different colors as shown in Figure 3.1. The gravity data used in this study were acquired from two marine surveys: Meteor 25/4 expedition, Meteor 40/1 expedition (Dehghani, 1994 and 1999) and combined with all the available gravity data from the GEODAS data base.

^{*1} A milligal unit of measurement of the gravity field. A milligal (mGal) is 10^{-3} Gals. The Gal is the basic unit in gravity, equals $1 \text{ cm s}^{-2} = 10^{-2} \text{ m s}^{-2}$ and is named after Galileo Galilei . i.e. $1 \text{ mGal} = 10^{-5} \text{ ms}^{-2}$.

In addition, several gravity profiles were obtained from B. G. I., and grid points representing gravity data obtained from the gravity map from a survey on Crete Island during 1997-1998 (Lange, 2000).

The marine gravity field data, which were obtained from GEODAS Data base, include the following parameters: latitude, longitude, water depth, observed gravity, and Free-Air anomaly. The marine gravity field data, which were obtained from B.G.I., include latitude, longitude, water depth (onshore), elevation (offshore), observed gravity, and Free-Air anomaly.

The marine gravity survey measurements were acquired from the: Meteor 25/4 and Meteor 40/1 expedition and recorded using the KSS 30 gyro-stabilized gravimeter system, no.15 and the GPS navigation of the Institute of Geophysics, University of Hamburg. The gravity values, together with the navigation data, were recorded continuously every ten seconds. Pre-processing of these data was done on the ship and the bathymetric data were measured continuously with HydroSweep (Dehghani, 1994 and 1999). The acquired data from two Meteor expeditions were combined with all available gravity data as mentioned above after applying the necessary reduction (see below). In general the data processing consists of the following steps: The data set is checked for erroneous values. After considering the frequency spectrum the recorded data are processed with a Gaussian, weighted average filter. Speed, heading and course are filtered before calculating the gravity anomalies, where with marine gravity surveys strong disturbing accelerations occur due to the sea state. These are short-periodic and can be eliminated by filtering (Dehghani, 1994 and 1999). A brief description of the processing and transformation of the gravity field data into Free-Air and Bouguer anomalies are presented below.

III.1.1. Evaluation processing of the Free-Air and Bouguer gravity field data

The gravity field data were processed and evaluated into Free-Air anomaly Δg_{FA} , using the following formula:

$$\Delta g_{FA} = g - \gamma_0 + \delta g_{Fr} + \delta g_{T(L,S)} + \delta g_{Eotv} \quad [mGal]$$

where g is the observed gravity value, γ_0 is the theoretical gravity value according to the international Gravity Formula of 1967 (Telford et al., 1990), δg_{Fr} is the Free-Air reduction, $\delta g_{T(L,S)}$ is the tide effect (see Liebe, 1986), and δg_{Eotv} is the Eötvös correction.

The Free-Air reduction δg_{Fr} depends on the altitude of the measured point and is zero in marine surveys and equal $+0.3086 \text{ h mGal/m}$ at the situation of land observation, where h is land elevation at the measured point (Dobrin, 1976). The Free-Air reduction concerns the fact

that gravity is decreasing with increasing distance to the reference height. As marine gravity measurements are carried out at the reference level, no extra height correction factor has to be applied.

The Eötvös correction is the most important reduction for marine gravity measurements. The Eötvös effect describes the vertical component of the Coriolis acceleration that occurs when the ship is moving. At sea, the main error in gravity investigations results from incorrect navigation data. The determination of the velocity over ground is most difficult. Consequently the accuracy of gravity measurements at sea is dependent on the correct determination of the Eötvös correction. Eötvös effect is described by the following equation (see Dehlinger, 1978):

$$\delta g_{\text{Eotv}} = 2 \omega v \cos \phi \sin \alpha + v^2 / R \quad [\text{mGal}]$$

where ω angular velocity due to earth's rotation, v is the velocity in [knots], ϕ is the geographic latitude in $[\circ]$ and α is the ships course with respect to north in $[\circ]$ and R is the earth's radius. The course α and the velocity v of the ship were determined from the GPS data recorded during the survey. δg_{Eotv} Eötvös reduction is zero if the survey is terrestrial from a non-moving platform.

The Bouguer anomaly Δg_{BA} was obtained by subtracting the Free-Air reduction δg_{Fr} , the Bouguer reduction δg_{Br} and the theoretical gravity value γ_0 from the observed gravity value g .

$$\Delta g_{\text{BA}} = g - \delta g_{\text{Fr}} - \delta g_{\text{Br}} - \gamma_0 \quad [\text{mGal}]$$

When the Bouguer reduction is applied to marine gravity measurements, the water body is substituted with a homogeneous material possessing the average crustal density. Accordingly, the Bouguer reduction is:

$$\delta g_{\text{Br}} = 2 \pi G \rho h = 0.04191 \rho h \quad [\text{mGal}]$$

with G being the gravitational constant, ρ = density, and h = depth of the ocean floor (Note: h = depth of ocean positive downward from the surface). In this study, the Bouguer reduction density of 2.67 g/cm^3 was used and the water density assumed as 1.03 g/cm^3 (Dobrin, 1976).

In this study, the Free-Air and Bouguer anomaly data were gridded and smoothed using the inverse-distance method to contour the raw potential field data. In general, the inverse distance method is the simplest interpolation method of scatter points. This method based on the assumption that the interpolating surface should be influenced most by the nearby points and less by the more distant points. The interpolating surface is a weighted average of the scatter

points and the weight assigned to each scatter point diminishes as the distance from the interpolation point to the scatter point increases (see Shepard, 1968). By interpolation of the original gravity data, a regular grid was obtained. The gravity data were gridded at a spacing of 0.005° or 0.555 km, using GMT software. Based on these grids contour maps were constructed. According to the accuracy of the gravity data, a contour interval of 10 mGal was still allowed. The compiled data were interpolated and plotted with contour intervals of 30, 20 and 10 mGal, respectively by using the GMT software. In order to do a more detailed qualitative analysis and also to obtain a clear image of the Free-Air and Bouguer anomalies a contour interval of 10 mGal is chosen as shown in Figures 3.1 and 3.2 respectively.

The image of the anomalies is only considered real where they are attached by shipboard profiles. Along a specific contour line, the distance between two points is irregular. The point density along a contour is usually low for straight lines and get higher as curvature of the contour increases. There are some mask specified areas around the boundaries of the area investigated which create overlay. These areas are not covered by gravity data, as shown in Figure 3.1, and in other maps in this study.

III.2. Magnetic investigations

The total intensity of the marine magnetic data are acquired from the GEODAS data base, including the following parameters: latitude, longitude, and total intensity of the magnetic field. These data refer to different decades valid for the different magnetic surveys. In addition, several profiles of the marine total intensity magnetic field measurements were acquired from Meteor 25/4 expedition. These data were recorded on profiles along the gravity lines in the area under study (Figure 3.3), and carried out with a proton precession magnetometer type ELSEC 7704 of the Institute of Geophysics, University of Hamburg. The analogue data by Meteor 25/4, 1993 have been digitized continuously and merged with the navigation data (Dehghani, 1994).

In order to produce a uniform total intensity magnetic anomaly map of the area investigated, all available total intensity magnetic field data have been compiled, and then plotted using the GMT software. The data from the GEODAS data base are displayed in red lines, and the data recovered during the Meteor 25/4 expedition are outlined in yellow (Figure 3.3).

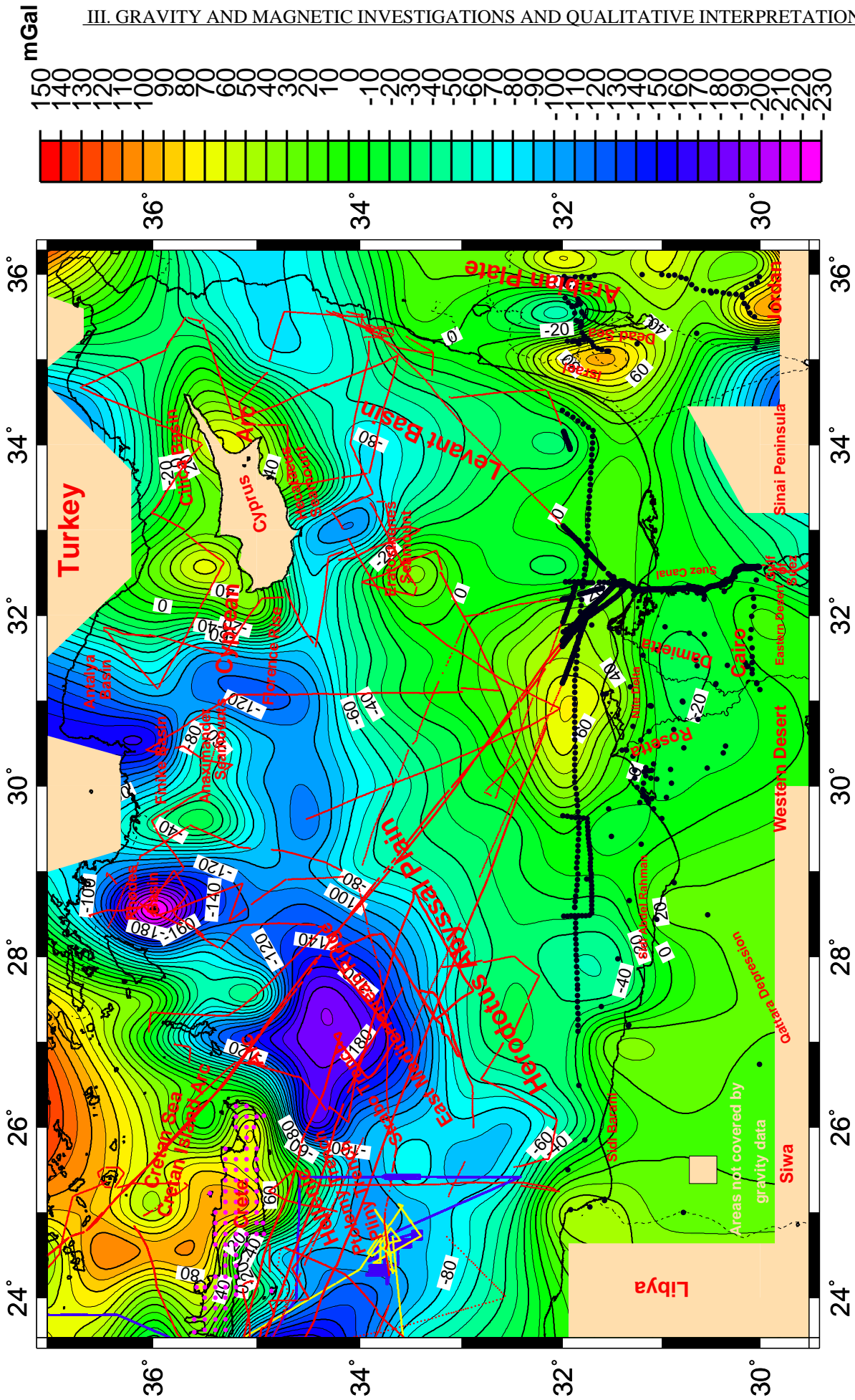


Figure 3.1: Free-Air gravity anomaly map of the southeastern Mediterranean Sea and the northern section of Egypt
 "Contour interval is 10 mGal". Data Sources : **GEODAS-Data**; **Meteor 25/4**; **Meteor 40/1** ; **B.G.I.&** grid points were obtained from
 gravity map of a survey on Crete Island during 1997-98 (Iange, 2000).

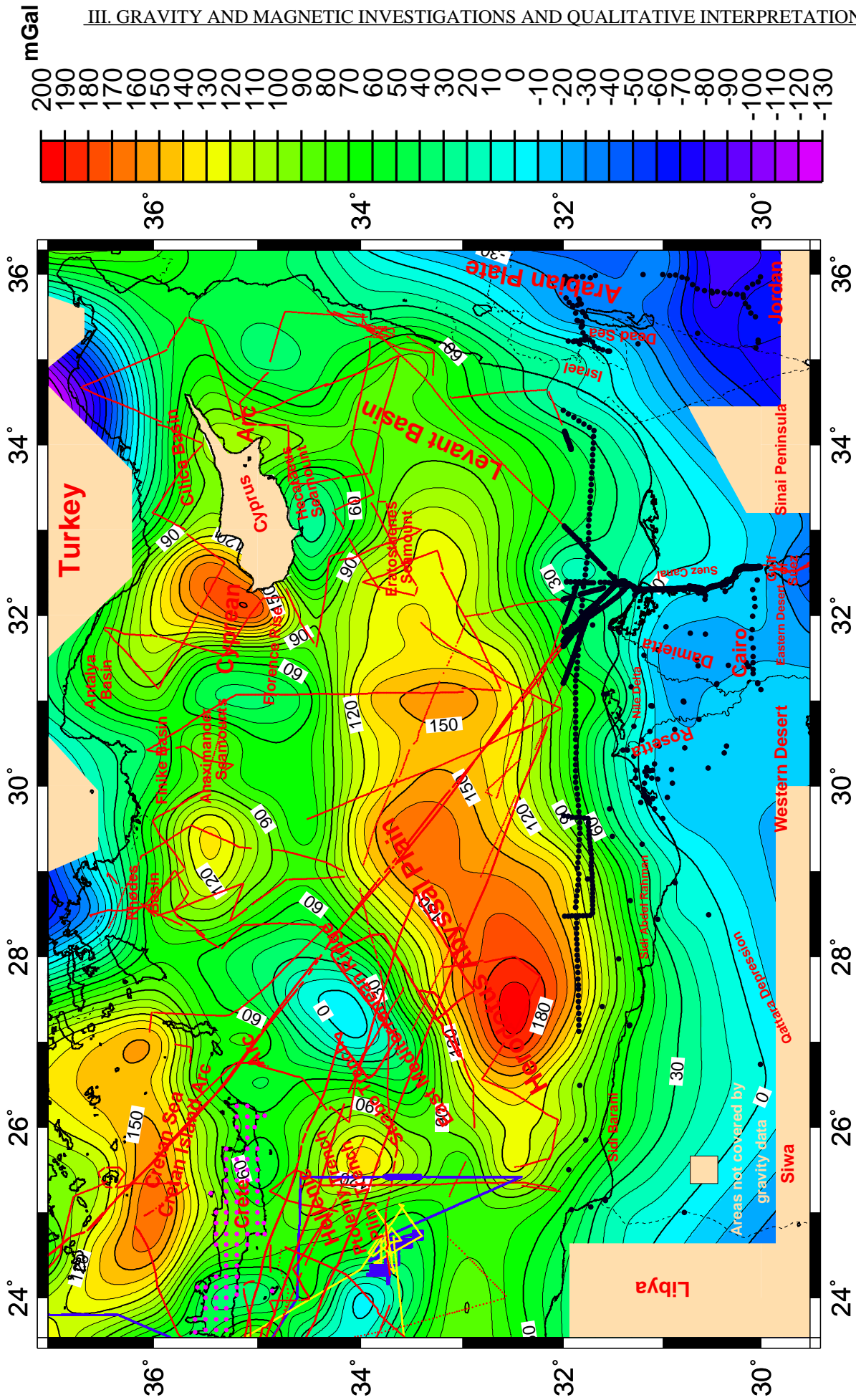


Figure 3.2: Bouguer gravity anomaly map of the southeastern Mediterranean Sea and the northern section of Egypt.

"Contour interval is 10 mGal". Data Sources : **GEODAS-Data**; **Meteor 25/4**; **Meteor 40/1** ; **B.G.I.& Meteor 40/1** grid points were obtained from gravity map of a survey on Crete Island during 1997-98 (Iange, 2000).

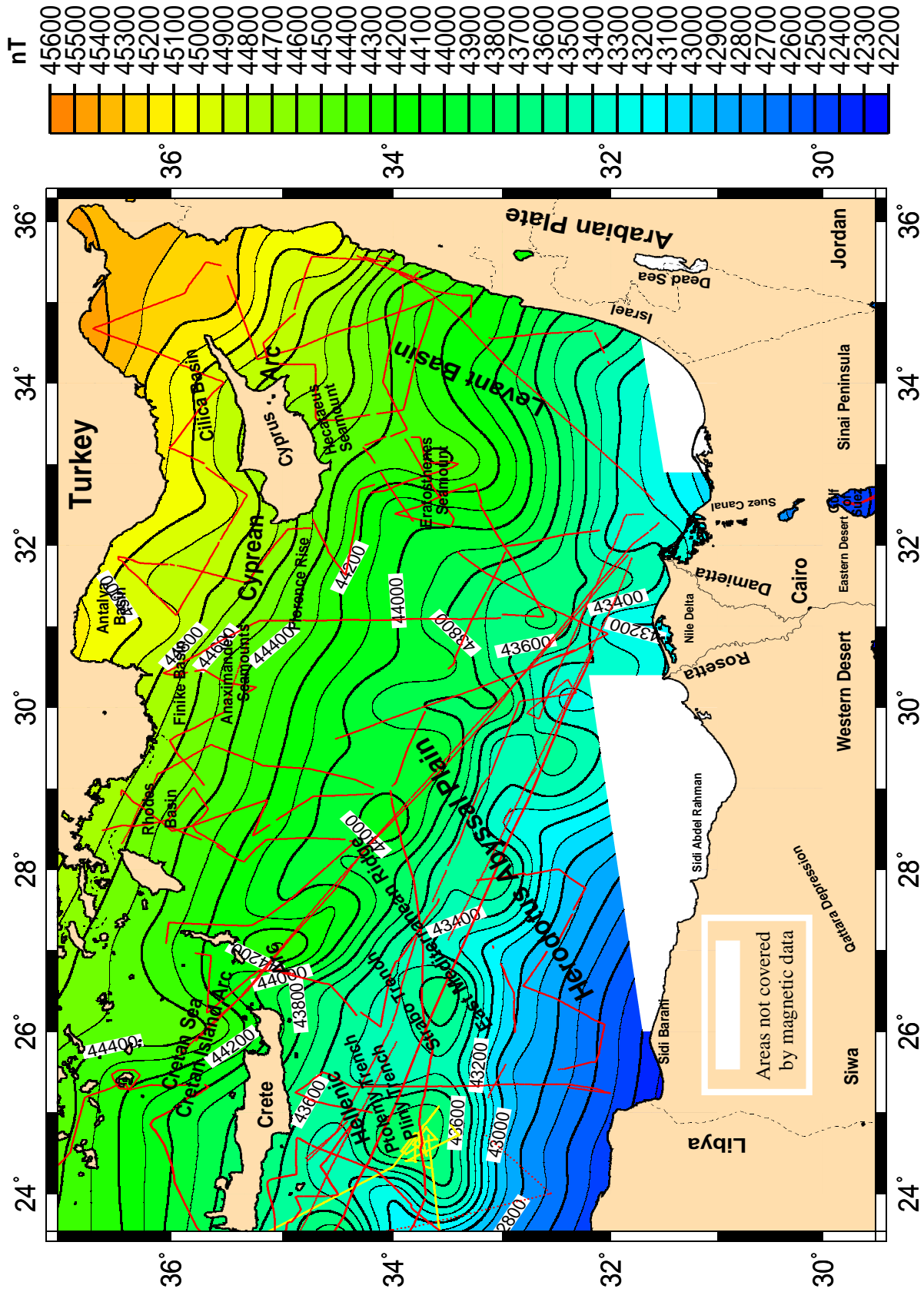


Figure 3.3: Total intensity magnetic anomaly map of the southeastern Mediterranean Sea and the northern section of Egypt.

"Contour interval is 100 nT". Data Sources: **GEODAS - Data** & **Meteor 25/4**

III.3. A qualitative interpretation of the gravity and magnetic data

A qualitative interpretation is very important for interpreting gravity and magnetic anomalies data. Its first stage of an interpretation involving recognition of source bodies and structures. This interpretation depends on a number of variables involve identifying linear features formed by anomaly shapes, gradients, and inferring structures analogous to important structures mapped from other data (Romberg, 1958).

In order to discuss the correlation of the gravity and magnetic field with geological structures, the Free-Air and Bouguer gravity, and the total intensity magnetic field anomaly maps are presented together with main tectonic features of the study area as shown in Figures 3.1, 3.2 and 3.3 respectively.

III.3.1. A qualitative interpretation of the Free-Air gravity data

Figure 3.1 shows the Free-Air anomaly map of the study area. The Free-Air anomalies cover the range from -230 to +150 mGal. A qualitative analysis of the Free-Air anomalies reveals the following features:

Free-Air anomalies in the Eastern Mediterranean Sea are generally negative. Positive values are found only over the Nile cone. The minimum and maximum values are located in the Rhodes Basin (less than -220 mGal) and on the region north of the Cretan Island Arc with up to +120 mGal. The negative Free-Air anomaly values are located in the Rhodes Basin between 28° N and 29° N and the southern Hellenic Arc between 27° S and 28° S and can probably be related to a deep crustal structure.

The Free-Air anomaly map contains information on tectonic features at regional and local scale, which may reflect the effect of the bathymetric and topographic features in a very general way. There is an almost continuous concave anomaly pattern extending from the south of Crete to the northeast of the Rhodes Basin and Turkey and in the south of Cyprus between Cyprus and the Eratosthenes Seamount.

A major discontinuity in the negative anomaly occurs south of Cyprus over the Anaximander Seamounts, where the Free-Air anomaly exhibits a relative maximum of -60 mGal. A series of local negative Free-Air anomalies point to the northern flank of the East Mediterranean Ridge, the Pliny, Strabo Trenches and Rhodes Basin. These mostly lie over the -120 mGal boundary contour line.

The region of long linear features pointing at the Herodotus Abyssal Plain and Nile cone, corresponds to increasingly less negative Free-Air anomalies, with the only major positive

anomaly in the marine areas situated over the mouth of the Nile, owing to the load of the deltaic sediments. A comparison between the bathymetric and topographic features pattern map (Figure 2. 1) and the Free-Air anomaly map reveals many similarities. i.e. gradients of the Free-Air anomalies are large in the vicinity of Cyprus. These anomalies range from more than +20 mGal along the coastline of Cyprus to less than -80 south of Cyprus. They rise again to more than -20 over Eratosthenes Seamount.

The Free-Air anomaly describes the state of isostatic equilibrium of a large-scale structure like a geological basin. It is very small if a region is totally compensated. The structure has to be at least ten times than the compensation depth. The Free-Air anomaly is positive if the structure is only partially compensated or not compensated at all. It is negative if the structure is over-compensated. By observed the orientation of the Free-Air anomalies in the study area, indicated that the isostatic equilibrium is far from being achieved.

III.3.2. A qualitative interpretation of the Bouguer gravity data

Figure 3.2 shows the Bouguer gravity anomaly map of the study area. The qualitative analysis of the Bouguer anomalies reveals the following features:

The anomalies field lies in the area with values ranging from -130 to +200 mGal. Bouguer anomalies in the Eastern Mediterranean Sea are predominantly positive, as it might be expected for an oceanic area. Elongated and longer shape anomalies are present. The long linear anomalies in the map are clear and well defined, being narrow and high gradient anomalies. Most of the broad changes in the Bouguer anomalies can be related to changes in crustal thickness.

The Bouguer anomalies in the Eastern Mediterranean Sea are dominated by an elongated NE-SW trending positive Bouguer anomaly, with a maximum of about +200 mGal coinciding with the elongated anomaly of the Herodotus Abyssal Plain.

The Bouguer anomaly values, in the southeast corner of the area investigated generally decrease towards the east and southeast due to transition from the oceanic crust of the Eastern Mediterranean to the continental crust of the Arabian plate.

To the northwest of the East Mediterranean Ridge there is a broad, relatively elongated high Bouguer anomaly. A negative Bouguer anomaly occurs near the East Mediterranean Ridge between 27° N and 28° N, as indicated by the bathymetric features and crustal thickening.

The Bouguer anomalies of Cyprean Arc and the eastern part of the Hellenic Arc coincide with bathymetric features. The area south of the Rhodes Basin has a depth of about -3000 meters and a Bouguer anomaly of nearly +120 mGal. On the other hand, the Anaximander Seamounts

are marked by a relative low Bouguer anomaly of only +60 mGal.

To the north of the Cretan Island Arc, the Bouguer anomalies strike nearly E-W with an oval shape, following the bathymetric and morphological features. The maximum reaches a value of +170 mGal, its position coinciding with a minimum Mohorovicic (Moho)^{*2} discontinuity depth of 17 km (see Chapter V).

There is a concave northward positive gravity anomaly with a maximum of nearly +190 mGal near the NW extremity of Cyprus which is expected to be related to Cretaceous ophiolites overlying the continental crust of Cyprus. The maximum part of this positive anomaly is associated with the ophiolite.

A broad Bouguer anomaly more than +60 mGal covers most north east of the Nile Delta front and the south west of the Eratosthenes Seamount. The Bouguer anomaly reaches +120 mGal, which is expected to be caused by the rapid decrease of low density sediments and incidence of high density crystalline or igneous rocks.

There are negative Bouguer anomalies located over the Dead Sea and the Northwestern East Mediterranean Ridge that are caused by thickening of the crust. Negative Bouguer anomalies are also located in the NE Cilicia Basin, in southern Turkey, and in the NW Rhodes Basin, and can also probably be related to crustal thickening.

In the Nile valley and Delta, where the bathymetry varies from 0 to 500 m, the negative Bouguer anomaly value ranges only from -10 to -30 mGal. This corresponds to the thickness of the Nile Quaternary sediment. A strong negative Bouguer anomaly is observed in the Gulf of Suez which is caused by thick sediments in this region.

The Bouguer anomaly is negative for a totally or partially compensated structure, an excess of less dense material beneath the measurement station. It is zero for a noncompensated structure. The Bouguer anomaly is positive when an excess of especially dense material is present. The absence of a large Bouguer anomaly associated with the extreme relief indicates that the area is, as could be expected, not isostatically compensated by local variations in the crustal or mantle structure. If the area is not completely isostatically compensated by local variations in the crust or mantle an additional dynamic compensation mechanism must be considered.

III.3.3. A qualitative interpretation of the total intensity magnetic data

The total intensity magnetic anomaly map with a contour interval of 100 nT (nanoTesla)^{*3} is given in Figure. 3.3. A qualitative analysis of the total intensity magnetic anomalies re-

^{*2} Mohorovicic discontinuity is the boundary surface or sharp seismic - velocity discontinuity that separated the Earth's crust from the subjacent mantle. It is named in honor of its discoverer, Andrija Mohorovicic (1857-1936), Croatian seismologist. Syn Moho; M-discontinuity.

^{*3} nano Teslas unit of measurement of the magnetic field. (A nano Tesla is 10^{-9} Teslas).

veals the following features: The total intensity magnetic anomalies in the area range from +42200 to +45600 nT. Smaller and longer shape features anomalies are present.

The total intensity magnetic anomalies are generally oriented from NW to the SE trend and correlated strongly with bathymetric and topographic features. For example, the complex bathymetric structure of the Cyprean Arc is characterized by a series of magnetic anomalies that are produced by the ophiolites located within the sedimentary sequence, or overthrust the continent.

There is an arcuate magnetic high value over Cyprus and the Cyprus structure that is connected to the Turkish mainland in the northwest. The low value in anomalies in the Levant Basin, the Eratosthenes Seamount, and at the Egyptian coast are related to thick sediments in these areas. A series of high magnetic anomalies around the Cyprean Arc run from the Antalya Basin across Cyprus to the coast of the Arabian plate. They coincide with a comparatively strong positive Bouguer gravity anomaly, which is related to the presence of the ophiolite over Cyprus, in southern Turkey, and on the northwest Cyprean Arc as mentioned above.

III.4. Separation of the gravity and magnetic data

Geophysical maps usually contain a number of features (anomalies, structures, ect.) which are superposed on each other. For instance, a gravity map may be composed of regional, local, and micro-anomalies. The aim of an interpretation of such maps is to extract as much useful information as possible from the data. Since one type of anomaly often masks another, the need arises to separate the various features from each other. In addition, the objective of the separation of gravity and magnetic data is to extract any deep seated anomaly features that are beyond the limits of the local disturbances. The removal of the regional field from the observed field produces a residual. These residuals are very important in deducing shallow anomalous features which are usually of primary interest in geophysical prospecting.

To isolate the gravity and magnetic field caused by the earth's crustal sources, a regional - residual gravity and magnetic anomaly maps were produced (see Figures 3.4, 3.5, 3.6, and 3.7) respectively. In general, the regional-residual separation of the gravity and magnetic data is non-unique and not all the regional trends may be excluded and not all the local anomalies are retained in the residual fields. Therefore, these maps may only be used for a qualitative interpretation.

III.4.1. Separation acquisition and methods

There are some classical methods proposed for the separation of the gravity and magnetic data (e.g. Nettleton, 1954, Abdelrahman et al., 1985). The simplest is the graphical method in which a regional trend is drawn manually for profile data. Determination of the trend is based upon the interpreter's understanding of the geology and related field distribution. This is a subjective approach and also becomes increasingly difficult with large 2-D data sets. In the second approach, the regional field is estimated by least-squares fitting a low-order of the observed field (Abdelrahman et al., 1991). This reduces subjectively, but still needs to specify the order of the polynomial and to select the data points to be fit. The third approach applies a digital filter. In this study, one of the 2-D data sets processing techniques was applied. This method namely the polynomial trend surface and wavelength filtering method, and was used in separating the residual from the regional fields provided by using GMT software (Wessel and Smith, 2001).

Generally, wavelength filtering helps in determining the depth of the different anomalous bodies. Wavelength filtering assumes that long wavelengths are due to regional but short wavelengths are due to local anomalies. High pass filtering will reveal the shallow local anomalies. In the following, a brief account of theoretical concepts of the polynomial trend surface method is presented:

The polynomial trend surface method is widely used by geologists, particularly in petroleum exploration, as a means of separating a mapped variable into two components, the regional and residual trends. The trend corresponds to the concept of regional features while residuals represent local features. This method is based on the assumption that the spatial distribution of a particular phenomenon can be represented by some form of continuous surface, usually a defined geometric function. It is assumed that an observed spatial pattern can be regarded as the summation of such a surface and a regional or residual term. The surface is a function of the two orthogonal coordinate axes; mathematically, this can be represented by (see Davis, 1973):

$$Z = f(x, y) + \epsilon$$

in which the variate Z at the point (x,y) is a function of the coordinate axes, plus the error term ϵ . This expression is the generalised form of the general linear model, which is the basis of the most common trend methods. The function $f(x,y)$ is expanded (approximated) with various terms to generate polynomial equations.

As a common example, consider fitting a trend surface as a polynomial regression using

(x,y) coordinates as the predictor variable. In the case of a third order polynomial (cubic), the fit takes the form:

$$Z(x,y) = m_1 + m_2X + m_3Y + m_4XY + m_5X^2 + m_6Y^2 + m_7X^3 + m_8X^2Y + m_9XY^2 + m_{10}Y^3$$

In general, the polynomial trend surface is considered as a filtering operation, where a surface fitted by polynomial regression emphasizes the coarse-scale pattern in the data while essentially ignoring and thus removing any finer scale pattern. This is easy to visualize by considering the range of variability that can be captured by polynomials of increasing order, i.e. a first order (linear) regression can capture only strictly increasing or decreasing trends, a second order (quadratic) regression can capture a single extrema (a minimum or a maximum, corresponding to a concave or convex surface), a third-order polynomial (cubic) can capture two extrema, and so on. Any finer scale pattern is lost as residual variation. Thus, hypothetically, the polynomial trend surface method partitions the original data into two components: the coarse-scale pattern captured by the regional trend at a resolution dictated by the order of the polynomial, and the finer-scale variability that is relegated to the residuals. Furthermore, the polynomial trend surface represent match the regional by a polynomial surface of low orders. The rest is assumed to be residual anomalies.

In this study, the regional trend was applied as either a first, a second or third order polynomial surface in order to assess which order number was most specify and significantly the order number of polynomial surface. A polynomial surface processing to the order of a third provides the best approximation to the observable gravity and magnetic field. The data were gridded and smoothed using the inverse distance method. In general, the polynomial surface trend was fitted to the two-dimensional gridded data by a weighted least-squares method provided by GMT software. The program will iteratively reweight the data based on a robust scale estimate, in order to converge to a solution insensitive to outliers. Thus, the planer trend of the regional field is separated from the observed gravity field.

III.4.2. Interpretation of the regional and residual gravity anomalies

In Figures 3.4 and 3.5 respectively, the regional and residual gravity anomaly maps are displayed and plotted with a contour interval of 5 mGal and 10 mGal to show more detail.

Generally, the regional field in the area under study is characterized by an oval shape and reveals that the orientation is mainly to ENE-WSW direction (Figure 3.4). It is considered to be

mainly influenced by the density contrast between the crust and upper mantle, and the undulating Moho discontinuity.

The regional anomaly field values generally decrease towards the E-W direction. This behaviour trends reflect the effect of the transition from oceanic crust to the continental crust of the Eastern Mediterranean towards the Arabian plate.

In the northern part of Egypt, the regional anomaly shows an increase from -10 to +60 mGal. This indicates that the crustal thickness decreases towards the Mediterranean Sea.

Figure 3.5 shows the residual gravity anomaly map with the alternatively high and low gravity anomalies of different orientation, gradients and shapes. This reflects the effect of the difference in density between the crystalline or igneous crust and the sediments, the variation of the basement geometry, and the effect of the bathymetric and topographic features.

In the south east of Crete, the negative residual gravity anomalies with a minimum value of -120 mGal are associated with the thick sedimentary sequences below the Eastern Mediterranean Ridge, as well as the negative anomalies of -40 mGal around southern Cyprus. This is related to the structures of the sedimentary sequences and the basement geometry.

The residual gravity anomalies in the Herodotus Abyssal Plain are dominated by an elongated NE-SW trend with a maximum value of about +100 mGal, which coincides with the elongated bathymetric and topographic features of the Herodotus Abyssal Plain.

There is a remarkable minimum in the residual gravity anomaly in the Gulf of Suez. This is due to the effect of sedimentary cover, which has a thickness of 6 km (Said, 1962). In the Nile Delta area, the negative residual gravity anomaly is -60 mGal, due to thick sediments in the Delta. A number of local residual gravity anomaly lows and highs are also apparent.

In general, the features of the gravity field such as the gradients and elongated anomalies, can be divided into three groups according to their trends: The first group, oriented in ENE-WSW and influenced by the density contrast between the crust and upper mantle. The second group, oriented in NE-SW direction parallel to the coastal line, reflects mainly the thickness variations of the Tertiary sediments. The third group, oriented NW-SE, may be related to the young tectonic dislocations.

III.4.3. Interpretation of the regional and residual magnetic anomalies

The total intensity magnetic anomaly map of the area under study is also resolved into its regional and residual components using a polynomial trend surface and wavelength filtering method. The regional and residual magnetic anomaly maps are shown in Figures 3.6 and 3.7

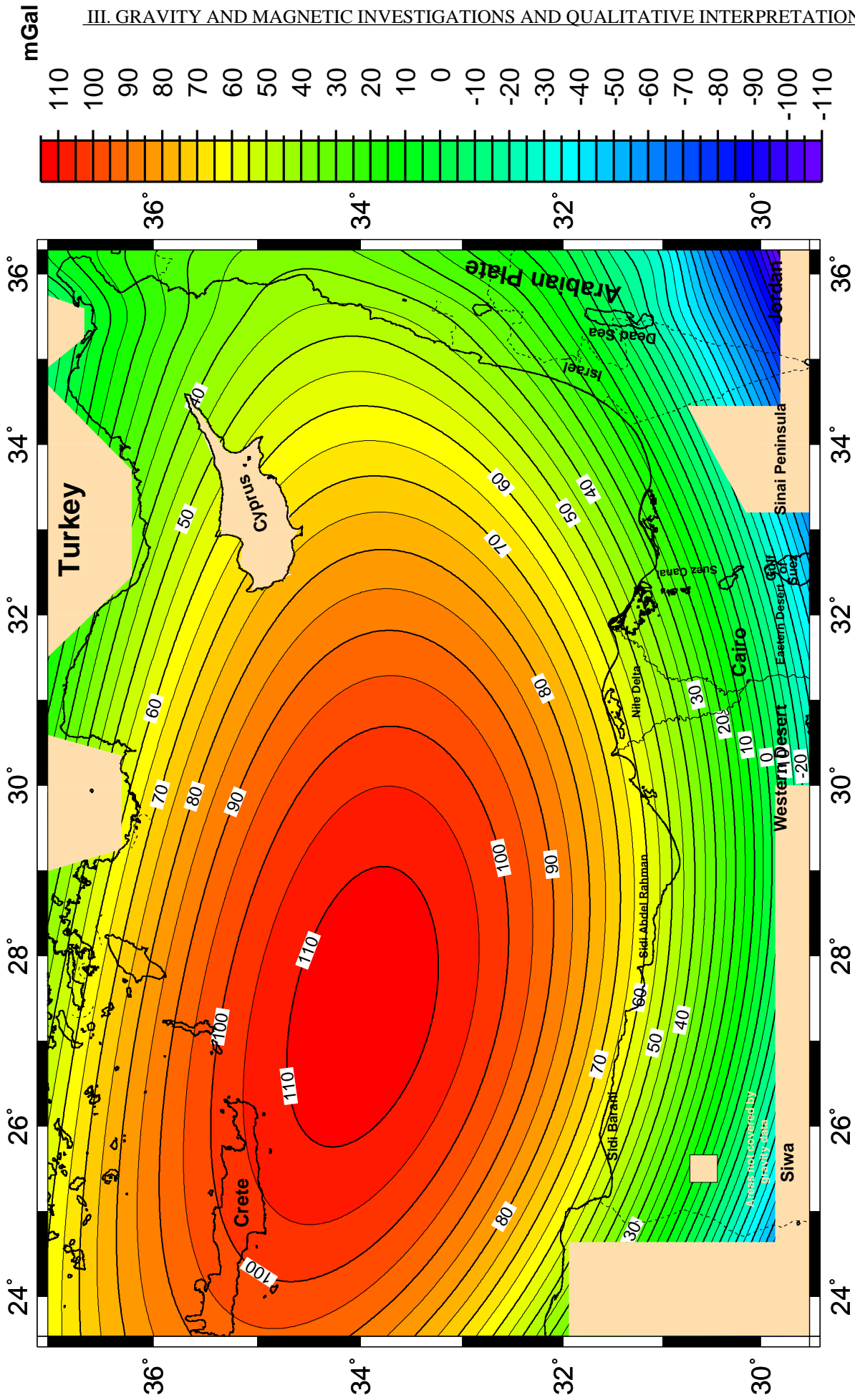


Figure 3.4: Regional Bouguer gravity anomaly map of the southeastern Mediterranean Sea and the northern section of Egypt.
 "Contour interval is 5 mGal".

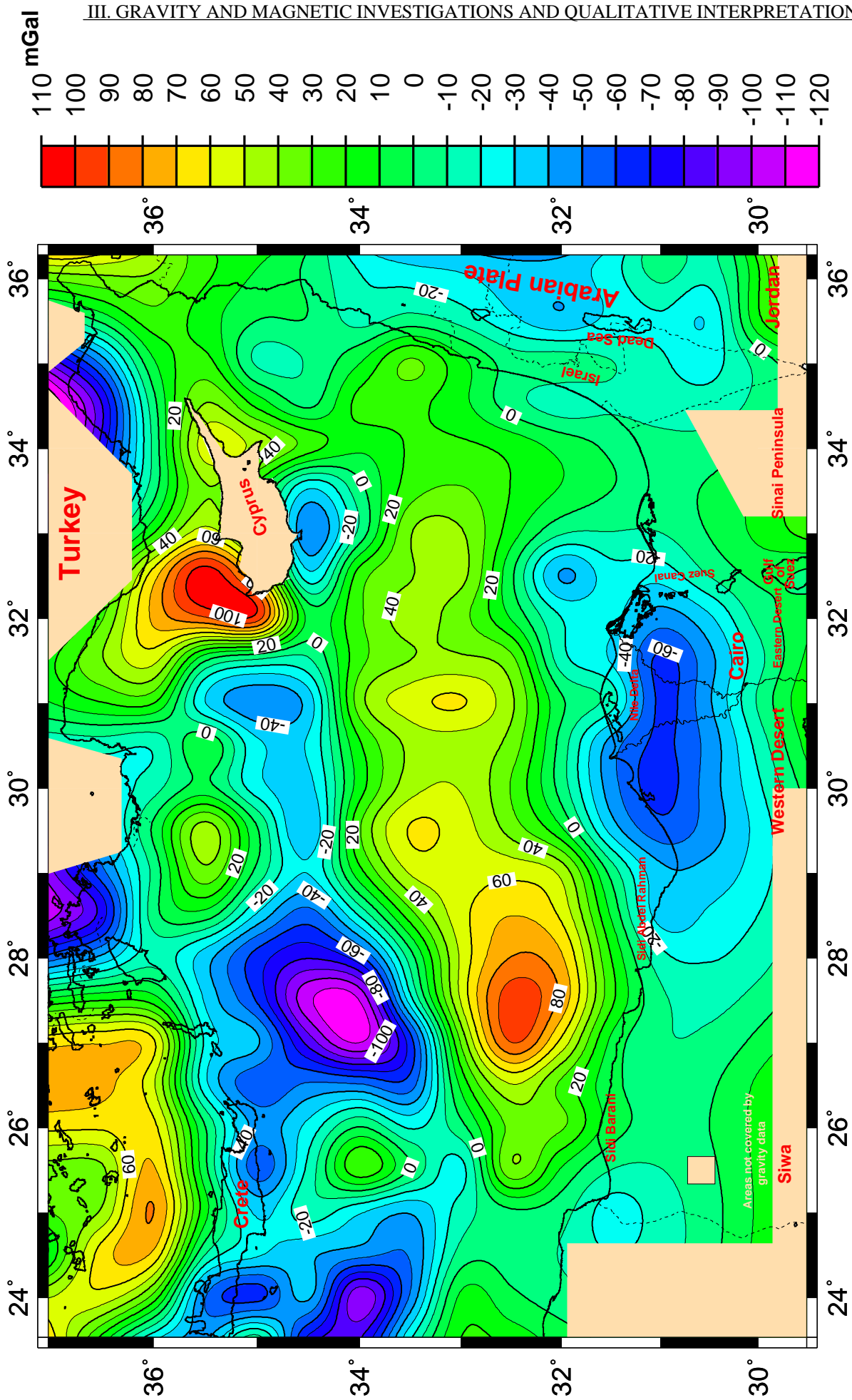


Figure 3.5: Residual Bouguer gravity anomaly map of the southeastern Mediterranean Sea and the northern section of Egypt.

respectively. Generally, the regional magnetic anomalies are dominant in NW-SE trends and the regional magnetic anomalies increases in northward direction, which may reflect the shallow depth of the basement rocks in this direction. The regional magnetic anomalies may reflect the global regional magnetic field trends over the region as also suggested by Woodside and Bowin (1970). The close inspection of the distribution of the residual magnetic anomalies exhibits a very complex pattern with different polarities and magnitudes values.

Correlation of the residual magnetic anomaly with the observed bathymetric and topographic features of the area investigated reveals a very good match between the various magnetic anomalies, the bathymetric and topographic features, and the main tectonic elements.

The residual magnetic anomalies are characterized by broad anomalies covering large areas in the different natural positive and negative anomalies. In the south east Crete region, the residual anomaly trend reflects the regional trends. This indicates relatively shallower basement rocks in this zone. The negative magnetic anomaly in the Levant Basin, and the offshore Egypt, could be caused by the combined effects of a thick sediment layer and the reversed remanent magnetization of the old oceanic crust.

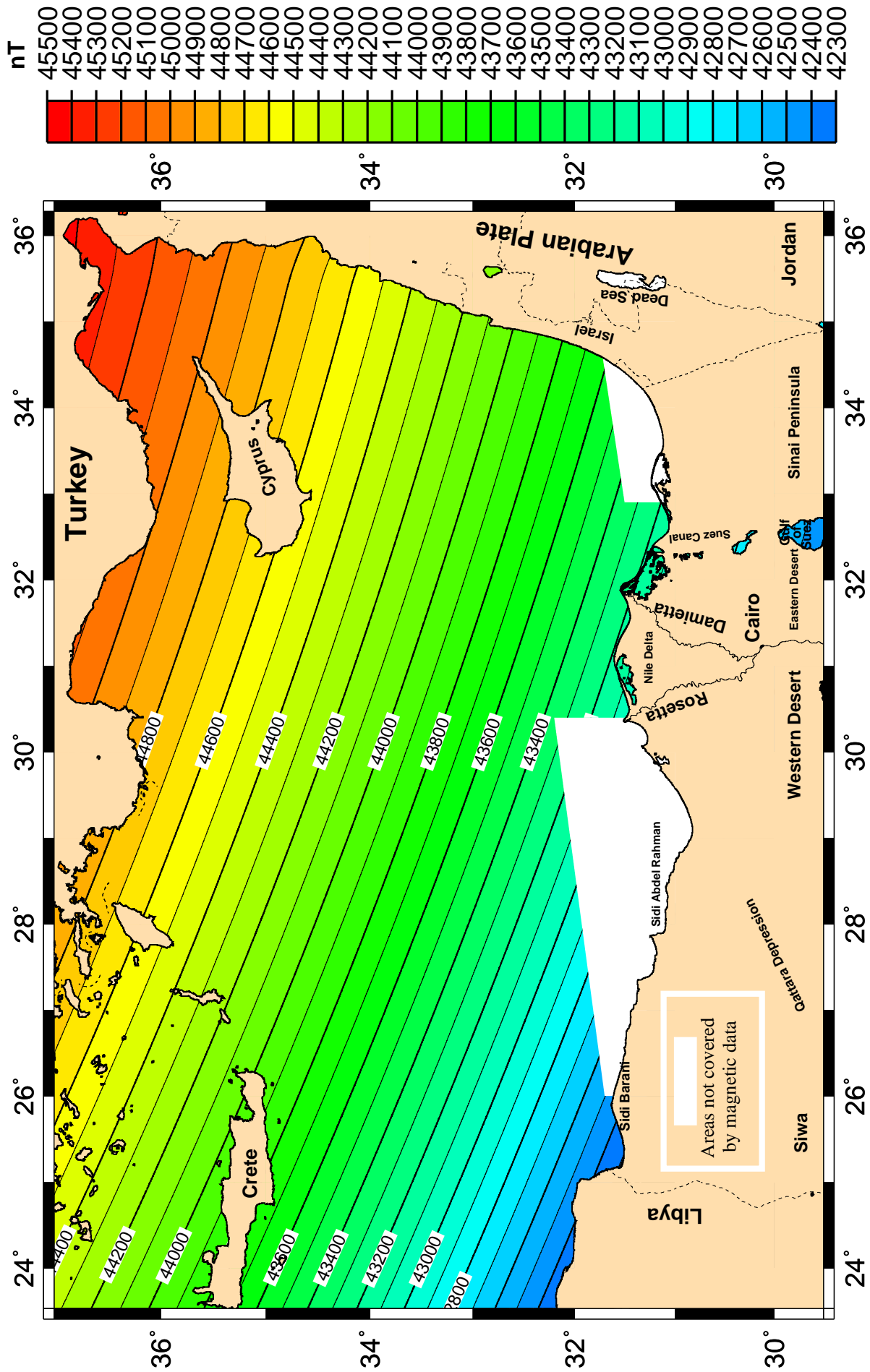


Figure 3.6: Regional magnetic anomaly map of the southeastern Mediterranean Sea and the northern section of Egypt.

"Contour interval is 100 nT".

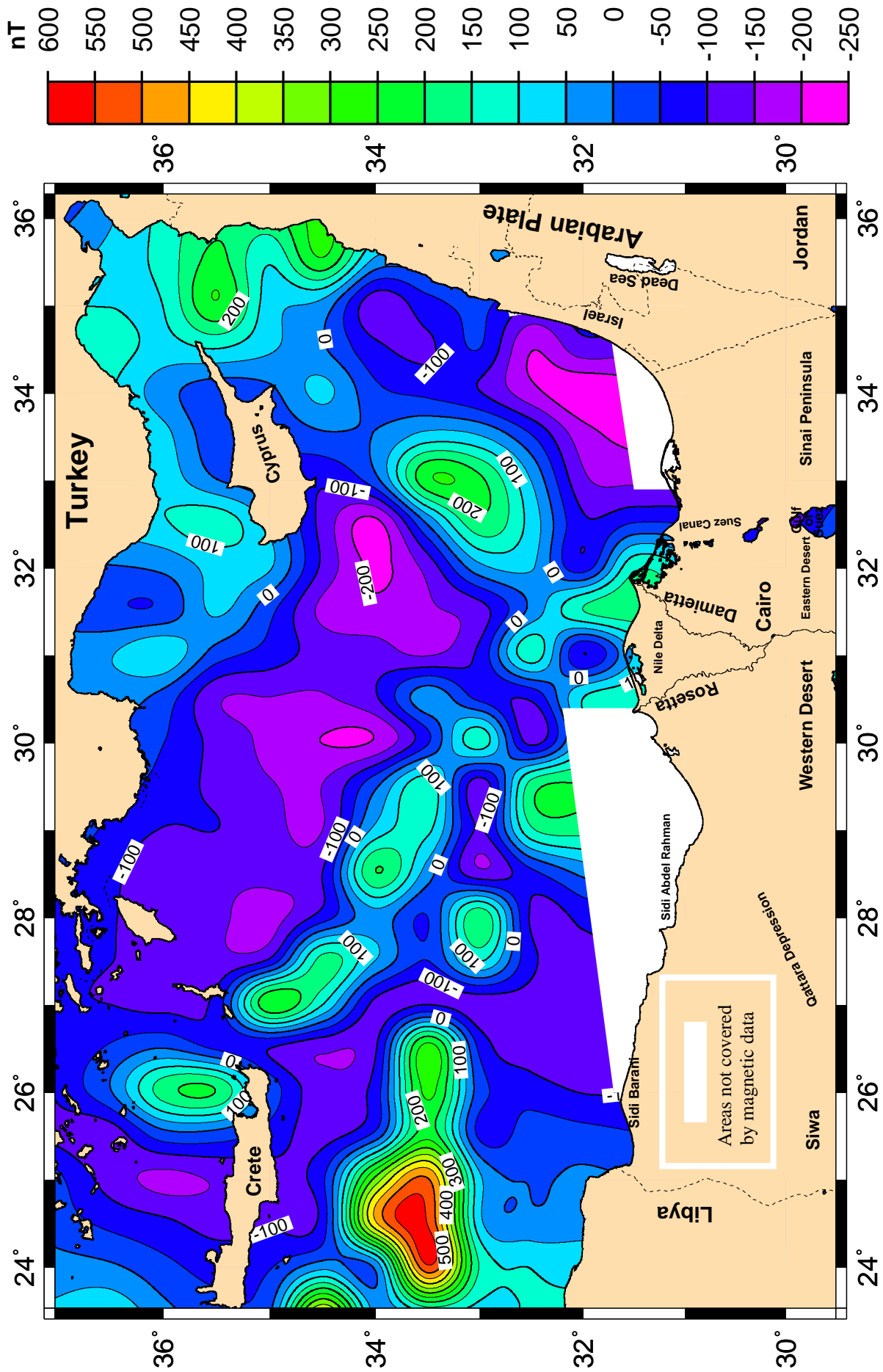


Figure 3.7: Residual magnetic anomaly map of the southeastern Mediterranean Sea and the northern section of Egypt.

"Contour interval is 50 nT".

III.5. Satellite Gravity

The Earth's surface has been monitored for nearly 20 years from satellites altimeters. Global mapping of the Earth gravity fields from different data sources has previously been presented by, e.g. Haxby (1987); Balmino et al. (1987); Sandwell and Smith (1997a); Andersen and Knudsen (1995), and the first gravity field from the full ERS-1 geodetic mission were presented by Andersen et al. (1995).

Satellite altimetry has enhanced our understanding of marine gravity, seafloor bathymetry and ocean circulation. Two satellites have operated in geodetic mission configurations. GEOSAT (1985-1986) where the satellite was operated in a non-repeating orbit, which yielded a very dense, though not completely homogeneous coverage of observations, and ERS-1 which covers all oceans between -82° and $+82^{\circ}$ latitudes and provides a very dense and homogeneous coverage. Satellite altimetry GEOSAT and ERS-1 provides the opportunity for geodesists to make very detailed mapping of the marine gravity field, and to supplement their own data set (Sandwell and Smith, 1997a).

The concept of determining marine gravity anomalies from satellite radar altimetry are as follows: The altimeter essentially measures the distance between the satellite and the sea surface along the nadir using pulse-limited radar at a series of footprints along the sub-satellite tracks (Fu and Cazenave, 2001). After modelling tidal effects and applying geophysical corrections, these measurements are then averaged (stacked) to give the mean shape of the sea surface with respect to a prescribed reference ellipsoid, knowing the position of the satellite from tracking, dynamic orbit modelling or both. To a first coarse approximation, the mean sea surface coincides with the geoid. However, these two surfaces depart by up to ~ 2 m due to sea surface topography, which is caused by oceanographic effects (Hipkin, 2000). Therefore, techniques to model and/or mitigate the effects of sea surface topography from the altimeter measurements form an integral part of estimating marine gravity anomalies from satellite altimetry.

Over the past two decades, marine gravity anomalies have been computed from satellites altimetry, starting with the work of Haxby et al. (1983) and Brenneke and Lelgemann (1983). There are now several different altimeter-derived gravity anomaly grids available in public domains, which have been computed by various groups using different data combinations and different computational philosophies. The data used in this study covers only the most recent satellite altimeter marine gravity field. A brief overview of this data is given below.

- Sandwell's version 10.1 satellite altimeter gravity field (Sandwell et al., 1997)

For two decades, Sandwell of Scripps Institute of Oceanography, California, USA, has

produced global gravity anomalies from multi-mission satellite altimetry. Sandwell's version 10.1 global grid of marine gravity anomalies is the most recent in this series, with the developments leading to the model reported in Sandwell (1992) and Sandwell and Smith (1997a). The version 10.1 global grid is available on 1 or 2 arc-minute spatial resolution grids from http://topex.ucsd.edu/marine_grav/mar_grav.html. Only the 2 arc-minute grid is used in this study so as to be compatible with KMS grids.

- The KMS99, KMS02 satellite altimeter gravity field (Andersen and Knudsen, 1998)

For nearly a decade, Andersen and Knudsen of Kort-og Matrikstyrelsen (KMS), Copenhagen, Denmark, have computed global marine gravity anomalies from multi-mission satellite altimetry. The progressive developments in their techniques are reported for example in Andersen and Knudsen (1998) and Andersen et al. (1999). The KMS02 and KMS99 gravity anomaly grids are the most recent in this series and result from refinements in the techniques described by Andersen and Knudsen, 1998. Both grids are supplied at a 2 arc-minute by 2 arc-minute spatial resolution, and are available in the public domain via anonymous ftp from <ftp.kms.dk/GRAVITY>.

There are several methods to compute gravity anomalies from satellite altimetry such as: *Method 1*: Gravity anomalies from point-mass models; *Method 2*: Gravity anomalies from geoid heights using an inverse Stokes integral; *Method 3*: Gravity anomalies from vertical deflections using an inverse Vening-Meinsz integral; and *Method 4*: Gravity anomalies from vertical deflections via Laplace's equation (Featherstone, 2001 and Featherstone, et al. 2002).

Also there are some significant differences between marine gravity anomalies computed by different groups from satellite rader altimetry (e.g. Sandwell's version 10.1 global grid and KMS grids satellite altimetry). These tend to become larger in coastal regions, which is due to the numerous problems associated with correcting altimeter data in these regions. Therefore, these data should be used with extreme caution in these regions. Since the altimeter grids are derived from predominantly the same altimeter data sources (mostly GEOSAT and ERS-1), the differences are due to the data treatment (notably outlier detection, gridding and filtering), models of sea surface topography and tides, and the computational philosophies taken by each group (Andersen and Knudsen, 1995).

In general, Sandwell's version 10.1 global grid is derived from multi-mission satellite altimetry from ERS-1, TOPEX, and GEOSAT, and refinements in filtering during gridding and Fourier transform conversion to procedures set out in Sandwell and Smith (1997a). To summa-

rise, the along-track gradients (vertical deflection) were computed and gridded iteratively using splines that include Wiener-type filter. The gravity anomalies were computed from this grid using the Fourier transform implementation of the Laplace-based inversion of the vertical deflection method (Sandwell and Smith, 1997 a; Method 4 as mentioned above). However, these KMS grid have been computed using a combination of ERS-1 and GEOSAT satellite altimetry via geoid (Andersen and Knudsen, 1998, Method 2 as mentioned above).

The marine gravity data derived from satellite altimetry have been used in an evaluation of the gravity field of the area investigated. The following section presents the investigation of the gravity field data derived from two most recent satellite altimetries of the area investigated. Furthermore, a comparison of the result of the shipboard marine Free-Air gravity data with the gravity data derived from satellite altimetry of the study area also is presented.

III.5.1. The available satellite altimetry marine gravity field of the area investigated

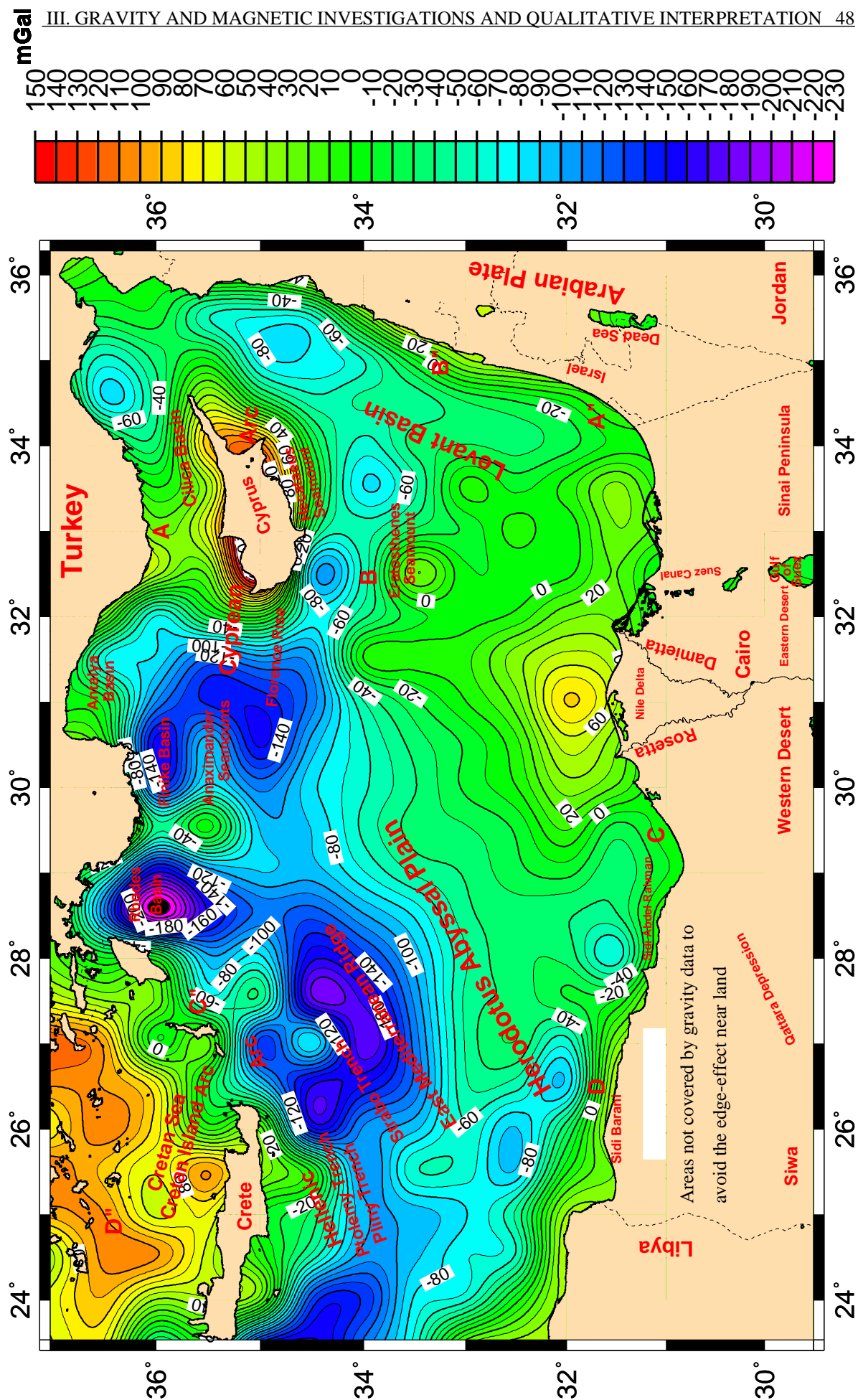
The available marine gravity field data derived from satellite altimetry and used in this study were obtained from: Sandwell's version 10.1 global grid (Sandwell et al., 1997); and KMS99, KMS02 (Andersen and Knudsen, 1998). Figures 3.8, 3.9, and 3.10 show the Free-Air gravity anomaly map based on satellite data from Sandwell et al., 1997 and KMS99, KMS02 respectively.

The Free-Air gravity anomaly map based on satellite altimetry from Sandwell's version 10.1 global grid was carried out relative to the altimetry data reduction to gravity data. The altimetry data are separated into ascending and descending profiles for each repeat cycle and differentiated in the along-track direction to obtain along-track vertical deflections (geoid slopes). The vertical deflections for all the repeat cycles are then averaged into a single ascending and descending profile which are combined to produce grids of the eastern and northern components of vertical deflection. These grids are used to compute both gravity anomaly and vertical gravity gradient grids (Sandwell et al., 1997). The marine gravity field derived from satellite altimetry by Sandwell's version 10.1 global grid shows a wavelength of 10 to 15 km (Sandwell and Smith 1997a, 1997b).

The Free-Air gravity anomaly mapping of the KMS99; KMS02 gravity field was carried out relative to the geoid using the GRAVSOF software. The processing of data and conversion of observations into gravity field were carried out in small cells of size 2° latitude by 10° longitude and sea surface variability (Knudsen and Andersen, 1998). The primary difference is between the longitude. The selection of such small sub-areas was essential to the modelling of



The thick red line represents location of the profiles B-B^{||}, C-C^{||} and D-D^{||}.



orbit errors KMS99 and KMS02 grids is a further fine-tuning of the filter characteristics, both in gridding of geoid height to gravity anomalies.

Observed more closely, the marine gravity anomaly maps of the area investigated derived from satellite altimetry are seen to have a large gradient as a direct effect of bathymetric changes close to the coast. It has a very large gravity signal ranging between -230 and +150 mGal (Figures 3.8, 3.9, and 3.10). This major gravity signal is related to the Hellenic Arc and the Cyprean arc where steep bathymetric changes occur within a few kilometres. The gravity field is seen to fall dramatically just south of Cyprus (Figures 3.8, 3.9, and 3.10), where the depth rapidly grows to more than 2000 meters (see Figure 2.1 in Chapter II).

III.5.2. Comparison with the shipboard marine Free-Air gravity and bathymetric data

As an example of estimating, and to show a comparison result of the shipboard gravity anomaly data of the area investigated and the satellite data, a comparison with the shipboard gravity anomaly data was made in two regions along two profiles (e.g. B-B^{||} and C-C^{||}). The regions belonging to these profiles are chosen to avoid edge-effect of the gravity anomaly near land in the study area. Also these regions have very different gravity signatures as shown in Figures 3.8, 3.9, and 3.10. Furthermore, these profiles cross the main tectonic elements in the investigated area. The location of the profiles are shown in Figure 3.8.

In comparison with the shipboard gravity data, the satellite data show only minor deviations in some partially regions of the area investigated (Figures 3.11 and 3.12). Also there are a significant dip and peak at all the gravity anomalies along the profiles B-B^{||} and C-C^{||}.

However, the comparison of processed marine gravity data, and the resolution of satellite gravity data still seems to be limited. The major limitation of the satellite altimetry data is not of high precision but a poor data coverage (Sandwell, 1992 and Knudsen and Andersen, 1998).

Also, in comparison with the wavelength gradient of the gravity anomaly, the long wavelength gradient can be observed and decrease in values towards the E-W direction. This behaviour shows the edge-effect at the transition from oceanic to continental crust (Figures 3.8, 3.9, and 3.10).

Furthermore, a comparison of the measured shipboard bathymetric data with the satellite data (e.g. from Sandwell et al., 1997) was made along seismic profile D-D^{||} as shown in Figure 3.13 [A]. This profile corresponds in most part with plane 15 of the three-dimensional model (see Figures 3.8 and 5.10). The largest difference in depth between the two data sets amounts to 250 m and is located at subduction trenches as shown in Figure 3.13 [B].

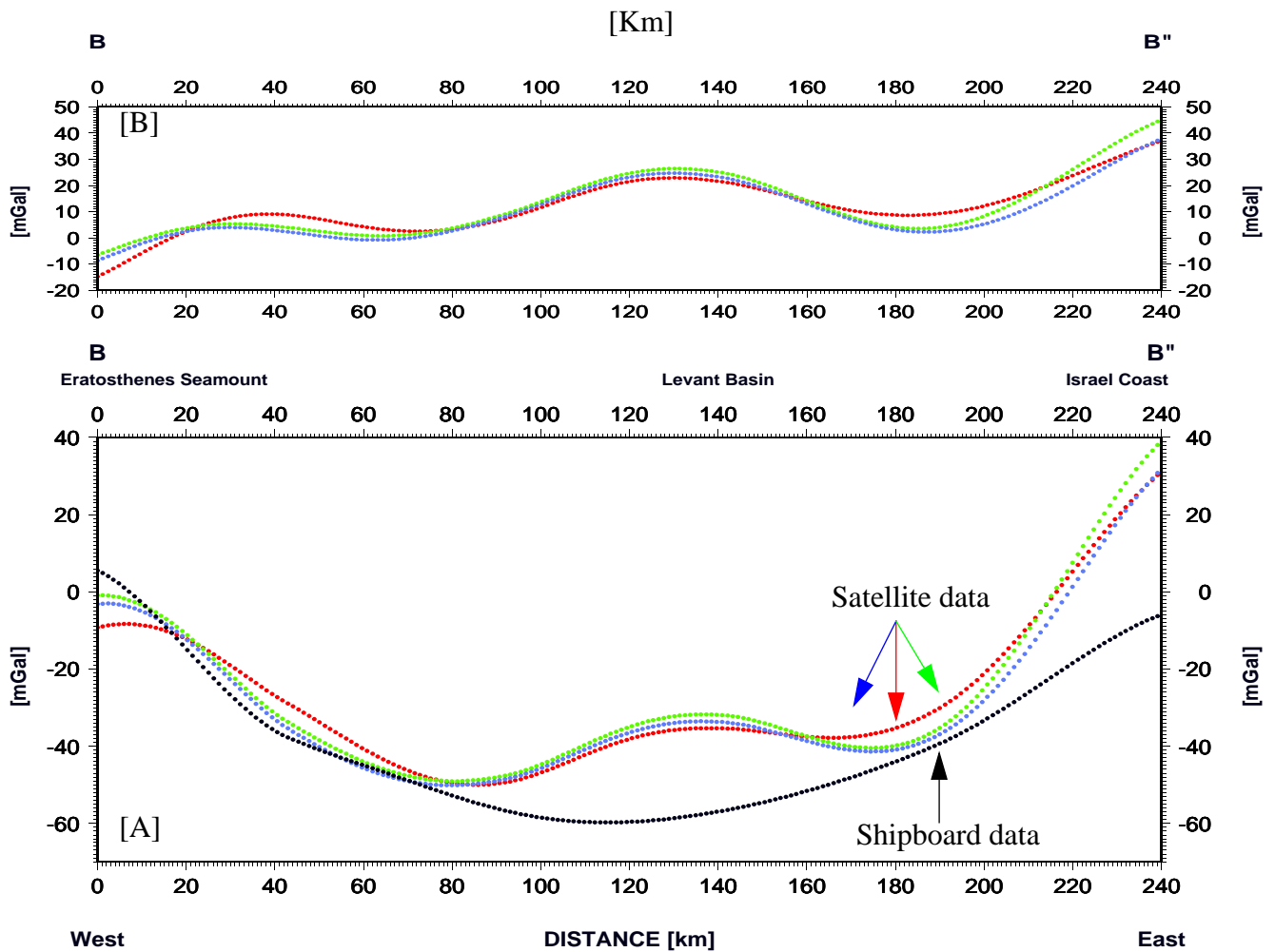


Figure 3.11: [A] : A comparison of the shipboard gravity data with the satellite gravity data along profile B-B^{||}

[B] : The difference between satellite and shipboard gravity data.

The red curve describes the satellite gravity data were obtained from Sandwell et al., 1997. The green and blue curves mark the KMS99 and KMS02 satellite gravity data were obtained from Andersen and Knudsen, 1998.

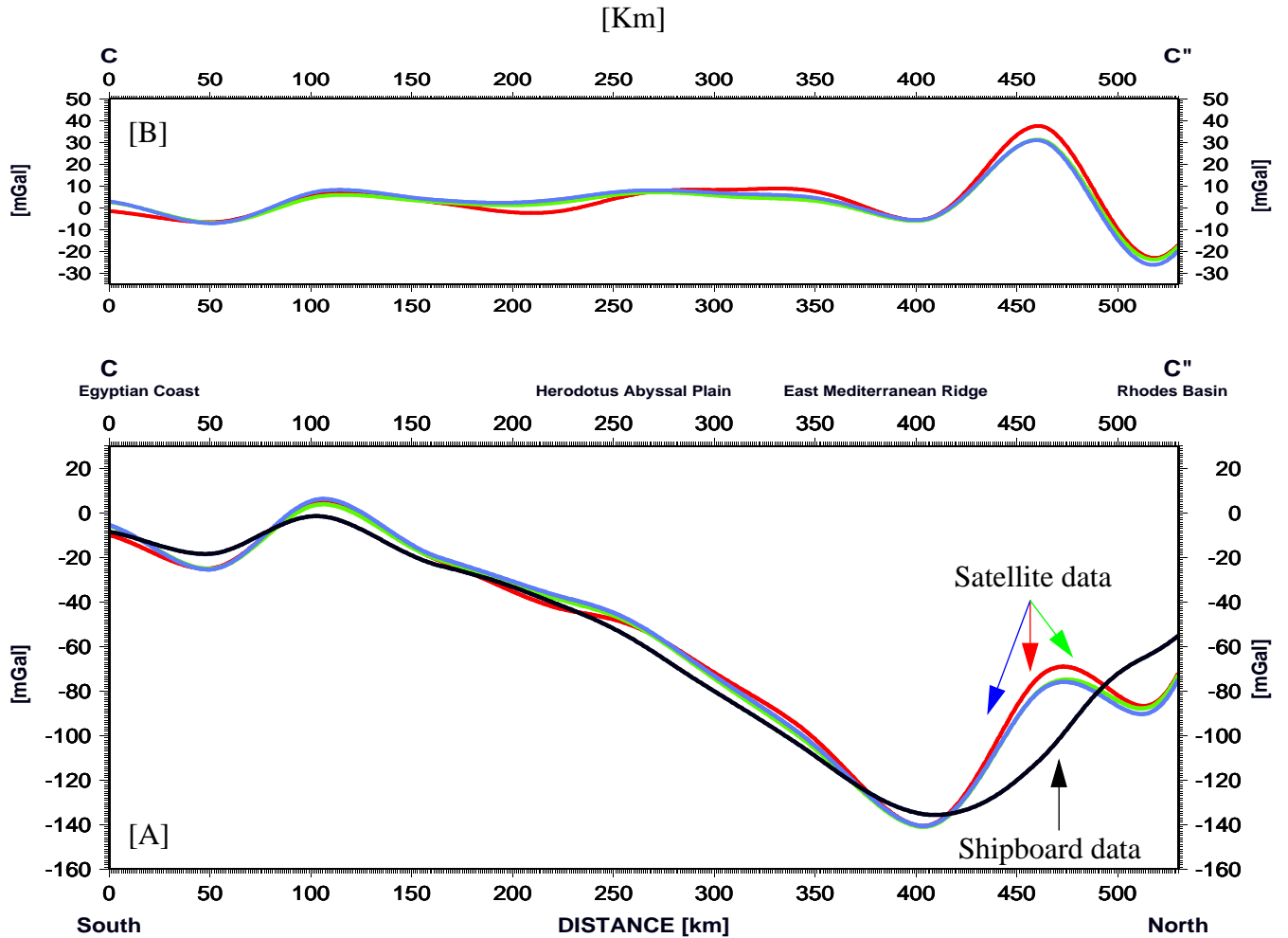


Figure 3.12: [A] : A comparison of the shipboard gravity data with the satellite gravity data along profile C-C''

[B] : The difference between satellite and shipboard gravity data.

The red curve describes the satellite gravity data were obtained from Sandwell et al., 1997. The green and blue curves mark the KMS99 and KMS02 satellite gravity data were obtained from Andersen and Knudsen 1998.

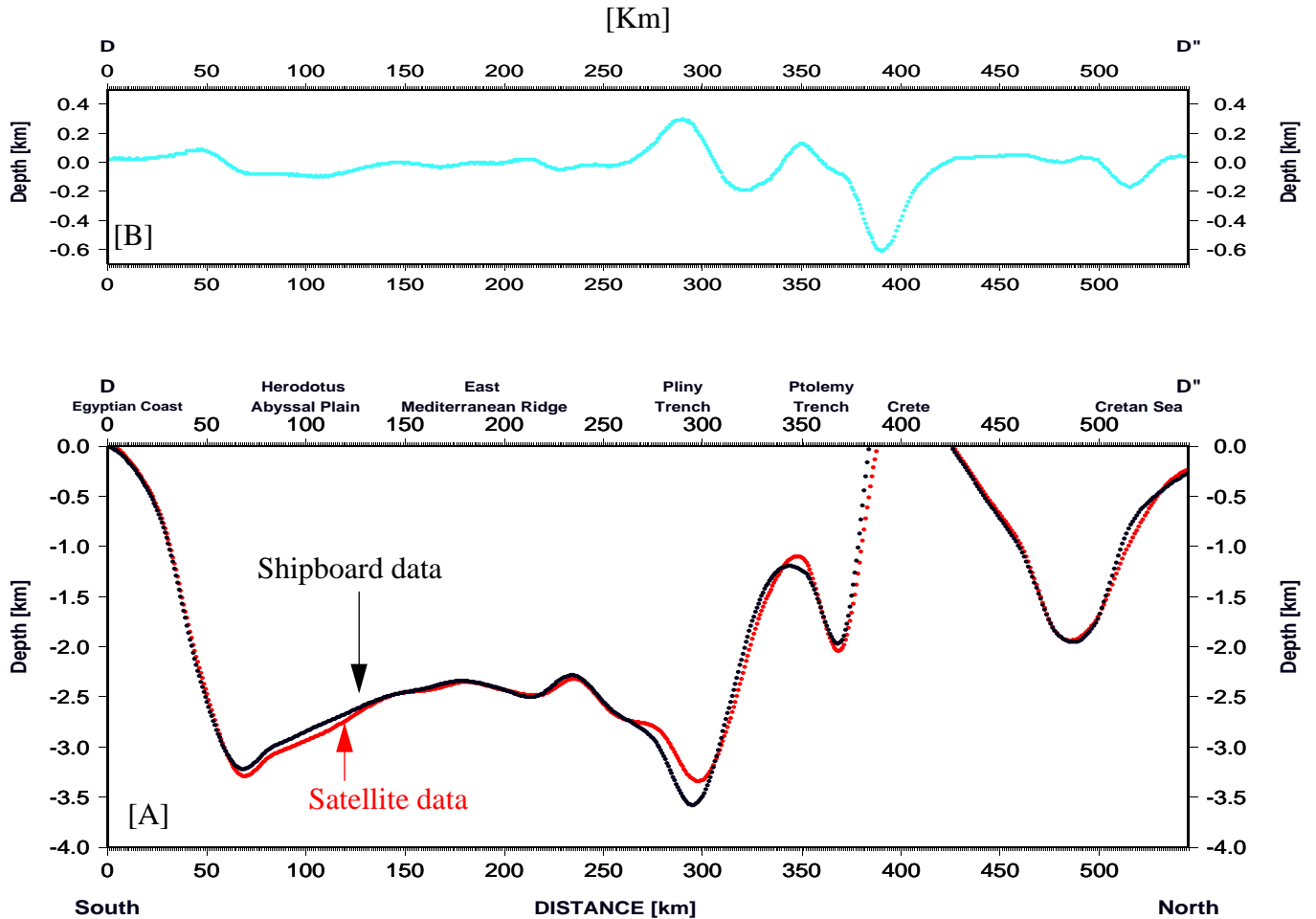


Figure 3.13: [A] : A comparison of the shipboard bathymetric data with the bathymetric data provided by satellite altimetry. [B] : The difference between satellite and shipboard data.

This line represents profile D-D^{||}. (The satellite data were obtained from Sandwell et al., 1997).

III.5.3. The differences between the satellite and the shipboard gravity anomaly data

Figure 3.14 shows as one example the differences between the satellite and the shipboard data. This map was created by using the “grdmath” option in GMTsoftware (Generic Mapping Tools, Wessel and Smith, 2001) for two grid files of the satellite and the shipboard gravity anomaly data.

In general, the differences between the satellite and the shipboard data are small in some regions of the area investigated. These occurred mostly near to land. Furthermore, some strong deviations in some regions, which are spatially correlated with bathymetric depth and geological structures become obvious from Figure 3.14.

There are also differences in polarities and gradients of the gravity anomalies. These occur mostly in regions of steep gravity gradients (i.e. in the northeast of Crete and Cyprean Arc). This reflects the effect of the structural features in the areas.

A series of local maxima and minima of the gravity anomalies in areas near the Libyan and Egyptian coastlines may be related to young tectonic dislocations (Figure 3.14).

Overall, the shipboard data are important near the coast lines and the regions of strong bathymetric depths and highs of showed wavelength. However, the precision of the satellite data is, in the study region, sufficient when large scale features are studied.

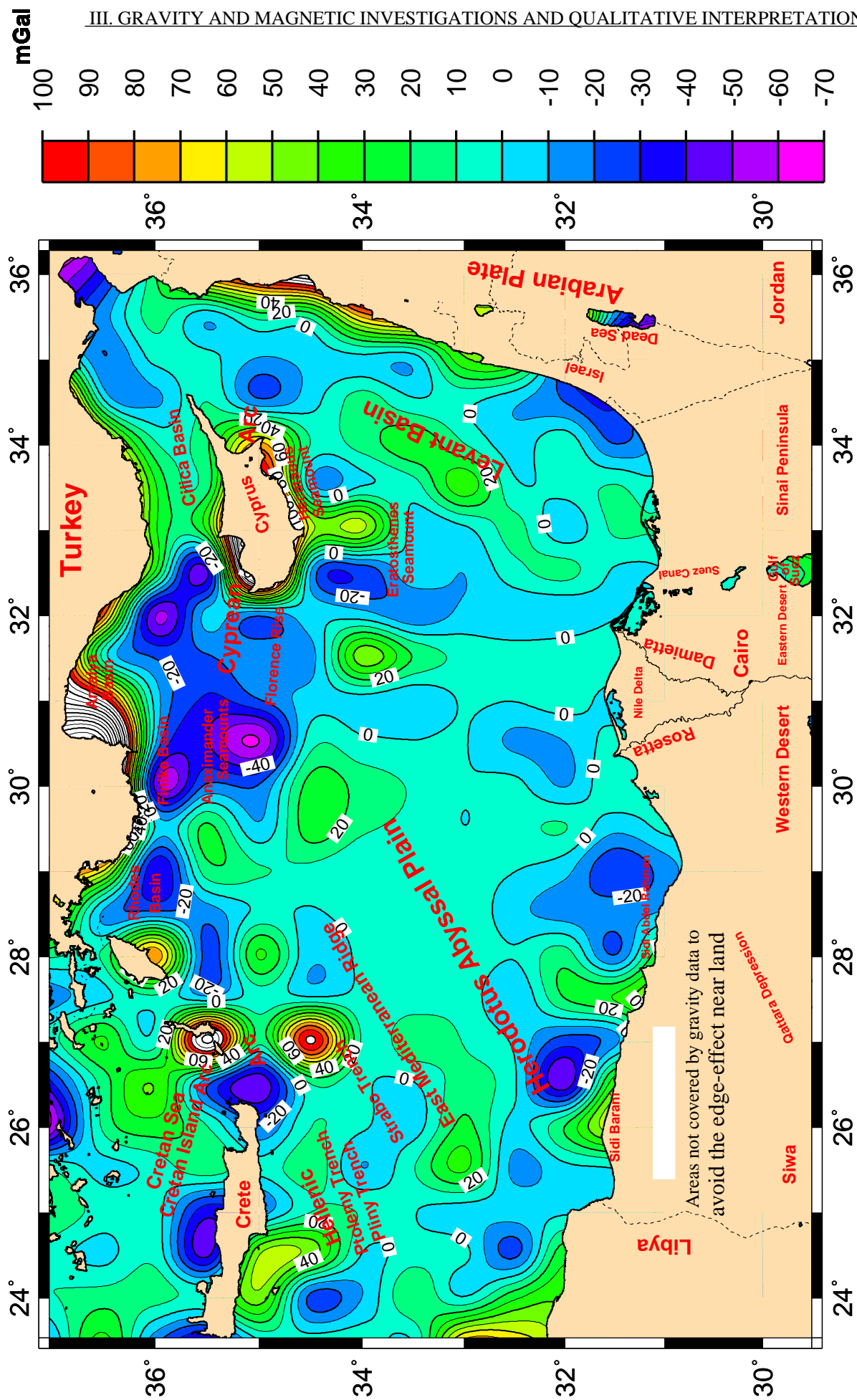


Figure 3.14: The differences between the KMS02 satellite and shipboard gravity data. Satellite obtained from Andersen and Knudsen, 1998.

IV. RESULTS OF THE SEISMIC STUDIES

To estimate a tectonic model for the study area within the regional tectonic concepts, results of the available seismic studies were obtained. These results were used to constrain layer geometry and thickness and to provide initial estimates of the layer densities along some seismic profiles crossing the main tectonic elements in the investigation area.

Various international organizations carried out deep seismic sounding experiments (DSS), wide-angle reflection / refraction seismic (WARRS) experiments and expanding spread profiles (ESP) of a two-ship refraction survey in the Eastern Mediterranean Sea. The seismic information directly concerning the tectonic models of the study area is described in detail below. In addition, some results from seismic profiles in several parts of the study area will be described as shown in Figure 4.1 and also in Figure Appendix [A4].

IV.1. Deep seismic sounding experiments (DSS)

IV.1.1. Seismic profile of Cyprus-Israel

In October 1978, a long seismic refraction profile was recorded between southern Israel and Cyprus to provide information on the structure of the crust and upper mantle between Cyprus and Israel. This was carried out by the Institute of Geophysics, University of Hamburg, Germany, in cooperation with the following organizations: Oceanographic and Limnologic Research Ltd of Israel, the Institute of Geophysics of the Free University of Berlin, the Department of Geophysics and Planetary Science, Tel Aviv University, Institut de Physique du Globe, Université Pierre et Marie Curie, Paris, the Institute of Oceanographic Sciences, Wormly, and the Geological Survey of Cyprus, Nicosia. This seismic profile is 540 km long and marked by line A-A^{II} in Figure 4.1. The seismic energy was generated by 33 Sea shots each of 800 kg fired explosives and were recorded by land stations in Israel and Cyprus and by ocean bottom seismographs (OBS) deployed along the profile. The data was evaluated using two-dimensional ray-tracing techniques (Makris et al., 1983). The calculated crustal velocity depth model is shown in Figure 4.2. The following points may be taken from the results:

- The continental crust of southern Israel thins towards the Mediterranean, under a northward thickening sedimentary cover. Cyprus is underlain by an about 25 km thick continental crust thinning southwards and extending to Eratosthenes Seamount. The upper crust has a velocity of 6.0 km/s and reaches a maximum thickness of about 20 km beneath Cyprus.

- The Eratosthenes Seamount is a continental fragment with a crustal thickness of about

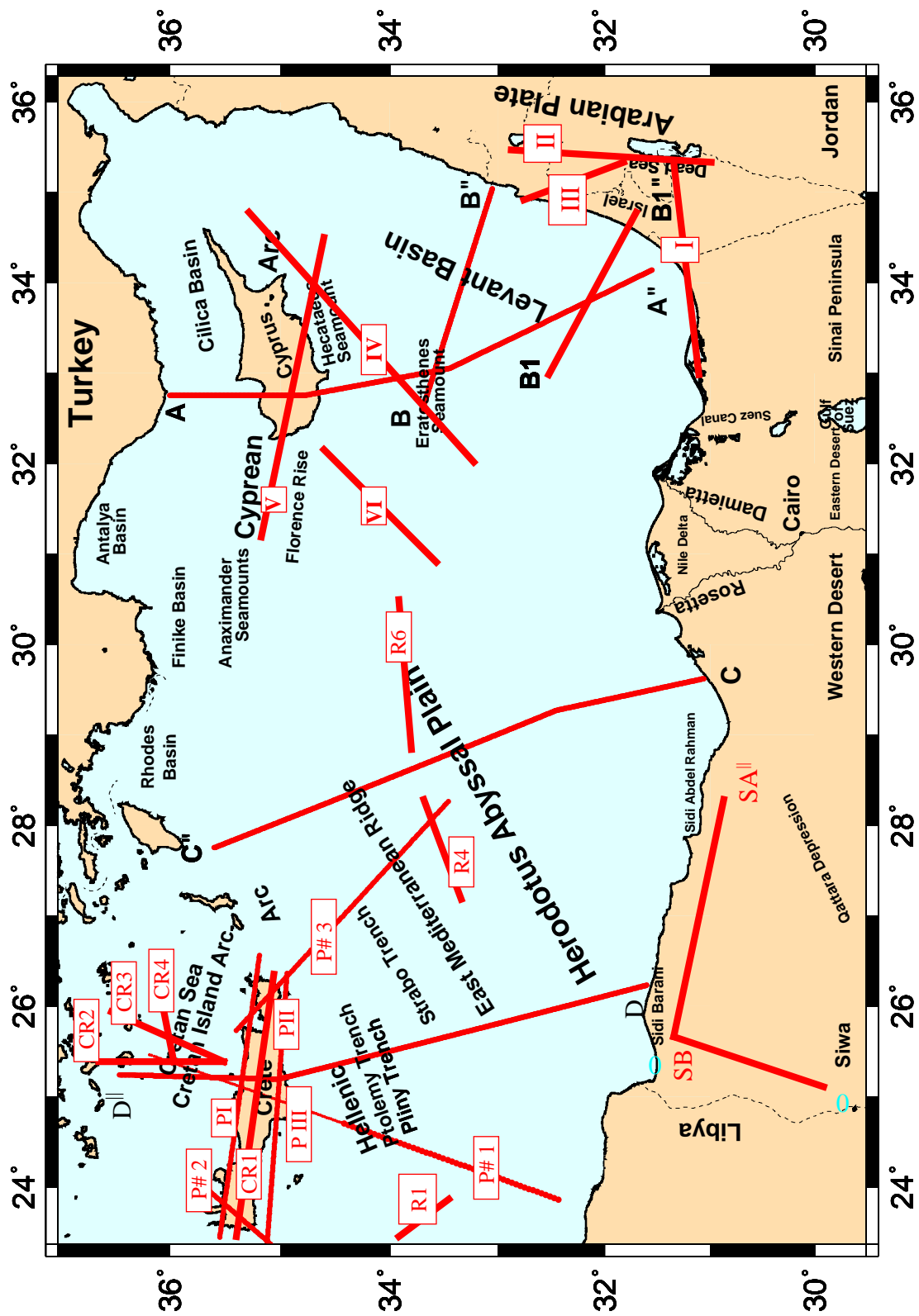


Figure 4.1: Location map of the seismic profiles performed on the southeastern Mediterranean Sea and the northern section of Egypt.

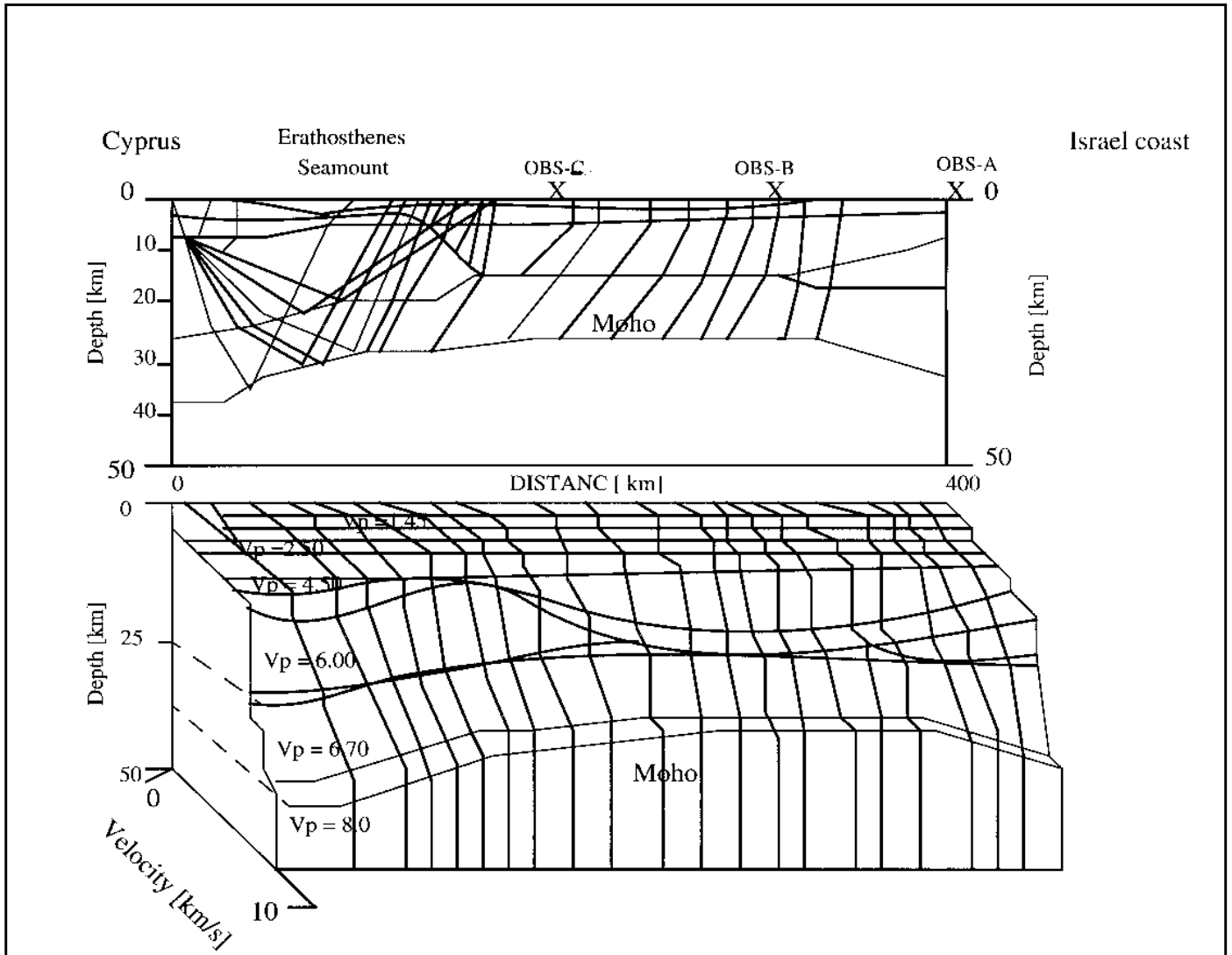


Figure 4.2: Sketch diagram shows velocity depth model of the profile Cyprus-Israel, shown as line A- A^{||} in Figure 4.1. Compiled from Makris et al. (1983).

22 km (Makris et al., 1983). Between the Eratosthenes Seamount and the Israel continental shelf the crystalline crust is composed of high velocity (6.5 km/s) material and is about 8 km thick. It is covered by 12 -14 km of sediments and may represent a fossil oceanic crust (Makris et al., 1983).

-Southern Israel is floored by a continental crust. The Moho lies at a depth of about 27 km beneath the coast of Israel. The sediment thickness is 5 km beneath the continental shelf of Israel suggesting the existence of a transition zone, where the crystalline crust thins rapidly, while the sedimentary cover thickens considerably towards the Levant Basin.

-The upper mantle has a normal P-wave velocity of 8.0 km/s (Makris et al., 1983).

IV.1.2. Seismic profiles of Eratosthenes Seamount-Israel and Levant Basin-Israel

In December 1989, a wide-angle reflection / refraction seismic experiment extending from the Levant Basin to the coastal area of Israel was undertaken by the Institute of Geophysics, University of Hamburg, Germany and the Department of Geophysics and Planetary Science, Tel Aviv University. Two profiles shown as lines **B-B^{||}** and **B1-B1^{||}** trending WNW-ESE (Figure 4.1) were recorded. The seismic energy was generated by airguns for both profiles. Ocean bottom seismograph (OBS) stations were deployed offshore to record the shots, while land stations were used onshore. The data was evaluated by two-point kinematic and dynamic ray-tracing seismic modelling (Trey, 1991). A brief description of the results of these profiles are given in the following:

-The sedimentary cover over the Eratosthenes Seamount has an average thickness of about 4 km. The sediment thickness increases rapidly to about 12 km in SE direction of the Eratosthenes Seamount and under the Levant Basin (Figure 4.3). The continental crust thins in SE direction and is abruptly truncated by an oceanic crust to about 10 km thick in the Levant Basin (Figure 4.3).

-The continent-ocean transition was identified near the coast by a single onshore recording station. Beneath the coast of Israel, the thickness of the sedimentary sequences are 6 km, while the depth to the Moho lies at about 24 km (Ginzburg et al., 1994). The P-wave velocity for the compressional waves travelling along the Moho has normal values of 8.0 km/s (Trey, 1991).

-The seismic results of these profiles conform that the Levant Basin is floored by oceanic crust. The sediment is interpreted to be about 10 km thick and is underlain by a 6.5-6.9 km/s velocity crystalline basement (Trey, 1991). In general, the crustal structure of the Levant Basin

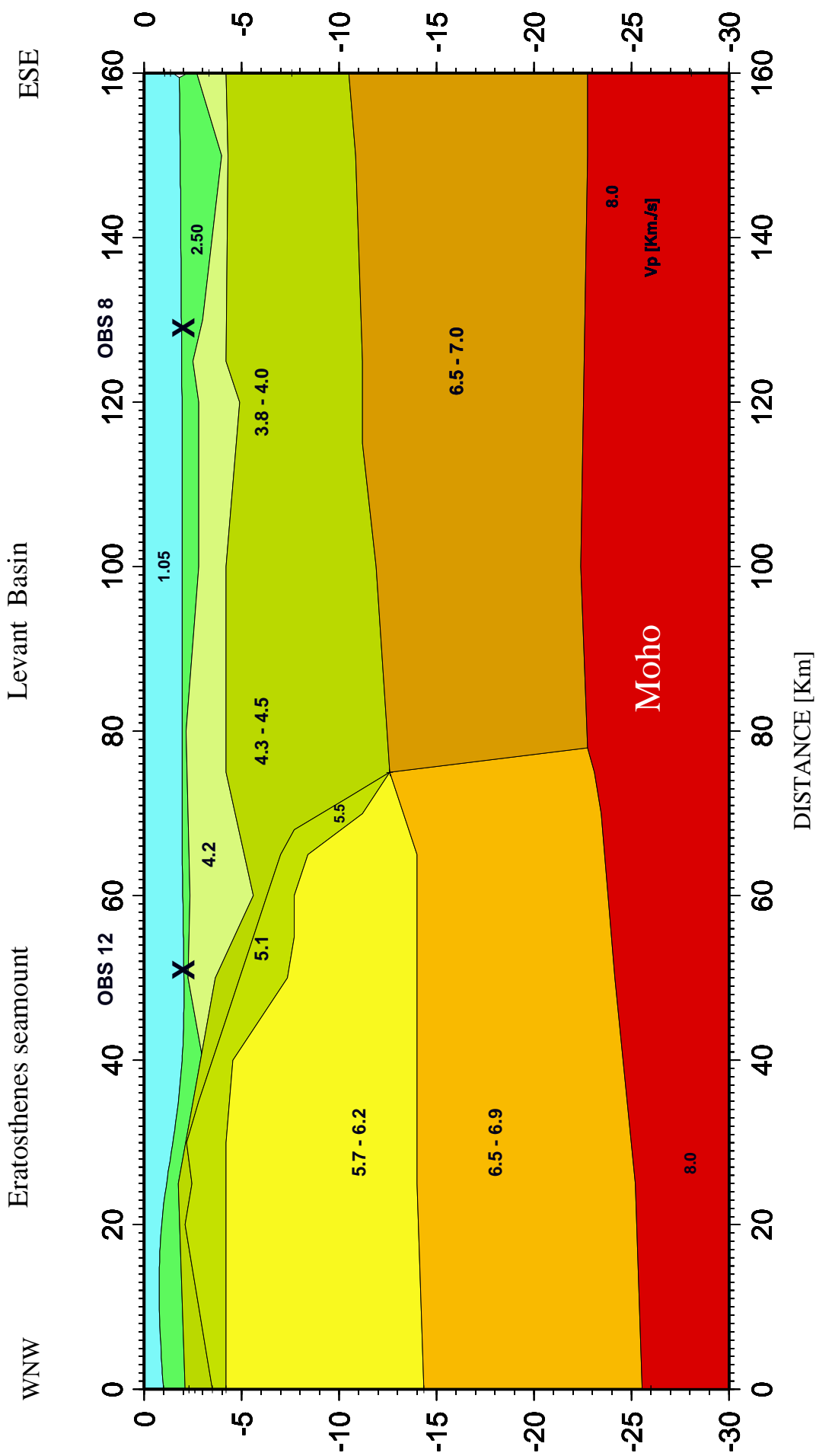


Figure 4.3: Velocity depth model from the Eratosthenes Seamount across the Levant Basin, based upon the Israel' 89 seismic project, shown as line B-B^{||} in Figure 4.1, Compiled from Trey (1991).

is oceanic, while the Eratosthenes Seamount is continental (Makris et al., 1983; Ginzburg et al., 1993).

IV.1.3. Seismic profiles of Egypt-Rhodes and Egypt-Crete-Santorin

These profiles run from the coast of Egypt, extending in NNW direction, and crossing the Herodotus Abyssal Plain and the East Mediterranean Ridge. Profile **C-C^{II}** (Egypt -Rhodes) is about 580 km long and terminates about 10 km west of the Island of Rhodes, while profile **D-D^{II}** (Egypt-Crete-Santorin) is about 570 km long and crosses Crete, the Cretan Sea and ends near the Island of Santorin as shown in Figure 4.1 (Wang, 1995).

Based on the drilling information of the sedimentary sequences at the Egyptian coast (Said, 1962), and the results of refraction seismic experiments, Malovitskiy et al. (1975) presented a geological cross-section from the Egyptian coast across the Herodotus Abyssal Plain to the Hellenic Arc “near the Island of Rhodes” (Figure 4.4). The location of the offshore part of this cross-section is shown in Figure 4.1, as line **C-C^{II}**. The Palaeozoic and Mesozoic sediments are shown to have a thickness of about 6 km at the Egyptian coast, and thicken towards the Eastern Mediterranean Sea and reach about 11-12 km below the Herodotus Abyssal Plain (Figure 4.4).

IV.1.4. Seismic profiles of Sidi Barani-Sidi Abdel Rahman

A refraction seismic profile was surveyed between Sidi Barani-Sidi Abel Rahman along the Egyptian coast. This profile is 250 km long and divided into sub-profiles as lines **SB -SA^{II}** in Figure 4.1 (Marzouk, 1988). The crust along this profile is 26 km thick below the Mediterranean Sea and the thickness increases towards the east to 30 km (Figure 4.5). The Egyptian coast is underlain by a continental crust covered by a 4-6 km thick sedimentary layer (Makris et al., 1988).

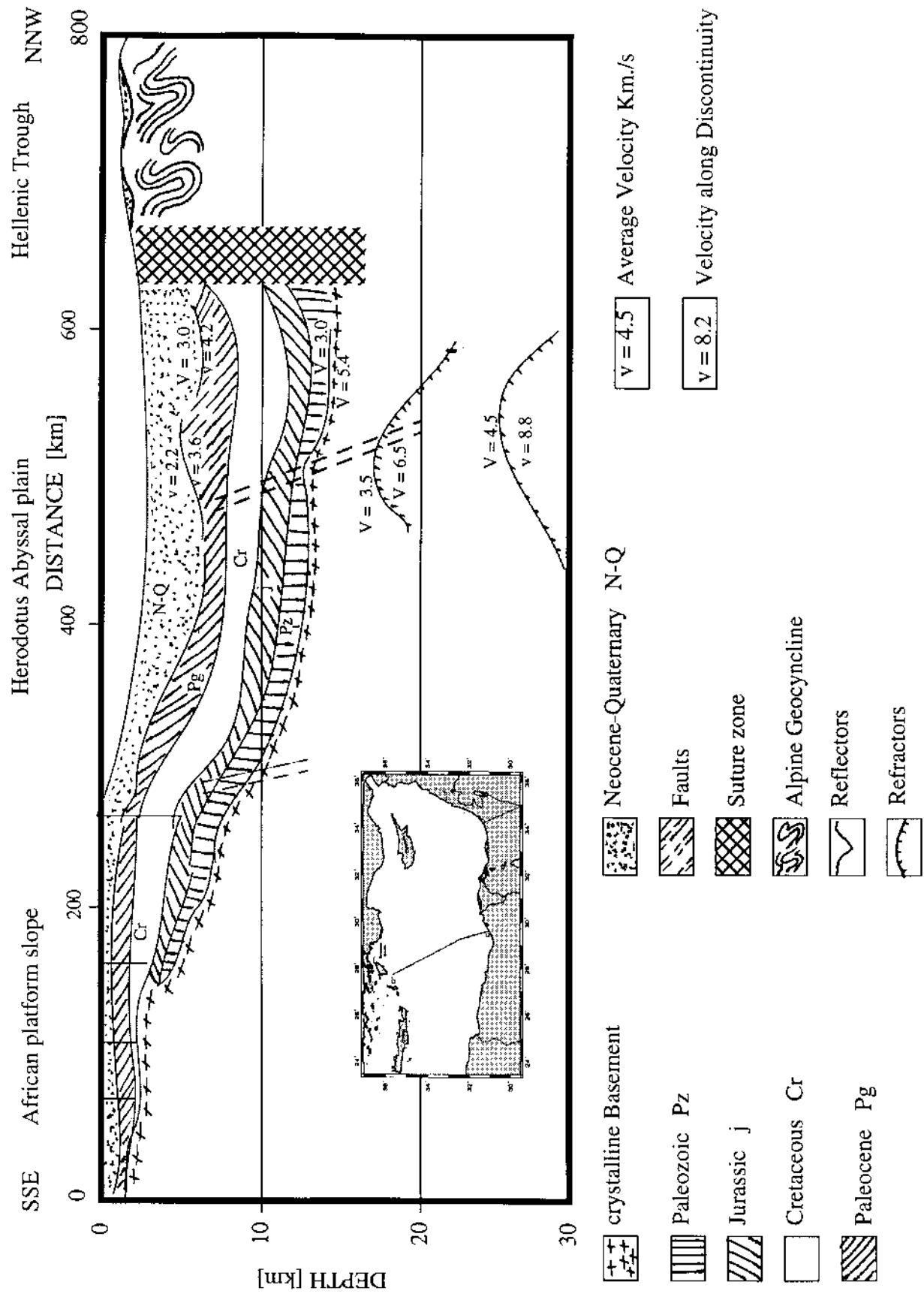


Figure 4.4: Sketch diagram shows geological cross-section between Egypt and Rhodes based on geological studies and borehole data. Compiled from Malovitskiy et al. (1975).

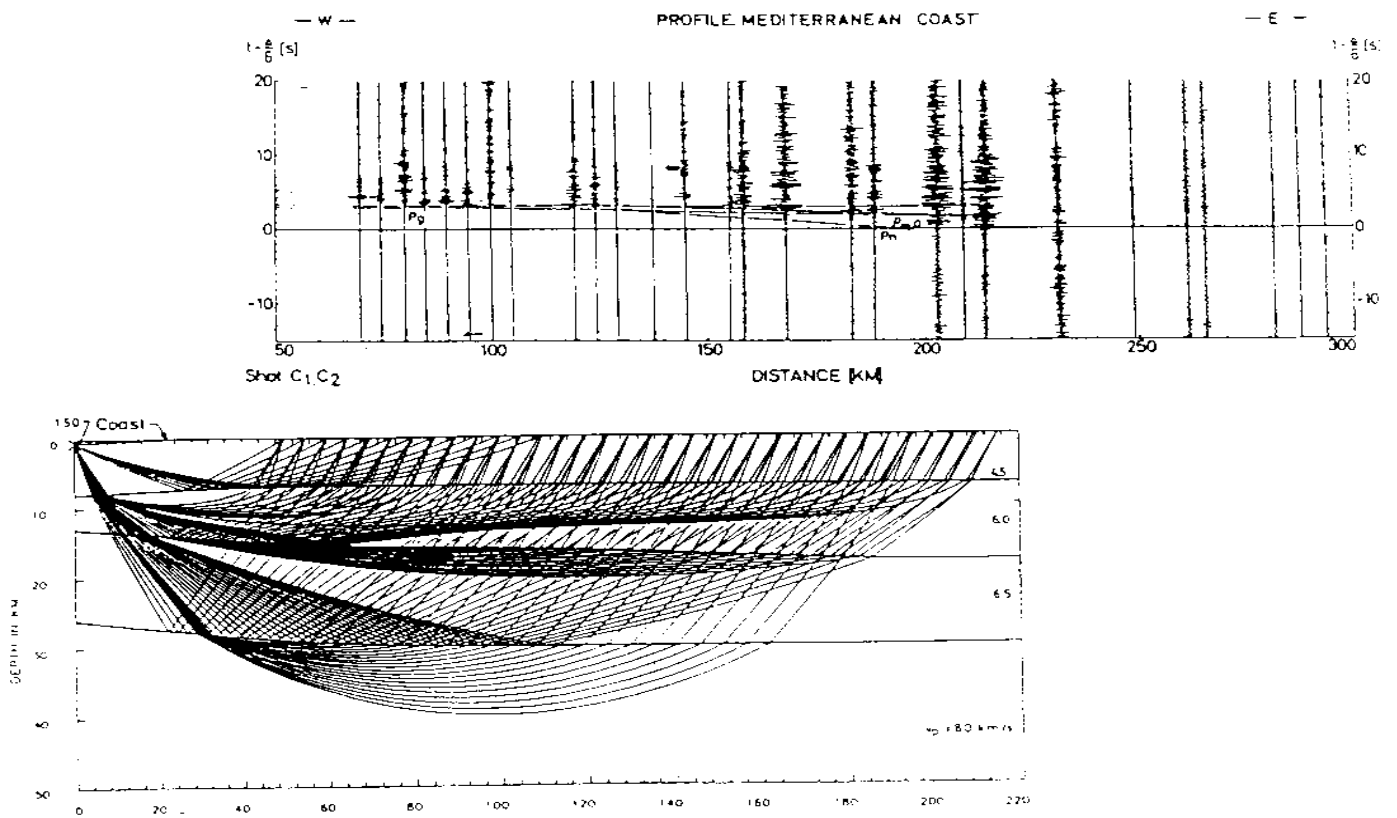


Figure 4.5: The travel time plot of seismic recordings and velocity depth model of the crustal structure below Sidi Barani-Sidi Abdel Rahman profile, after Marzouk (1988).

IV.2. Wide-angle reflection / refraction seismic profiles in and around the Cretan region

Makris and Vees (1977), Makris (1978 a, b), Makris (1985) and Hartung (1987), studied the crustal thickness and velocity structure by several wide-angle reflection / refraction seismic (WARRS) experiment profiles in the Cretan region, as lines CR1, CR2, CR3 and CR4 in Figure 4.1. The results of these seismic experiments are summarized as follows:

- The sedimentary thickness varies from about 1 km below Crete (Figure 4.6) to about 2-3 km beneath the Cretan Sea (Figure 4.7). The thin sediment covers are mainly post upper Miocene sediments, although there are remnants of older nappes, which are mainly confined to the southern border of the Cretan Sea (Makris, 1978 a).

- The Cretan Sea seabed is a stretched continental crust forming to an E-W elongated dome of the upper mantle striking along the Cretan Trough. The maximum thinning of the crust is located at the central deep part of the trough, where the minimum depth of Moho is only about 17 km (Figure 4.7).

- Below Crete and the Cretan Sea, the upper crust has a velocity of 6.0 to 6.2 km/s. The lower crust is controlled by a gradually increasing velocity from about 6.4 to 6.8 km/s (Figures 4.6 and 4.7). The upper mantle here shows a velocity of 7.7 to 7.9 km/s, which is slightly lower than the normal value of 8.0 km/s obtained elsewhere in the Eastern Mediterranean Sea (Makris et al., 1983). Below Crete, the crustal thickness increases and the depth of the Moho is 30 - 32 km (Figure 4.6).

In addition, Bohnhoff (2000) studied the crustal investigation of the Cretan region using wide aperture seismic data consisting of three seismic data lines PI, PII, and PIII see Figure 4.1. These seismic lines were carried out at Crete region in order to investigate the crustal structure of the region. Bohnhoff (2000) developed 2D P-wave velocity-depth models for each of the three seismic lines which reveal strong lateral variations in crustal and sedimentary thickness as shown in Figures 4.8, 4.9, and 4.10. A brief account of the results of these seismic experiments are summarized:

- The crust in the Cretan region was identified to be continental with a maximum thickness of 32.5 km below northern Central Crete, thinning towards the north and south to 15 and 17 km respectively and thinning also along the strike of the main morphological structures on Crete (E-W) to 24 km (east) and 26 km (west).

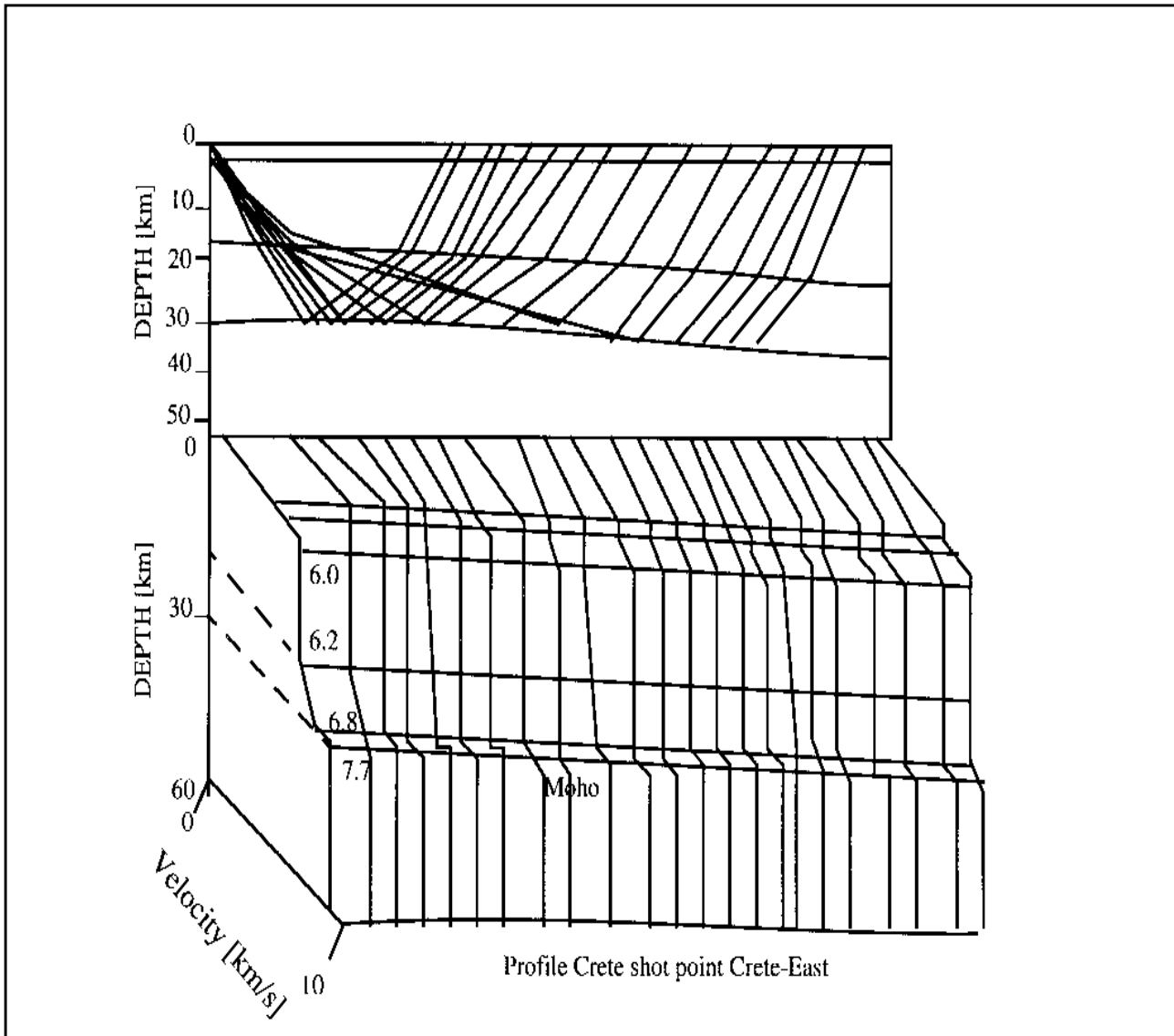


Figure 4.6: Sketch diagram shows velocity depth model along the Island of Crete, shown as line CR1 in Figure 4.1. Compiled from Makris (1978 a).

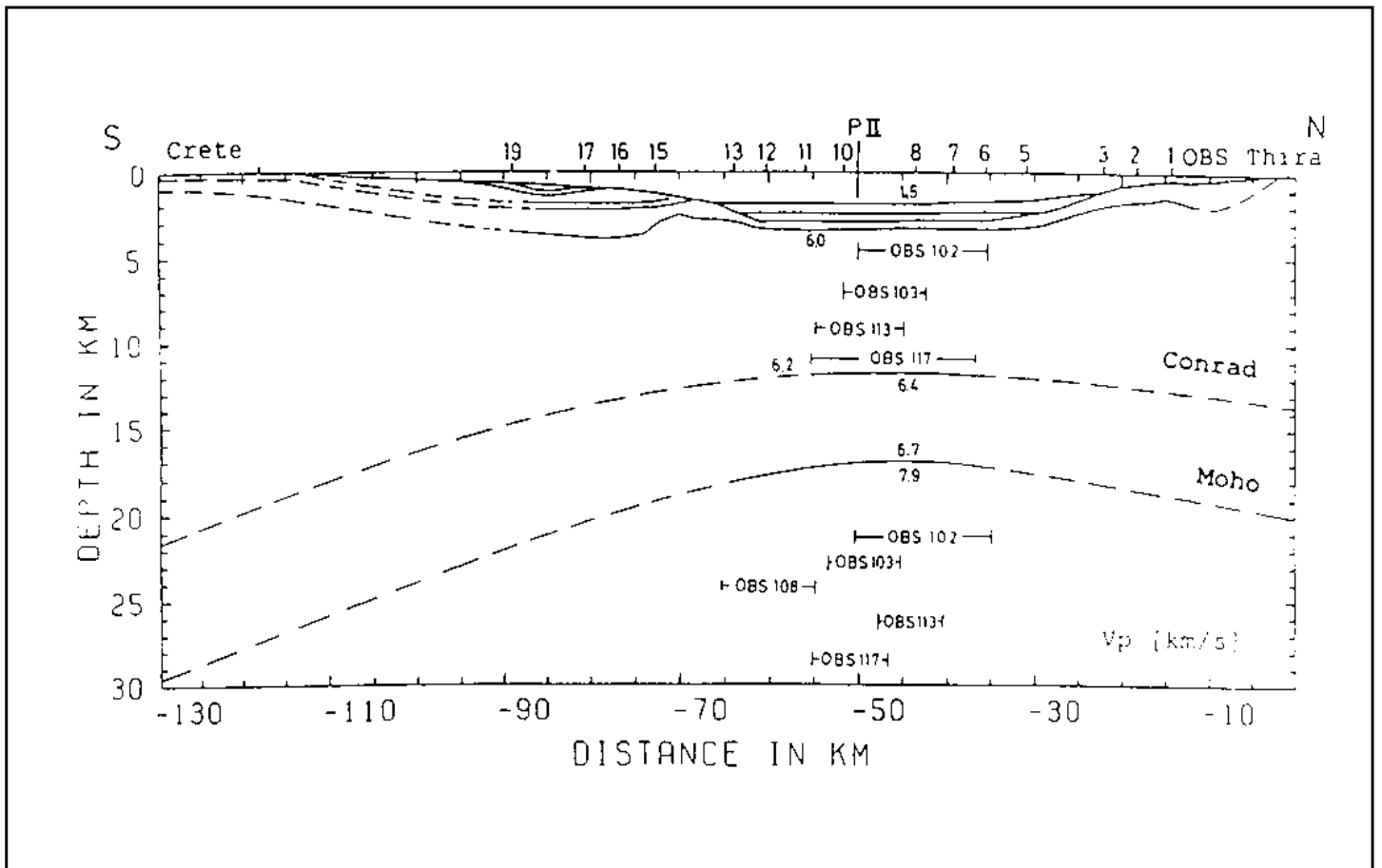


Figure 4.7: Velocity depth model across Cretan Sea, shown as line CR3 in Figure 4.1, Interfaces controlled by the seismic data are marked by continuous lines, after Hartung (1987).

-The velocity structure shows lateral variations within the upper crust (5.8-6.3 km/s, locally 6.5 km/s) being larger than those of the lower crust (6.4-6.9 km/s).

- The intracrustal discontinuity was encountered at most parts of the seismic profiles with velocity contrasts reaching from 0.15 to 0.6 km/s.

- Below the continental Cretan crust, lies a NNE-ward dipping layer that is decoupled from the overlying continental crust at approximately central Crete. This layer is presently under subduction as oceanic crust below the Aegean Sea. This is indicated by a change of crustal composition moving along with an increasing thickness of the sediments from some hundreds of meters to more than 7 km just before the northern slope of the central Mediterranean Ridge.

-The prominent reduction of the Moho depth north of central Crete is interpreted to represent the northern end of a microcontinent that was subducted in Oligocene times (Stöckhert, 1999).

Furthermore, Helms (2001), Planert (2001), and Brönnner (2003) studied the crustal and velocity structures between Crete and Libyan margin-East Mediterranean Sea in WARRS survey (Crete-Project 99, Distribution of OBS-and land stations). The locations of the three seismic lines between Crete and Libyan margin-East Mediterranean Sea are shown in Figure 4.1 as lines P#1, P#2, and P#3. Helms (2001), Planert (2001), and Brönnner (2003) generated 2 D P-wave velocity-depth models for each of these seismic lines and identified at least four sedimentary layers, upper and lower continental crust and oceanic crust as shown in Figures 4.11, 4.12, and 4.13. A brief account of the results of these seismic experiments are summarized:

-The crustal structure of the African margin is complex and varies laterally. The complexity and lateral variability of the Mediterranean margin of north Africa are demonstrated in a simplified way for the Libyan coastal areas (Figures 4.11, 4.12, and 4.13).

-The passive continental margin at seismic line P#2 shows thick and strongly tectonized units of sediments lying on thin continental crust. The African margin-basement and sediments along seismic line P#1 are barely affected by faulting.

-The African passive continental margin extends to nearly 90 km offshore the coastal line and has an abrupt transition to an oceanic crust buried under 12 to 14 km of sediments. The continental crust is 23 km thick and thickens towards the coast to a value of about 28 km (Figure 4.11).

-The continental structure along the seismic line P#2 (Figure 4.12) extends at least to 160 km off the Libyan coast and is severely tectonized. The crust is 22 to 25 km thick including 6

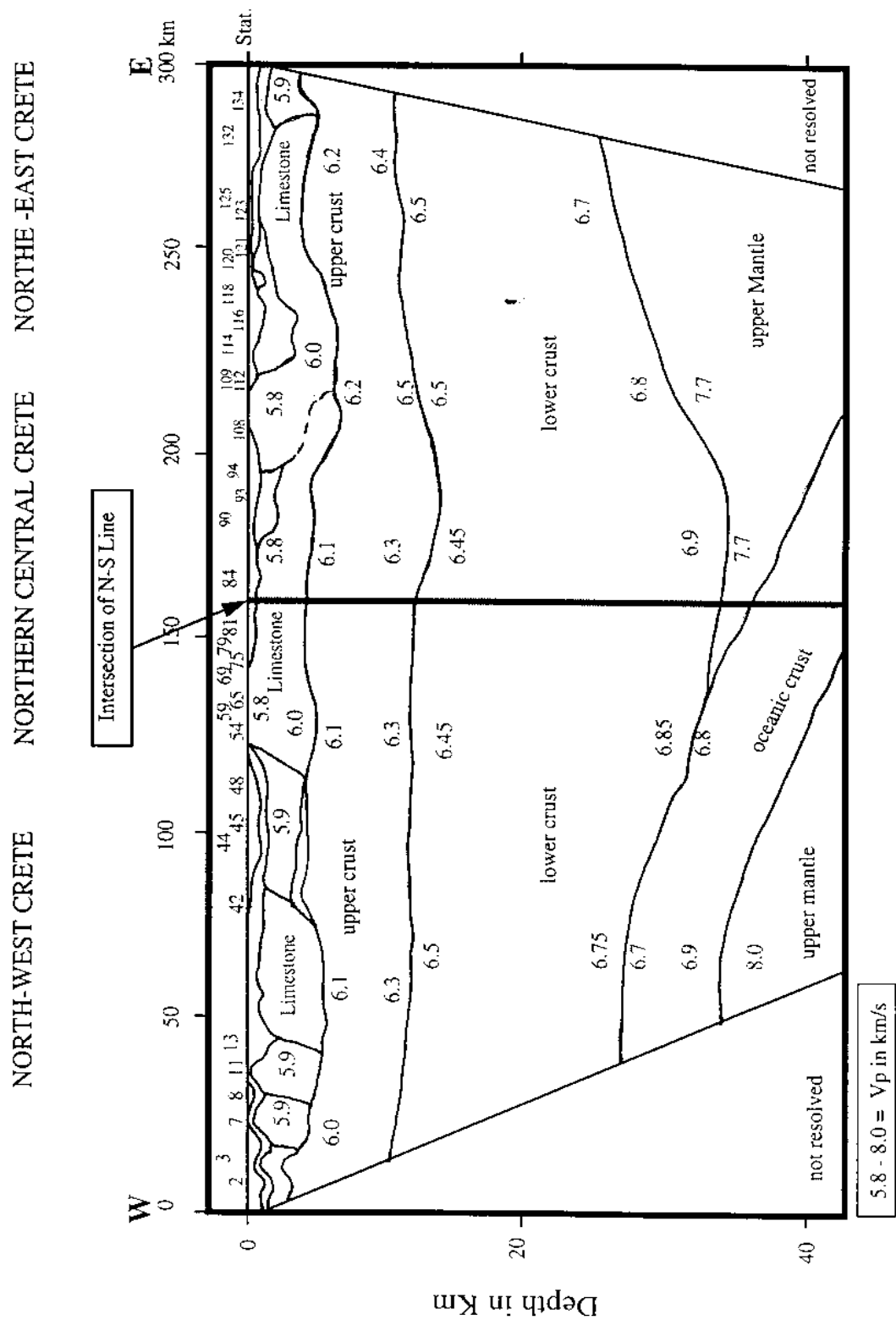


Figure 4.8: 2D P-wave velocity depth model for northern shore profile on the Cretan region, based on Crete seismic experiment, shown as line PI in Figure 4.1, compiled from Bohnhoff (2000).

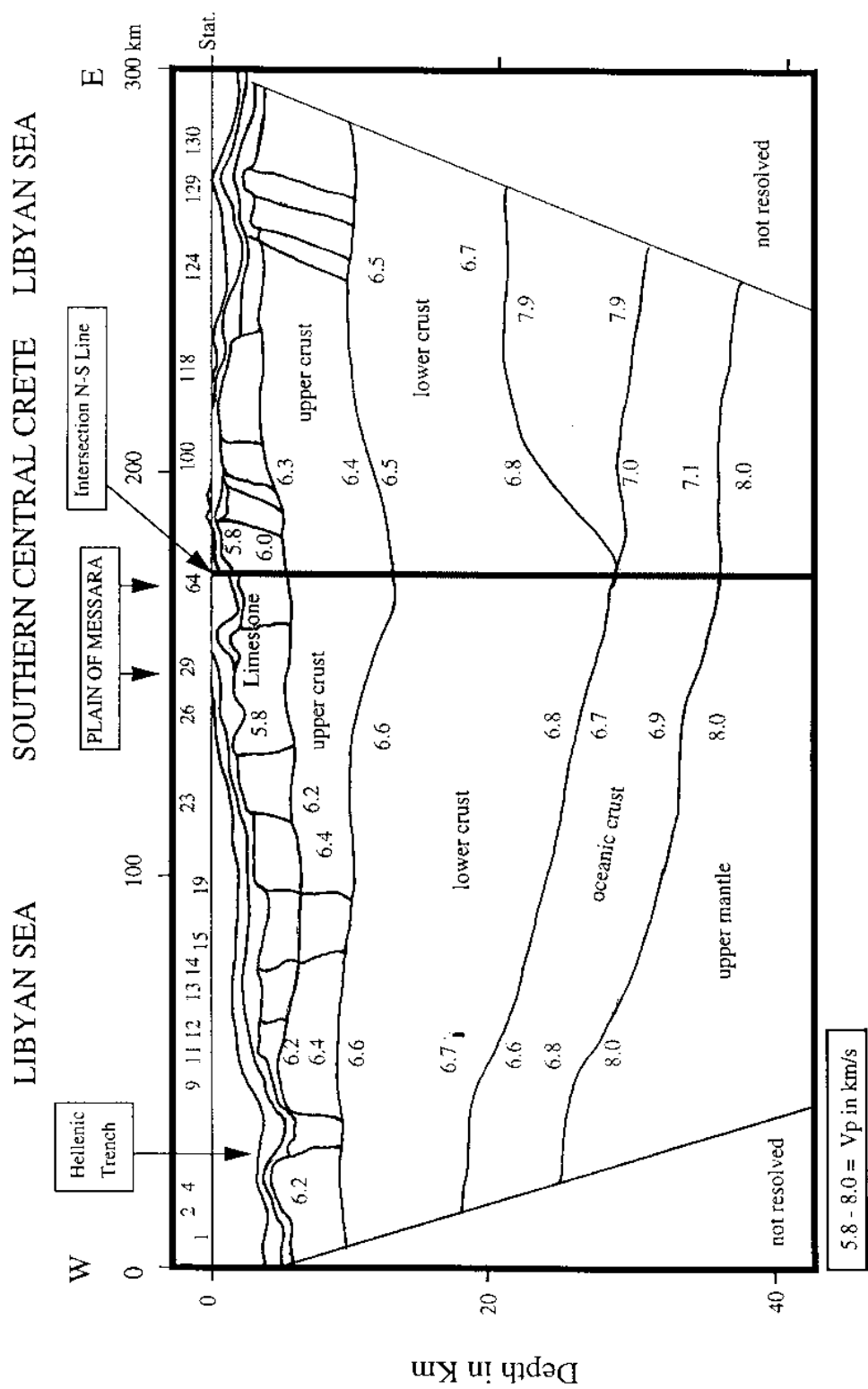


Figure 4.9: 2D P-wave velocity depth model for southern shore profile on the Cretan region, based on Crete seismic experiment, shown as line PII in Figure 4.1, compiled from Bohnhoff (2000).

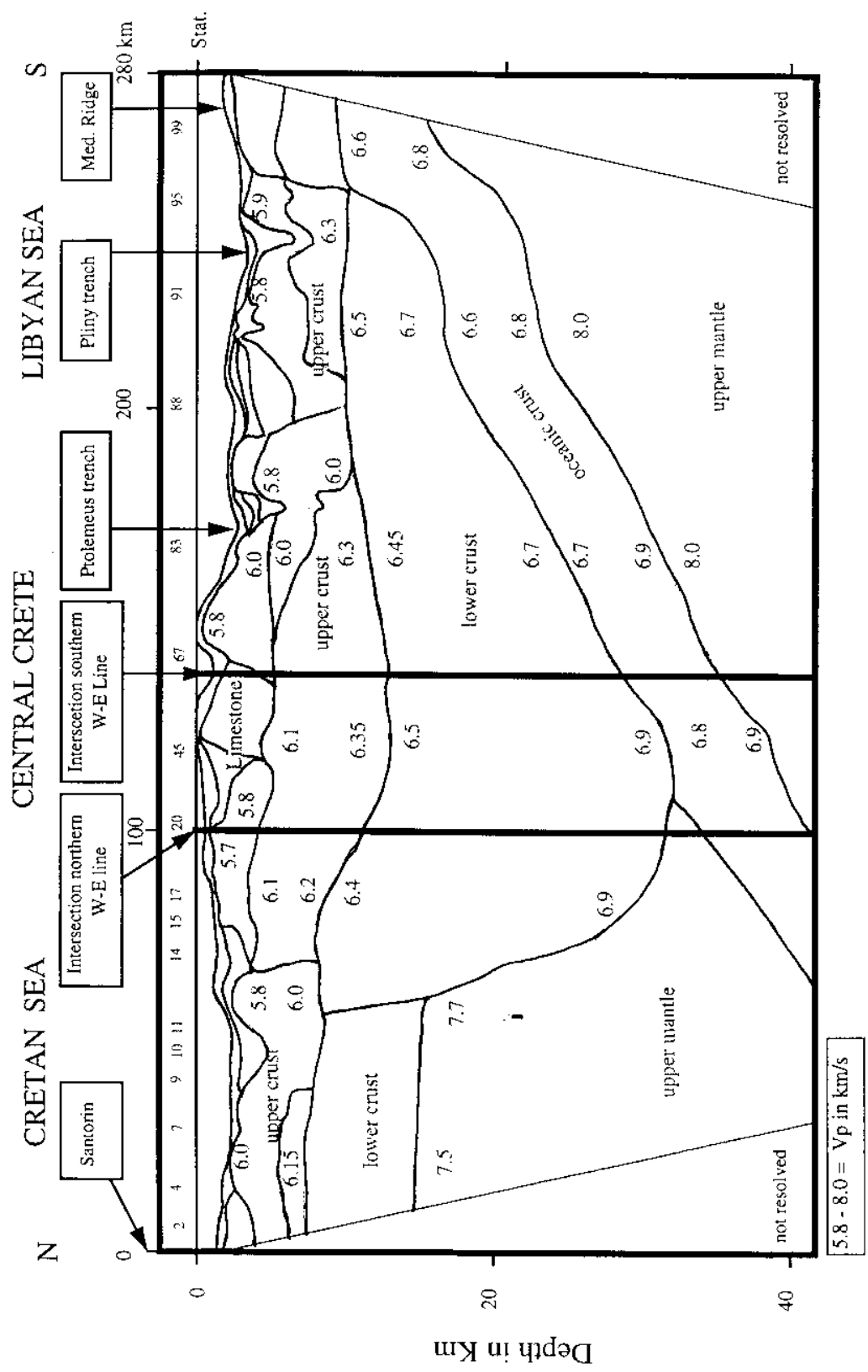


Figure 4.10: 2D P-wave velocity depth model for north-south traverse profile on the Cretan region, based on Crete seismic experiment, shown as line PIII in Figure 4.1, compiled from Bohnhoff (2000).

to 7 km sediments under 2 to 2.5 km water depth. The oceanic structure has a limited extension to not more than 50 km wide and is covered by 12 to 13 km of strongly tectonized sediments (Figure 4.12).

IV.3. Other deep seismic refraction profiles in the Eastern Mediterranean Sea

Based on deep seismic refraction profiles R1, R2 and R6 as shown in Figure 4.1 (Lort, 1973), Morelli (1975) presented a schematic crustal section of the Mediterranean Ridge and Herodotus Abyssal Plain (Figure 4.14). The result shows the existence of a thick sedimentary cover along profile R1 (about 10 km) in SW direction of the Crete beneath the Mediterranean Ridge and along profiles R4 and R6 (about 12 -15 km) beneath the Herodotus Abyssal Plain.

Some Deep seismic sounding experiments (DSS) and Expanding spread profiles in the Mediterranean Sea (ESP) were performed on several parts of the study area. The results of these seismic profiles are described in detail in Appendix [A] for example, results of the seismic profiles around and adjacent Dead Sea rift, the Cyprean region, the Mediterranean Ridge and Herodotus Abyssal Plain.

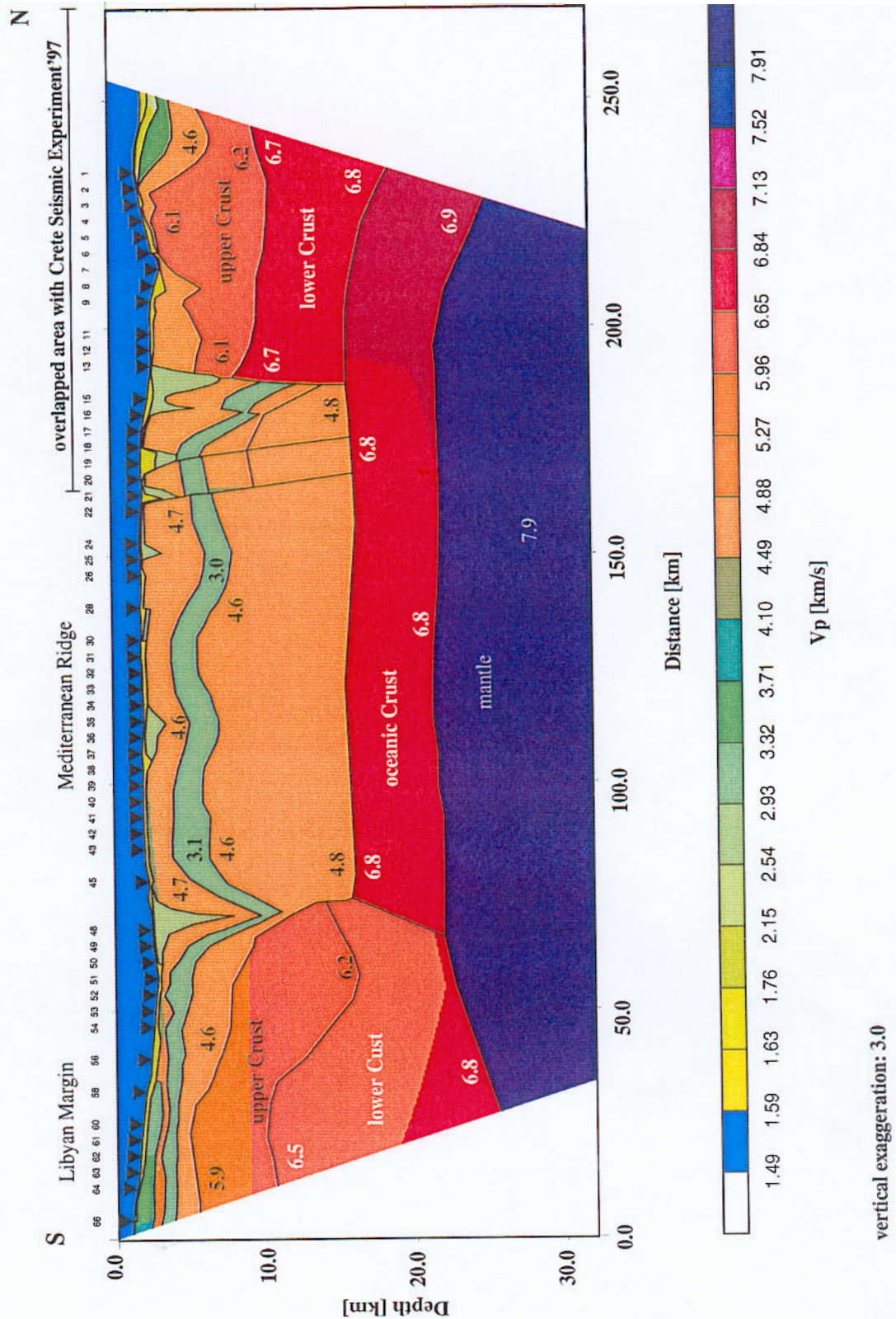


Figure 4.11: Velocity depth model along the central profile between Crete and Libyan margin-East Mediterranean Sea, based on Crete-Project 99, shown as line P#1 in Figure 4.1, after Helms (2001).

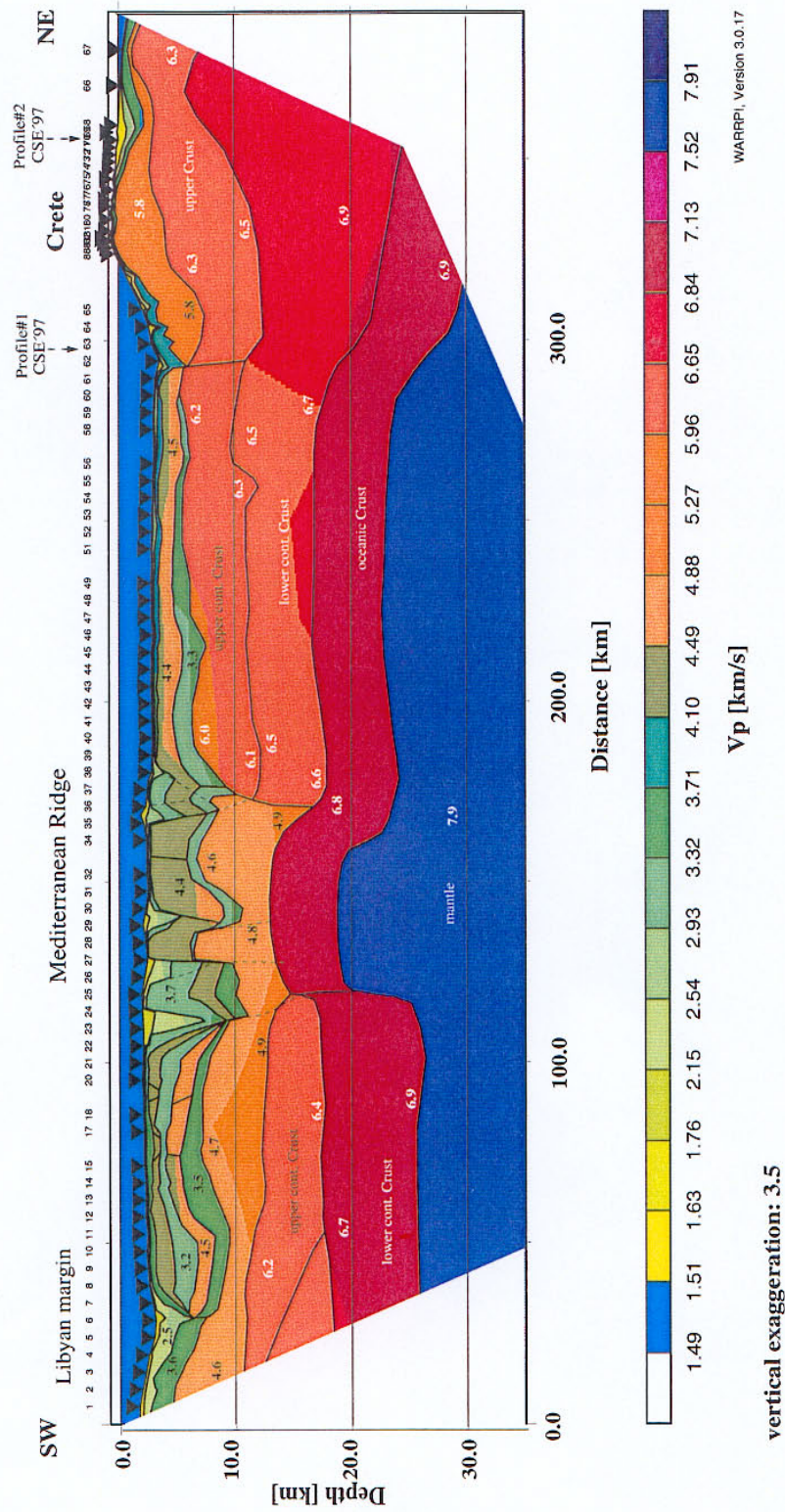


Figure 4.12: Velocity depth model along the west profile between Crete and Libyan margin-East Mediterranean Sea, based on Crete-Project 99, shown as line P#2 in Figure 4.1, after Brönnner (2003).

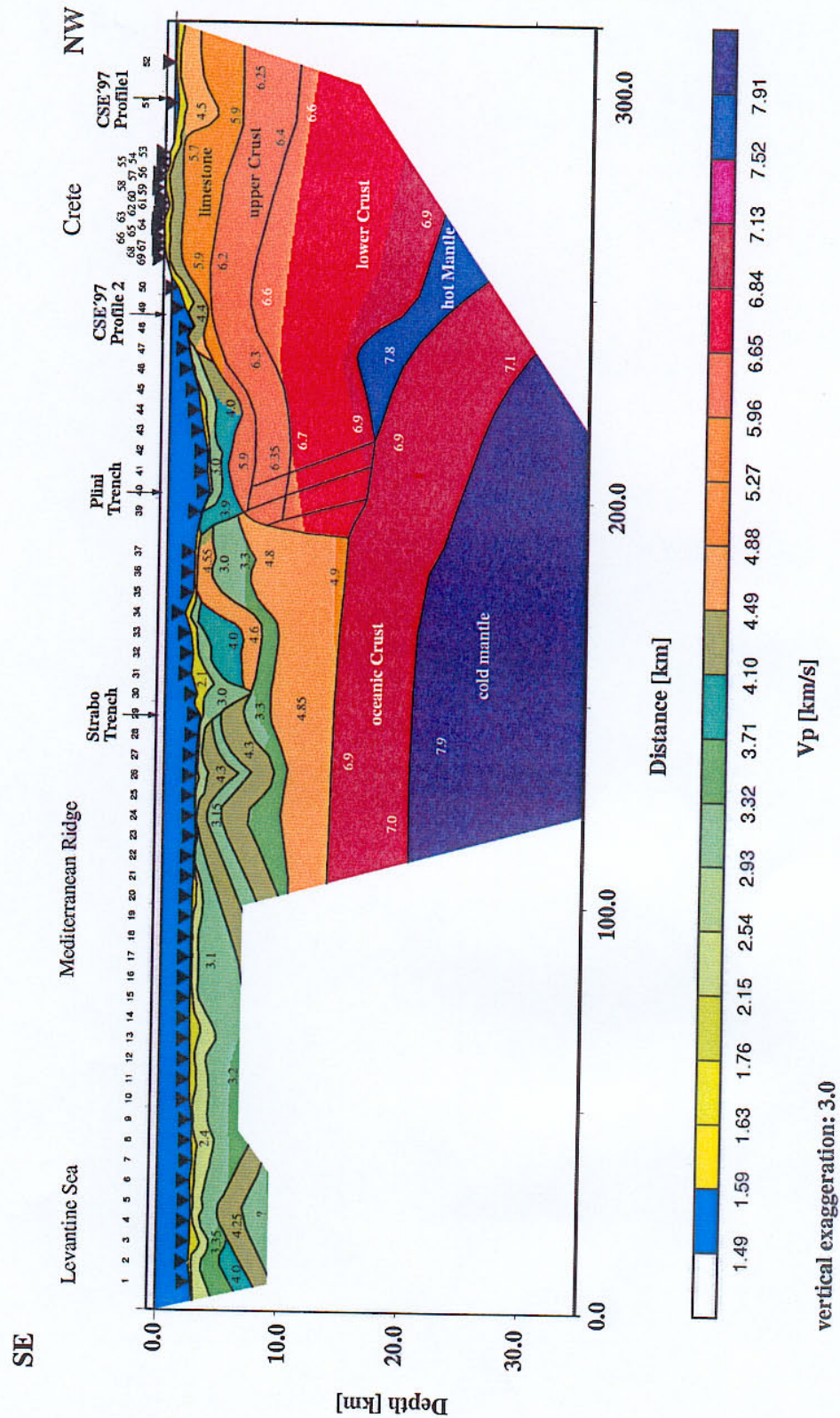


Figure 4.13: Velocity depth model along the east profile between Crete and Libyan margin-East Mediterranean Sea, based on Crete-Project 99, shown as line P#3 in Figure 4.1, after Planert, 2001.

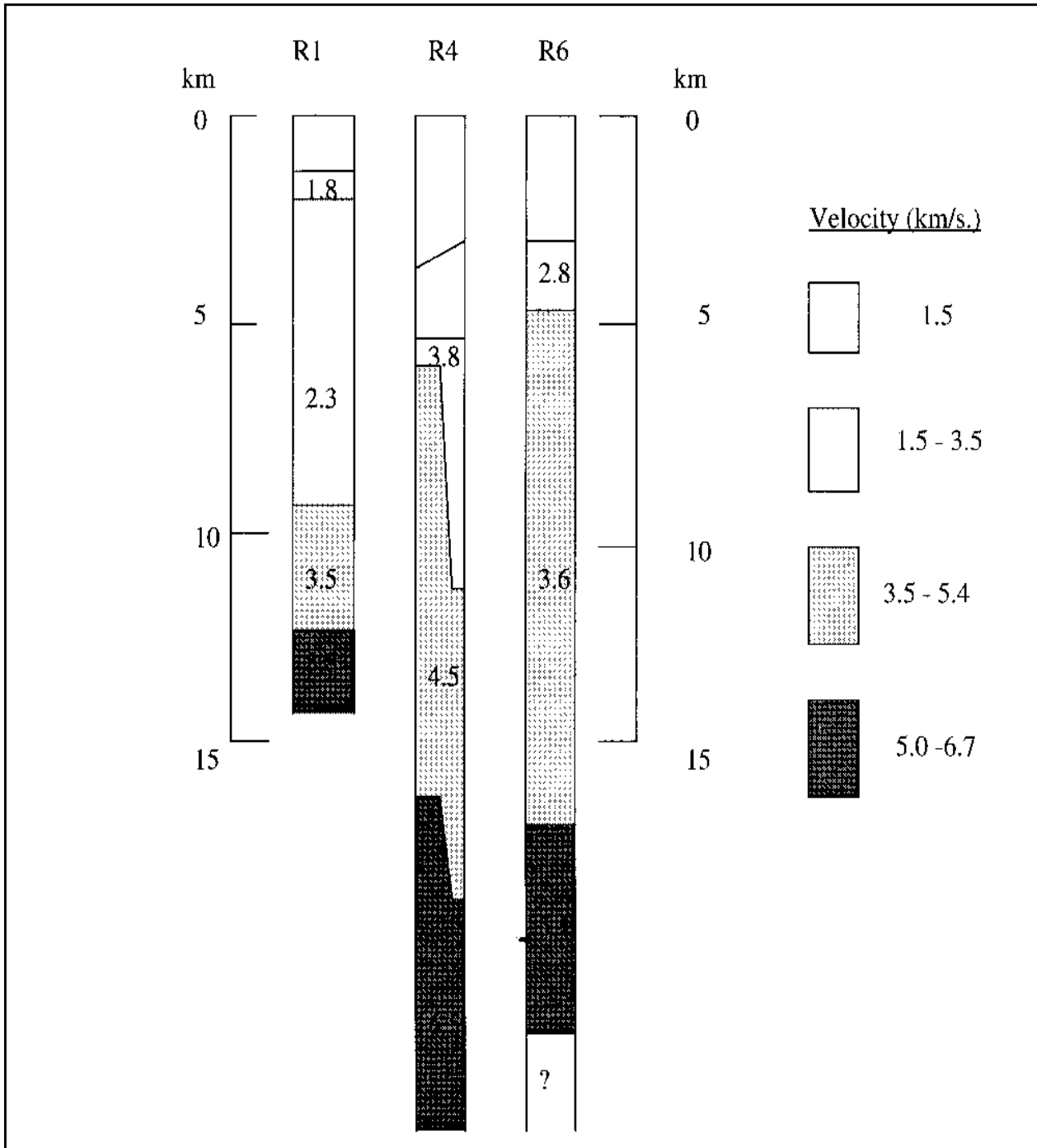


Figure 4.14: Schematic crustal sections in the Eastern Mediterranean Sea, based on deep seismic refraction profiles. Compiled from Morelli (1975).

V. TWO AND THREE-DIMENSIONAL GRAVITY MODELLING

Two and three-dimensional gravity modelling has become increasingly important in applied geophysics and geophysical research. In order to contribute to a better understanding of the crustal structure of the study area and its relation to the adjacent areas, a quantitative interpretation of the Free-Air gravity field was undertaken by developing two and three-dimensional gravity modelling.

Since there is no unique solution to a gravity effect, because it is more complex, geological, seismic, and any other available information are used to constrain the density models. To calculate the gravity anomalies produced by the subsurface structures, crustal models are assumed. If the calculated gravity values of the density models are in agreement with the measured ones, then these models should represent a good evaluation to the prevailing conditions.

In the present work, the two-dimensional gravity modelling was calculated along four seismic profiles, which cross the main tectonic elements of the area investigated (Figure 5.1). A two-dimensional gravity model was created using the software TWGRAV (Talwani two-dimensional gravity modelling) by applying the technique developed by Talwani et al. (1959). The quantitative interpretation of gravity data provided only two-dimensional gravity modelling images of the crustal structure along the profiles. In order to get a better understanding of the main tectonic features in the study area, three-dimensional gravity models were created using the IGMAS software (Interactive Gravity and Magnetic Application System) developed by Götze et al., 2000. The modelling parameter is constrained by the seismic profile results presented in the previous chapter.

For the two and three-dimensional gravity modelling, the Free-Air gravity data was used, since the Bouguer gravity anomalies may contain additional errors. For the calculation of the Bouguer gravity field the water depth is substantial. As the bathymetry along the modelling profile and the model areas, is not satisfactory enough, the Bouguer gravity field may contain inaccuracies. In the following section, a brief description of the modelling procedures are presented and the main results of these gravity models are discussed.

V.1. Two-dimensional gravity modelling

Many geological structures are approximately linear, and the problems connected with them can be solved with two-dimensional forms of analysis. Various methods exist for the computation of the gravitational attraction caused by irregularly shaped two-dimensional bod-

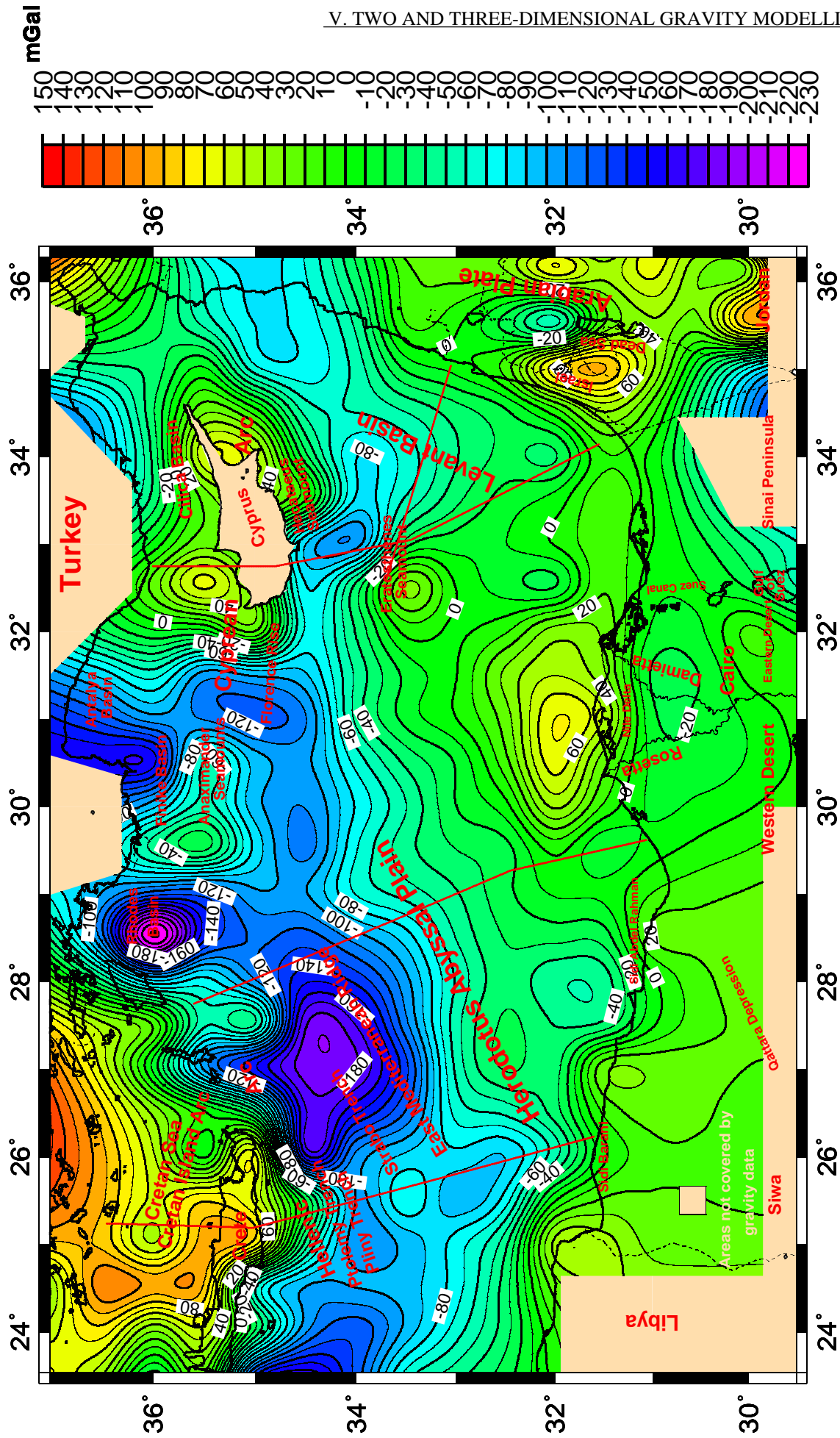


Figure 5.1: Free-Air gravity anomaly map of the southeastern Mediterranean Sea and the northern section of Egypt. The thick lines A-A", B-B", C-C" and D-D" are two-dimensional gravity modelling profiles, which coincide with the seismic lines (see Figure 4.1).

ies (e.g. Talwani et al., 1959; 1965; and Parker, 1972). These methods describe a two-dimensional system operation on a geological cross section in which the bodies for gravity effects are calculated and defined by a polygon. In the following the theory of two-dimensional calculation according to Talwani et al. (1959) is presented.

V.1.1. Theory of two-dimensional calculation according to Talwani et al., 1959

A two-dimensional body is divided into several small bodies of different size but regular shapes. In this way a two-dimensional body is approximated by a polygon with a sufficiently large number of sides. Both the vertical and the horizontal components of the gravitational attraction due to this polygon can be computed at any given point. Figure 5.2 is an arbitrary polygon ABCDEF with n sides.

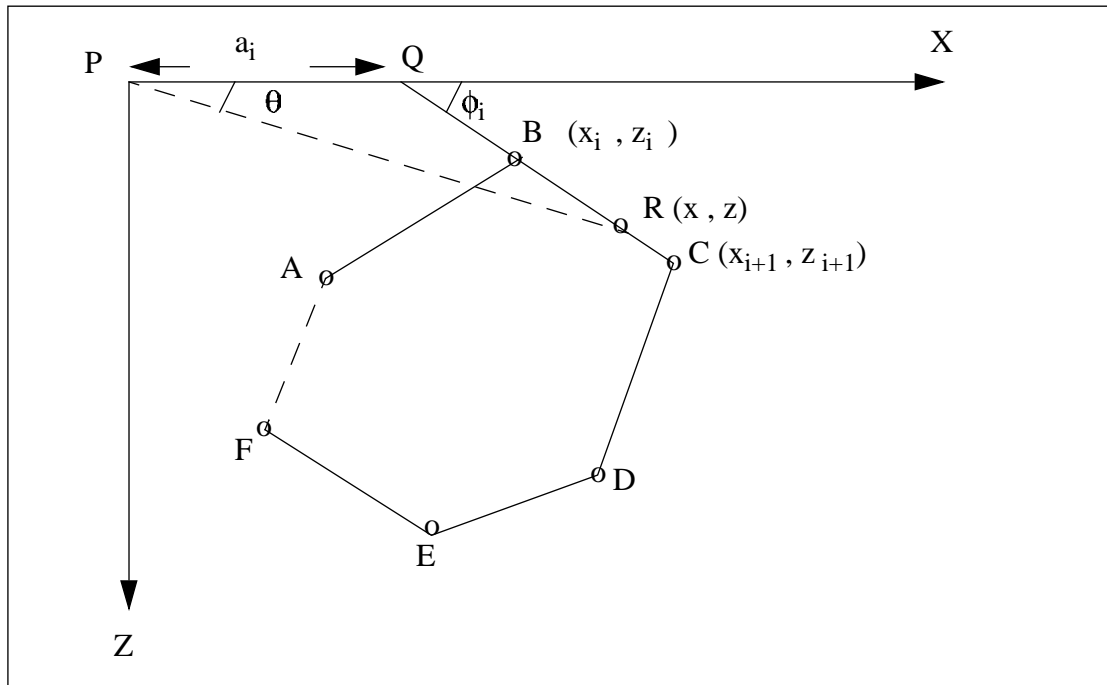


Figure 5.2: Geometrical elements involved in the gravitational attraction of an n - sided polygon.

Let P be the point at which the attraction has to be determined. Imagine P being the origin of an xz system of coordinates, where the polygon also lies within the xz plane. Let positive z be defined downwards (vertical) and let θ be measured from the positive x axis towards the positive z axis as shown in Figure 5.2.

The vertical and horizontal components (V and H respectively) of gravitational attraction due to such a two-dimensional body are calculated at the origin as follows:

$$V = 2 G \rho \oint z d\theta \quad (5.1)$$

$$H = 2 G \rho \oint x d\theta \quad (5.2)$$

Where G is the universal constant of gravitation, and ρ is the density of the body.

To evaluate the two integrals $\oint z d\theta$ and $\oint x d\theta$ for the polygon above, the contribution to $\oint z d\theta$ from the side BC of the polygon can be first computed. Produce CB to meet the x axis at Q at an angle ϕ_i . Let $PQ = a_i$. Now

$$z = x \tan \theta \quad (5.3)$$

For any arbitrary point R on the line BC . Also

$$z = (x - a_i) \tan \phi_i \quad (5.4)$$

The z from equations (5.3) and (5.4) can be calculated using the following formula:

$$z = \frac{a_i \tan \theta \tan \phi_i}{\tan \phi_i - \tan \theta} \quad (5.5)$$

The following formula is based on a substituting of z in the equations (5.3) and (5.4) followed by an integration:

$$\int_{BC} z d\theta = \int_B^C \frac{a_i \tan \theta \tan \phi_i}{\tan \phi_i - \tan \theta} d\theta = Z_i \quad (5.6)$$

$$\int_{BC} x d\theta = \int_B^C \frac{a_i \tan \phi_i}{\tan \phi_i - \tan \theta} d\theta = X_i \quad (5.7)$$

The vertical and horizontal components of gravitational attraction due the whole polygon are then given respectively by

$$V = 2 G \rho \sum_{i=1}^n Z_i \quad (5.8)$$

and

$$H = 2 G \rho \sum_{i=1}^n X_i \quad (5.9)$$

The summations are made over n sides of the polygon. It now remains to solve the integrals involved in the expressions for Z_i and X_i

In the most general case it can be shown that

$$Z_i = a_i \sin \phi_i \cos \phi_i (\theta_i - \theta_{i+1} + \tan \phi_i + \log \frac{\cos \theta_i (\tan \theta_i - \tan \phi_i)}{\cos \theta_{i+1} (\tan \theta_{i+1} - \tan \phi_i)}) \quad (5.10)$$

$$X_i = a_i \sin \phi_i \cos \phi_i (\tan \phi_i (\theta_{i+1} - \theta_i) + \log \frac{\cos \theta_i (\tan \theta_i - \tan \phi_i)}{\cos \theta_{i+1} (\tan \theta_{i+1} - \tan \phi_i)}) \quad (5.11)$$

where

$$\theta_i = \tan^{-1} \frac{Z_i}{X_i},$$

$$\phi_i = \tan^{-1} \frac{Z_{i+1} - Z_i}{X_{i+1} - X_i},$$

$$\theta_{i+1} = \tan^{-1} \frac{Z_{i+1}}{X_{i+1}},$$

and

$$a_i = \frac{X_{i+1} - X_i}{Z_i - Z_{i+1}}.$$

θ_i , θ_{i+1} , ϕ_i and a_i are all expressed simply in terms of Z_i , and X_i to calculate both V and H

By applying this theoretical concept based on a full grid approach, Talwani et al. (1959) developed an algorithm for the calculation of potential fields which was later modified by Dehghani and Kaminski (pers. communication). They calculated multi layer models of the subsurface geology.

The densities of the two and three gravity modelling were constrained by the V_p velocities by means of the Nafe and Darke (1963) and Birch empirical functions (Birch, 1960; 1961). Nafe and Darke (1963) developed an empirical relationship between seismic velocities and densities. This relationship was originally based on marine shelf and deep sea sediments but was extended to a wider range of rocks with higher velocities. The Nafe, Darke and Birch relation was used to convert the V_p velocity into the density ρ . This yielded the following density values which were applied in the calculations.

$\rho = 2.35\text{-}2.5 \text{ g/cm}^3$ for the sediments with $V_p=1.5\text{-}4.5 \text{ km/sec}$.

$\rho = 2.82 \text{ g/cm}^3$ for the upper crust with $V_p=6.0 \text{ km/sec}$.

$\rho = 2.9 \text{ g/cm}^3$ for the lower crust with $V_p=6.5 \text{ km/sec}$.

$\rho = 2.95 \text{ g/cm}^3$ for the oceanic crust with $V_p=7.0 \text{ km/sec}$.

$\rho = 3.10 \text{ g/cm}^3$ for the upper mantle with $V_p=7.5 \text{ km/sec}$.

$\rho = 3.30 \text{ g/cm}^3$ for the Moho with $V_p=8.0 \text{ km/sec}$.

V.1.2. Results of the two -dimensional gravity models of the profiles A-A^{||}, B-B^{||}, C-C^{||} and D-D^{||}

Two-dimensional gravity models were calculated along the four lines A-A^{||}, B-B^{||}, C-C^{||} and D-D^{||} of the gravity profiles shown in Figure 5.1. These profiles are coincident with the seismic profiles presented in Figure 4.1 This means that the seismic results can be directly used to constrain a first density model. From Figure 5.1 Free-Air anomaly values were sampled every 0.5 km along the lines in order to obtain a smooth model.

The two-dimensional gravity modelling processes on the four profiles are shown in Figures 5.3, 5.4, 5.5 and 5.6. For a better comprehension of the results of the models and also to make a comparative and a quantitative analysis between the gravity anomalies of the area investigated and its geological sources, the main results of the two-dimensional gravity modelling (e.g. variability in crustal structure, density and layer thickness) for these profiles are described below.

V.1.2.1. Two-dimensional gravity model along profile A-A^{||} (Cyprus-Israel)

The location of this profile is shown as line A-A^{||} in Figure 5.1. The profile is 540 km long, extends from north to south, and runs from Cyprus, Eratosthenes Seamount to the Levant Basin. Density gravity modelling along this profile was constrained by the result from the seismic profile Cyprus-Israel A-A^{||} (Figure 4.1).

Two-dimensional gravity modelling along profile A-A^{||} is shown in part [C] of Figure 5.3. For comparison, the bathymetry of this profile is also presented in part [A]. The gravity data calculated from the density model and from the observed field are shown in part [B] of the same Figure. Generally, the observed gravity field was satisfied by the layer modelling thickness and the densities are indicative for the high reliability of the results obtained.

Along the profile, gravity values display lateral variations. e.g. South of Cyprus, a large negative anomaly of about -90 mGal coincides with the thickening of the sedimentary layers with a density of approximately 2.00 g/cm³. in the south of Cyprus. A thick sedimentary layer beneath the sea bed was identified by a recent seismic survey of the Geological Survey of Cyprus (Figure Appendix A2). This sedimentary basin separates the Island of Cyprus from the Eratosthenes Seamount.

The positive gravity field over north Cyprus coincides with the ophiolite overlays on Cyprus. It has a high density with a lateral variation from 2.95 to 3.00 g/cm³. It extends both to the south and to the north down to a depth of 4 km and is underlain by a 2 km thick sedimentary layer with a density of 2.60 g/cm³. In general, the ophiolite, known as the Troodos Massif are pieces of oceanic crust that have been thrust (obducted) onto the edge of continental crust. Such an ophiolite is also identified in southern Turkey and northwest Syria, i.e. the Troodos Massif is obducted onto the Taurus-Anatolian platform and Arabian plate by the end of the Mesozoic due to the closing of the Tethyan oceans during the Cretaceous period as suggested by Gillis and Robinson (1990). Furthermore, Robinson et al. (1983) and Robertson and Xenophontos (1993) showed that the Troodos ophiolite to have formed at several spreading axes in a supra-subduction zone environment resulting from the collision of the African and Eurasian plates in the Late Cretaceous.

The lower crust lies at a depth of about 22 km and the Moho lies at a depth of about 32 km beneath Cyprus. The upper crust was modelled with a density of 2.82 g/cm³ and the lower crust with a density of 2.90 g/cm³.

The top of the crystalline or igneous basement lies at a depth of about 6.0 km beneath the Eratosthenes Seamount. According to the seismic results from profiles through and across the

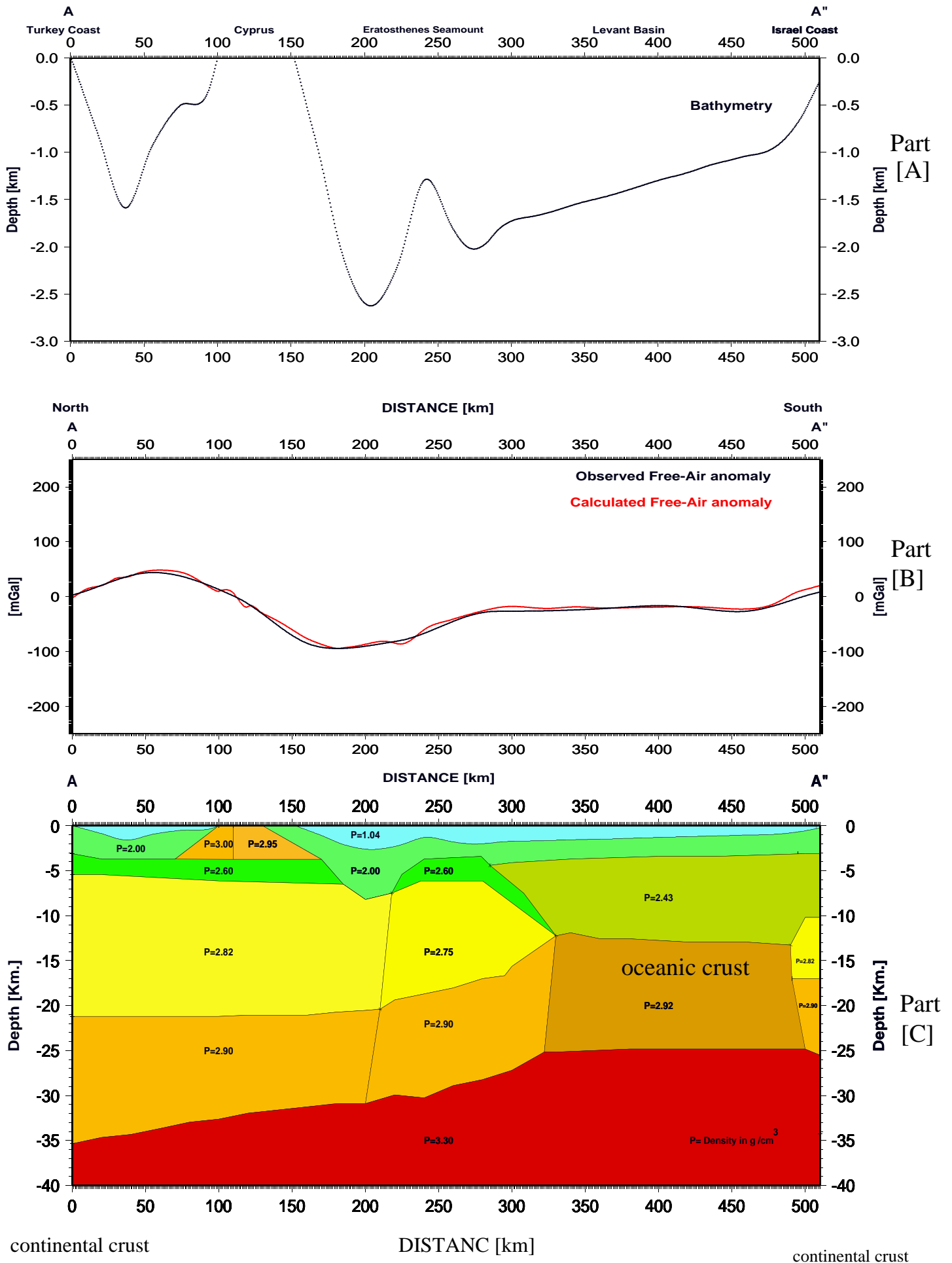


Figure 5.3: The final results of two-dimensional gravity modelling along profile A-A'' (Cyprus-Israel).

Seamount (Figures 4.3 and Appendix A2) a thin layer is situated above the crystalline crust. It was modelled with a density of 2.60 g/cm^3 . Also from the seismic surveys, the upper crust beneath this thin layer has a relative low velocity of about 5.7-6.2 km/s and was modelled with a density of 2.75 g/cm^3 . The lower crust was modelled with a density of 2.90 g/cm^3 .

South of the Levant Basin, the basement dips steeply to a depth of about 13 km. A thick sedimentary layer with an average density of 2.43 g/cm^3 lies beneath the Plio-Quaternary sediment with a density of 2.00 g/cm^3 . The oceanic crust beneath the sediments was modelled with a density of 2.92 g/cm^3 . The Moho lies at a depth of about 25 km.

Near the coast of Israel, the transition of oceanic-continental crust occurs. The same density values of the crust beneath Cyprus were used for modelling the continental crust according to the seismic results obtained by Makris et al. (1983). The Moho depth is about 27 km at the coast of Israel. The upper mantle has a density of 3.30 g/cm^3 .

V.1.2.2. Two-dimensional gravity model along profile B-B^{||} (Eratosthenes Seamount-Israel)

The two-dimensional gravity model along profile B-B^{||} is shown in part [C] of Figure 5.4. It is constrained by the Israel seismic profile B-B^{||} shown in Figure 4.1. It is mainly 240 km long, trending WNW-ESE and extends from the Eratosthenes Seamount across Levant Basin to Israel coast. In part [B] of the Figure 5.4, the gravity calculated from the density model and the observed field are shown. The bathymetry of this profile is presented in part [A] of the same Figure. In the following the main features of the two-dimensional gravity modelling along profile B-B^{||} are given.

In general, the Free-Air anomaly along profile B-B^{||} has negative values varying from -0.5 to -60 mGal, and shows a rapid decrease at the edges of the profile. This is reflected in a sharp drop of the basement and in an increase of the sedimentary cover, such that in the Levant Basin a thick sedimentary cover lies beneath the Plio-Quaternary sediment. The densities in the sedimentary cover are between 2.0 to 2.5 g/cm^3 and the oceanic crust has a density of 2.92 g/cm^3 .

At the left edge of the profile, the densities of the continental crust are between 2.75 and 2.90 g/cm^3 for the upper and lower parts respectively. The thin layer lies above the crystalline crust. It was modelled with a density of 2.60 g/cm^3 . However, at the right side of the profile, the transition between the oceanic and continental crust occurs at a distance of about 60 km from the Israel coast based on the seismic result of the profile B-B^{||} (see Figure 4.3). The densities

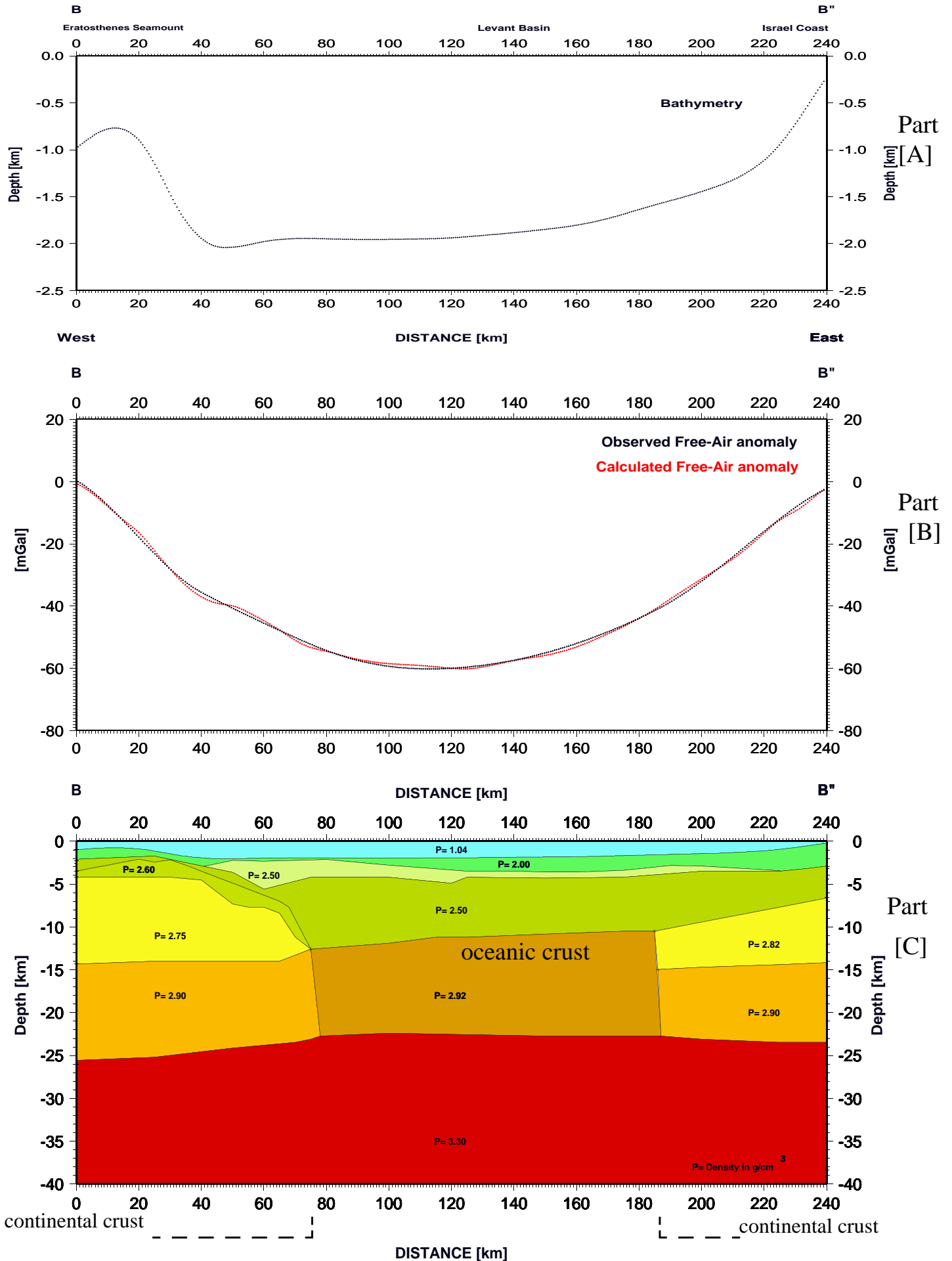


Figure 5.4: The final results of two-dimensional gravity modelling along profile B-B'' (Eratosthenes Seamount-Israel).

of the continental crust beneath the Israel coast are 2.82 and 2.90 g/cm³ for the upper and lower part respectively.

The depth of the crystalline or igneous basement changes from about 4 km at the left side of the profile beneath the Eratosthenes Seamount to about 13 km in the Levant Basin and decreases to about 6 km at the right side of the profile.

The Moho depth varies from about 26 km at the left side of the profile beneath the Eratosthenes Seamount to about 23 km under the Levant Basin, and to about 24 km at the right side of the profile, which is constrained by the Israel seismic profile B-B^{||}. The upper mantle has a density of 3.30 g/cm³.

V.1.2.3. Two-dimensional gravity models along profile C-C^{||} (Egypt -Rhodes) and D-D^{||} (Egypt-Crete-Santorin)

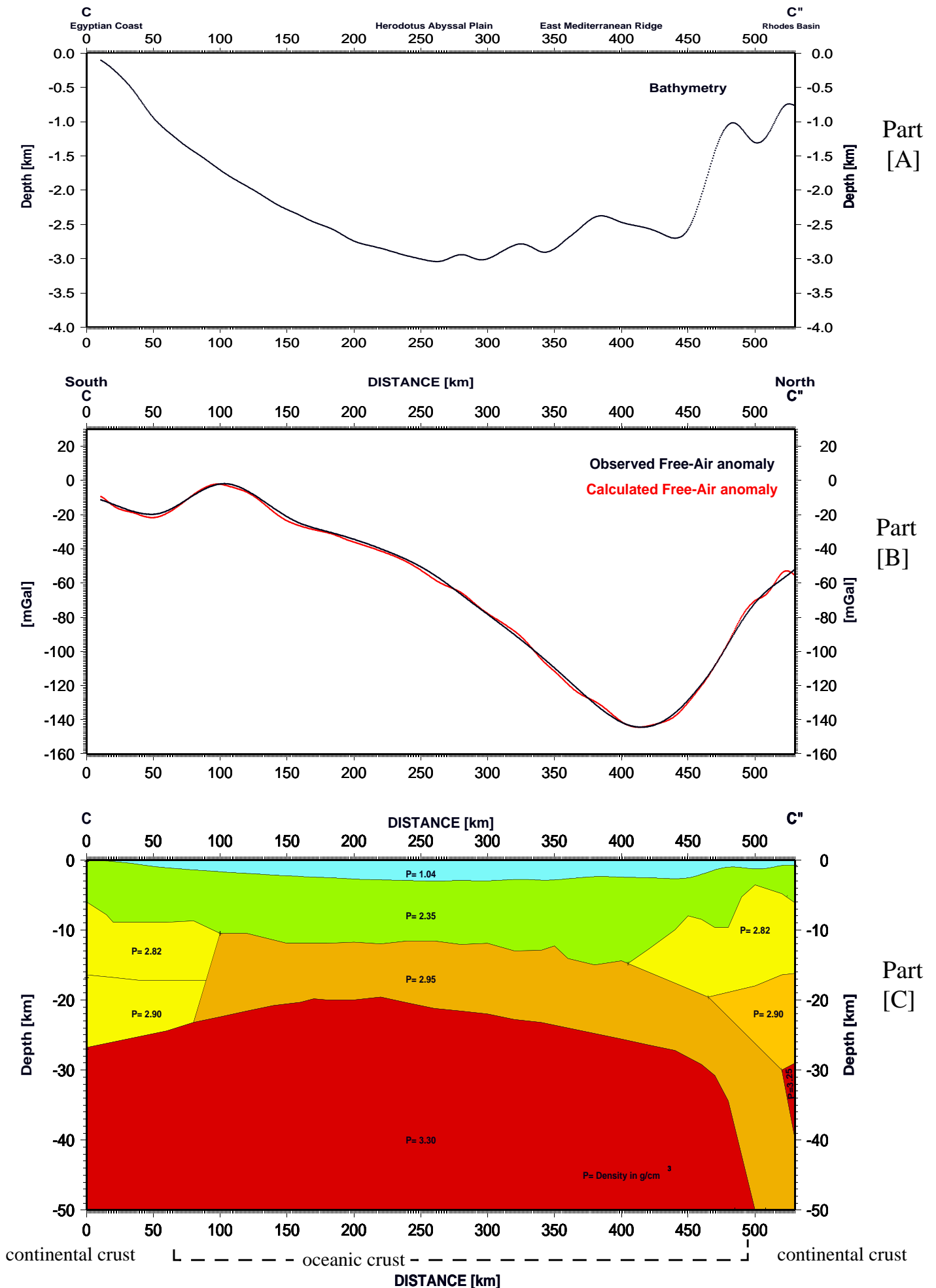
Two-dimensional gravity modelling along the profiles C-C^{||} (Egypt-Rhodes) and D-D^{||} (Egypt-Crete-Santorin) was constrained by the results of the deep seismic refraction profiles in the Eastern Mediterranean Sea and wide-angle reflection/ refraction seismic profiles (Figure 4.1) in and around Cretan region (e.g. Morelli, 1975, Makris and Veis, 1977, Makris, 1978 a; b and 1985, Hartung, 1987, Bohnhoff, 2000, Helms, 2001, Planert, 2001, and Brönnert, 2003).

Figures 5.5 and 5.6 show respectively the final results of the two-dimensional gravity modelling along the profiles C-C^{||} and D-D^{||}. They cross the Herodotus Abyssal Plain and the East Mediterranean Ridge, and start from the Egyptian coast and extend in a NNW direction (Figure. 5.1). The main features of the two-dimensional gravity modelling along these two profiles are described below.

V.1.2.3.1. Two-dimensional gravity model along profile C-C^{||} (Egypt-Rhodes)

The two-dimensional gravity modelling along profile C-C^{||} (Egypt-Rhodes) is displayed in Figure 5.5 and is mainly 530 km long. Along this profile, the Free-Air anomaly has negative values starting with -2 mGal, increasing to -140 mGal and at the end reaching values of -50 mGal. There are local gravity lows also at the East Mediterranean Ridge.

The two-dimensional gravity modelling along profile C-C^{||} is shown in part [C] of Figure 5.5. For comparison, the bathymetric value of this profile is also presented in part [A]. The gravity anomaly computed by the density model, which was derived from the seismic model, is shown in part [B]. At the left and right edges of the profile, the densities of the continental crust are between 2.82 and 2.90 g/cm³ for the upper and lower parts respectively.



The Moho depth values correlate considerably with the variations of gravity value along this profile. Here the Moho lies at a depth of about 27 km at the Egyptian coast, and then rises to a minimum depth of about 19 km beneath the Herodotus Abyssal Plain. The Moho depth increases again from about 26 km below the East Mediterranean Ridge to about 30 km below the Hellenic Arc. At the East Mediterranean Ridge, the increase in the negative gravity anomaly corresponds with the relatively large thickness of the sedimentary layer.

The transition from continental to oceanic crust within the African plate was modelled at a distance of about 100 km from the Egyptian coast constrained by the results of the Expanding spread profile 18 as shown in Figure Appendix [A4] in the Herodotus Abyssal Plain (De Voogd et al. (1992). The African oceanic crust is subducted beneath the Hellenic Arc with degree angle of approximately 110 as assumed by Le Pichon and Angelier (1979). Hence it is not only the Aegean continental crust but also the subducted crust that contributes to the Free-Air low associated with the Hellenic Arc.

The basement lies at about 6 km beneath the Egyptian coast coinciding with the Borehole results (Said, 1962 and Malovitskiy et al., 1975). However, the thickness of the sedimentary layer increases towards the East Mediterranean Ridge. In the Herodotus Abyssal Plain the depth lies between about 10 to 13 km and increases up to 14.5 km beneath the East Mediterranean Ridge. The sedimentary layer thins rapidly at the Hellenic Arc towards the west flank of Rhodes.

V.1.2.3.2. Two-dimensional gravity model along profile D-D^{||} (Egypt-Crete-Santorin)

The two-dimensional gravity modelling along profile D-D^{||} (Egypt-Crete-Santorin) is displayed in part [C] (Figure 5.6). It is about 545 km long and shows similarities to profile C - C^{||}. For comparison, the bathymetric value of this profile is also presented in part [A] of the Figure. The Free-Air gravity anomaly calculated from the density model and the observed anomaly are shown in part [B] of Figure 5.6. Generally, the observed anomaly is in agreement with the modelled seismic layers. The densities and layer thickness indicate the good reliability of the two-dimensional gravity model.

Along the profile, gravity values display intense lateral variations, especially along the left edge of the profile to about 300 km. A negative gravity anomaly coincides with the thickening of the sedimentary layers. The gravity values decrease abruptly towards the Pliny Trench region due to significant crustal thickening and the bathymetric slope.

The basement depth varies from about 9 km at the Egyptian coast to about 13 km in the

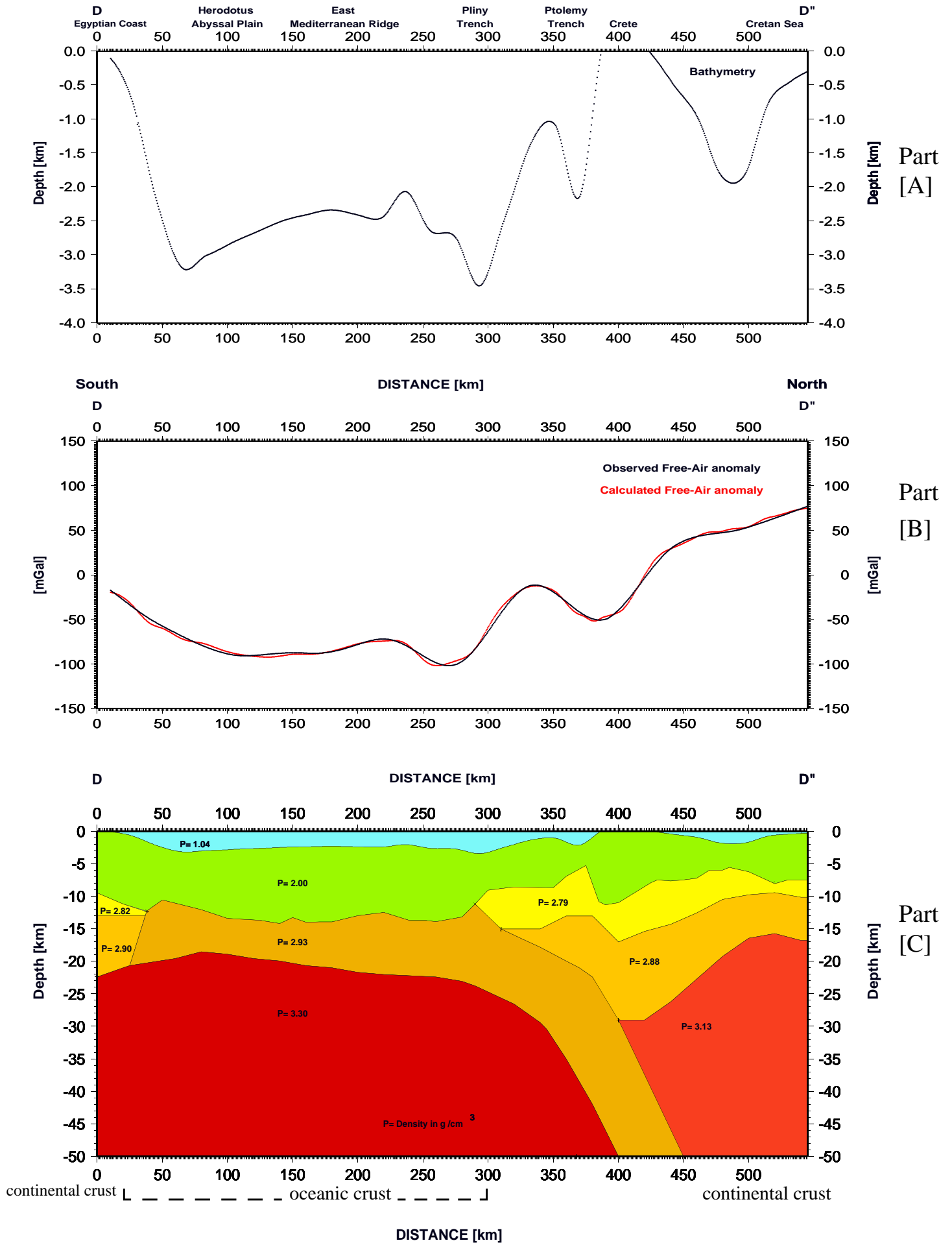


Figure 5.6: The final results of two-dimensional gravity modelling along profile D-D^{||} (Egypt-Crete-Santorin).

Herodotus Abyssal Plain and beneath the East Mediterranean Ridge. A thin layer of sediment with a thickness of about 5-7 km overlays the Aegean continental crust. The Moho depth at the Egyptian coast is about 23 km. However in the Herodotus Abyssal Plain and beneath the East Mediterranean Ridge, the depth ranges between about 20 and 24 km, while the Moho depth is about 31 km beneath Crete. These results coincide with the seismic results obtained by Makris (1978 a), Hartung (1987), and Bohnhoff (2000).

The transition from the continental to oceanic crusts within the African plate is modelled to extend offshore to a distance of about 40 km from the Egyptian coast (Figure 5.6) according to the drilling information of the sedimentary sequences at the Egyptian coast (Said, 1962), and the results of refraction seismic experiments by Malovitskiy et al. (1975). The African oceanic crust has been subducted beneath the Island of Crete with degree angle of approximately 110 according to the main driving force for the opening of the Cretan Sea as assumed by Le Pichon and Angelier (1979). Furthermore, the subduction occurs at uniform speed along the Hellenic Arc and that it was started because of the movement to the west of the Anatolian plate would have pushed in a SW direction the hypothetical Aegean plate as hypothesised by McKenzie (1972). In this hypothesis, to define it as a microplate, the Aegean zone should show a relatively rigid behaviour while it is clear that the Aegean Sea is actually a very deformed zone.

The East Mediterranean Ridge has been interpreted as an accretionary complex built up by off scrapping and piling of sediments deposited on top of the downgoing African plate as suggested by (Biju-Duval et al., 1978; Le Pichon et al., 1982 a; b and Truffert et al., 1993). The result of the two-dimensional gravity modelling along the profiles C-C^{||} and D-D^{||} confirm that the thickness of the accretionary complex is up to about 12 km at the East Mediterranean Ridge.

V.2. Three-dimensional gravity modelling

To get a better understanding of the crustal structure and the complicated geological structure of the investigated area and their relation to the adjacent areas, three-dimensional gravity modelling within the entire investigated area was performed using the software IGMAS. This program uses a polyhedral approach which makes it a very efficient tool for forward modelling in three dimensions. But the polyhedral approach aggravates a geometric inversion. The geometric layout is fixed and the inversion can only be calculated with respect to densities of the polyhedral in the model. In the following, a short summary is given of the methodical aspects of the three-dimensional gravity modelling equations and the calculation of the gravitational effect of a three-dimensional body as used in the program IGMAS (Götze, 1984; Götze and Lahmeyer, 1988).

V.2.1. Methodical aspects of the three-dimensional gravity modelling equations

The three-dimensional models consist of different bodies which are created as polyhedrons. The geometric layout of a polyhedron and the involved components are displayed in Figure 5.7. The polyhedrons are constructed of numerous vertices which are triangulated to form a triangle net.

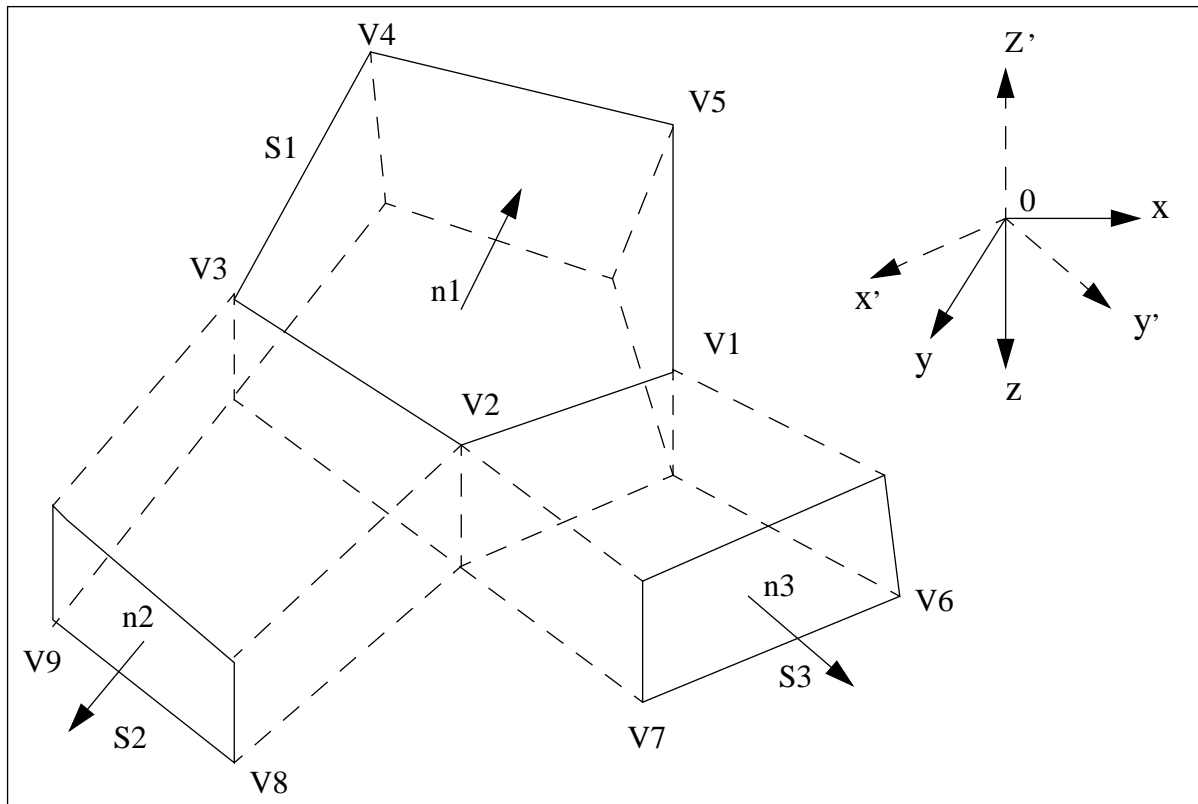


Figure 5.7: Geometric layout of a polyhedron (after Götze, 1984).

The analytical representation of the gravity effect of polyhedral bodies has been researched by many investigators (e.g. Paul (1974), Barnett (1976), and Götze and Lahmeyer, 1988). Most derivations consist of the same steps but result in different analytical expressions. The gravity effect g at an observation point caused by a homogenous polyhedron is represented as a volume integral:

$$g = f\rho \int_{Vol} \frac{\partial}{\partial z} \left(\frac{1}{r} \right) dv \quad (1)$$

with r the distance between the computation point and the volume dv . This volume integral is then transformed into a surface integral by application of Gauss' s divergence theorem:

$$g = f\rho \oint \cos(n, z) \frac{1}{r} ds \quad (2)$$

For a polyhedron the surface integral can be expressed as a sum of the contributions of each planar polygonal face S_i where the cosine term in formula (2) represents the outward normal, N_i of the element with respect to the z -axis.

$$g = f\rho \sum_{i=1}^m \left[\cos(n_i, z) \int \int_{S_i} \frac{1}{r} ds \right] \quad (3)$$

with facets S_i from $i = 1, \dots, m$, (m = total number of facets in the polyhedron). The next step is to transform into a new cartesian coordinate (x^1, y^1, z^1) system where the outward normal of facet S_i is concordant with new z^1 direction (see Figure 5.8). The final step is to convert the surface integral formula (3) into a line integral of a polygon limiting the facet S_i . The numerical result is conceived by inserting the limits of integration, which are the coordinates of the vertices of the polygon.

Götze and Lahmeyer (1988) and Götze (1984) developed a numerical solution for formula (1). An impression of the applied equations is provided in the following.

The attraction of a polyhedron of homogenous density ρ at a station P is based on the calculation of potential $U(P)$:

$$U(P) = f \int_{Poly} \frac{1}{R} dm \quad (4)$$

with $dm = \rho \, dx \, dy \, dz$ and R is the distance between the station P and dm . The vertical component of the gravity at the station, $g_z(P)$, is obtained by taking the derivative of the potential with respect to the z -component. This partial derivative can be reformulated into a surface integral:

$$\frac{\partial U}{\partial z}(P) = g_z(P) = f \rho \oint \cos(n, z) \frac{1}{R} dS \quad (5)$$

where the integral has to be calculated for the whole polyhedron surface and the cosine term determines the orientation of the surface element dS with respect to the cartesian coordinate system. For any polyhedron surface, S_j , $\cos(n_j, z)$ is constant and therefore the gravity effect of a polyhedron can be expressed via superposition of the effects of its whole surface:

$$g(P) = f \rho \sum_{j=1}^m \left[\cos(n_j, z) \oint_{S_j} \frac{1}{R} dS_j \right] \quad (6)$$

Götze and Lahmeyer then transformed the coordinate system for each surface (see Figure 5.7) for the geometry, so that the new x -axis, x^1 , is parallel to V_1V_2 , the new z -axis, z^1 , is parallel to the outward normal of the surface and the transformed y -axis, y^1 , is chosen to be orthogonal to x^1 and z^1 (x^1, y^1, z^1) = $\mathbf{TM}(x, y, z)$ and $(x, y, z) = \mathbf{TM}^T(x^1, y^1, z^1)$:

$$\mathbf{TM} = \begin{bmatrix} \alpha_1 & \alpha_2 & \alpha_3 \\ \beta_1 & \beta_2 & \beta_3 \\ \gamma_1 & \gamma_2 & \gamma_3 \end{bmatrix} \quad (7)$$

The surface integral now needs to be transformed into a line integral via polygon P_j limiting the surface S_j (see Figure 5.8 for the used syntax):

$$g(P) = f \rho \sum_{j=1}^m \cos(n_j, z) \left[\oint \frac{h_j}{r^2} \sqrt{(\overline{PP_j^*})^2 + r^2} dp_j + 2\pi \overline{PP^*} \delta \epsilon \right] \quad (8)$$

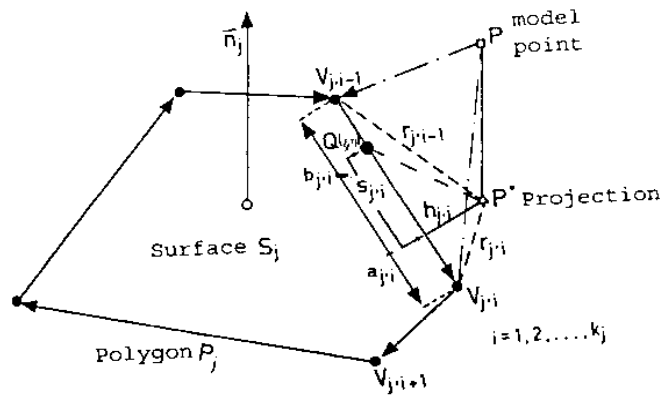


Figure 5.8: Geometric layout for the line integral (from Götze, 1984)

with $\delta = \begin{matrix} \nearrow & 0 \\ \searrow & 1 \end{matrix}$, if $P^* \begin{matrix} \nearrow & \notin S_j \\ \searrow & \in S_j \end{matrix}$

using k_j as the number of the sides in the current polygon the line in formula (8) can be evaluated to:

$$\tau = \sum_{i=1}^{k_j} \left[h_{j,i} \int_{a_{j,i}}^{b_{j,i}} \frac{\sqrt{PP_j^{*2} + h_{j,i}^2 + s_{j,i}^2}}{h_{j,i}^2 + s_{j,i}^2} ds_{j,i} \right] \quad (9)$$

with k_j number of sides of polygon P_j , $a_{j,i}$, $b_{j,i}$ limits of integration. The integral in (9) is of the general form:

$$I = \int \frac{\sqrt{H^2 + s^2}}{h^2 + s^2} ds \quad (10)$$

with $H > |h|$ and $H^2 = \overline{PP_j}^2 + h_{j,i}^2$ and $s^2 = s_{j,i}^2$. Substituting

leads to:

$$I = \int \frac{\frac{H}{2\sqrt{u}}(u+1)}{h^2 + \frac{H^2}{4u}(u-1)^2} \frac{H}{4} (u^{-\frac{1}{2}} + u^{-\frac{3}{2}}) du \quad (11)$$

which can be solved to:

$$I = \frac{1}{2} \left[\underbrace{\int \frac{u du}{z}}_A + \underbrace{\int \frac{2 du}{z}}_B + \underbrace{\int \frac{du}{uz}}_C \right] \quad (12)$$

$$\text{with } z = u^2 - 2u\lambda + 1 \quad \text{and } \lambda = 1 - \frac{2h^2}{H^2}.$$

using case differentiation the three integrals, A, B, C, in formula (12) can be solved, see Götze (1984) for the case differentiation. Finally the numerical formula for the attraction of a polygon and the gravity g in point P , caused by a polyhedron can be written as:

$$g(P) = f\rho \left[\sum_{j=1}^m \cos(n_{j,z}) \left[\sum_{i=1}^k h_{j,i} \left[T_1 + \frac{|\overline{PP_j^*}|}{h_{j,i}} (T_2 - T_3) \right] + 2\pi |\overline{PP_j^*}| \delta\epsilon \right] \right] \quad (13)$$

with

$$\begin{aligned} \tau_1 &= \ln \frac{b_{j,i} + \overline{PV_{j,i-1}}}{a_{j,i} + \overline{PV_{j,i}}} \\ \tau_2 &= \arctan \frac{r_{j,i-1}^2 + b_{j,i} \overline{PV_{j,i-1}}}{|\overline{PP_j^*}| |h_{j,i}|} \\ \tau_3 &= \arctan \frac{r_{j,i}^2 + a_{j,i} \overline{PV_{j,i}}}{|\overline{PP_j^*}| |h_{j,i}|} \end{aligned}$$

and

$$\delta = \begin{cases} 0 \\ 1 \end{cases}, \text{ if } P^* \begin{cases} \notin S_j \\ \in S_j \end{cases}$$

V.2.2. Brief description of the preparation of the model input according to IGMAS

IGMAS is an interactive graphical computer system for the interpretation of potential fields by means of numerical modelling (Götze, 1978; Götze, 1984; Götze and Lahmeyer, 1988). In order to assemble the body, a system to name and position the different planes needs to be developed. The polyhedron is organized using the coordinates of the vertices and by the assembly of the vertices to form the facets of the polyhedron. Okabe (1979) suggested a way in which all vertices are numbered and the vertex coordinates should be stored by number. Every facet is defined by the vertex numbers in anti-clockwise order about the outward facet normal. This approach is very time-consuming. Another complex question is how to fill all the space in the model with multiple polyhedron without gaps or overlaps.

Götze and Lahmeyer (1988) provided a practical approach which is used in their program IGMAS. The model is divided into parallel planes. The user defines the geological structures in each planar section and the polyhedral bodies are automatically assembled between the sections using a triangulation algorithm. This is shown in Figure 5.9.

In general, for the input of the structures to be modelled, a number of vertical planes suitable to represent the geometry were identified. In addition, either all closed unit polygons including their density indices on these vertical planes or all open lines including their density indices right and left were also identified. The necessary definitions are only two-dimensional. The final construction of the three-dimensional structures (i.e. triangulation between the vertical planes) was automatically done by IGMAS.

An IGMAS structure requires the use of vertical planes, which are used to define the location of the vertex coordinates. These vertical planes are always parallel to each other, but the distance between them is variable. In order to achieve the greatest flexibility, these vertical planes should be defined perpendicular to the dominating strike direction of the structures to be modelled. The vertical planes should have small distances where high variation of the geometry is expected.

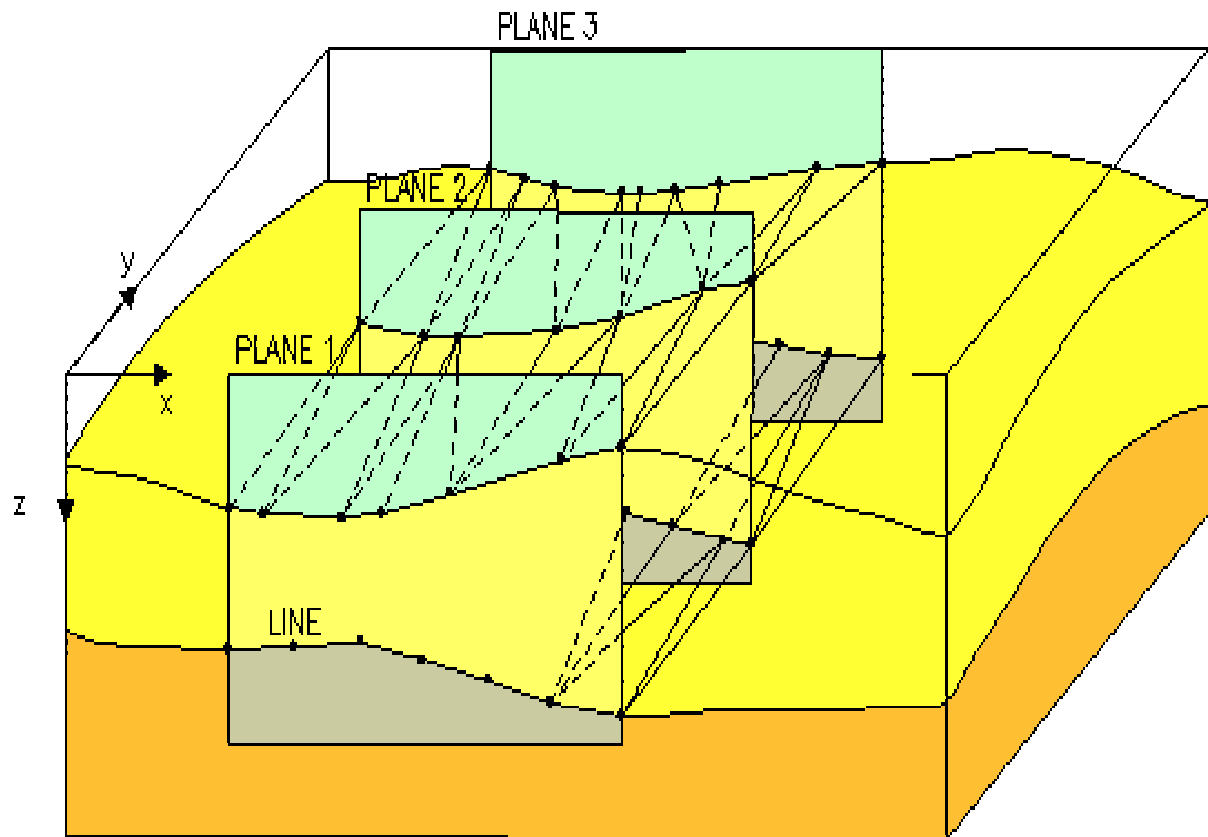


Figure 5.9: Polyhedral assembly using triangulation as used in IGMAS (from Götze, 1984) .

V.2.3. The area of three-dimensional gravity model

The area of three-dimensional gravity model is displayed in Figure 5.10. This area covers the whole subduction area and shows the model geometry of the contact between the African and Eurasian plate, and is selected as a part containing main tectonic and geological structures of the investigated area, i.e, Hellenic arc, Cretan Island Arc, East Mediterranean Ridge, Herodotus Abyssal Plain, and subduction trenches. Furthermore, it has a relatively dense distribution of seismic profiles, gravity anomalies, and variations of the bathymetric and topographic features.

The area of three-dimensional gravity model is located between 31.01° N and 36.49° N and was constructed along 18 parallel vertical planes extending from the coast of Egypt in NW direction. It crosses the main geological structures of the modelled area such as the Herodotus Abyssal Plain, bathymetric ridges Island arcs, subduction trenches, basins or major Seamounts. These planes are located at a distance of 50 km from each other. The distance between the different plane is small enough to resolve the existing structures and it is adequately large considering the immense size of the modelled area. Each vertical plane includes a part of the southeastern Mediterranean Sea region and the northern section of Egyptian coast.

The location of all the vertical planes and also the seismic profiles which can be directly used to constrain the modelled area is displayed in Figure 5.10. The vertical planes actually engaged for gravity modelling are displayed by green lines. The red lines represent the distribution of seismic profiles of the modelled area. The lateral extension along and beyond the vertical planes are marked by blue lines which are used to avoid edge-effects (see Figure 5.10). In general, the amount of lateral extension depends on the thickness of the modelled blocks, the difference between the mean density of the modelled blocks and the surroundings density, and on the desired high modelling precision. The reference density is determined in such a way, that the edge-effect is as small as possible. This signifies that the average difference between the model densities and the reference density is close to zero. If there are no edge-effects an arbitrary constant value may be added to all density values, but as a shift value is added, the densities given are relative values.

V.2.3.1. Accuracy and resolution of the modelled area

In general, the geometry of the modelled area was not changed during three-dimensional gravity modelling along the existing seismic profiles. It was only changed in some parts, modifications were required to keep the model smooth. The final geometry of the modelled area is

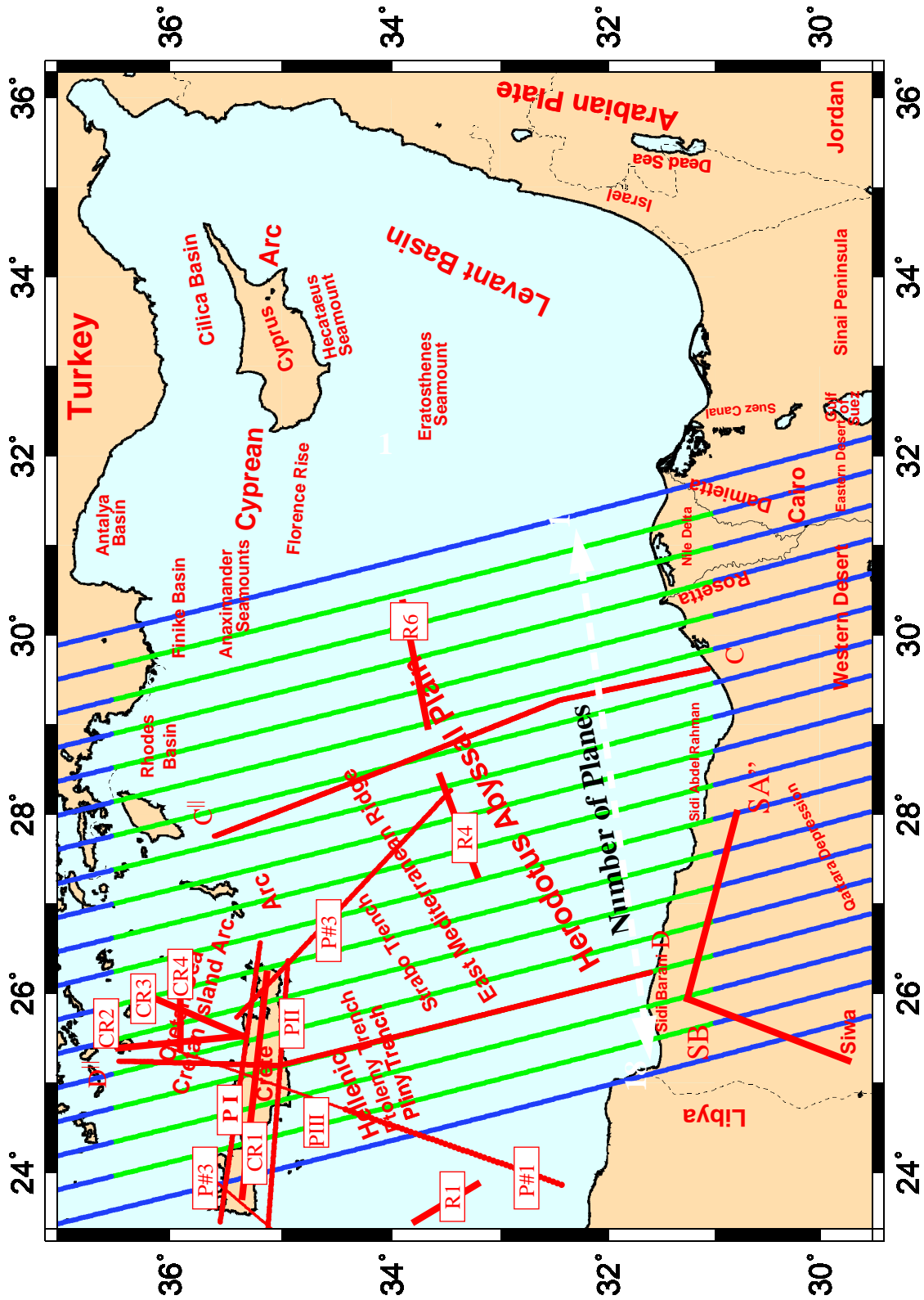


Figure 5.10: The area of three-dimensional modelling. The green lines depict the planes of gravity modelling. The blue lines describe the extension of the model which are necessary to avoid edge effect. The red lines mark the seismic profiles performed only on the modelled area (see Figure 4.1).

generally in agreement with the seismic structural data.

The results of the seismic profiles i.e. C-C^{||}, D-D^{||}, PI, PII, PIII, P#1, P#2, P#3 as shown in Figure 5.10 are used to constrain layer geometry and thickness of the three-dimensional gravity model and to provide initial estimates of the layer densities. Firstly, on the basis of seismic structural data, two-dimensional models were constructed. The profiles which are constrained by the seismic velocity model were duplicated several times and laterally extrapolated in both directions. Accordingly were determined sensitive velocity densities, providing the best fit between calculated and observed gravity anomalies. After the accomplishment, the appropriate gravity, and bathymetric data were appointed to the different vertical planes. The layer geometries of the profiles which are constrained by seismic data were kept fixed and the layer densities were iteratively adjusted until a satisfactory fit between the observed and the calculated anomalies was achieved.

In general, some problems occurred when attempting to integrate the seismic information into the three-dimensional gravity model. The seismic models were often very detailed and the different seismic layers may produce similar gravity effects. Such a detailed model which consists of numerous bodies causing almost the same gravity anomalies, is not sensible for gravity modelling.

The area of three-dimensional gravity model possesses a different resolution in the y- and in the x- direction. In the y-direction the distance between the vertical planes forming the model determines the resolution (Figure 5.10). In the modelled area, the defined distance between the planes is adequate to resolve the observed geological structures. In the x-direction, i.e. along the planes, the data density is approximately one kilometer. The gravity value is extracted from the data grids presented in Chapter III.1. In addition, the modelled area parameters are constrained by the bathymetric and topographic data. This is also extracted from the data grids presented in Chapter II.1.

Integration of the bathymetric and topographic features and seismic profiles has allowed for the construction of a perspective sketch of the modelled area as shown in Figure 5.11. According to this sketch the continental crust is modelled in a different way to the upper and lower continental crust. The modelled area reaches depth of 50 km. On the whole, this sketch of the modelled area consists of the sediment layer, upper continental crust, lower continental crust, oceanic crust, hot mantle, and mantle.

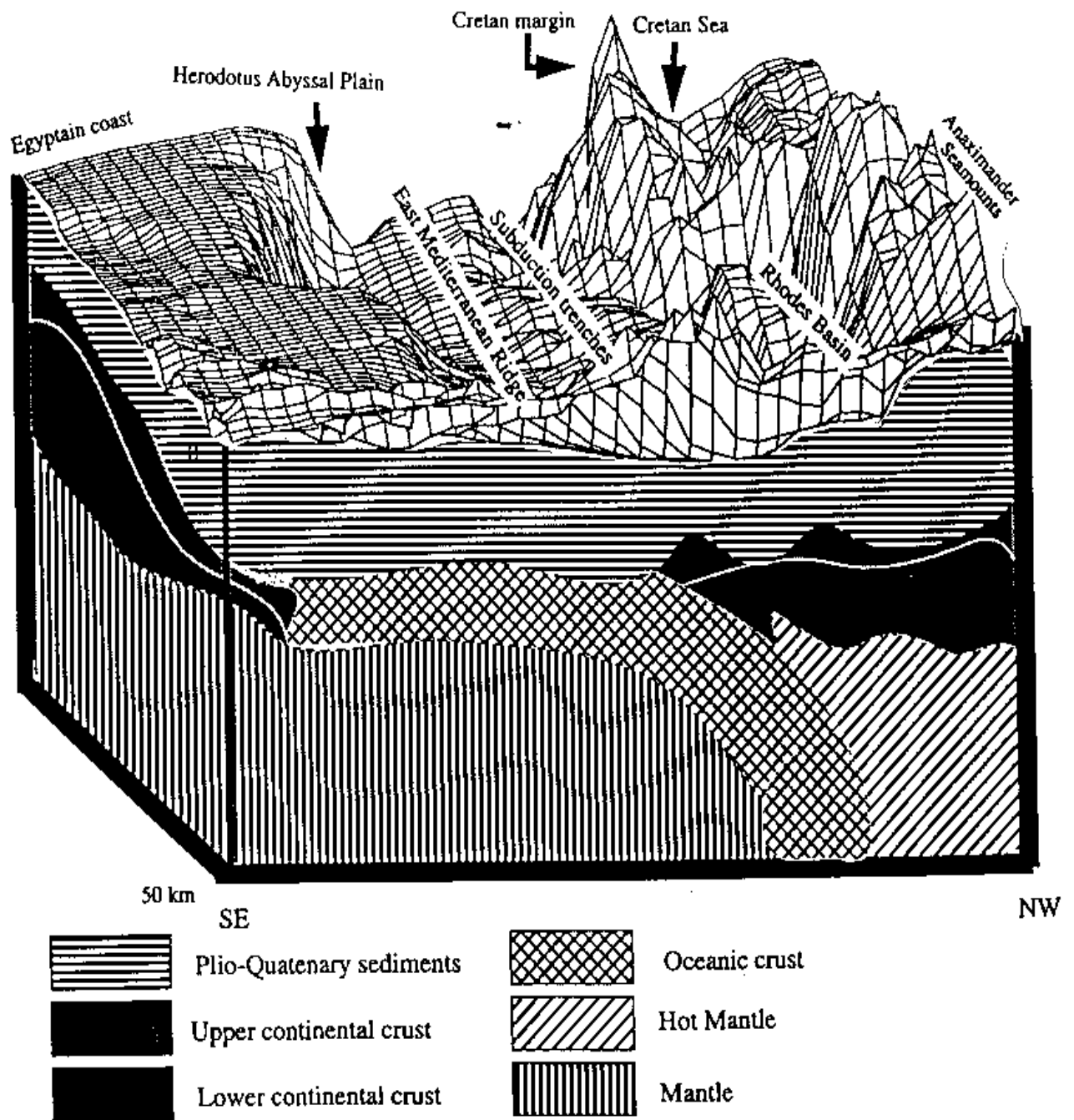


Figure 5.11: Interpretative 3D perspective sketch of the modelled area, based on the bathymetric and topographic features and seismic profiles.

V.2.3.2. Results of the area of three-dimensional gravity model

In the following, all the planes of the three-dimensional model area are presented. Planes 1 and 18 are the east-westward extension of the model. These planes prevent the occurrence of edge-effects. The actual gravity field modelling starts on plane 2. In general, in all the mentioned Figures 5.12 to 5.27, the vertical planes through the modelled area are shown in the lower part of the Figures, where the different densities have different colours. The calculated gravity curve is shown as a dotted black line, and the measured curve is shown as a red line in the upper part of the Figures.

Figures 5.12 and 5.13 show planes 2 and 3 respectively. These planes lie at most of eastern planes and cross the Nile Delta and the Anaximander Seamounts at the south-eastern and the north-western parts of the modelled area, respectively (Figure 5.10). As mentioned before, a shift value is added to the calculated anomalies and therefore the densities are relative values. The average thickness of the oceanic crust on planes 2 and 3 ranges from 25 to 30 km below Anaximander Seamounts respectively. The depth to the basement is about 16 km beneath the Nile Delta, However, the sedimentary layer thins rapidly towards the Anaximander Seamounts. The calculated and measured gravity curves show values around +70 to -131 mGal. A bathymetric high, causing a local gravity high, is located around 500 km. Underneath the East Mediterranean Ridge, the oceanic crust is markedly thin with a thickness of about 7-8 km. The Moho lies at a depth of about 22 km beneath Nile Delta, the Herodotus Abyssal plain and the East Mediterranean Ridge.

On planes 4 and 5 the upper and continental crust is significantly thickened at the north-western part around km 500 as shown in Figures 5.14 and 5.15. The average thickness of the oceanic crust on planes 4 and 5 is about 22 km below Rhodes Basin. Planes 4 and 5 cross the Nile Delta and Egyptain coast and Rhodes Basin at the south-eastern and the north-western parts of the modelled area, respectively (Figure 5.10).

Observed more closely, planes 4 and 5 show very smooth gravity curves and the gravity values decrease abruptly towards the Rhodes Basin at 550 km. Negative gravity reaches -208 mGal at Rhodes Basin and can probably be related to significant crustal thickening (see Figure 5.15). There are local gravity lows also at the East Mediterranean Ridge at 400 km on plane 4. The sedimentary layer shows its normal thickness for the modelled area. Furthermore, the continental crust layers are almost parallel. The Moho lies at a depth of about 22 km at the Egyptian coast and then increases to a depth of about 25 km beneath the East Mediterranean Ridge.

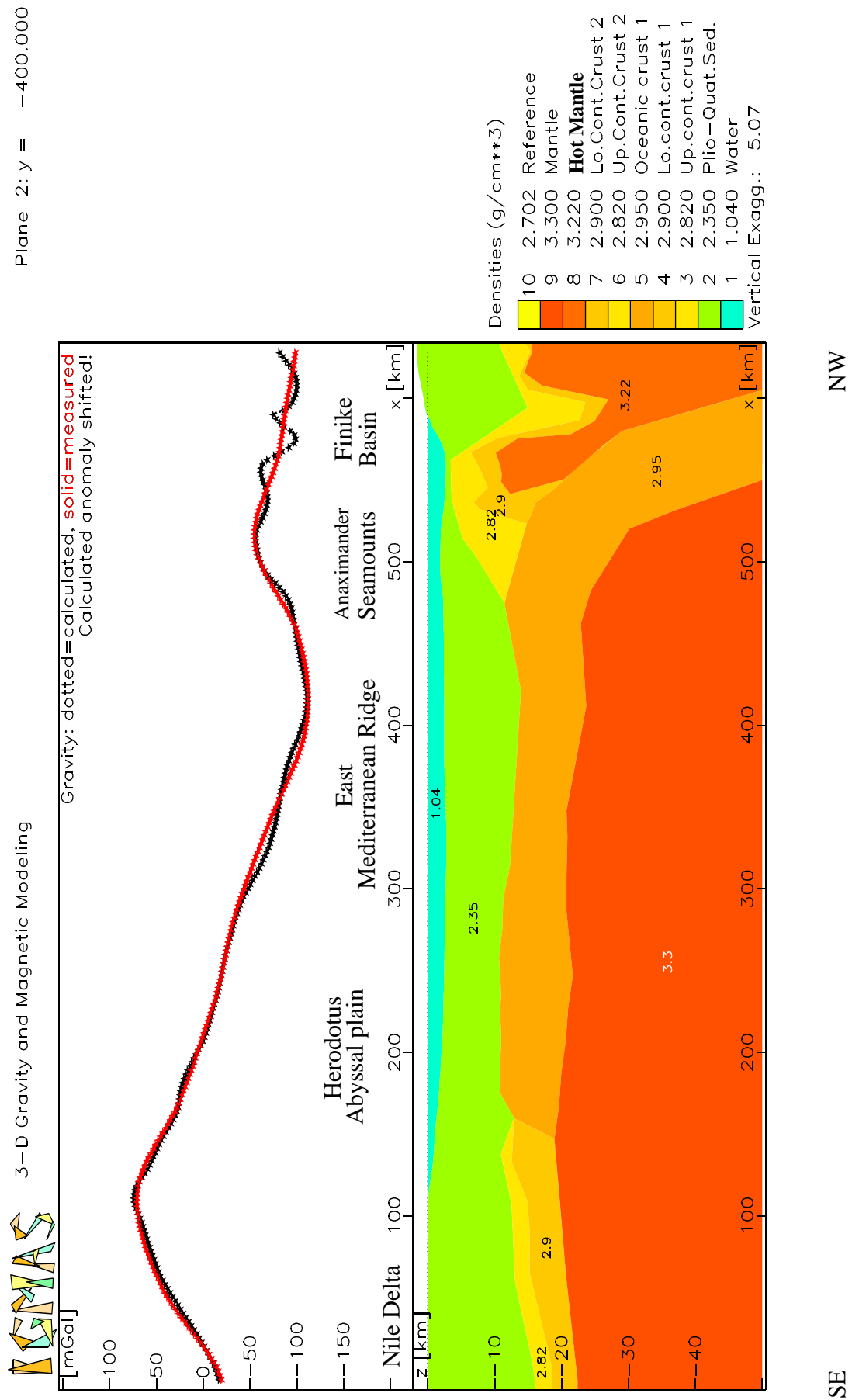


Figure 5.12: The final results of the vertical plane 2 through the three-dimensional gravity model and the related Free-Air anomaly.

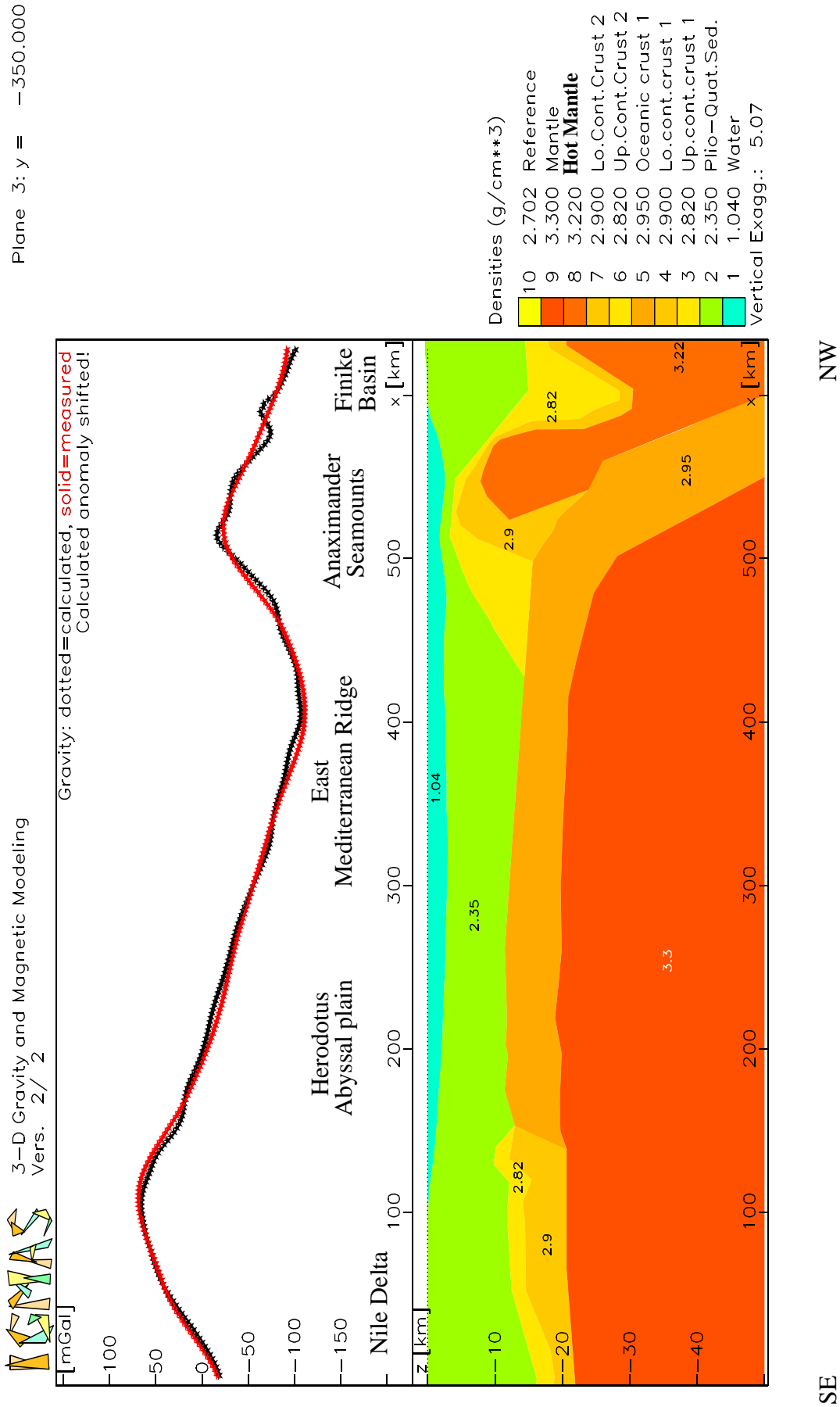


Figure 5.13: The final results of the vertical plane 3 through the three-dimensional gravity model and the related Free-Air anomaly.

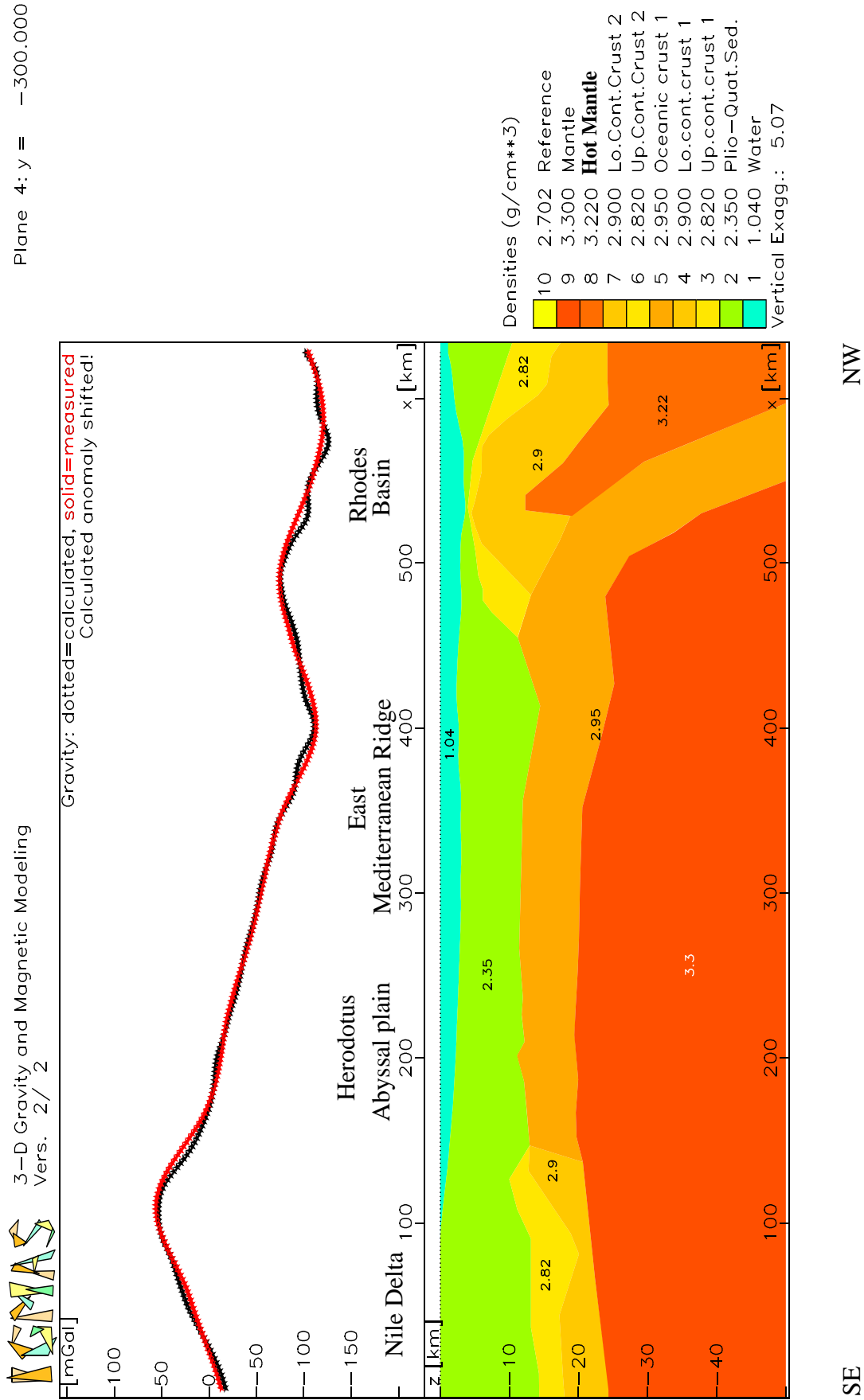


Figure 5.14: The final results of the vertical plane 4 through the three-dimensional gravity model and the related Free-Air anomaly.

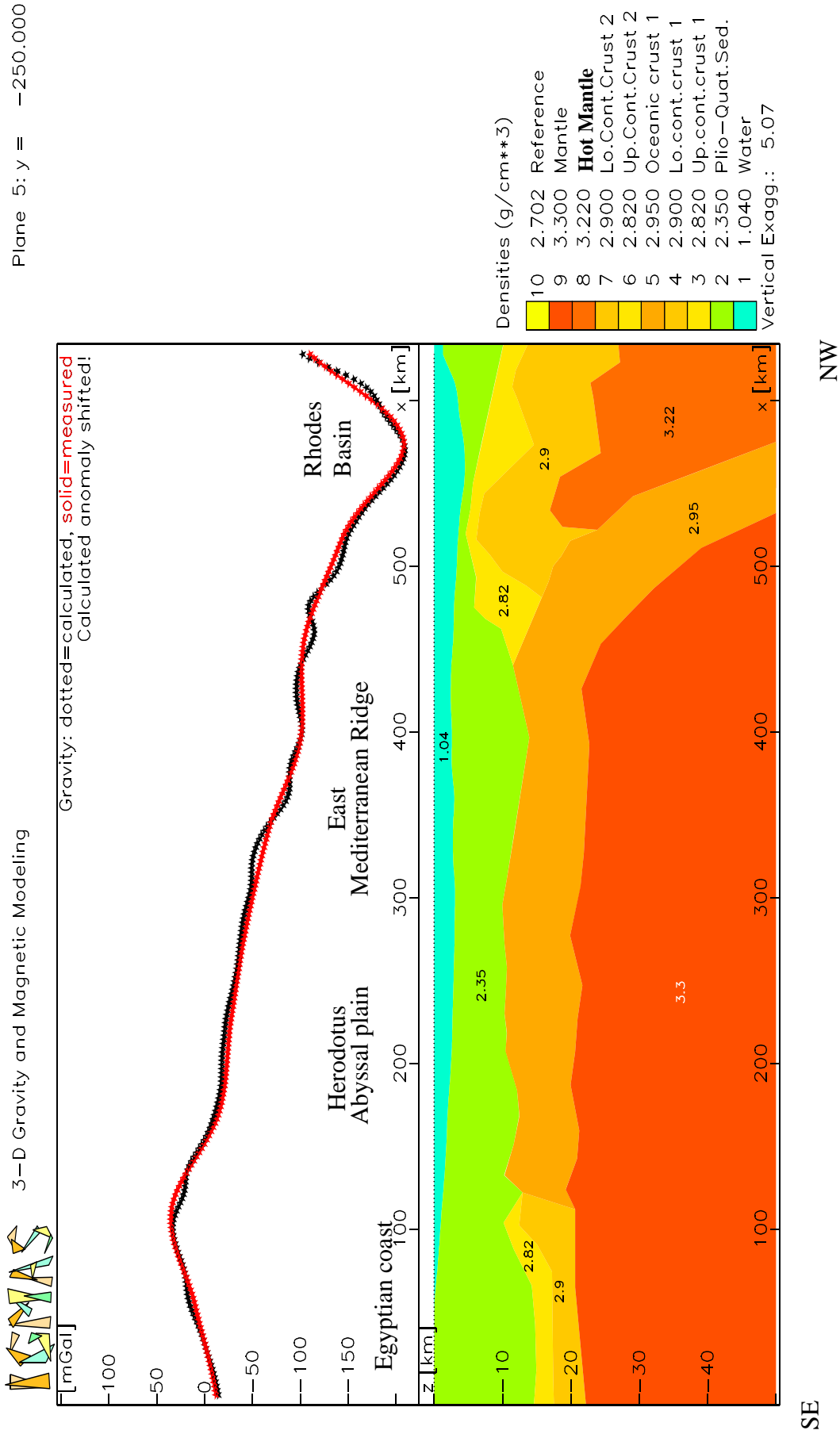


Figure 5.15: The final results of the vertical plane 5 through the three-dimensional gravity model and the related Free-Air anomaly.

On planes 6 and 7 as shown in Figures 5.16 and 5.17, respectively, the calculated and measured gravity curves show values around +12 to -186 mGal as shown in Figures 5.16 and 5.17, respectively. On plane 6 the sedimentary layer thins rapidly near 500 km towards the west flank of Rhodes. The Free-Air anomalies reflect the lateral variation of thickness in water layer. i.e. there are local gravity lows at the NW Rhodes Basin on plane 6.

On plane 7 the increase of a negative gravity anomaly at 400 km near the East Mediterranean Ridge corresponds with the relatively large thickness of the sedimentary layer. Plane 7 shows several undulations of the continental crust between 400 and 620 km. The oceanic crust is markedly thin underneath the East Mediterranean Ridge.

On plane 6 and 7 the Moho depth values are very considerable and correlate with the variations of gravity value. The Moho lies at a depth of about 25 km at the Egyptian coast, and then rises to about 19 km beneath the Herodotus Abyssal Plain. The Moho depth increases again to about 25 km below the East Mediterranean Ridge.

Plane 8 shows the same plateau in the gravity curve as plane 7 (see Figure 5.18). Near 400 km the sedimentary layer increases in thickness and causes a local gravity low. Above the continental crust at the south-eastern and the north-western parts on plane 8, the gravity curve shows only small variations around +55 mGal.

Plane 9 shows a very smooth gravity curve (see Figure 5.19). The calculated and measured gravity curves show values around +55 to -183 mGal. The depth to the oceanic crust is significantly increasing, at 350 km just before the oceanic crust starts to subduct with the continental crust. Along plane 9 there are alternatively high and low gravity curve with different gradients. This may reflect the effect of the difference in density between the continental crust and the sediment layer, and the effect of the bathymetric and topographic features. On plane 8 and 9 the Moho depth is about 22 km beneath the Herodotus Abyssal Plain and the East Mediterranean Ridge

In general, from planes 2 to 9, at the south-eastern part of the modelled area, the transition from continental to oceanic crust within the African plate was modelled at a distance between 100 and 150 km from the Egyptian coast. At the north-western part of the modelled area, the transition between the oceanic and continental crust occurs between 400 to 450 km through these planes.

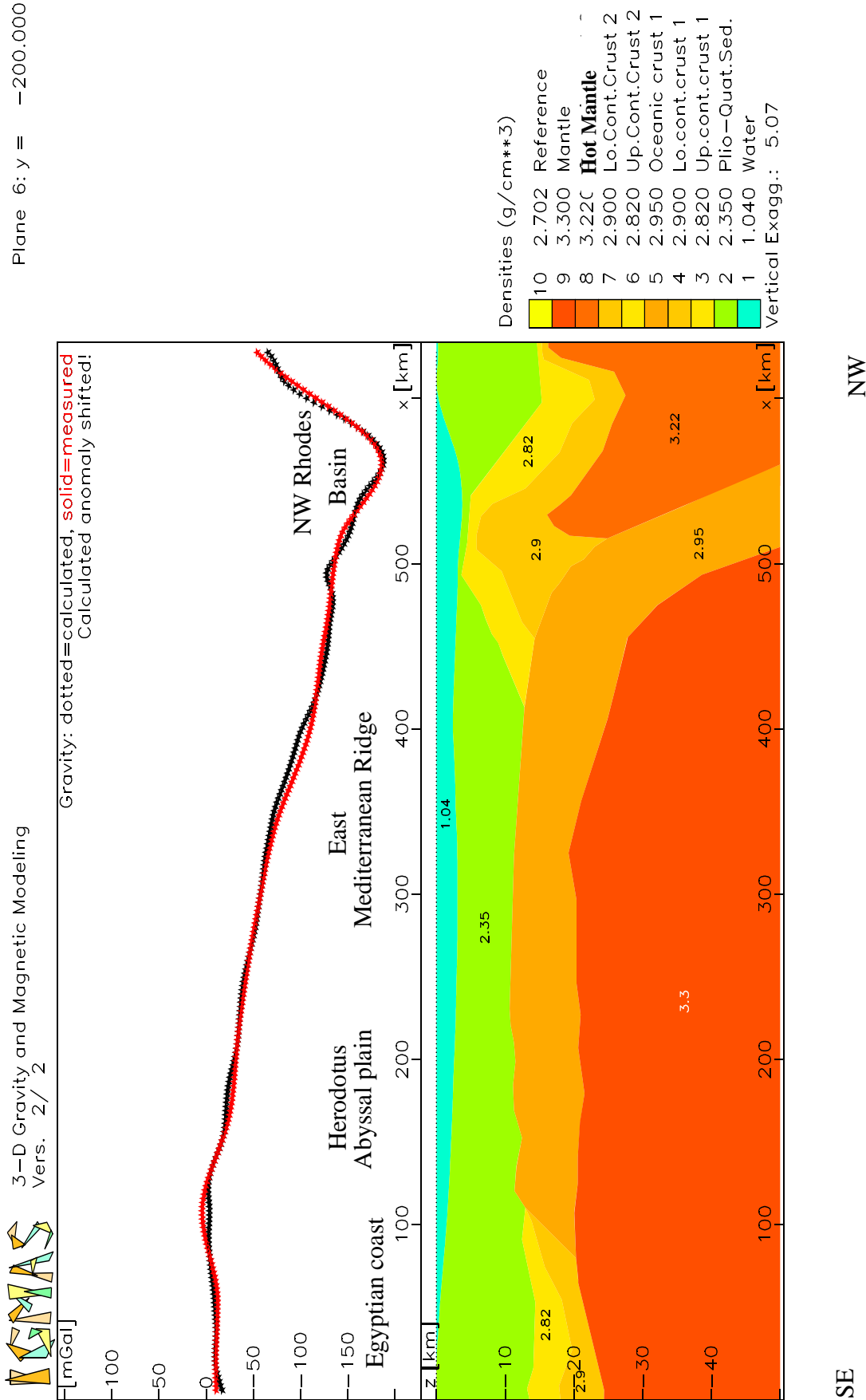


Figure 5.16: The final results of the vertical plane 6 through the three-dimensional gravity model and the related Free-Air anomaly.

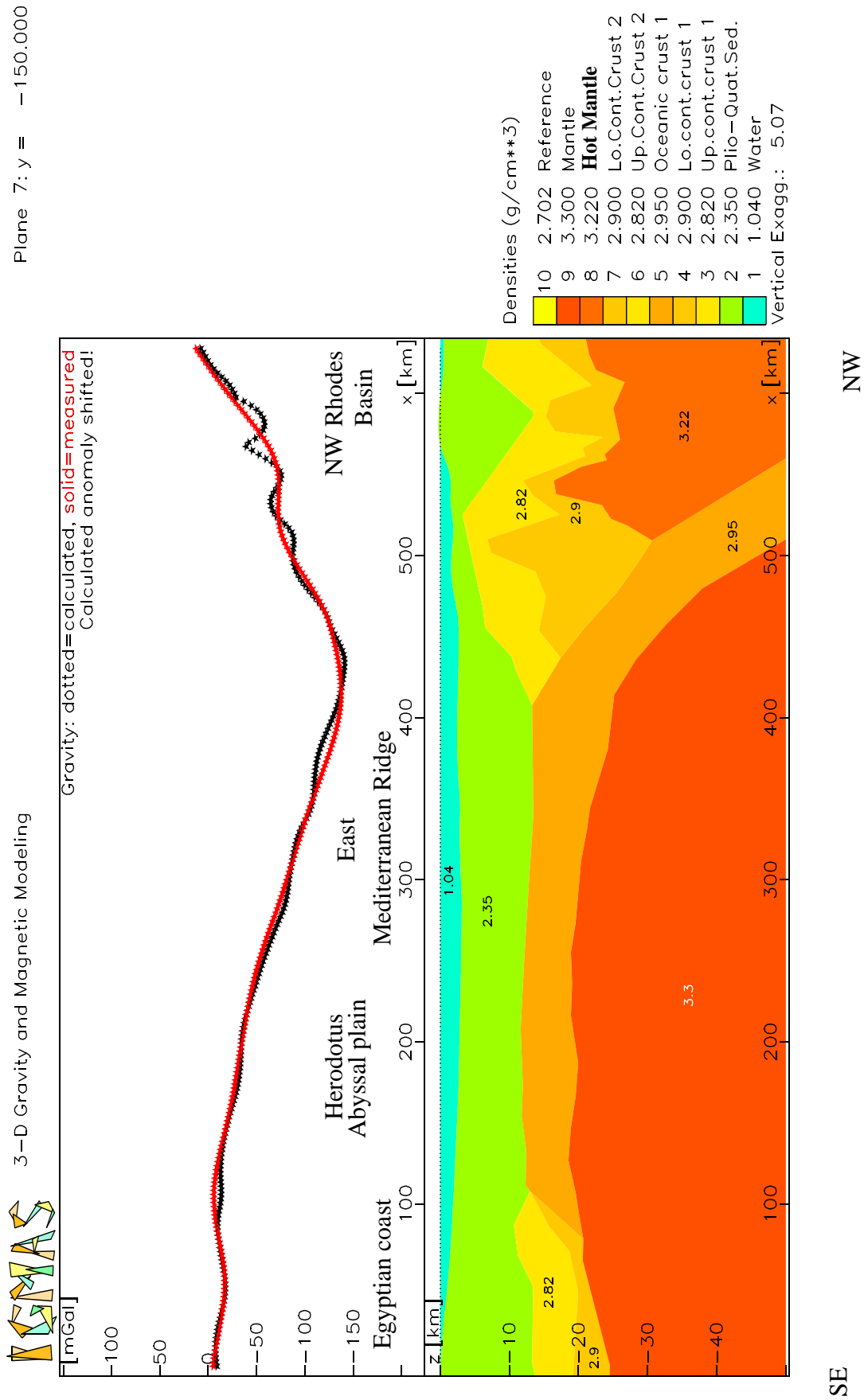


Figure 5.17: The final results of the vertical plane 7 through the three-dimensional gravity model and the related Free-Air anomaly.

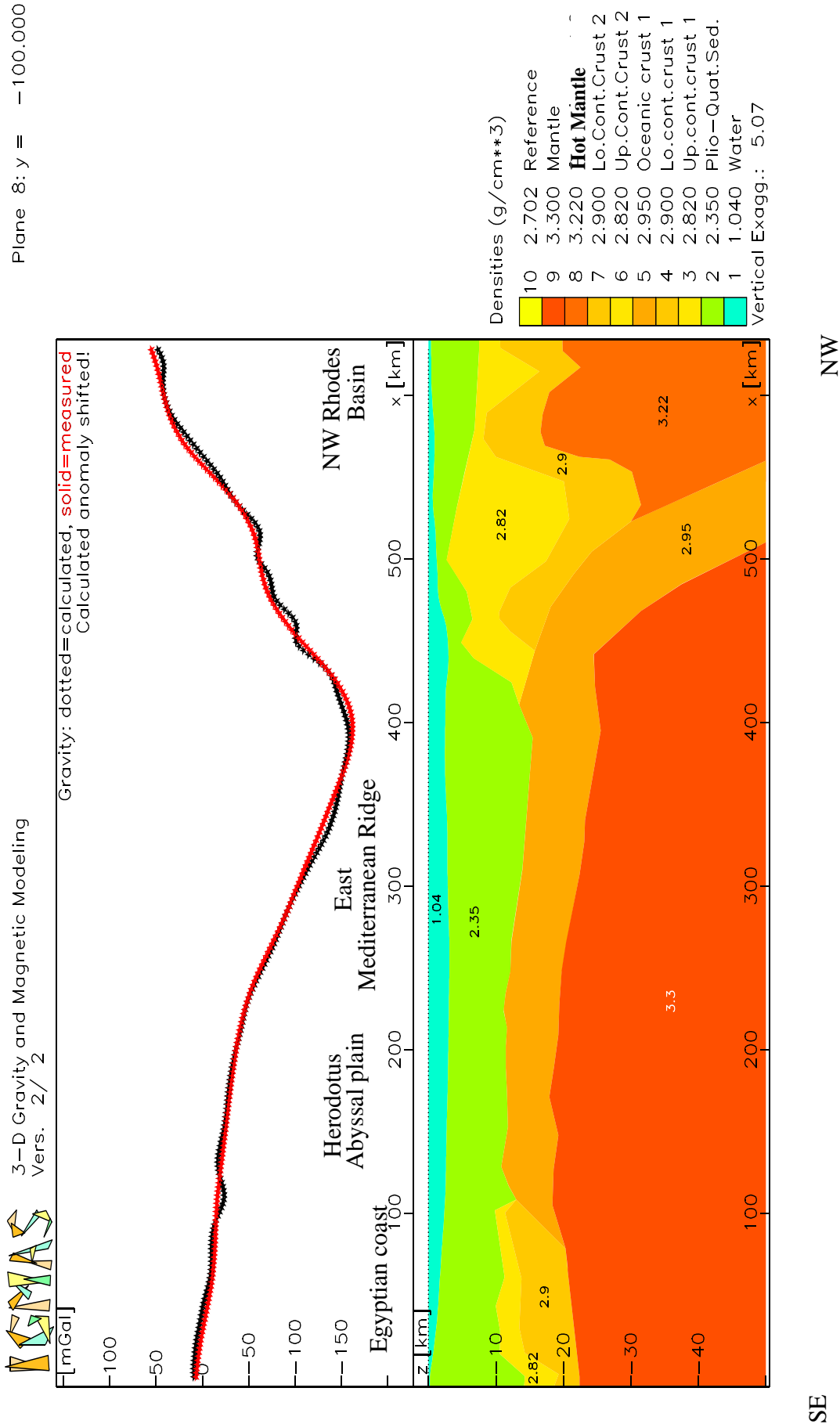


Figure 5.18: The final results of the vertical plane 8 through the three-dimensional gravity model and the related Free-Air anomaly.

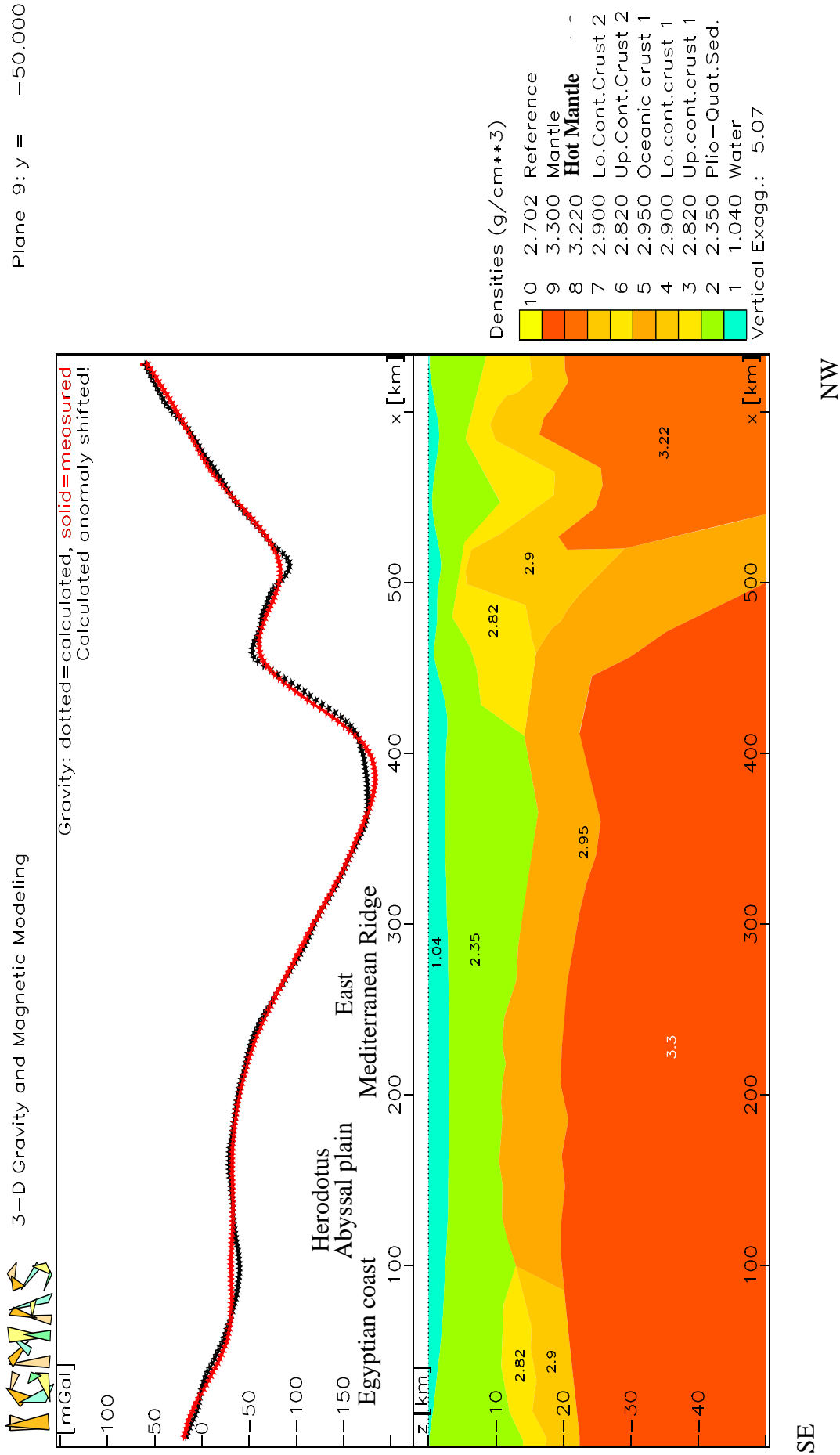


Figure 5.19: The final results of the vertical plane 9 through the three-dimensional gravity model and the related Free-Air anomaly.

Figures 5.20 and 5.21 show planes 10 and 11 respectively. These planes start from the Egyptian coast and cross the Herodotus Abyssal Plain, the East Mediterranean Ridge, the subduction trenches, Island arcs, and Cretan Sea (see Figure 5.10). The calculated and measured gravity curves show values around +70 to -190 mGal. Near 390 km, towards the East Mediterranean Ridge, the sedimentary layer increases in thickness and causes a gravity low. In addition, this layer is markedly thin towards the Herodotus Abyssal Plain and subduction trenches.

The gravity curves show high and low values towards the Herodotus Abyssal Plain, and the Egyptian coast on planes 10 and 11. This may reflect the effect of the variation of the basement geometry, and the effect of the bathymetric and topographic features. The gravity values decrease abruptly towards the Strabo Trench due to significant crustal thickening. Above the continental crust at the north-western part on the planes 10 and 11, the gravity curve shows small variations around +70 mGal. The oceanic crust is significantly thickened between 390 and 440 km, towards subduction trenches, and resulting in a gravity low.

Figures 5.22 and 5.23 show planes 12 and 13 respectively. These planes start from the Egyptian coast and cross the main geological structures of the modelled area such as the Herodotus Abyssal plain, the East Mediterranean Ridge, the subduction trenches, Island arcs, and Cretan Sea (Figure 5.10). The calculated and measured gravity curves show values around +85 to -176 mGal. A prominent minimum of -176 mGal is located at Strabo Trench. The gravity values rise to +85 mGal at Crete region and exhibit very sharp edges. At the north-western part, the continental crust is markedly thickened towards Crete region (see Figures 5.22 and 5.23).

Through planes 10, 11 and 12 the transition from continental to oceanic crust within the African plate was observed more closely and modelled offshore to a distance of about 40 km from the Egyptian coast. At the north-western part of the modelled area, the transition between the oceanic and continental crust through these planes occurs between 300 to 350 km.

From the Egyptian coast, the transition from continental to oceanic crust within the African plate decreases in a distance from 100 km through plane 9 to 40 km on plane 10. However the transition from continental to oceanic crust within the African plate increases from 40 km through plane 12 to 100 km on plane 13.

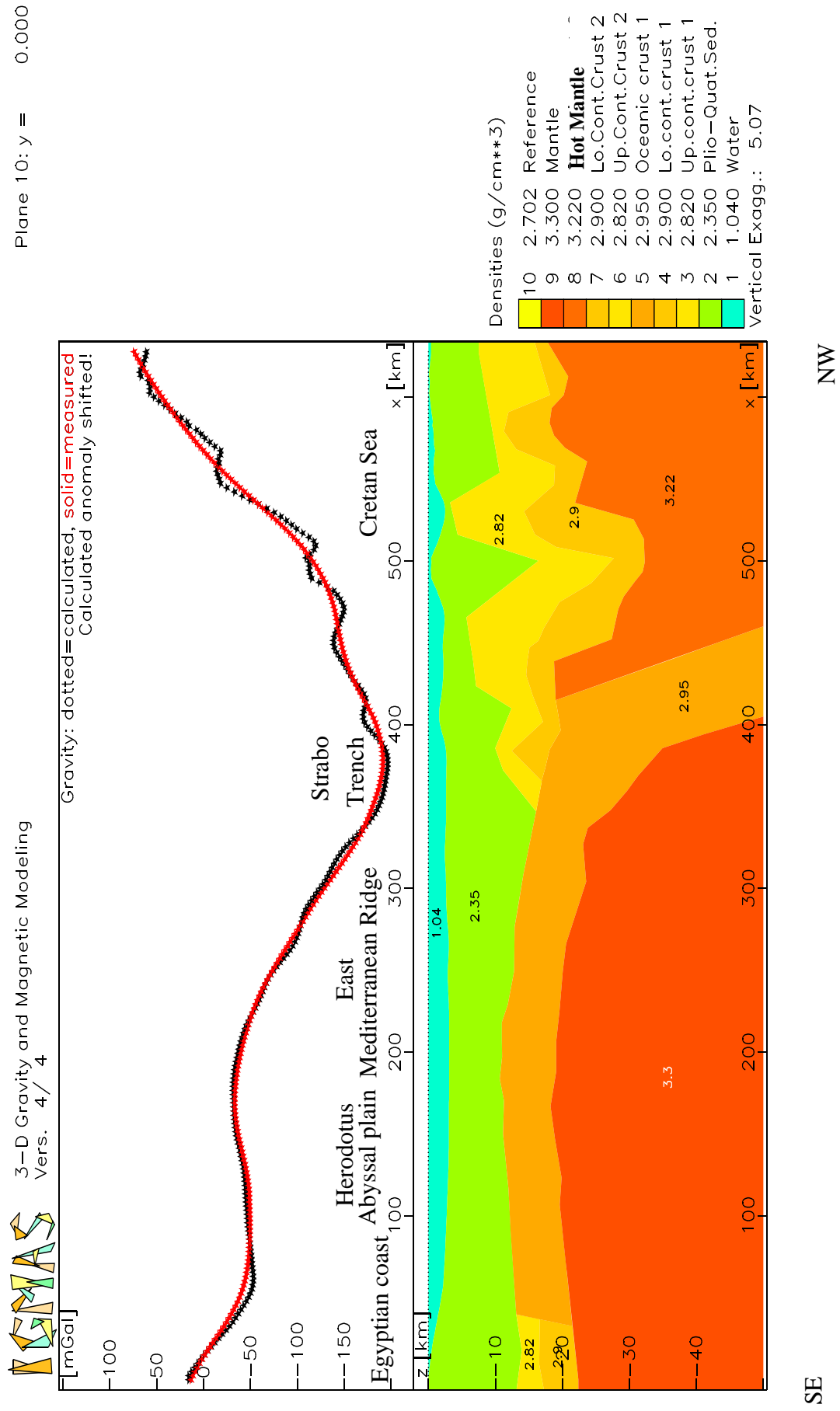


Figure 5.20: The final results of the vertical plane 10 through the three-dimensional gravity model and the related Free-Air anomaly.

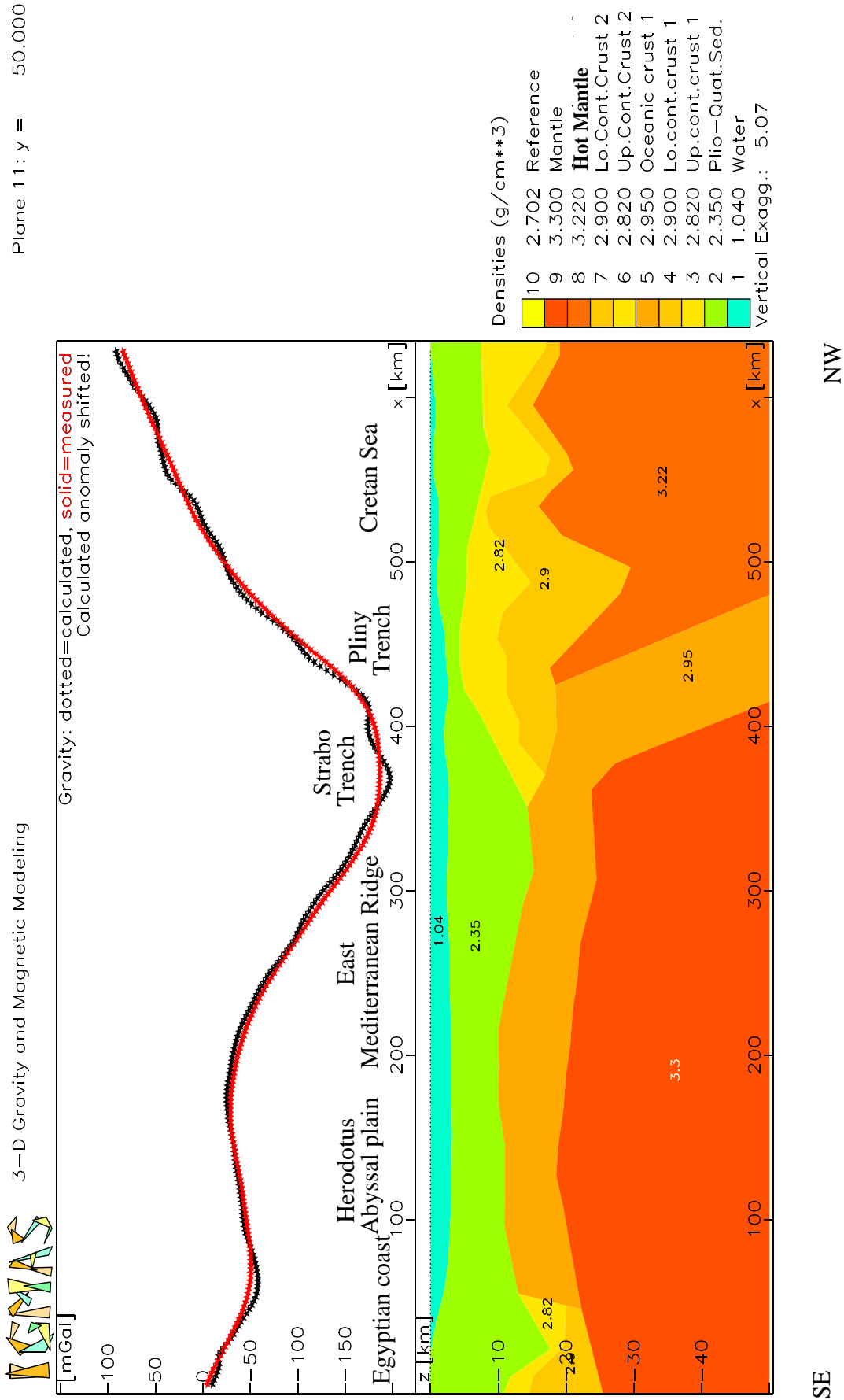


Figure 5.21: The final results of the vertical plane 11 through the three-dimensional gravity model and the related Free-Air anomaly.

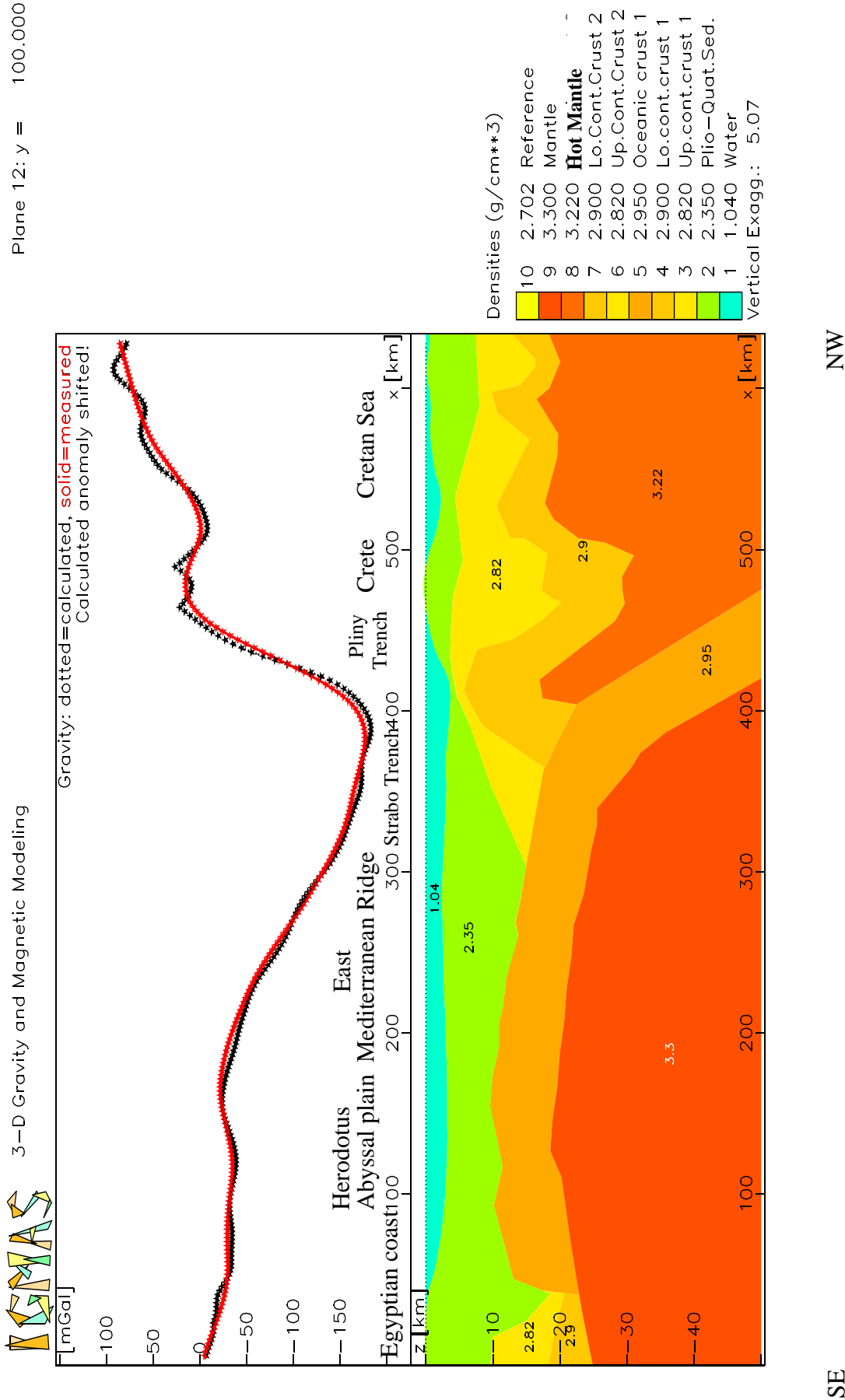


Figure 5.22: The final results of the vertical plane 12 through the three-dimensional gravity model and the related Free-Air anomaly.

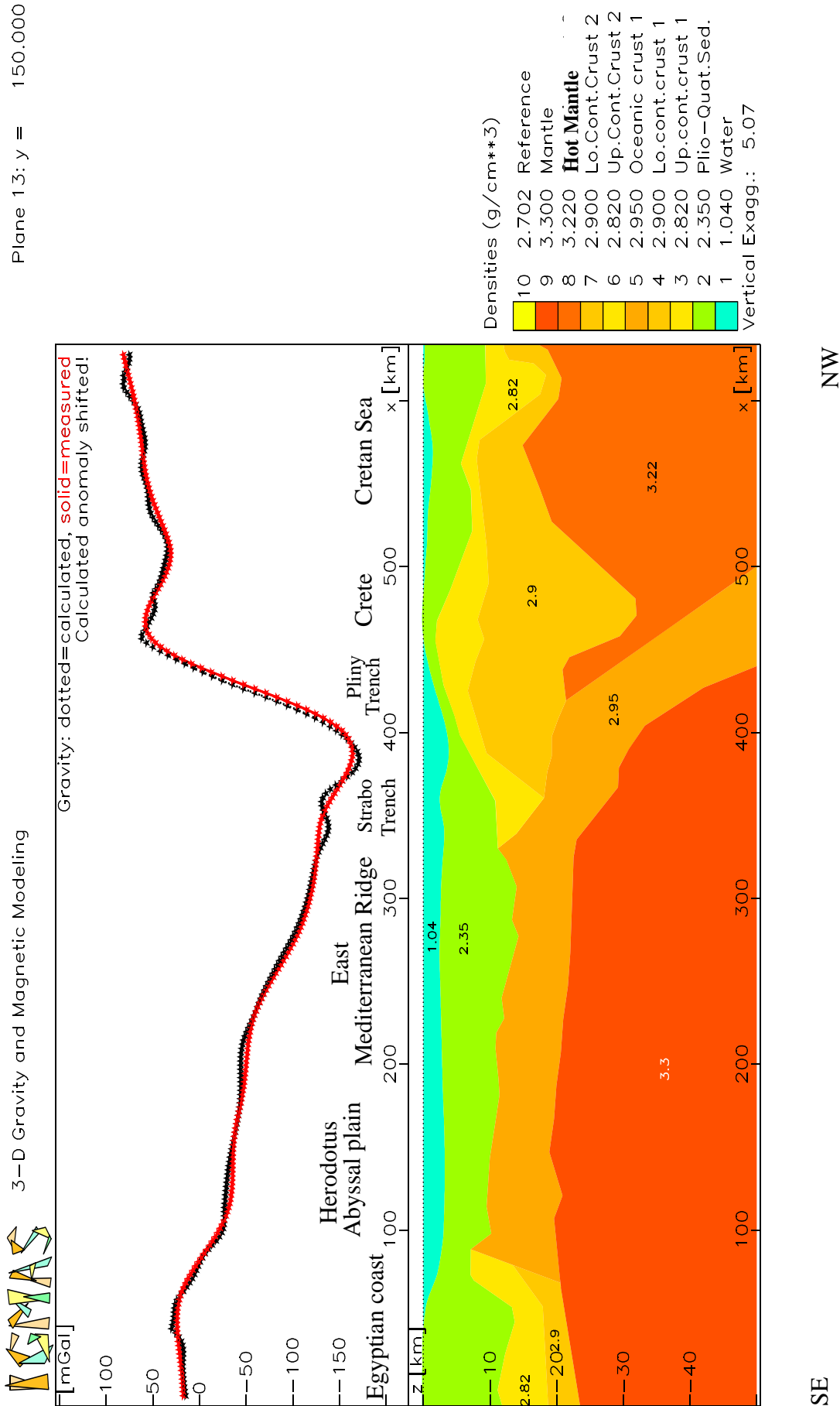


Figure 5.23: The final results of the vertical plane 13 through the three-dimensional gravity model and the related Free-Air anomaly.

Planes 14 and 15 as shown in Figures 5.24 and 5.25 respectively, show several undulations of the oceanic crust between 100 and 350 km. Several undulations of the mantle layer between 100 and 350 km can be also observed. The calculated and measured gravity curves show values around +86 to -107 mGal. Plane 14 shows the same plateau in the gravity curve as plane 15.

At about 475 km the layers of the continental crust well up and cause a high gravity curve. In addition, the gradient of the gravity values comparatively higher above the continental crust than over the oceanic crust. Between 330 and 450 km, the subduction trenches such as Pliny and Ptolemy trenches are visible through the planes 14 and 15. These trenches causes a minimum of -107 mGal. A thin layer of sediments overlaying the continental crust can be observed towards Crete Island.

Planes 14 and 15 start from the Egyptian coast and cross the Herodotus Abyssal Plain, the East Mediterranean Ridge, subduction trenches, Island arcs, Crete, and Cretan Sea (Figure 5.10).

Figures 5.26 and 5.27 show planes 16 and 17 respectively. These planes are located at the most of the western planes and cross the Egyptian coast and the Crete region at the south-eastern and the north-western parts of the modelled area respectively (Figure 5.10). The calculated and measured gravity curves show values around +102 to -114 mGal. A negative gravity curve between 100 and 400 km coincides with a thickening of the sedimentary layers through the planes. There are high gravity values above the continental crust towards the Crete region. This may reflect the effect of the bathymetric and topographic features.

Strong undulations of the oceanic crust are observed towards the Herodotus Abyssal Plain and the East Mediterranean Ridge through this planes. In addition, the oceanic crust is substantially thickened near 100 km through the plane 16. The continental slop features a striking elevation of the sediment layer beneath the Herodotus Abyssal Plain and the Crete region. This causes a high gravity curve.

When considering the advantages and disadvantages of the three-dimensional compared with the two-dimensional models, the following factors, which are sometimes disregarded, should be remembered with regard to the fitting and resolution of the models. In general, three-dimensional models provide more flexibility but are very hard to build. Some advantages of the three-dimensional models are shown, for example the image of the subsurface structure can be more realistic. Moreover, the description of three dimensional model geometry is simple and

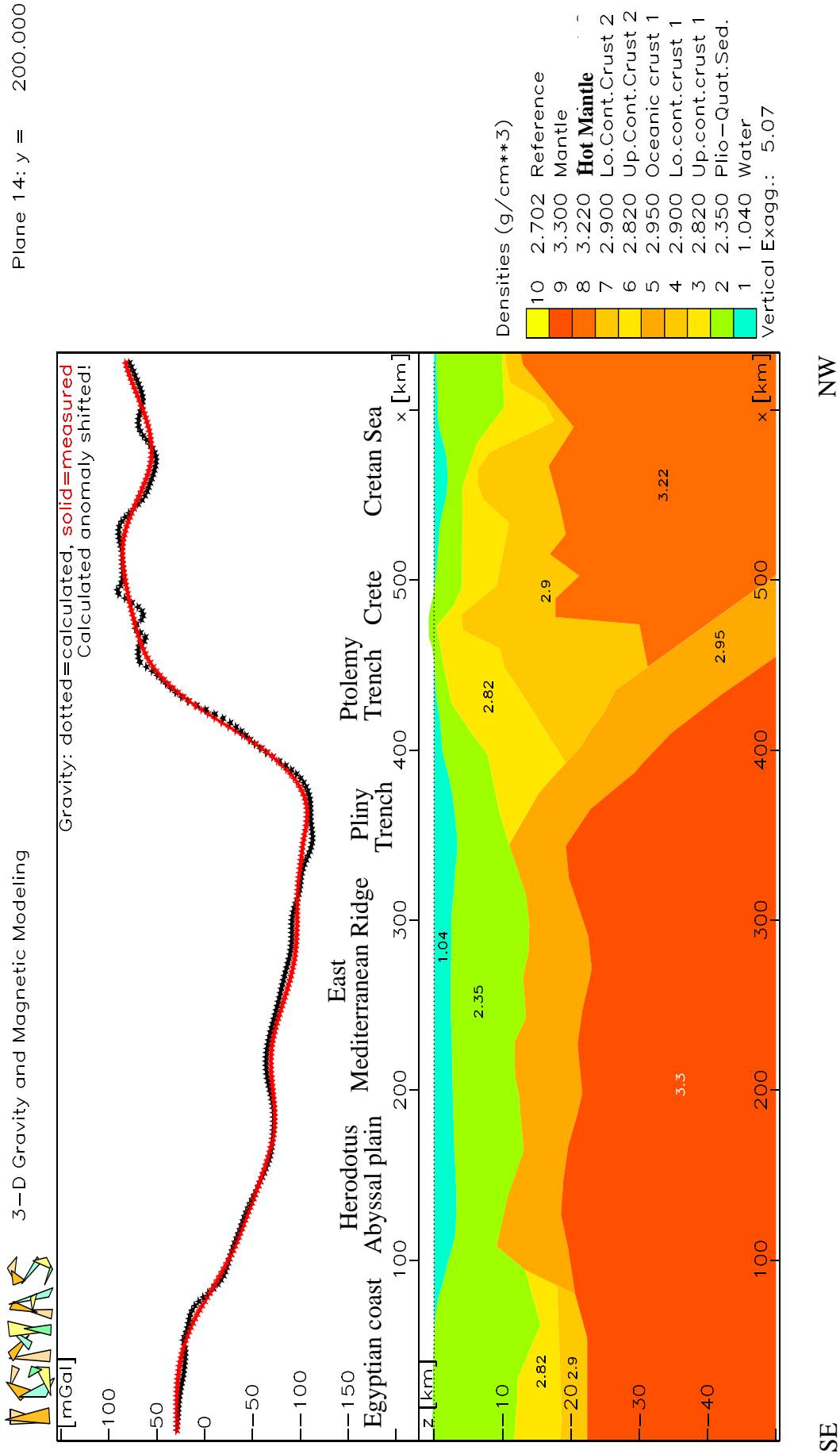


Figure 5.24: The final results of the vertical plane 14 through the three-dimensional gravity model and the related Free-Air anomaly.

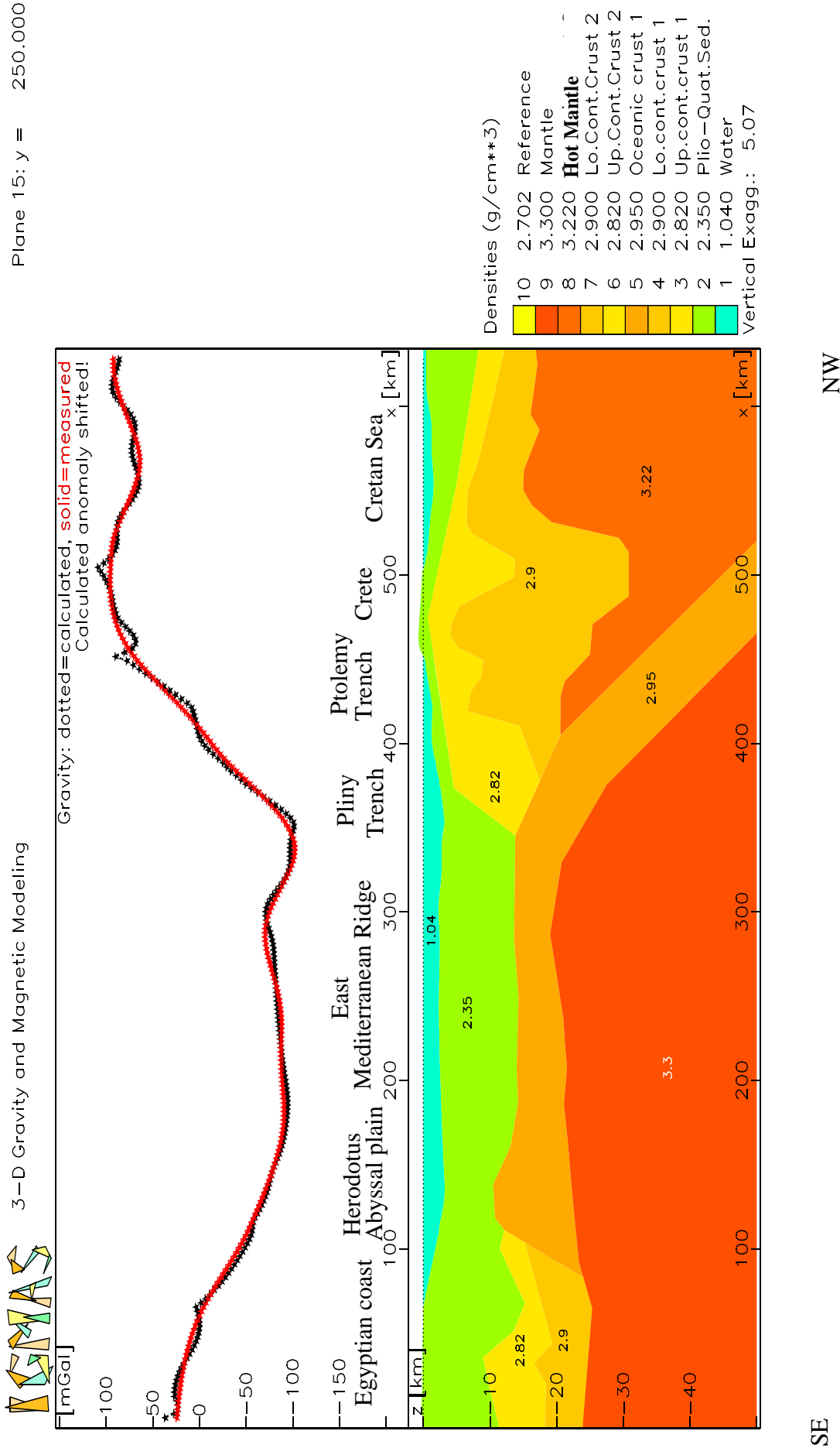


Figure 5.25: The final results of the vertical plane 15 through the three-dimensional gravity model and the related Free-Air anomaly.

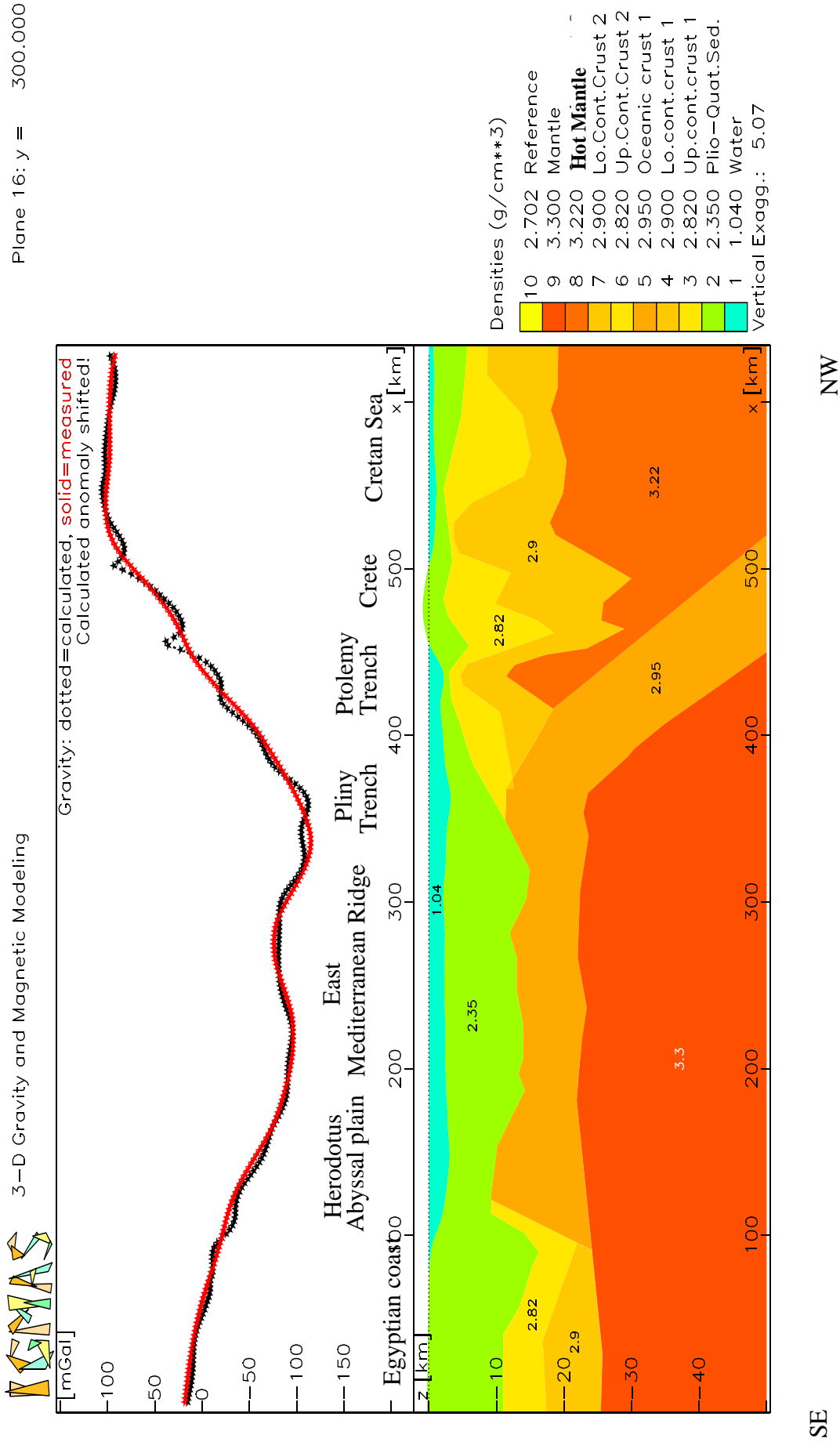


Figure 5.26: The final results of the vertical plane 16 through the three-dimensional gravity model and the related Free-Air anomaly .

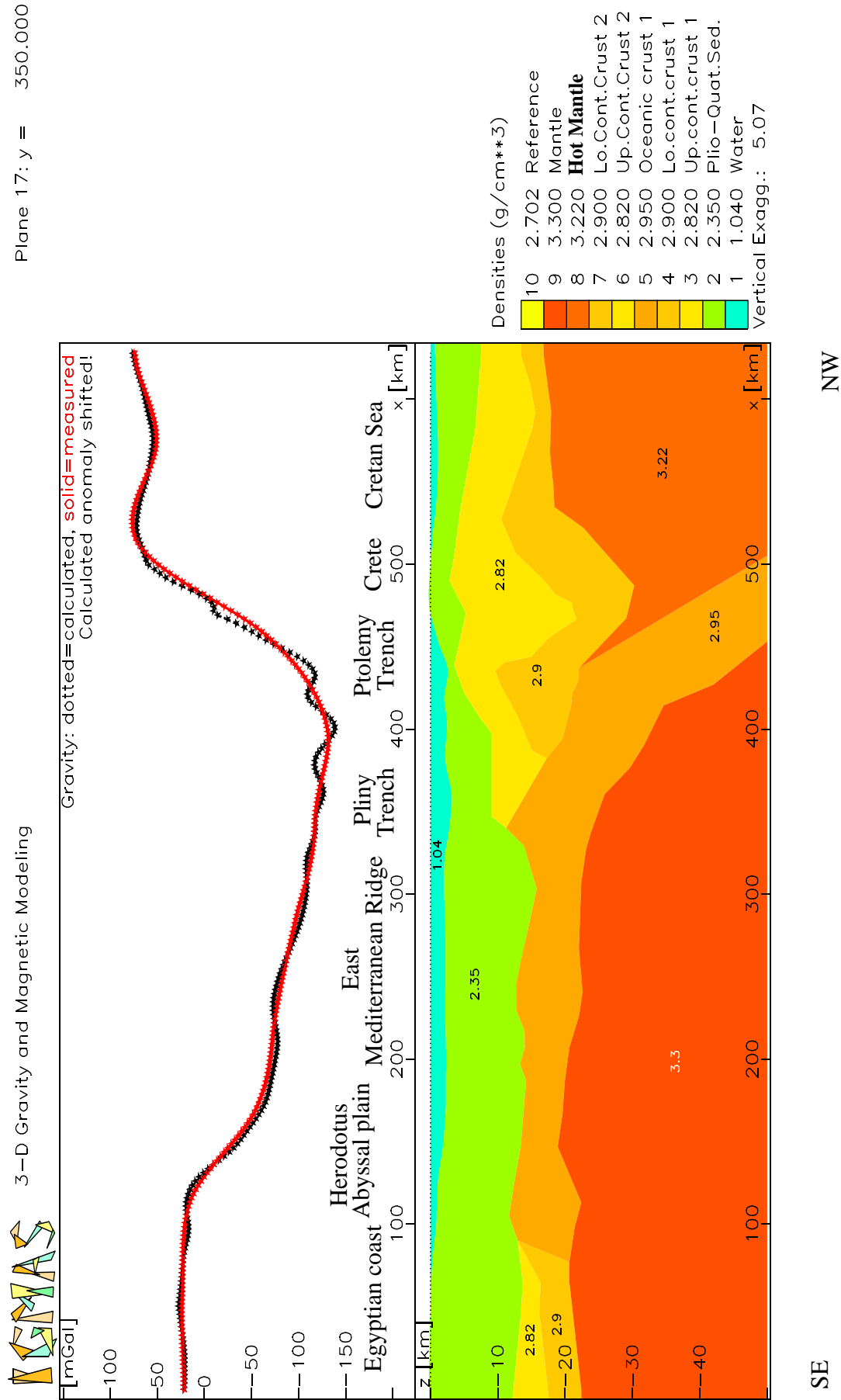


Figure 5.27: The final results of the vertical plane 17 through the three-dimensional gravity model and the related Free-Air anomaly.

flexible enough to cover the wide field of potential field modelling. However, in two-dimensional models the longitudinal extent of a modelled structure should be three or four times its width. The view of the subsurface structure through the two-dimensional model is orthogonal to the planar cross section and displayed in the same planar cross section. The view of the subsurface structure through the three-dimensional model enables any number of planar cross section to be displayed.

In general, the two-dimensional model geometry using TWGRAV software have fixed pre-calculated view points through all the model areas. However, some capabilities requested and several functions for display and calculation of potential fields are available in the three-dimensional model area by using IGMAS software. In the following section some several functions is given such as a comparison of the measured and modelled gravity field, differences between the measured and the modelled anomalies, and the thickness of a single geometry body.

- In Figure 5.28 a comparison of the measured and modelled gravity fields without adaptation (i.e. without variability of the layer geometry and layer thickness of the modelling area) is plotted. This Figure shows that the images of the gravity anomalies are clearly deviating from each other in the southeast as well as in the northwest of the modelled area. In Figure 5.29 a comparison of the measured and modelled gravity fields with adaptation (i.e. with variability of the layer geometry and layer thickness of the modelling area) is presented. The modelled anomalies resemble the measured anomalies in detail. The black lines represent the different vertical planes which build up the area of three-dimensional model. In Figures 5.28 and 5.29 the buffer zone surrounding the three-dimensional model is apparent. This zone surrounds the area documented by gravity field data to exclude edge-effects. The imaged planes represent the extent of the model. The gravity data are located only on planes 2 to 17.

- The differences between the measured and the modelled anomalies are displayed in Figure 5.30. This Figure shows the minimal differences between these gravity anomalies. For the area of three-dimensional model a standard deviation of 9.61 and a correlation coefficient of 0.99 were achieved.

- At the north-western part of the modelled area, the average thickness of the oceanic crust near 550 km, below the Anaximander Seamounts on plane 2 is about 30 km. This is decreases to a thickness of about 25 km, near 500 km towards NW Rhodes Basin on planes 6 and 9 as shown by pointing arrows in Figure 5.31. However it increases from about 25 km, near 500 km on plane 9 to about 35 km between 400 to 430 km below the subduction trenches on planes 10 and 11 as shown by pointing arrows in the same Figure.



3-D Gravity and Magnetic Modeling

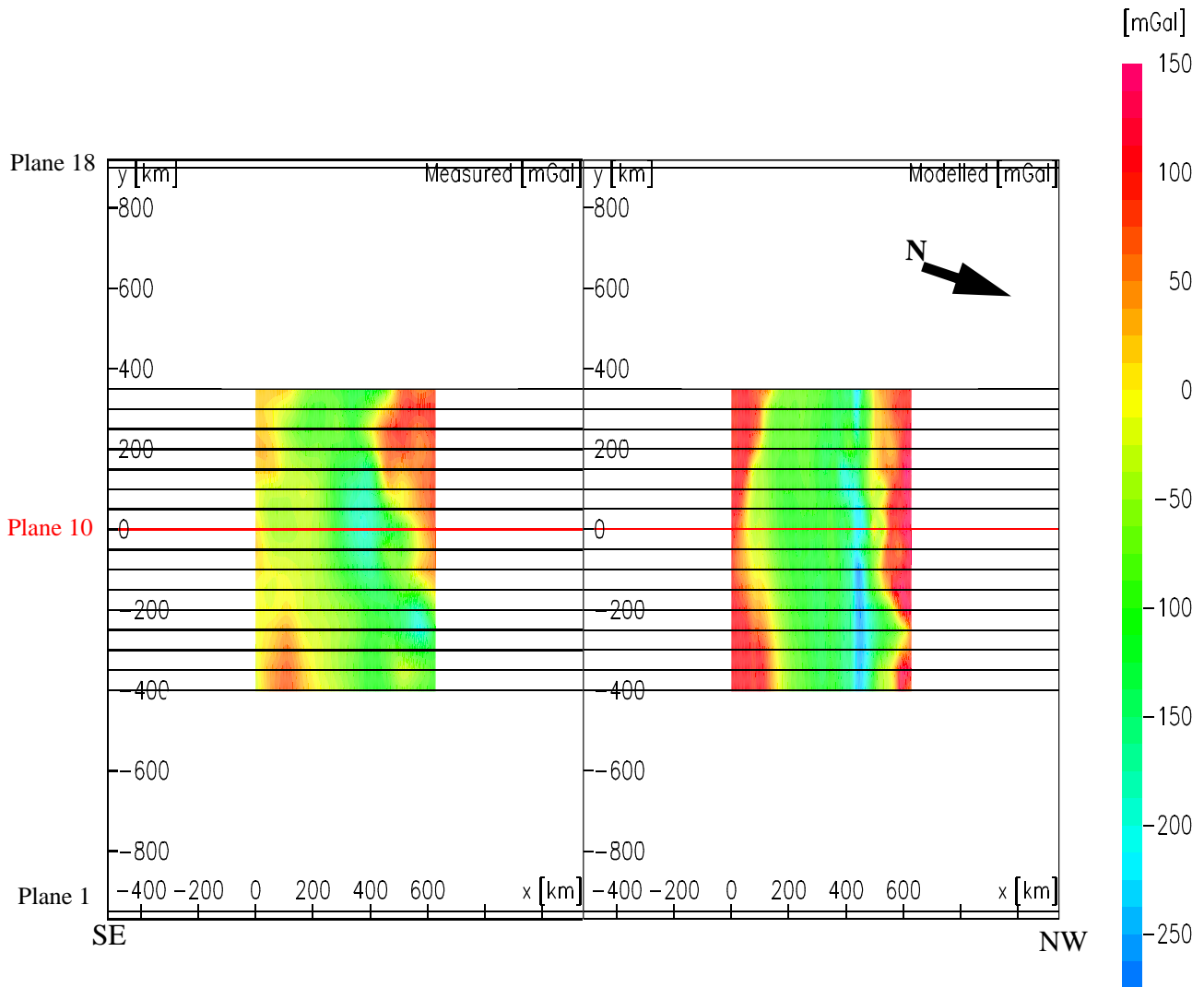


Figure 5.28: The modelled and the measured gravity fields without adaptation within the modelling area. The position of the vertical planes is indicated by black lines and the actual plane is marked by a red line



3-D Gravity and Magnetic Modeling

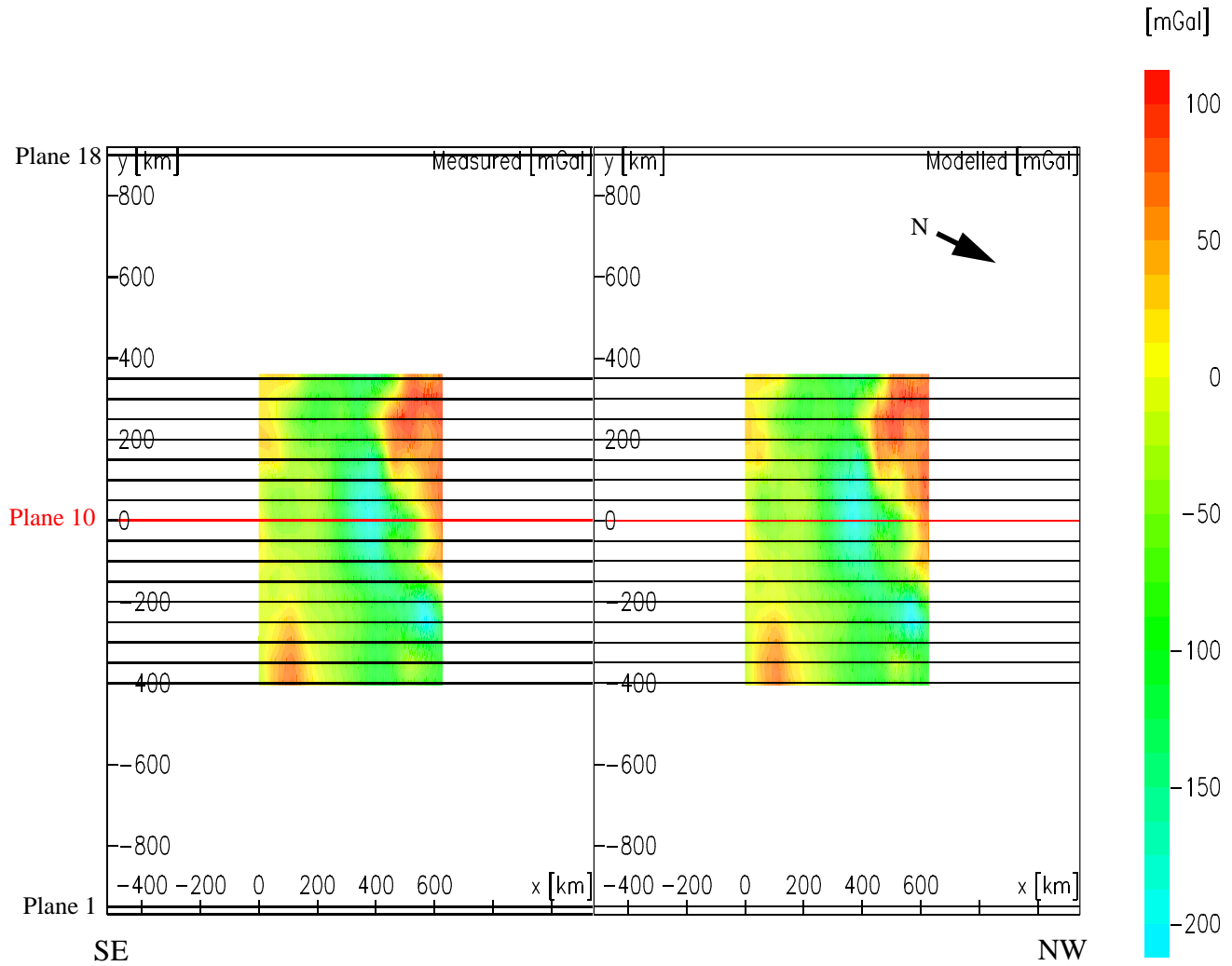


Figure 5.29: The modelled and the measured gravity fields with adaptation within the modelling area. The position of the vertical planes is indicated by black lines and the actual plane is marked by a red line

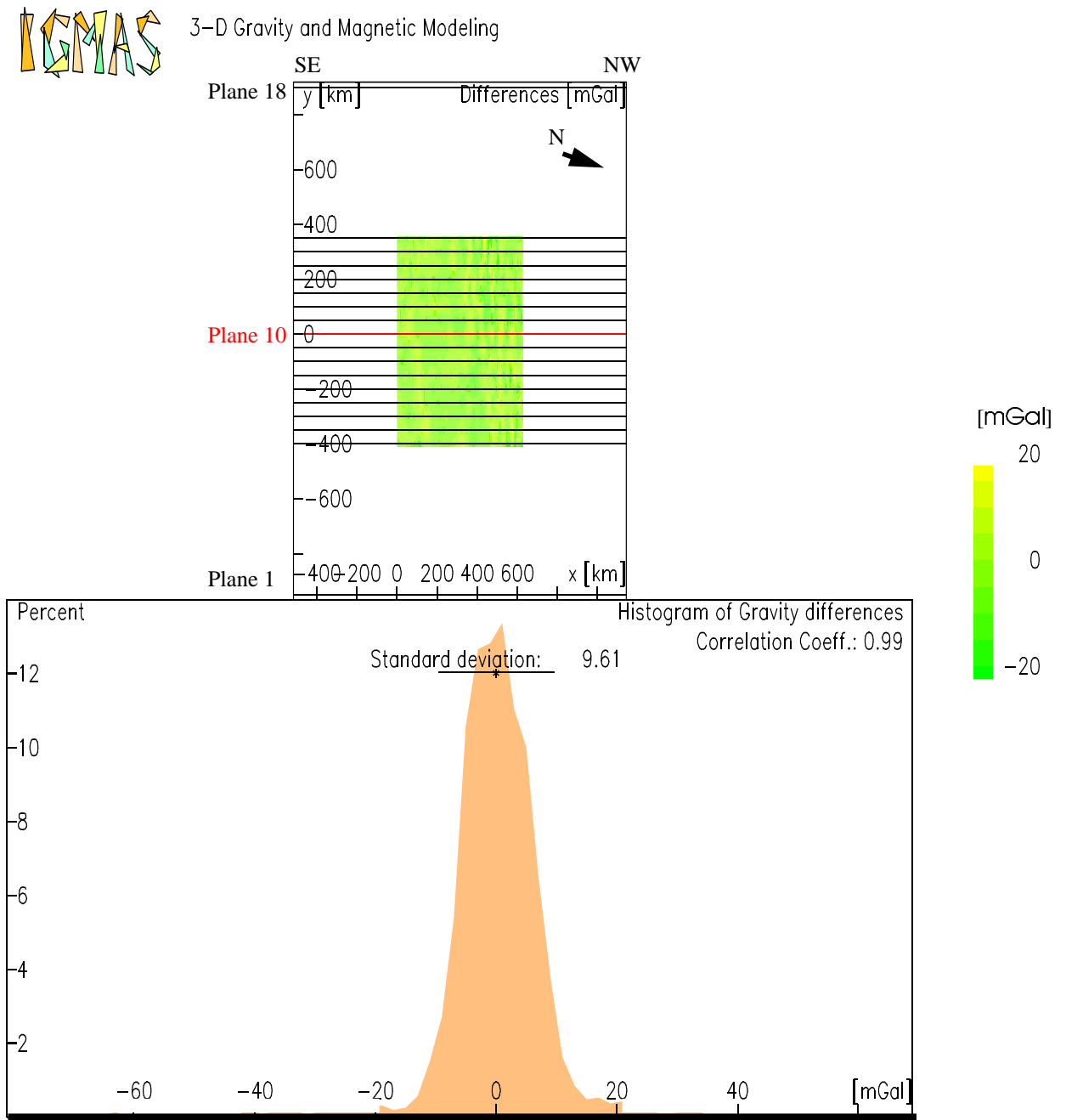


Figure 5.30: The differences between the modelled and the measured gravity anomalies within the modelling area. The position of the vertical planes is indicated by black lines and the actual plane is marked by a red line.

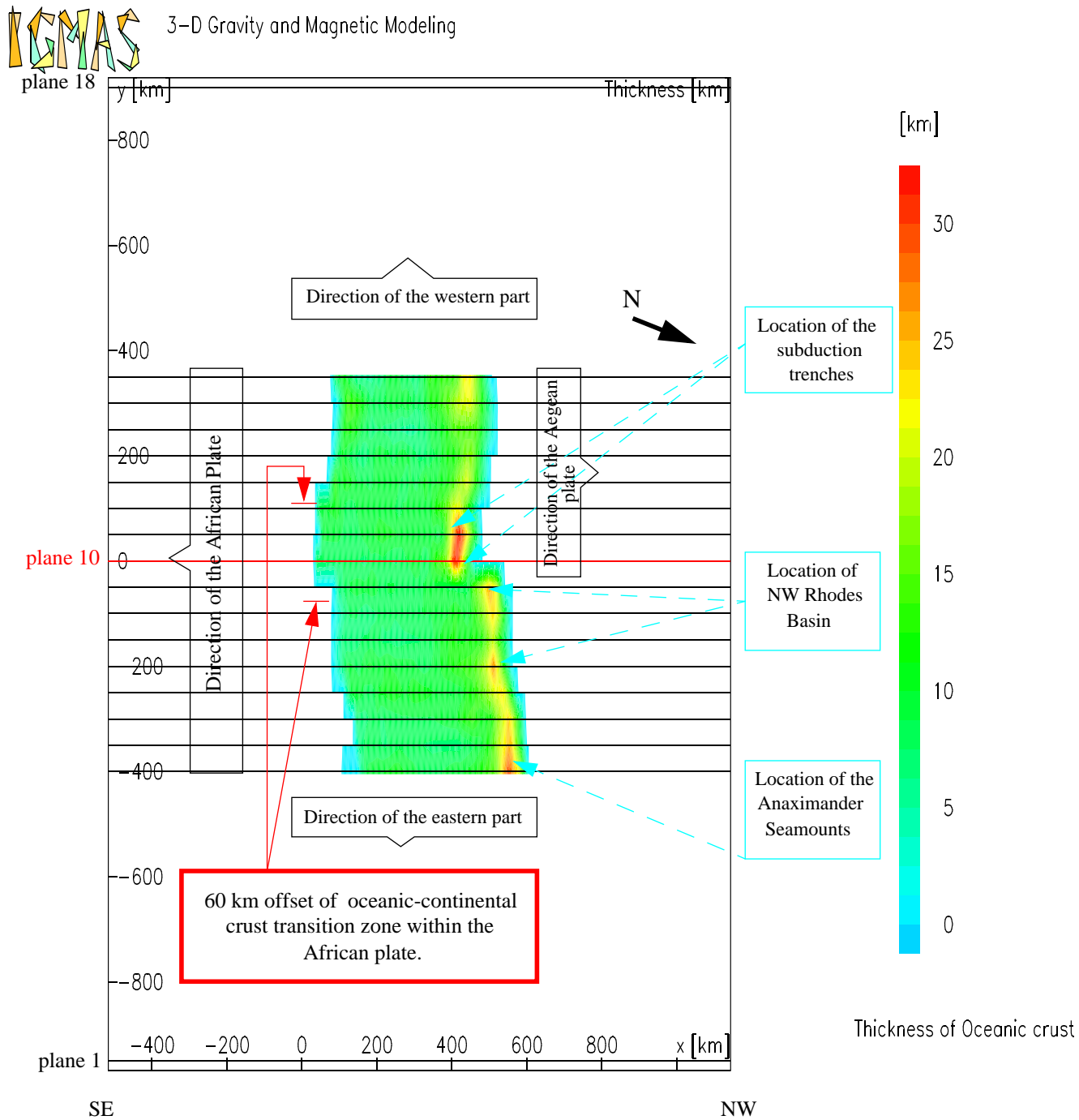


Figure 5.31: Isopach map displays the thickness of the oceanic crust on the modelling area. The position of the vertical planes is indicated by black lines and the actual plane is marked by a red line. The red arrows marks the position of the oceanic-continental crust transition zone within the African plate.

- Figure 5.32 shows several undulations in average thickness of the deepest layer in the model (mantle layer). In the north-western part of the modelled area, between 350 to 550 km the average thickness of the mantle layer ranges from about 10 to 22 km through the planes 2 to 17. In the south-eastern part of the modelled area, the average thickness of the mantle layer is 27 km towards the Egyptian coast. In the middle part the average thickness of the mantle layer is about 30 km. There are strong lateral undulations in the average thickness of the mantle layer at the western part on the modelled area towards Cretan Island Arc through planes 11 to 17. This may reflect the effect of the main driving force for the opening of the Cretan Sea through these planes (see Figure 5.32).

- Furthermore, the modelled area reproduces the observed gravity anomalies successfully. The anomalies are oriented roughly parallel to the bathymetric and topographic features as observed in all the planes of the modelled area. The calculated and measured gravity have negative values increasing gradually from -220 to -2 mGal. Local high and low gravity values were observed. For example as shown at Anaximander Seamounts (plane 3, see Figure 5.13), at Rhodes Basin (plane 5, see Figure 5.15), and at Strabo Trench (plane 13, see Figure 5.23). This is due to significant crustal thickening in these regions.

- Along the Nile Delta region, a prominent positive anomaly can be followed through planes 2 to 4 (Figures 5.12, 5.13, 5.14, and 5.15) as well as along the Egyptian coast through planes 5 to 17 (Figures 5.16 to 5.27). In addition, the gravity values seaward of the subduction trenches form a complicated pattern.

- There are several undulations of the hot mantle layer between 500 and 627 km through the planes 2 to 17 at the north-western part of the modelled area.

- As mentioned before, in the south-eastern part of the modelled area, the transition from continental to oceanic crust within the African plate decreases abruptly from about 100 km through plane 9 (see Figure 5.19) to about 40 km through planes 10, 11, and 12 as illustrated in Figures 5.20, 5.21, and 5.22 respectively (see also Figure 5.31). Then it increases to about 100 km through plane 13 (see Figure 5.23). This reflects a very good match between the bathymetric and topographic features along the Egyptian coast and the main tectonic elements in this area (see Figure 2.1). Also, it reflects the effect of an active eastern Mediterranean transcurrent fault system (EMTS) running through the Ionian Sea, the continental margin of Eastern Libya and Western Egypt, into the land area through the Nile Delta and eventually into the Gulf of Suez (see Figure 2.2) as suggested by Ben-Avraham et al. (1987).



3-D Gravity and Magnetic Modeling

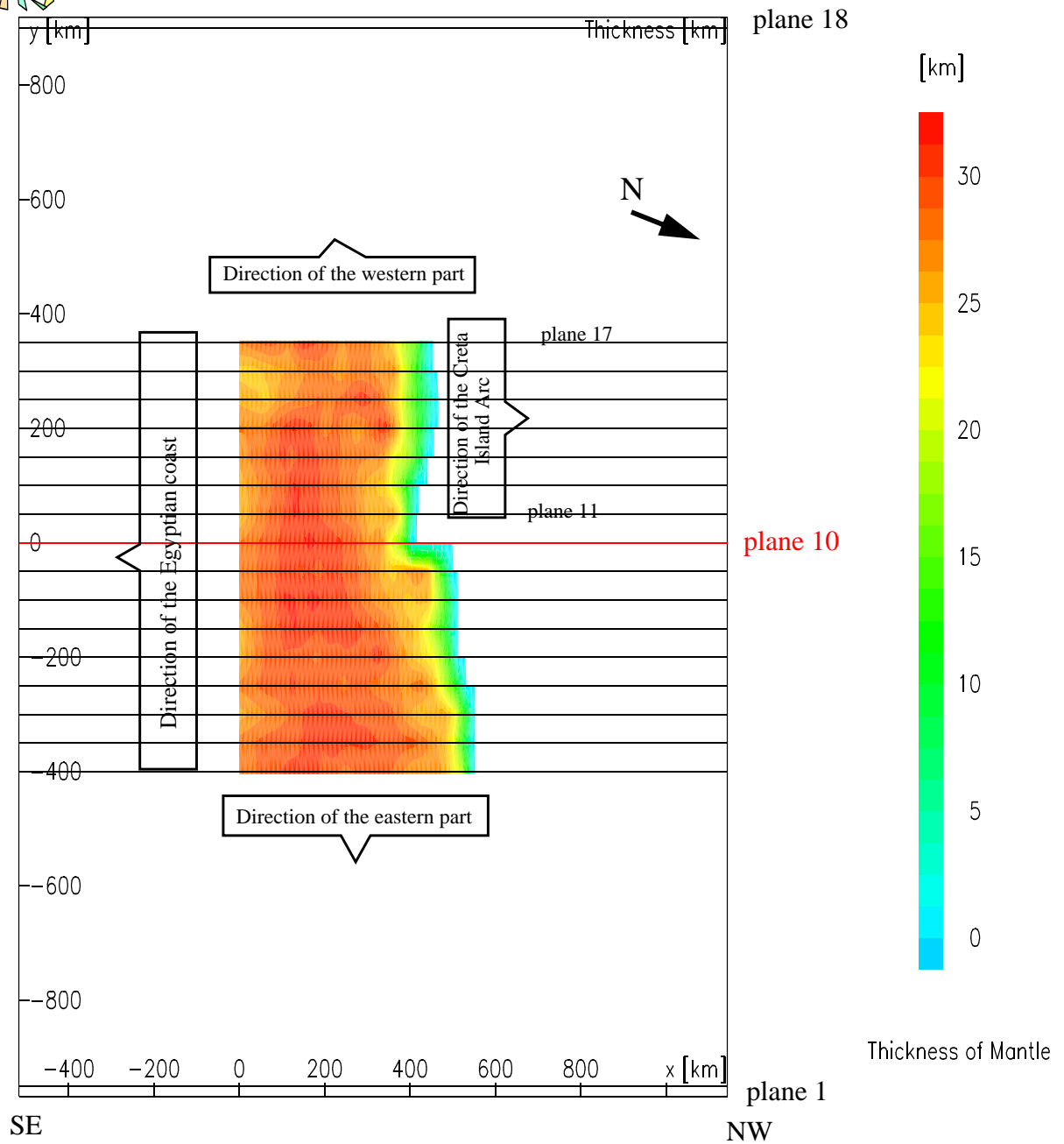


Figure 5.32: Isopach map displays the thickness of the mantle layer on the modelling area. The position of the vertical planes is indicated by black lines and the actual plane is marked by a red line.

- On the other hand, in the north-western part of the modelled area, the transition between the oceanic and continental crust at a distance between 400 to 450 km can be followed through planes 2 to 9 (see Figures 5.12 to 5.19) and also at a distance between 300 to 350 km through planes 10 to 17 (see Figures 5.20 to 5.27). This may be related to the African oceanic crust being subducted beneath the Hellenic Arc. Not only the subduction of the oceanic lithosphere along the belts of the Aegean continental crust but also the subducted crust contributes to the gravity low associated with the Hellenic Arc. In addition, the African oceanic crust is subducted beneath the Island of Crete, according to the main driving force for the opening of the Cretan Sea.

VI. TECTONIC ACTIVITY AND REGIONAL STRESS PATTERN

It is generally accepted that the seismicity reflects the tectonic activity in the Lithosphere of any area (Kasahara and Stevens, 1969). Also the study of regional stress pattern distribution is a significant step towards understanding the tectonic setting and the direction of relative plate movement in any area and its adjacent areas (Kawasumi, 1937; Stefansson, 1966). In recent years, and with the establishment of the plate tectonics theory, many studies have been published on the seismicity and tectonics in and around the study area (e.g. Papazachos, 1969; Papazachos and Comninakis, 1978; Mckenzie et al., 1970; Comninakis and Papazachos, 1972; Mckenzie, 1972; Halsey and Grandner, 1975, Ben-Menahem et al., 1976; Makris, 1976; Nur and Ben-Avraham, 1978; Garfunkel and Freund, 1981; Garfunkel and Almagor, 1985; Ben-Avraham and Nur, 1986; Darkal et al., 1990; Kebeasy, 1990; Girdler, 1991 and Ben-Menahem, 1991; Rabai et al., 1992; Aboulela, 1994; Salamon, et al., 1996; Barka and Reilinger, 1997; Mantovani et al., 1997; Ambraseyes and Jackson, 1998; Ylmaztürk and Burton. 1999; Badawy and Horvath, 1999 a, and b; Knapmeyer and Harjes, 2000; Harjes, 2001; Pondrelli et al., 2002; Mahmoud, 2003).

In the following, a distribution of earthquake epicentres obtained during the period of 1904-2002 covering the whole study area is presented (see Figure 6.1). The data was acquired from two different data base sources, (NEIC and ISC). To understand the regional stress pattern (i.e. P-axes orientation) currently taking place in the study area, available focal mechanism parameters data of earthquakes are collected for moderate to large events within the study area. These parameters are presented in Tables Appendix B1 and B2, which are extracted from the Harvard Seismology, CMT (Centroid-Moment Tensor database) catalogue search and WSM (World Stress Map database, Mueller et al., 2000). The epicentral locations and the stereographic projections of the lower focal hemisphere of some moderate to large earthquakes are plotted using GMT software as shown in Figure 6.2.

VI.1. Tectonic activity and seismicity pattern

In Figure 6.1 the seismicity of the area investigated is illustrated with respect to magnitudes and depth in kilometre. The earthquakes with variation body wave magnitude (M_b) are marked with different symbols. The focal depth (km) is represented by a color scale. The position of the two and three-dimensional gravity modelling areas are indicated by red lines and a green box respectively (Figure 6.1).

From figure 6.1 it can be observed that the seismicity of the study area is characterized

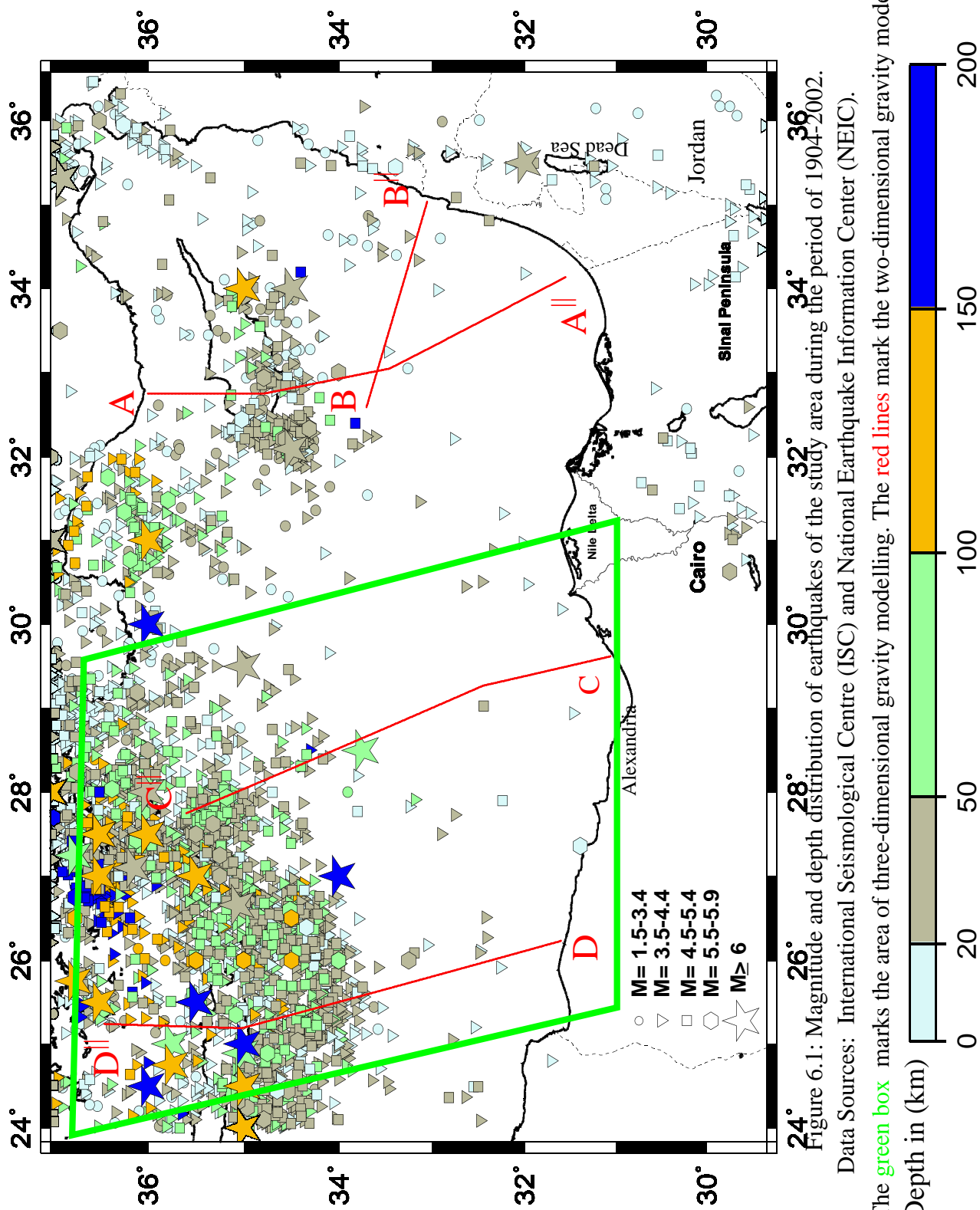


Figure 6.1: Magnitude and depth distribution of earthquakes of the study area during the period of 1904-2002.

Data Sources: International Seismological Centre (ISC) and National Earthquake Information Center (NEIC).

The green box marks the area of three-dimensional gravity modelling. The red lines mark the two-dimensional gravity modelling.

by widespread seismic activity in some areas and a scattering of events in others. Most of the active seismicity is concentrated along and around the main tectonic and geological structural area such as the Hellenic and Cyprean Arcs. There are also some activity areas along the trends of the Gulf of Aqaba - Dead Sea - Levant transform, and the Gulf of Suez - Cairo - Alexandria || northern Egypt || (see Figure 2.2). In the following a short description of these individual seismic areas is given, concentrating on several segments of the stronger seismic belts, which surround these regions.

The Hellenic Arc is the most seismically active zone of the investigated area due to the subduction of the African plate beneath the Aegean area. Most of the moderate events ($M \leq 5.9$) with a focal depth of less than 100 km are concentrated along the Hellenic Arc, while the strong events ($M > 5.9$) with a focal depth of 100 -150 km are concentrated mainly behind the Arc in the Cretan Island Arc. The Hellenic Arc is a significantly deep focus earthquake, which extends eastwards as far as the Rhodes Basin through the Junction between the Hellenic and Cyprean Arcs (see Figure 2.4). The macroseismic effects of the earthquakes occurred in the southern part of the Hellenic Arc and the intermediate depth seismicity in Cretan Island Arc is related to north-south convergence between the African and European plates as suggested by Delibasis et al. (1999). Moreover, the majority of the earthquakes beneath Crete are shallow events with a depth mainly from 10 to 20 km, which are separated from the subducting slab as suggested by Harjes (2001).

The strong and moderate earthquakes, including hypocenters as deep as 150 km are concentrated in and around the Cyprean Arc (i.e. southwestern and southeastern Cyprus- the Eratosthenes) as illustrated in Figure 6.1. Along this Arc, the earthquake distribution reveals that convergence takes place along the Western and central parts. Subduction takes place along the Western side of the Arc, while the processes along the central part are interrupted due to the collision of the Eratosthenes Seamount with the Cyprean Arc as suggested by Ben-Avraharm and Nur (1986).

The seismicity gradually decreases from west to east along the Cyprean Arc, and also decreasing southwards. In addition the seismicity associated with the Cyprean Arc is significantly lower than that associated with the Hellenic Arc. Recently, Rihm et al. (1999) studied the seismicity of Cyprus and identified numerous active faults concluding that the fault systems in Western Cyprus and their offshore extensions are activated by a subduction of an oceanic lithosphere below Western Cyprus.

The seismicity level along the Gulf of Aqaba- Dead Sea-Levant transform trend is quite

low and the depth of the events increases northward or northeastward of the Cyprus Island, where the depth of the events in the proximity of the Dead Sea rift zone and Cyprus Island is shallower compared to the depth of the activities in the Antalya Basin (Figure 6.1). This region is comparable with Dead Sea rift zone and the relative motion between the Sinai and Arabian plates as suggested by Le Pichon and Gaulier (1988).

The trend of Gulf of Suez-Cairo-Alexandria || northern Egypt || extends from the Sinai triple junction to the northwest along the Gulf of Suez towards the Nile Delta and the Mediterranean Sea. The activity in north Egypt spreads out with moderate events ($M \leq 5.5$) with a focal depth of less than 50 km. The trend of the Gulf of Suez-Cairo-Alexandria represents the major active trend and is characterized by the occurrence of shallow earthquakes activities.

The main earthquake activity in northern Egypt can be considered as a direct seismotectonic consequence of the Sinai subplate kinematics. The tectonic activity and seismicity of this trend may be related to the faults trending NW-SE, parallel to the trend of the Gulf of Suez and also perpendicular to the Gulf of Suez trending NE-SW. These faults may be of the Syrian Arc deformation trend. Also it reflects the effect of an active eastern Mediterranean transcurrent fault system (EMTS) as illustrated Figures 6.1 and 6.3. On the whole, the epicentral distribution of all earthquakes in northern Egypt is associated with the northward movement of the Arabian plate, reflecting the great influence of the regional stress affecting the northeastern corner of Africa. The effect of the stress direction is also reflected from much younger faulting documented in and around the Gulf of Suez as suggested by Garfunkel and Bartov (1977) and Abdel Aal et al. (2000).

VI.2. Regional stress pattern

To determine the stress pattern (i.e average P-axes orientations), a selection of the focal mechanisms of some moderate to large earthquakes are plotted as shown in Figure 6.2. These shocks occurred in the most seismically active areas of the study area and were separated into several groups with fault plane parameters data (Tables Appendix B1 and B2). Furthermore, Figure 6.3 shows the distribution and direction of the P-axes on a horizontal plane derived from focal mechanism solutions of moderate to large earthquakes in the study area. A short description of the focal mechanisms concept is given in Appendix [C]. In the following section, a brief description of the regional stress pattern (P-axes orientations) is presented, which was determined on the basis of the focal mechanisms of some moderate to large earthquakes as mentioned above in this study area.

In and around the Hellenic Arc, both extension and compression stresses are present resulting in complex fault tectonics characterized by important horizontal and vertical movements. Observed more closely, the P-axes orientations in and around the Hellenic Arc are north eastward directed at the border of the Arc as shown in Figures 6.2 and 6.3. Moreover, oblique reverse and normal faulting mechanisms are present along the Hellenic Arc, which may be related to subduction processes of the Africa plate under Eurasia.

The focal mechanisms of shallow earthquakes (focal depth of 0-50 km) along and around Cyprean Arc indicated that the P-axes is directed WNW-ESE which is perpendicular to the northern coast of the Eastern Mediterranean (Figure 6.3). In the region of Cyprus, the situation looks very complex because the P-axes direction is changing between WNW-ESE and NE-SW. It can tell which one is the true direction. This is in full agreement with the previously suggested concept by Nur and Ben-Avraham (1978) and Badawy and Horvath (1999 a), which stated that the shallow seismic activity along this coast is due to the convergence of the African and Eurasian plates in NNW-SSE direction. There are strike slip faults solutions in the western part of the Cyprean Arc (see Figure 6.2). This may be related to the difference in the convergence rates at the Hellenic and Cyprus arcs.

The focal mechanism solutions along the Gulf of Aqaba- Dead Sea-Levant transform trend indicated that the P-axes direction is changing from NW-SE to NNW-SSE (see Figure 6.3), which corresponds to a strike-slip mechanism in agreement with the geological evidence as suggested by Badawy and Horvath (1999 a). It may be also due to the relative movement between the Arabian and African plates. North to the main depression of the Dead Sea, the activity tends to take a north western direction into the Mediterranean Sea towards the Arabian plate to meet the Cyprean Arc somewhere east of Cyprus.

The focal mechanisms of shallow earthquakes in northern Egypt show that the average P-axes orientation is nearly parallel to the direction of the absolute plate motion of Africa. Along the Gulf of Suez and north eastern Egypt, the orientation of the P-axes is in a NW-SE direction (Figure 6.3) and also in north western Egypt the direction of the P-axes is in a NW-SE parallel to some young active faults in the Gulf of Suez. This corresponds with the faults active trends along the Gulf of Suez.

For the overall region, it seems that in and around seismic activity zones in the study area, the existence of extensional and compresional stress could be clearly seen. It can be observed that the average P-axes orientations in the study area is in good agreement with regional stress pattern within the global plate tectonic framework and it is broadly consistent with the absolute

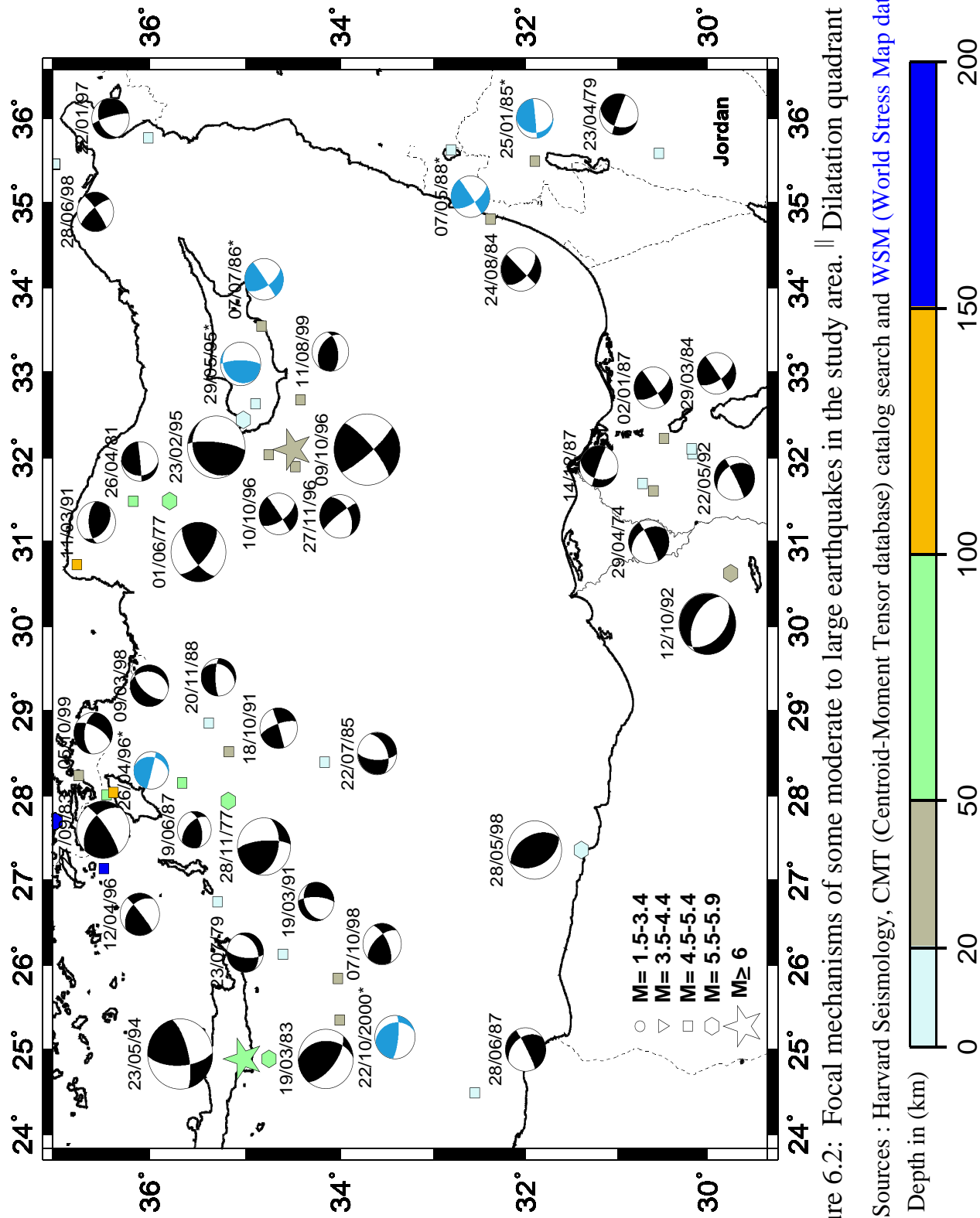
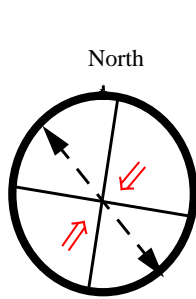


Figure 6.2: Focal mechanisms of some moderate to large earthquakes in the study area. || Dilatation quadrant are white ||

Data Sources : Harvard Seismology, CMT (Centroid-Moment Tensor database) catalog search and [WSM \(World Stress Map database\)*](#)

Along the Hellenic Arc :

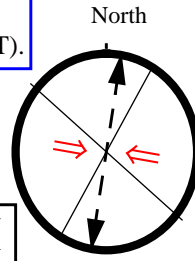
- The average P-axes direction is N25°E -S25°W.



II

Along the Cyprean Arc :

- The P- axes direction is changing between N25°E-S25°W and N85°W- S85° E.



I

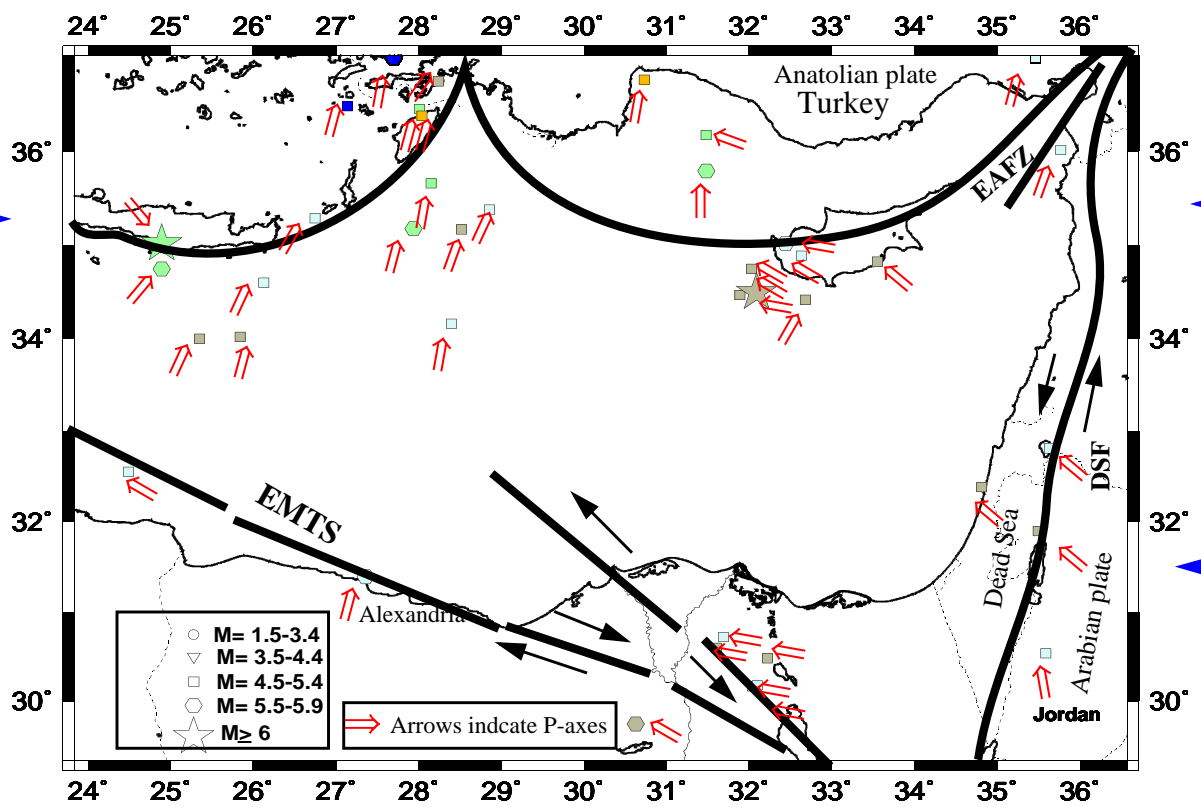
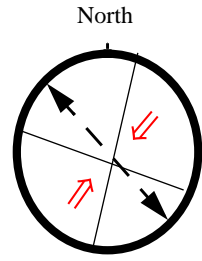
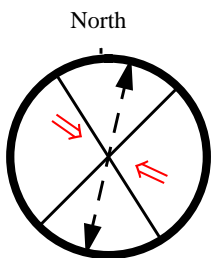


Figure 6.3: The distribution and direction of the P-axes on a horizontal plane derived from focal mechanism solutions of moderate to large earthquakes in the study area. (Faults, Subduction zone based on Mchenzie, 1972, Nur and Ben-Avraham ,1978, Ben-Avraham et al., 1987, and Jarriage et al., 1990)

- DSF=Dead Sea fault; EMTS= Eastern Mediterranean transcurent fault system; and EAFZ= East Anatolian fault zone.

Along the trend of Gulf of Suez-Cairo-Alexandria (Northern - Egypt):

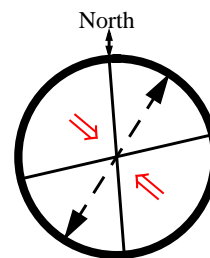
- The average P- axes direction is N50°W - S50°E.



III

Along the Gulf of Aqaba - Dead Sea-Levant transform trend:

- The average P- axes direction is N45°W - S45°E.



IV

plate motion of African and its collision with Eurasian plates as illustrated in plane view by boxes [I], [II], [III] and [IV] in Figure 6.3. Furthermore, comparing the seismicity map with results obtained from two and three-dimensional gravity modelling of the study area, it can be concluded that:

- The main characteristic of the distribution of earthquakes in the three-dimensional gravity modelling area, and also along two-dimensional gravity models, (e.g. profile C-C^{||} and D-D^{||}) is the concentration below the northern part of the East Mediterranean Ridge and the Hellenic Arc (see Figure 6.1). This is due to the compressional stresses caused by the convergence between the African plate and the Aegean subplate. The three-dimensional gravity modelling area of earthquakes with an intermediate focal depth more than 20 km at the Egyptian coast dips northwards to a depth of about 150 km below the Cretan Sea. This is attributed to the subduction of the African plate beneath the Aegean subplate.

- In the three-dimensional gravity modelling area there is a general relationship between the distribution and focal depth of earthquakes which then further relates to crustal thickness (see Figure 6.1). i.e. The Moho lies at a depth of about 27 km at the Egyptian coast and then rises to a minimum depth of about 19 km beneath the Herodotus Abyssal Plain. About 6 km sedimentary cover is present along the Egyptian coast as mentioned previously in Chapter V.

- The distribution of the earthquakes along and around a two-dimensional gravity model i.e. profile A-A^{||} (Figure 6.1) shows that both shallow and intermediate focal depth (20-100 km) earthquakes exist in the central part of the Cyprean arc underneath Cyprus. The intermediate focal depth earthquakes beneath Cyprus appear to be associated with collisions between Cyprus and the Eratosthenes Seamount as suggested by Robertson (1990).

- There are some local scattered activities with the intermediate focal depth in both the southern margin of the Levant Basin and the Eratosthenes Seamount along and around the two-dimensional gravity model i.e. profile B-B^{||} (Figure 6.1). This may be attributed to the underthrusting of the northern edge of the Eratosthenes Seamount beneath Cyprus as suggested by Robertson et al. (1995).

VII. DISCUSSION AND CONCLUSIONS

The area under investigation covers the northeastern margin of the African plate between Latitudes 29°:30'-37°:00' N and Longitudes 23°:30'-36°:00' E. It represents a unique opportunity for studying the beginning of such a collision between the passive margins of a major plate (Africa), locally acting as a continental indenter against the active margin of another plate (Eurasia).

In this work, large amount of data was extracted from the geophysical data which were acquired during field work within the area investigated as mentioned in the beginning of this study (see Chapter I). This study is an attempt to achieve a better understanding of tectonics, and geodynamical processes along a complex tectonization region such as crustal structure, thickness of sediments, transition between oceanic and continental crust and regional integrated model of the gravity field observed in the area investigated. In addition, a comparison between the marine gravity data and the gravity data derived from satellite altimetry was made to ensure that the marine gravity data compiled from different marine surveys were compatible. Furthermore, a successful attempt was made to understand the behaviour of the tectonic activity and regional stress pattern distributions within the area investigated using the seismicity data. In the following, a brief discussion and conclusions of the main principle results in this study are presented by evaluating all of the geophysical data with regard to the study area.

VII.1. Discussion

Based on the main principle results obtained in this study and combining it with the tectonic models of the study area, a sketch map of the area under investigation and its neighbouring areas showing simplified regional tectonic and geodynamic framework was produced and is presented in Figure 7.1. The sketch is also based on the results of geophysical and tectonic studies that have been observed within the study area (e.g. Mckenzie, 1972; Nur and Ben-Avraham, 1978; Ben-Avraham et al., 1987; Courtillot et al., 1987; Peter et al., 1998; Badawy and Horvath, 1999 b, and Mcklusky et al., 2000). For the overall area under investigation as illustrated in Figure 7.1, it seems that:

- The geographic setting and geology of the study area show that the Eastern Mediterranean region includes a short segment of the convergence boundary between Africa and Eurasia. Subduction in this segment is along two very small Arcs, the Hellenic and Cyprean Arcs as shown in Figure 7.1 part A. In both Arcs subduction has been documented by a large number of small block areas and subduction trenches (e.g. Crete Island and Cyprus, Ptolemy, Strabo

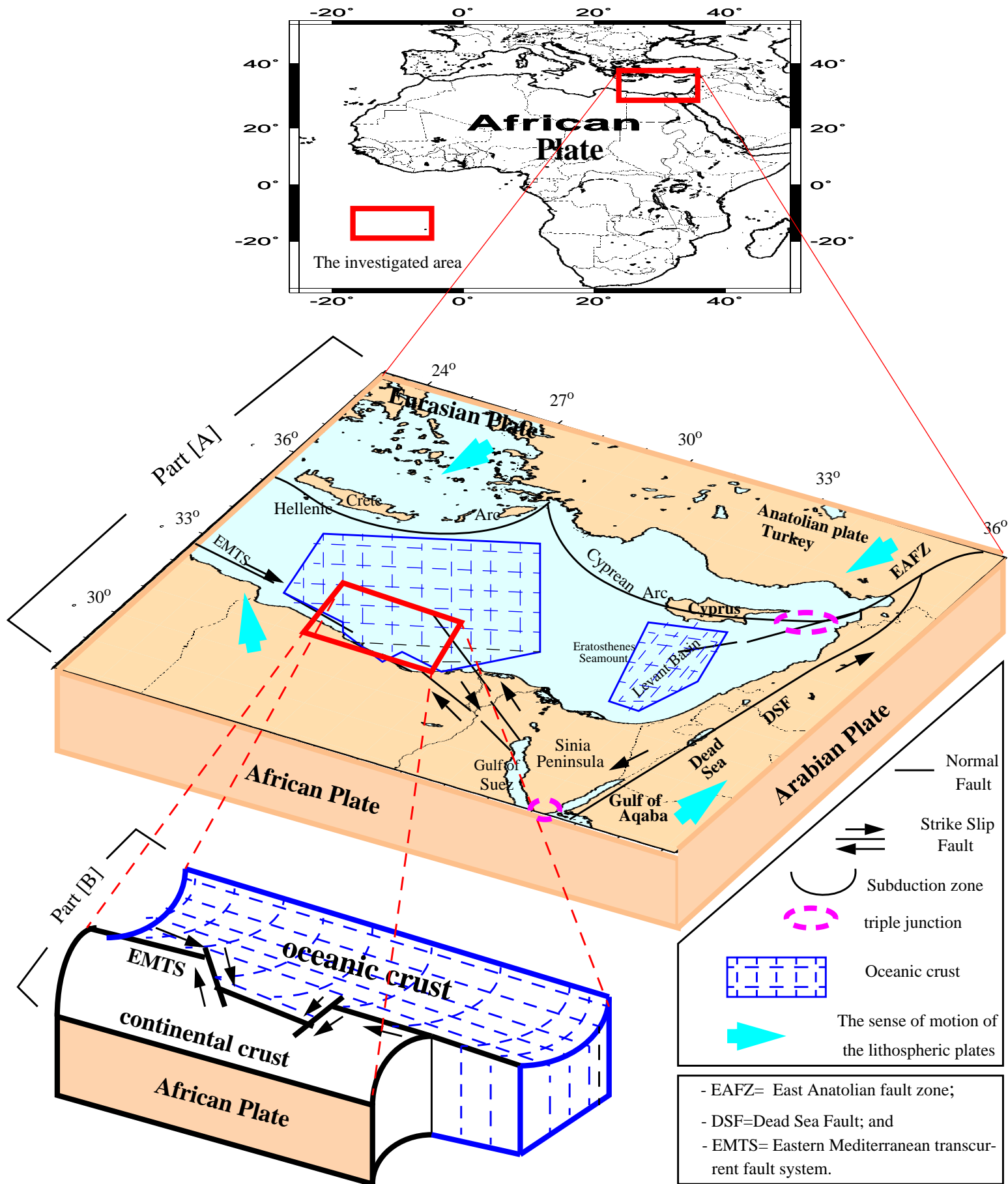


Figure 7.1: Part [A]: Sketch map showing simplified regional tectonics and geodynamic framework in the study area. Based on Mckenzi e (1972), Nur an d Ben-Avraham (1978); Ben-Avraham et al. (1987); Courtillot et al. (1987); Peter et al. (1998); Badawy and Horvath (1999 b), Mcklusky et al. (2000) and the principal results of this study. Part [B]: Structural model for the active EMTS at the base of the continental slope off the Egyptian coast.

and Pliny Trenches). Moreover, the study area has remarkably prominent morphogeologic features such as East Mediterranean Ridge, Herodotus Abyssal Plain, Levant Basin, Eratosthenes Seamount, Nile Delta and Sinai Peninsula (see Chapter II).

- Geologically, at the base of the continental slope of the Egyptain coast and eastern Libya, the shape and size of a bathymetric depressions strongly suggested that they originated from an active eastern Mediterranean transcurrent fault system (EMTS) as shown in Figure 7.1 part A. This fault runs through the Ionian Sea, the base of the continental margin of Eastern Libya and western Egypt, into the land area through the apex of the Nile Delta and eventually into the Gulf of Suez as suggested by Ben-Avraham et al., 1987. Assuming the EMTS is continuous through the above mentioned area, the question is then how does the fault terminate from the Ionian Sea to the eastern Egypt? It is proposed that it continues along the same trend southeast into the land area where a large topographic depression exist along the continental margin of eastern Libya and western Egypt. From there it cuts through the apex of the Nile Delta and enters into the Gulf of Suez (Figure 7.1 part A). Undulation in shape of the bathymetric and topographic features along the Egyptain coast can also be observed (Figure 2.1). Furthermore, Malovitsky et al. (1975) suggested that a major fault has been described along the continental margin of the Egyptain coast and eastern Libya on the basis of seismic refraction data. The activity of this area may be related to the faults trending NE-SW and NW-SE as suggested by many investigators (e.g. Youssef, 1968; Halsey and Grandner, 1975, Kebeasy, 1990; Mahmoud, 2003). Additionally, there is some moderate to large earthquake occurrences in land of this area (Figure 6.1).

- There is a few major fault systems such as the Suez rift and faults from Arabian plate, which extend into southeastern Mediterranean Sea as shown in Figure 7.1 part A. These faults are trending NW-SE and parallel to the trend of the Gulf of Suez as suggested by (e.g. Nur and Ben-Avraham, 1978 and Jarriage et al., 1990). It reflects activation of the Dead Sea Transform faults (DSF) and the Levant-Aqaba transform plate boundary as suggested by (e.g. Mckenzie, 1970; Kahle et al., 1998). The tectonic activity and seismicity along these faults spread out with moderate events ($M \leq 5.5$) and also with a focal depth of less than 50 km (see Figure 6.1). However, most of the active seismicity is concentrated along and around the Hellenic and Cyprean Arcs (Figure 6.1).

- Generally, in the southeast adjacent to the study area, most activity is concentrated at the southern end of the Gulf of Suez, where the triple junction* (Africa, Arabian, Sinai) is situated as suggested by (e.g. Courtillot et al., 1987; Badawy and Horvath, 1999 a, El-Dididy, 2001).

* A point that is common to three plate and which must also be the meeting place of three boundary features, such as divergence zones, convergence zones, or transform fault.

Furthermore, in the northeast, the neighbouring zone of the intersection between the Cyprean Arc, East Anatolian fault zone (EAFZ), and the Dead Sea Fault (DSF) represent a new triple junction zone along the EAFZ between the Africa, Anatolian and Arabian plates (see Figure 7.1 part A) as proposed by McClusky et al., 2000 and 2003, Best et al., 1993, and Beydoun, 1991. This zone is characterized by strong and moderate earthquakes decreasing from north to south (Figure 6.1). Kempler and Garfunkel (1994), Kiratzi and Papazachos (1995) and Jackson and Mckenzie (1988) stated that the deformation in the triple junction zone along EAFZ display a comple array of tectonic regimes with complex local variations and rapid tectonic facies changes from extension to strike-slip and shortening in the context of continental collision.

- The continental African plate extends from approximately 40 to 100 km offshore of the Egyptain coast and has an abrupt transition to an oceanic crust. This transition has been conformed and further constrained by three-dimensional gravity modelling of this study. It seems that the proposed extend reflects the effect of an active EMTS and the main tectonic elements in this area, which occur on the boundary between continental and oceanic crust units as shown in Figures 7.1 part B and 5.4).

- Moreover, the crustal structure of the Levant Basin is significantly different from that of the adjacent land. The gravity modelling results identify the continental-oceanic crust transition at Levant Basin (see Figures 7.1 part A and 5.4).

VII.2. Conclusions

In the following, and according to the results of the a qualitative interpretation of the observed gravity and magnetic anomalies, a quantitative interpretation of the Free-Air gravity field provided by two and three-dimensional gravity modelling, as well as the results of seismic deep soundings and tectonic activity and regional stress patterns, the main conclusions can be drawn.

- ◆ By studying the Free-Air and Bouguer gravity anomaly maps as well as the total intensity magnetic anomaly map, it can be revealed that:

- Over most of the study area, the Free-Air anomaly range from -230 to +150 mGal and are generally negative. However, the Bouguer anomalies range from -130 to +200 mGal and are predominantly positive, as might be expected for an oceanic area.

- The Free-Air and Bouguer anomalies are characterized by the presence of linear and closed anomalies of different polarities which could be attributed to either structural breaks or lateral density variations.

- The broad region of negative Free-Air anomalies, as shown in tectonic models, coincide with the East Mediterranean Ridge and widen to cover the area of the Pliny, Ptolemy and Strabo Trenches southeast of Crete.

- The positive Bouguer anomalies over the Anaximander Seamounts and Eratosthenes Seamount are probably an indication of upwelling of the crust or a large dense mass rising in this region.

- In the north port of Egypt, at the Nile valley and Delta, the topography varies between 0 and 500 m. The negative Bouguer anomalies values range from -10 to -30 mGal. This corresponds with the thickening of the Nile Quaternary sediment. Negative Bouguer anomalies are observed in the Gulf of Suez, this is caused by the thick sediments in the Gulf.

- By observing the orientation of the Free-Air anomalies in the study area, it was shown that the isostatic equilibrium is far from being achieved. The absence of a large Bouguer anomaly associated with the extreme relief indicates that the area is, as could be expected, not isostatically compensated by local variations in the crustal or mantle structure.

- The lack of significant magnetic anomalies across the East Mediterranean Ridge puts in doubt whether this Ridge is constructed of faulted, folded, uplifted and sedimentary strata. A series of high magnetic anomalies around the Cyprean Arc, runs from the Antalya Basin across Cyprus to the coast of Arabian plate. It coincides with a large positive Bouguer gravity anomaly suggesting that the ophiolites in Cyprus, in southern Turkey and northwest Arabian plate have a common base, and that ophiolites probably exist around the whole Cyprean Arc.

- The regional gravity anomaly values in the study area decrease generally towards the E-W and SE directions. The cause of the regional gravity trend is the transition from oceanic crust of the Eastern Mediterranean to the continental crust of the Arabian plate. The regional magnetic anomalies in the study area on the other hand are dominant in NW-SE trends and the regional magnetic field increases towards the north, which may reflect the shallow depth of the basement rocks in this direction.

◆ Furthermore, based on a comparison between result of the shipboard gravity anomaly data of the area investigated and the satellite data, it can be showed that:

- The satellite data show only minor deviations in some partial regions of the area investigated such as at Levant Basin and nearest Rhodes Basin.

- The largest difference in depth between the measured shipboard bathymetric data and the satellite data (e.g. Sandwell's version 10.1 global grid from Sandwell et al., 1997) amounts to 250 m and is located at subduction trenches.

- The differences between the satellite and the shipboard data are small in some regions of the area investigated. These occurred mostly near to land. Furthermore, some strong deviations in some regions are spatially correlated with bathymetric depth and geological structures can be also obvious.

◆ In general, as the potential field data alone do not provide definite models of the geological structures, the seismic constraints are necessary. Additionally, the results of geological studies and other geophysical experiments play a major role in the creation of the models. The two and three-dimensional gravity modelling performed render very satisfactory results. The modelling parameters are constrained by the bathymetric models, gravity anomalies and the seismic results. The following main conclusions can be drawn from interpreting the gravity data:

- Two-dimensional gravity modelling derived along seismic profile A-A^{||} (Figure 5.3) showed that the positive gravity field along and in the north of Cyprus coincides with the ophiolite cover over Cyprus, which is obducted over a continental crust. Such an ophiolite is also identified in southern Turkey and northwest Arabian plate. The transition of the oceanic-continental crust occurs near the coast of Israel, the Moho lies at a depth of about 32 km beneath Cyprus, and at a depth of about 27 km at the coast of Israel.

- Two-dimensional gravity modelling derived along seismic profile B-B^{||} (Figure 5.4) revealed that the deep parts of the Levant Basin is covered by about 13 km of sediments. The crust is oceanic and about 9 to 10 km in thickness, with an abrupt transition to the continental margin to the east indicating the existence of a shear zone. The Moho depth varies from about 26 km beneath the Eratosthenes Seamount to about 23 km under the Levant Basin, and to about 24 km under the Israel coast.

- Two-dimensional gravity modelling derived along seismic profile C-C^{||} (Figure 5.5) showed that the depth to the basement lies at about 6 km beneath the Egyptian coast. However, the thickness of the sedimentary layer increases towards the East Mediterranean Ridge. In the Herodotus abyssal plain, the depth to the basement varies between about 10 to 13 km and increases up to about 14.5 km beneath the East Mediterranean Ridge. The sedimentary layer thins rapidly at the Hellenic Arc towards the west flank of Rhodes. The Moho lies at a depth of about 27 km at the Egyptian coast and then rises to a minimum depth of about 19 km beneath the Herodotus abyssal plain. The depth to the Moho increases again from about 26 km below the East Mediterranean Ridge to about 30 km below the Hellenic Arc. Also at the East Mediterranean Ridge, the increase in negative gravity anomaly corresponds with the relatively large thickness

of the sedimentary layer. The transition from continental to oceanic crust within the African plate occurs at a distance of about 100 km from the Egyptian coast.

- Two-dimensional gravity modelling derived along seismic profile D-D^{||} (Figure 5.6) revealed that the basement depth varies between about 9 km at the Egyptian coast and about 13 km at the Herodotus Abyssal Plain and beneath the East Mediterranean Ridge. A thin layer of sediments covers the Aegean continental crust. The transition of continental to oceanic crust within the African plate is modelled to extend offshore to a distance of about 40 km from the Egyptian coast. The African oceanic crust is subducted beneath the Island of Crete, according to the main driving force for the opening of the Cretan Sea. The thickness of the accretionary complex is up to about 12 km at the East Mediterranean Ridge. The boundary of the accretionary wedge and the crustal backstop of the outer Hellenic Arc is located at 100 -130 km seaward from the coast of Crete within the northern part of the Mediterranean Ridge.

- ◆ This study presents the three-dimensional gravity modelling along an area which covers the whole subduction region in the area of study in order to contribute to a better understanding of the crustal structure of this region and its relation with the adjacent areas. Furthermore it shows the model geometry of the contact between the African and Eurasian plate. The area of three-dimensional gravity modelling was located between 31.01° and 36.49° N and was constructed along 18 parallel vertical planes extending from the coast of Egypt in NW direction. From interpreting the gravity data, the following main conclusions have been reached:

- The modelled area reproduces the observed gravity anomalies successfully. The anomalies are oriented roughly parallel to the bathymetric and topographic features as observed in all the planes of the modelled area.

- The calculated and measured gravity have negative values increasing gradually from -220 to -2 mGal. Local high and low gravity values were observed. As shown for example at Anaximander Seamounts (Figure 5.13), at Rhodes Basin (Figure 5.15), and at Strabo Trench (Figure 5.23). This is due to significant crustal thickening in these regions. The gravity values seaward of the subduction trenches form a complicated pattern.

- In the south-eastern part of the modelled area, the transition from continental to oceanic crust within the African plate decreases abruptly from about 100 km through plane 9 (Figure 5.19) to about 40 km through planes 10, 11, and 12 as illustrated in Figures 5.20, 5.21, and 5.22 respectively. It increases again to about 100 km through plane 13 (Figure 5.23). This reflects a very good match between the topographic features along the Egyptian coast and the main tectonic elements in this area (see Figure 2.1). Also, it reflects the effect of an active eastern Med-

iterranean transcurrent fault system running through the Ionian Sea, the continental margin of Eastern Libya and western Egypt, into the land area through the Nile Delta and eventually into the Gulf of Suez (Figure 2.2).

- In the north-western part of the modelled area, the horizontal distance of the transition between the oceanic and continental crust at a distance between 400 to 450 km can be followed through planes 2 to 9 (Figures 5.12 to 5.19) and also at a distance between 300 to 350 km through planes 10 to 17 (Figures 5.20 to 5.27). This may be related to the African oceanic crust being subducted beneath the Hellenic Arc. In addition, the African oceanic crust is subducted beneath the Island of Crete, according to the main driving force for the opening of the Cretan Sea.

- There are several undulations in average thickness of the mantle layer of the model. In the north-western part of the modelled area, between 350 to 550 km the average thickness of the mantle layer ranges from about 10 to 22 km. In the south-eastern part of the modelled area, the average thickness of the mantle layer is 27 km towards the Egyptian coast. In the middle part the average thickness of the mantle layer is about 30 km.

- Strong lateral undulations in the average thickness of the mantle layer are substantial at the western part on the modelled area towards Cretan Island Arc through planes 11 to 17. This may reflect the effect of the main driving force for the opening of the Cretan Sea through these planes (Figure 5.32).

- At the north-western part of the modelled area, the average thickness of the oceanic crust near 550 km, below the Anaximander Seamounts on plane 2 is about 30 km. This decreases to a thickness of about 25 km, near 500 km towards NW Rhodes Basin on planes 6 and 9. However it increases from about 25 km, near 500 km on plane 9 to about 35 km between 400 to 430 km below the subduction trenches on planes 10 and 11 as shown by the arrows in Figure 5.31.

◆ The seismic experiments performed on the investigated area were conducted by various international organizations. From these investigation, the following may be deduced:

- The main tectonic elements of the study area reflect the geological evolution of the Eastern Mediterranean Sea. Seismic profile results indicate that the thickness and velocity values of the crystalline unit under the Levant Basin are similar to the values determined for a normal oceanic crust.

- The crustal structure of the Levant Basin is oceanic, while that of the Eratosthenes Seamount is continental. The seismic results indicated a continental crust 35 km thick under Cyprus and an oceanic crust 8 km thick, in the Levant Basin between the continental margin of

southern Israel and the Eratosthenes Seamount. The oceanic crust is covered by 12 -14 km of sediments.

- To the south and southwest of Crete, the continental crust gradually thins to a minimum of 17 km and at the southern coast of Crete is about 10 km. The eastern part of Crete shows a significantly thinner crust of 24 to 26 km. To the North, the crustal thickness decreases to 15 km below the central Cretan Sea. Furthermore, the crustal structure of the African margin is complex and varies laterally.

- The seismic results of the Western Desert of Egypt showed that the Egyptian coast is underlain by a continental crust covered by 4-6 km thick sedimentary layer. The crust is about 26 km thick below the Mediterranean Sea and the thickness increases towards the east to about 30 km.

- In the trench areas, the Ptolemy, Pliny and Strabo Trenches, the thickness of the sedimentary cover below is less than that beneath the Mediterranean Ridge. The formation of these trenches is not attributed to the subduction of the African plate but to the strike-slip movements within the Aegean continental lithosphere.

- ◆ Finally, the study of the seismicity and focal mechanisms in the study area is in good agreement with the geodynamic and plate tectonic model (see Figure 7.1 and Chapter VI) derived from this and previous studies.

ACKNOWLEDGEMENTS

I would like to express my deep gratitude to Prof. Dr. Torsten Dahm, Professor of Seismology, Institute of Geophysics, Faculty of Earth Sciences, University of Hamburg for his keen supervision, review of this work, valuable suggestions and for his constructive comments.

Gratitude and thanks are due to Dr. G. Ali Dehghani, Scientist and Faculty member at the Institute of Geophysics, Faculty of Earth Sciences, University of Hamburg, head of the Marine gravity and magnetic group for suggesting the research task, his careful supervision, helpful suggestions, and encouragement.

Many sincere thanks to Dr. Sabine Schmidt, Gravity Research Group, Institute of Geophysics, University of Berlin for enabling me to work with the program IGMAS.

Great appreciation is also extended to Dr. Georges Balmino and Mr. Gilles Balma, Bureau Gravimétrique International (B. G. I), Avenue Edouard Belin, France, for providing the onshore and offshore of geophysical field data on the study area. It is my pleasure to thank Prof. Dr. Ole B. Andersen, Senior Research Scientist, at the Kort & Matrikelstyrelsen (National Survey and Cadastre), Geodetic Department, Copenhagen, Denmark for his help in providing KMS99, KMS02 satellite altimeter gravity and bathymetry data necessary for the study area.

Deepest gratitude also goes to all members and colleagues at the Institute of Geophysics, Faculty of Earth Sciences, University of Hamburg; especially Gesa Netzeband, Tina Kaschwich, Jörg Reinhardt, and Marco Brönnner for their unfailing help. I express my gratitude to Dr. Kate Richards at the Institute for Meteorology, University of Hamburg, and Dr. Raafat El Awaady, Radiotherapy Unit, Hospital of Hamburg University for reviewing the manuscript of this thesis.

I wish to express my appreciation to the members of my dissertation committee: Prof. Dr. Torsten Dahm, Dr. G. Ali Dehghani, Prof. Dr. Claus-Dieter Reuther, Dr. Sabine Schmidt, and Dr. Christian Hübscher.

I am particularly indebted to the Cultural Department and Study Mission, Arab Republic of Egypt, for their financial support and encouragement during the course of this study. Last but not least my heartfelt gratitude are due to my family. I thank my wife and both sons for their patience, and understanding throughout the period of my study.

Hamdy A. M. Aboulela

2003

REFERENCES

Abdel Aal, A.; El Barkooky, A.; Gerrits, M.; Meyer, H.; Schwander, M. and Zaki, H. and Shell Egypt Deep Water B. V., 2000. Tectonic evolution of the Eastern Mediterranean Basin and its significance for hydrocarbon prospectivity in the ultradeepwater of the Nile Delta. The Leading Edge, October, Pp. 1086-1102.

Abdelrahman, E.; Riad, S.; Refai, E. and Amin, Y., 1985. On the least-squares residual anomaly determination. Geophysics, Vol. 50, No. 3, Pp. 473-480.

Abdelrahman, E.; Bayoumi, H. and EL-Araby, H., 1991. A least -squares minimization approach to invert gravity data. Geophysics, Vol. 56, Pp. 115-118.

Aboulela, H., 1994. A study on the tectonic activity and seismicity in the Suez Canal region. M. Sc. Thesis, Fac. Sci., Suez Canal Univ., Egypt, P. 133.

Adam, J.; Reuther, C.; Grasso, M. and Torelli, T., 2000. Active fault kinematics and crustal stresses along the Ionian margin of southeastern Sicily. Tectonophysics, Vol. 326, Pp. 217-239.

Allan, T. and Morelli, C., 1971. A geophysical study of the Mediterranean Sea. Bollettino Di Geofisica Teorica ED Applicata, Vol. 13, No. 50, Pp. 99-142.

Ambraseyes, N. and Jackson, J., 1990. Seismicity and associated strain of central Greece between 1890 and 1988. Geophysical Journal International, Vol. 101, Pp. 663-708.

Ambraseyes, N. and Jackson, J., 1998. Faulting associated with historical and recent earthquakes in the eastern Mediterranean region. Geophysical Journal International, Vol. 133, Pp. 390-406.

Anastasakis, G. and Kelling, G., 1991. Tectonic connection of the Hellenic and Cyprus arcs and related geotectonic elements. Marine Geology, Vol. 97, Pp. 261-277.

Andersen, O. and Knudsen, P., 1995. Global gravity field from the ERS-1 geodetic mission. Earth Observation Quarterly (EOQ), ESRIN, Vol. 47, Pp 1-5.

Andersen, O.; Woodworth, P. and Flather, R., 1995. Intercomparison of recent global ocean tide models. *Journal of Geophysical Research*, Vol. 100, C 12, Pp. 25261- 25282.

Andersen, O. and Knudsen, P., 1998. Global marine gravity field from the ERS-1 and Geosat geodetic mission altimetry. *Journal of Geophysical Research*, Vol. 103, No. C4, Pp. 8129-8137.

Andersen, O.; Knudsen, P.; Kenyon, S. and Trimmer, R., 1999. Recent improvements in the KMS global marine gravity field. *Bollettino Di Geofisica Teorica ED Applicata*, Vol. 40, No. 3-4, Pp. 369-377.

Badawy, A. and Horvath, F., 1999 a. Recent stress field of the Sinai subplate region. *Tectonophysics*, Vol. 304, Pp. 385-403.

Badawy, A. and Horvath, F., 1999 b. Seismicity of the Sinai subplate region: Kinematic implications. *Journal of Geodynamics*, Vol. 27, Pp. 451-468.

Badawy, A. and Abdel Fattah, A., 2001. Source parameters and fault plane determinations of the 28 December 1999 northeastern Cairo earthquakes. *Tectonophysics*, Vol. 343, Pp. 63-77.

Balmino, G.; Moynot, M.; Sarrailh, M. and Vales, N., 1987. Free Air gravity anomalies over the oceans from Seasat and Geos3 altimeter data. *EOS Trans., AGU*, Vol. 68, No. 2, Pp. 17-18.

Barka, A., 1992. The North Anatolian fault zone. *Annales Tectonicae*, Vol. 6, Pp. 164-195.

Barka, A. and Reilinger, R., 1997. Active tectonics of the Eastern Mediterranean region: deduced from GPS, neotectonic and seismicity data. *Annali Di Geofisica*, Vol. XL, No. 3, Pp. 587-610.

Barnett, C., 1976. Theoretical modeling of the magnetic and gravitational field of an arbitrarily shaped three-dimensional body. *Geophysics*, Vol. 41, No. 6, Pp. 1353-1364.

Ben-Avraham, Z. and Nur, A., 1976. Slip rates and morphology of continental collision belts. *Geology*, Vol. 4, Pp. 661-664.

Ben-Avraham, Z. and Nur, A. and Vered, M., 1976. Tectonic, seismicity and structure of the Afro-Eurasian junction the breaking of an incoherent plate. *Physics of the Earth and Planetary Interiors*, Vol. 12, Pp. 1-50.

Ben-Avraham, Z., 1978. The structure and tectonic setting of the Levant continental margin, Eastern Mediterranean. *Tectonophysics*, Vol. 46, Issues 3-4, Pp. 313-331.

Ben-Avraham, Z. and Nur, A., 1986. Collisional processes in the Eastern Mediterranean. *Geol. Rundschau*, Vol. 75, Pp. 209-217.

Ben-Avraham, Z.; Nur, A. and Cello, G., 1987. Active transcurrent fault system along the north African passive margin. *Tectonophysics*, Vol. 141, Pp. 249-260.

Ben-Avraham, Z.; Kempler D. and Ginzburg, A., 1988. Plate convergence in the Cyprean Arc. *Tectonophysics*, Vol. 146, Pp. 231-240.

Ben-Avraham, Z., 1989. Multiple opening and closure of the Eastern Mediterranean and south China Basins. *Tectonics*, Vol. 8, No. 2, Pp. 351-362.

Ben-Avraham, Z.; Tibor, G.; Limonov, A.; Leybov, M.; Ivanov, M.; Tokarev, M. and Woodside, J., 1995. Structure and tectonics of the Eastern Cyprean Arc. *Marine and Petroleum Geology*, Vol. 12, No. 3, Pp. 263-271.

Ben-Avraham, Z.; Ginzburg, A.; Makris, J. and Eppelbaum, L., 2002. Crustal structure of the Levant Basin, Eastern Mediterranean. *Tectonophysics*, Vol. 346, Pp. 23-43.

Ben-Menahem, A.; Nur, A. and Vered, M., 1976. Tectonics, seismicity and structure of the Afro-Eurasian junction-the breaking of an incoherent plate. *Physics of the Earth and Planetary Interiors*, Vol. 12, Pp. 1-50.

Ben-Menahem, A., 1991. Four thousand years of seismicity along the Dead Sea rift. *Journal of Geophysical Research*, Vol. 96, No. B12, Pp. 20195-20216.

Best, J.; Barazangi, M.; Al-Saad, D.; Sawaf, T. and Gebran, A., 1993. Continental margin evolution of the northern Arabian platform in Syria. *American Association Petroleum Geologists Bulletin*, Vol. 77, Pp. 173-193.

Beydoun, Z., 1991. Arabian plate hydrocarbon geology and potential? a plate tectonic approach. *Studies in geology*, 33, American Association of Petroleum Geologists, Tulsa, Oklahoma, USA, 77 p.

Biju-Duval, B.; Letouzey, J. and Montadert, L., 1978. Structure and evolution of the Mediterranean basins. In: Hsue, K. and Montadert et al. (Editors), *Initial Report of the Deep Sea Drilling project*, Vol. 42, Part 1, Pp. 951-984.

Birch, F., 1960. The velocity of compressional waves in rocks to 10 Kilobars, Part I. *Journal of Geophysical Research*, Vol. 65, No. 4, Pp. 1083-1102.

Birch, F., 1961. The velocity of compressional waves in rocks to 10 Kilobars, Part II. *Journal of Geophysical Research*, Vol. 66, No. 7, Pp. 2199-2224.

Bohnhoff, M., 2000. Untersuchung der Krustenstruktur der region Kreta durch Weitwinkelseismische Vermessungen. Ph. D. Thesis, Institute of Geophysics, University of Hamburg, Germany, No. 19, P. 150.

Bohnhoff, M.; Makris, J.; Papanikolaou, D. and Stavrakakis, G., 2001. Crustal investigation of the Hellenic subduction zone using wide aperture seismic data. *Tectonophysics*, Vol. 343, Pp. 239-262.

Brenneke, J. and Lelgemann, D., 1983. Geoid and gravity anomalies in the North Sea area derived from SEASAT altimeter data. *Manuscripta geodaetica*, Vol. 8, Pp. 301-320.

Brönnner, M., 2003. Untersuchung des krustenaufbaus entlang des Mediterranen Rückens abgeleitet aus geophysikalischen Messungen. Ph. D. Thesis, Institute of Geophysics, University of Hamburg, Germany, No. 21, P. 170.

Cagatay, M.; Görür, N.; Alpar, B.; Saatçilar, R.; Akkök, R.; Sakinc, M.; Yüce, H.; Yaltrirak, C. and Kusu, I., 1998. Geological evolution of the Gulf of Saros, NE Aegean Sea. *Geo-Marine Letters*, Vol. 18, Pp. 1-9.

Chaumillon, E.; Mascle, J. and Hoffmann, H., 1996. Deformation of the western Mediterranean Ridge: importance of Missinian evaporitic formations. *Tectonophysics*, Vol. 263, Pp. 163-190.

Comninakis, P. and Papazachos, B., 1972. Seismicity of the Eastern Mediterranean and some tectonic features of the Mediterranean Ridge. *Geological Society of America Bulletin*, Vol. 83, Pp. 1093-1102.

Courtillot, V.; Armijo, R. and Tapponnier, P., 1987. The Sinai triple junction revisited. *Tectonophysics*, Vol. 141., Pp. 181-190.

Darkal, A.; Krauss, M. and Ruske, R., 1990. The Levant fault zone. *Zeitschrift von geologische Wissenschaft*, 18, Pp. 549-562.

Davis, J., 1973. *Statistics and data analysis in geology*: John Wiley and Sons, New York.

Dehlinger, P., 1978. *Marine Gravity*: Elsevier scientific publishing company, Amsterdam-Oxford-New York.

Dehghani, G. A., 1994. Meteor-Berichte: Mittelmeer 1993, Cruise No. 25, 12 May-20 Aug, 1993. Hieke, W.; Halbach, P.; Türkay, M. and Weikert, H. (Eds.), *Int. reports*, Pp. 188-192.

Dehghani, G. A., 1999. Meteor-Berichte: Mittelmeer 1997/98, Cruise No. 40, 28 Oct, 1997-10 Feb, 1998. Hieke, W.; Helmleben, C.; Linke, P.; Türkay, M. and Weikert, H. (Eds.), *Int. reports*, Pp. 42-45.

Dehghani, G. A. and Kaminski, J. (pers. communication). Modified of the two-dimensional gravity model of software TWGRAV (Talwani two-dimensional gravity modelling).

Delibasis, N.; Ziaziaa, M.; Voulgaris, N.; Papadopoulos, T.; Stavrakakis, G.; Papanastassiou, D. and Drakatosb, D., 1999. Microseismic activity and seismotectonics of Heraklion area (central Crete Island, Greece). *Tectonophysics*, Vol. 308, Pp. 237-248.

DeMets, C.; Gordon, R.; Argus, D. and Stein, S. 1990. Effect of recent revisions to the geomagnetic reversal time scale on estimates of current plate motions. *Geophysical Research Letters*, Vol. 21, No. 20, Pp. 2191-2194.

Dercourt, J.; Zoneshain, L.; Ricov, L.; Kazmin, V.; Le Pichon, X.; Knipper, A.; Grandjacquet, C.; Sbertshikov, I.; Geyssant, J.; Lepvrier, C.; Perchersky, D.; Bovlin, J.; Sibuet, J.; Savostin, L.; Sorokhtin, O.; Westphal, M.; Bazhenov, M.; Lauer, J. and Biji-Duval, B., 1986. Geological evolution of the Tethys belt from the atlantic to the pamirs since the LIAS. *Tectonophysics*, Vol. 123, Pp. 241-315.

DESERT 2000 Group., 2000 a. Multinational geoscientific research effort kicks off in the Middle East. *EOS, Transactions, AGU*, Vol. 81, No. 50, Pp. 609, 661-617.

DESERT 2000 Group., 2000 b. The DESERT passive seismic experiment 2000/2001 in the Middle East. *Observatories and research facilities for european seismology*, Vol. 4, No. 1, May 2002.

De Voogd, B.; Truffert, C.; Chamot-Rooke, N.; Huchon, P.; Lallemand, S. and Le Pichon, X., 1992. Two-ship deep seismic soundings in the basins of the Eastern Mediterranean Sea (Pasiphae cruise). *Geophysical Journal International*, Vol. 109, Pp. 536-552.

Dewey, J.; Pitman, W.; Ryan, W. and Bonnin, J., 1973. Plate tectonics and the evolution of the Alpine system. *Geological Society of America Bulletin*, Vol. 84, Pp. 3137-3180.

Dobrin, M., 1976. *Introduction to geophysical prospecting: Third Edition*, Mc. Graw-Hill Book Co. Inc., New York. P. 867.

Egeran, E., 1948. *Tektonique de la Turquie et relation entre les runites tectoniques et les gites metalliferes de la Turquie*. Nancy, 1947 adly eseri üzerine. Ankara Üniversitesi DTCTF. Dergisi.

Cilt VI, Say: 3, Pp. 208-212.

El-Dididy, S., 2001. Notes on the earthquake hazard and risk in Egypt. Global blueprints for change. International workshop on disaster reduction convened on Aug. 19-22.

El-Kelani, R.; Abu-Ayyash, K.; Ben-Avraham, Z.; Mechie, J.; Weber, M. and DESERT 2000 Group., 2000. A wide angle seismic profile across the Jordan-Dead Sea rift (Transform). A multi-national and interdisciplinary study. DESERT workshop-July, 2002.

Erwan, G.; Doglioni, C. and Fernandez, M. 1998. On the post-25 Ma geodynamic evolution of the western Mediterranean. *Tectonophysics*, Vol. 298, Pp. 259-269.

Featherstone, W. 2001. Comparison of recent satellite altimeter-derived gravity anomalies with one another, EGM96 and ship-borne gravimetry around Australia. "on-line at", <http://www.cage.curtin.edu.au/~will/altimeter5.pdf>.

Featherstone, W.; Kirby, J.; Holmes, S.; Fotopoulos, G. and Goos, J., 2002. Recent research towards an improved geoid model for Australia. Joint Aur. Inst. Surv. Conf., Adelaide, south Australia, 25-30 Nov.

Finetti, I. and Morelli, C., 1973. Geophysical exploration of the Mediterranean Sea. *Bollettino Di Geofisica Teorica ED Applicata*, Vol. 15, No. 60, Pp. 261-341.

Freund, R.; Garfunkel, Z.; Goldberg, M.; Weissbrod, T. and Derin, B., 1970. The shear along the Dead Sea rift. *Philos. Trans. Roy. Soc. London, A* 267, Pp. 107-130.

Freund, R.; Goldberg, M.; Weissbrod, T.; Druckman, Y. and Derin, B., 1975. The triassic - jurassic structure of Israel and its relation to the origin of the Eastern Mediterranean. *Geol. Surv. Israel Bull.*, Vol. 65, Pp. 1-26.

Fu, L. and Cazenave, A., 2001. *Satellite Altimetry and Earth Sciences: A handbook of techniques and applications*. Int. Geophys. Ser., Vol. 69, Academic Press, San Diego, USA, P. 463.

- Garfunkel, Z. and Bartov, Y., 1977. The tectonics of the Suez rift. *Geol. Surv. Israel Bull.*, Vol. 71, Pp. 1-41.
- Garfunkel, Z. and Freund, R., 1981. Active faulting in the Dead Sea rift. *Tectonophysics*, Vol. 80, Pp. 1-26.
- Garfunkel, Z., 1984. Large-scale submarine slumps and growth faults in the Eastern Mediterranean. *Marine Geology*, Vol. 55, Pp. 303-324.
- Garfunkel, Z. and Almagor, G., 1985. Geology and structure of the continental margin off northern Israel and the adjacent part of the Levantine basin. *Marine Geology*, Vol. 62, Pp. 105-131.
- Garfunkel, Z., 1998. Constrains on the origin and history of the Eastern Mediterranean basin. *Tectonophysics*, Vol. 298, Pp. 5-35.
- Gass, I. and Masson-Smith, D., 1963. The geology and gravity anomalies of the Troodos Massif, Cyprus. *Philosophical Transactions of the Royal Society of London, Series A, Mathematical and Physical Sciences*, Vol. 255, No. 1060, Pp. 417-467.
- Giermann, G., 1969. The Eastern Mediterranean Ridge. *Rapp. Comm. Int. Mer Medit.*, Vol. 19, Pp. 605-607.
- Giermann, G., 1971. Some geophysical profiles in the Eastern Mediterranean. *Geological Society of America Bulletin*, Vol. 82, No. 1, Pp. 91-100.
- Gillis, K. and Robinson, P., 1990. Patterns and processes of alteration in the lavas and dykes of the Troodos Ophiolite, Cyprus. *Journal of Geophysical Research*, Vol. 95, Pp. 21523-21548.
- Ginzburg, A.; Makris, J.; Fuchs, K.; Prodehl, C.; Kaminski, W. and Amitai, A., 1979 a. A seismic study of the crust and upper mantle of the Jordan-Dead Sea rift and their transition toward the Mediterranean Sea. *Journal of Geophysical Research*, Vol. 84, No. B4, Pp. 1569-1582.

Ginzburg, A.; Makris, J.; Fuchs, K.; Perathoner, B. and Prodehl, C., 1979 b. Detailed structure of the crust and upper mantle along the Jordan-Dead Sea rift. *Journal of Geophysical Research*, Vol. 84, No. B10, Pp. 5605-5612.

Ginzburg, A. and Folkman, Y., 1980. The crustal structure between the Dead Sea rift and the Mediterranean Sea. *Earth and Planetary Science Letters*, Vol. 51, Pp. 181-188.

Ginzburg, A.; Makris, J.; Fuchs, K. and Prodehl, C., 1981. The structure of the crust and upper mantle in the Dead Sea rift. *Tectonophysics*, Vol. 80, Pp. 109-119.

Ginzburg, A.; Folkman, Y.; Rybakov, M.; Rostein, Y., Assael, Y. and Yuval, Z., 1993. Israel: Bouguer gravity map, scale 1:250,000. Survey of Israel.

Ginzburg, A.; Ben-Avraham, Z.; Makris, J.; Hubral, P. and Rotstein, Y., 1994. Crustal structure of northern Israel. *Marine and Petroleum Geology*, Vol. 11, No. 4, Pp. 501-506.

Girdler, R., 1991. The Afro-Arabian rift system-an overview. *Tectonophysics*, Vol. 197, Pp. 139-153.

Glover, C. and Robertson, A., 1998. Neotectonic intersection of the Aegean and Cyprus tectonic arcs: extensional and strike-slip faulting in the Isparta Angle, SW Turkey. *Tectonophysics*, Vol. 298, Pp. 103-132.

Götze, H.-J., 1978. Ein numerisches verfahren zur berechnung der gravimetrischen feldgrößen drei-dimensionaler modellkörper. *Arch. Met. Geoph. Biokl., Ser. A*, 25, Pp. 195-215.

Götze, H.-J., 1984. Über den einsatz interaktiver computergraphik im rahmen 3-dimensionaler interpretationstechniken in gravimetrie und magnetik. *Habilitations-Schrift*, 121 Seiten, Technische Universität Clausthal.

Götze, H.-J. and Lahmeyer, B., 1988. Application of three-dimensional interactive modeling in gravity and magnetics. *Geophysics*, Vol. 53, No. 8, Pp. 1096-1108.

- Götze, H.-J., Schmidt, S., Goltz, G., Alvers, M., Klesper, Ch. and Hoffman, M., 2000. IGMAS Interactive Gravity and Magnetic Application System. http://userpage.fu-berlin.de/~sschmidt/Sabine_IGMAS.html.
- Guiraud, R. and Bosworth, W., 1999. Phanerozoic geodynamic evolution of the northeastern Africa and the northwestern Arabian platform. *Tectonophysics*, Vol. 315, Pp. 73-108.
- Halsey, G. and Grandner, W., 1975. Tectonic analysis of Egypt using ERTS-1 satellite Data. A lecture delivered at the GPC, Cairo, Egypt.
- Hancock, P. and Atiya, M., 1979. Tectonic significance of mesofracture systems associated with the Lebanese segment of the Dead Sea transform fault. *Journal of Structural Geology*, Vol. 1, Pp. 143-153.
- Harjes, H., 2001. Imaging the Hellenic subductions zone near Crete by using microseismicity. *Schriftenreihe der deutschen geologischen gesellschaft*, Heft 14. Roth, S. & A. Rüggeberg (eds.). Margins meeting, Kiel, C3, Oct 2-6, P. 82.
- Harrison, J., 1955. An interpretation of gravity anomalies in the Eastern Mediterranean. *Philosophical Transactions of the Royal Society of London, Series A, Mathematical and Physical Sciences*, Vol. 248, No. 947, Pp. 283-325.
- Hartung, M., 1987. Geophysikalische vermessung des Kreta-Meeres unter besonderer Beruecksichtigung refraktionsseismischer daten. M. Sc.Thesis, Institute of Geophysics, University of Hamburg, Germany, P. 241.
- Haxby, W., 1987. Gravity field of the worlds oceans: a portrayal of gridded geophysical data derived from GEOSAT rader altimeter measurements of the shape of the ocean surface, Department of the US Navy, Office of Naval Research and NOAA Data Center, Boulder, Colorado. USA.
- Haxby, W.; Karner, G.; LaBrecque, J. and Weissel, J., 1983. Digital images of combined oceanic and continental data sets and their use in tectonic studies. *EOS*, Vol. 64, No. 52, Pp. 995-

1004.

Helms, S., 2001. Der aufbau des Mediterranen Rückens, abgeleitet aus weitwinkelreflexions- und refraktionsseismischen Messungen. M. Sc. Thesis, Institute of Geophysics, University of Hamburg, Germany, P. 73.

Hipkin, R., 2000. Modelling the geoid and sea-surface topography in coastal areas. Physics and chemistry of the Earth, Vol. 25, No. 1, Pp. 9-16.

Hübscher, C.; Dehghani, A.; Gohl, K.; Pätzold, J. and GEMME Working Group., 2002. New data from the easternmost Nile system-the gemme project. Mediterranean and Black Seas turbidite systems and deep Sea fans, CIESM workshop series, Bucarest, 5-8 June, Pp. 39-42.

Huguen, C.; Mascle, J.; Chaumillon, E.; Woodside, J.; Benkhelil, J.; Kopf, A. and Volkonskaia, A., 2001. Deformational styles of the Eastern Mediterranean Ridge and surroundings from combined swath mapping and seismic reflection profiling. Tectonophysics, Vol. 343, Pp. 21-47.

Ilinski, D.; Makris, J. and Casten, U., 2000. 3 D density model of Crete constrained by seismic data. ICDP/KTB Kolloquium, Wissenschaftliches programm und Abstract, Ruhr-Universität Bochum, Pp. 99-104.

Jackson, J. and Mckenzie, D., 1984. Active tectonics of the Alpine-Himalayan Belt between western Turkey and Pakistan. Geophysical Journal of the Royal Astronomical Society, Vol. 77, No. 1, Pp. 185-265.

Jackson, J. and Mckenzie, D., 1988. The relationship between plate motions and seismic moment tensors, and the rates of active deformation in the Mediterranean and Middle East. Geophysical Journal, Vol. 93, Pp. 45-73.

Jackson, J., 1992. Partitioning of strike-slip and convergent motion between Eurasia and Arabia in eastern Turkey and the Caucasus. Journal of Geophysical Research, Vol. 97, Pp. 12471-12479.

- Jarriage, J.; D'Estevou, P.; Burrollet, P.; Montenat, C.; Part, P.; Richert, J. and Thiriet, J., 1990. The multistage tectonic evolution of the Gulf of Suez-northern Red sea continental rift from field observations. *Tectonics*, Vol. 9, No. 3, Pp. 441-465.
- Jestin, F.; Huchon, P. and Gaulier, J., 1994. The Somalia plate and East African rift system: present-day kinematics. *Geophysical Journal International*, Vol. 116, Pp. 637-654.
- Joffe, S. and Garfunkel, S., 1987. Plate kinematics of the circum Red Sea-re-evaluation. *Tectonophysics*, Vol. 141, Pp. 5-22.
- Kahle, H.-G.; Straub, C.; Reilinger, R.; McClusky, S.; King, R.; Hurst, K.; Veis, G.; Kastens, K. and Cross, P., 1998. The strain rate field in the eastern Mediterranean region, estimated by repeated GPS measurements. *Tectonophysics*, Vol. 294, Pp. 237-252.
- Kasahara, K. and Stevens, A., 1969. A symposium on processes in focal region. *Publ. Dominion Obs. Ottawa*, Vol. 37, Pp. 183-235.
- Kasahara, K., 1981. *earthquake mechanics*: Cambridge Uni., Press, P. 221.
- Kastens, K., 1991. Rate of outward growth of the Mediterranean ridge accretionary complex. *Tectonophysics*, 199, Pp. 25-50.
- Kawasumi, H., 1937. An historical sketch of the development of knowledge concerning the initial motion of an earthquake. *Publications du Bureau central seismologique international, series A, Travaux Scientifique*, 15, Pp. 1-76.
- Kebeasy, R., 1990. Seismicity: In *The Geology of Egypt* (Said, R. Eds.), A. A. Balkema, Brookfield, Pp. 51-59.
- Kempler, D. and Ben-Avraham, Z., 1987. The tectonic evolution of the Cyprean Arc. *Annales Tectonicae*, Vol. 1, Pp. 58-71.
- Kempler, D. and Garfunkel, Z., 1991. The northeast Mediterranean triple junction from a plate

kinematics point of view. Bull. Tech. Uni. Istanbul, Vol. 44, Pp. 425-454.

Kempler, D. and Garfunkel, Z., 1994. Structures and kinematics in the northeastern Mediterranean: A study of an irregular plate boundary. Tectonophysics, Vol. 234, Pp. 19-32.

Kempler, D., 1998. Eratosthenes Seamount: the possible spearhead of incipient continental collision in the Eastern Mediterranean. Proceeding of the Ocean Drilling program, Scientific Results, Vol. 160, Pp. 709-721.

Kiratzi, A., and Papazachos, C., 1995. Active crustal deformation from the Azores triple junction to the Middle East. Tectonophysics, Vol. 243, Pp. 1-24

Klinger, Y.; Avouac, J.; Dorbath, L.; Abou Karaki, N. and Tisnerat, N., 2000. Seismic behaviour of the Dead Sea fault along Araba valley. Jordan. Geophysical Journal International, Vol. 142, Pp. 769-782.

Knapmeyer, M. and Harjes, H.-P., 2000. Seismic Discontinuities in the Vicinity of the Islands of Crete and Santorini (Greece). General Assembly, European Geophysical Society, Nice, France, Geophysical Research Abstracts, 2, P. 111. [C3].

Knudsen, P., and Andersen, O. 1998. Global marine gravity and mean sea surface from multi-mission satellite altimetry. In "Geodesy on the Move, Gravity, geoid, geodynamics and Antarctica", Proceedings IAG scientific assembly, IAG symposia, 119, Springer, Berlin, Pp. 132-138.

Kovachev, S.; Kuzin, I. and Soloviev, S. 1992. Microseismicity of the frontal Hellenic Arc according to OBS observations. Tectonophysics, Vol. 201, Pp. 317-327.

Lallemant, S.; Truffert, C.; Jolivet, L.; Henry, P.; Chamot-Rooke, N. and De Voogd, B., 1994. Spatial transition from compression to extension in the Wetsren Mediterranean Ridge complex. Tectonophysics, Vol. 234, Pp. 33-52.

Lange, H., 2000. 2D-Schweremodell der Lithosphäre kretas. M. Sc. Thesis, Institute of Geophysics, University of Hamburg, Germany, P. 57.

Le Pichon, X. and Angelier, J., 1979. The Hellenic Arc and trench system: A key to the neotectonic evolution of the Eastern Mediterranean. *Tectonophysics*, Vol. 60, Pp. 1-42.

Le Pichon, X.; Lyberis, N.; Angelier, J. and Renard, V., 1982 a. Strain distribution over the East Mediterranean Ridge: A synthesis incorporating new Sea-Beam data. *Tectonophysics*, Vol. 86, Pp. 243-274.

Le Pichon, X.; Huchon, P.; Angelier, J.; Lyberis, N.; Boulin, J.; Bureau, D.; Cadet, J.; Dercourt, J.; Glacon, G.; Got, H.; Karig, D.; Mascle, J.; Ricou, L. and Thiebault, F., 1982 b. Subduction in the Hellenic Trench: probable role of a thick evaporitic layer based on seabeam and submersible studies. In: Leggett, J. K. (ED). *Trench Forearc Geology*. Spec. Publ. Geol. Soc. Lond., 10, Pp. 319-333.

Le Pichon, X. and Gaulier, J., 1988. The rotation of Arabia and the Levant fault system. *Tectonophysics*, Vol. 153, Pp. 271-294.

Le Pichon, X.; Chamot-Rooke, N.; Lallemant, S.; Noomen, R. and Veis, G., 1995. Geodetic determination of the kinematics of central Greece with respect to Europe: Implications for eastern Mediterranean tectonics. *Journal of Geophysical Research*, Vol. 100, No. B7, Pp. 12675-12690.

Le Pichon, X.; Lallemant, S.; Chamot-Rooke, N.; Lemeur, D. and Pascal, G., 2002. The Mediterranean Ridge backstop and the Hellenic nappes. *Marine Geology*, Vol. 186, Pp. 111-125.

Liebe, T., 1986. Genauigkeitsbetrachtungen und Kriterien zur Erstellung einer seegravimetrischen Karte. M. Sc. Thesis, Institute of Geophysics, University of Hamburg, Germany, P. 86.

Lort, J., 1971. The tectonics of the Eastern Mediterranean: A geophysical review. *Reviews of Geophysics and Space Physics*, Vol. 9, No. 2, Pp. 189-216.

Lort, J., 1973. Summary of seismic studies in the Eastern Mediterranean. *Geol. Soc. Greece Bull.*, Vol. 10, No. 1, Pp. 99-108.

Lort, J.; Limond, W. and Gray, F., 1974. Preliminary seismic studies in the Eastern Mediterranean. *Earth and Planetary Science Letters*, Vol. 21, Pp. 355-366.

Maamoun, M.; Allam, A.; Megahed, A. and Abu El-Ata, A., 1980. Neotectonics and seismic regionalisation of Egypt. *Bull. IISSE*, Vol. 18, Pp. 27-39.

Mahmoud, S., 2003. Seismicity and GPS-derived crustal deformation in Egypt. *Journal of Geodynamics*, Vol. 35, Pp. 333-352.

Makris, J., 1976. A dynamic model of the Hellenic Arc deduced from geophysical data. *Tectonophysics*, Vol. 36, Pp. 339-346.

Makris, J. and Veas, R., 1977. Crustal structure of the central Aegean Sea and the Islands of Evia, Crete, Greece, obtained by refractive seismic experiments. *Journal of Geophysics*, Vol. 42., Pp. 329-341.

Makris, J., 1978 a. The crust and upper mantle of the Aegean region from deep seismic soundings. *Tectonophysics*, Vol. 46, Pp. 269-284.

Makris, J., 1978 b. Some geophysical considerations of the geodynamic situation in Greece. *Tectonophysics*, Vol. 46, Pp. 251-268.

Makris, J.; Ben-Avraham, Z.; Behle, A.; Ginzburg, A.; Giese, P.; Steinmetz, L.; Whitmarsh, R. and Eleftheriou, S., 1983. Seismic refraction profiles between Cyprus and Israel and their interpretation. *Geophysical Journal of the Royal Astronomical Society*, Vol. 75, Pp. 575-591.

Makris, J. and Stobbe, C., 1984. Physical properties and state of the crust and upper mantle of the Eastern Mediterranean Sea deduced from geophysical data. *Marine Geology*, Vol. 55, Pp. 347-363.

Makris, J., 1985. Geophysics and geodynamic implications for the evolution of the Hellenids. In Stanley, D. and Wezel, F. (EDS). *Geological evolution of the Mediterranean Basin*, Pp. 231-248.

Makris, J.; Rihm, R. and Allam, A., 1988. Some geophysical aspects of the evolution and the structure of the crust in Egypt. Eds. El-Gaby and Geriling, R., The Pan African belt of Northeast Africa and adjacent areas. Pp. 345-369.

Makris, J.; Wang, J.; Odintsov, S. and Udintsev, G., 1994. The Magnetic field of the Eastern Mediterranean Sea. In: Krashenininnikov, V. A. & Hall, J. K. (editors), Geological structure of the Northeastern Mediterranean. Cruise 5 of the Research Vessel, Akademik Nikolagj strakhov , Chapter 4, Pp. 75-85.

Makris, J. and Wang, J., 1994. Bouguer gravity anomalies of the Eastern Mediterranean Sea. In: Krashenininnikov, V. A. & Hall, J. K. (editors), Geological structure of the Northeastern Mediterranean. Cruise 5 of the Research Vessel, Akademik Nikolagj strakhov, Chapter 3, Pp. 87-98.

Malovitskiy, Y.; Emelyanov, E.; Kazakov, O.; Moskalenko, V.; Osipov, G.; Shimkus, K. and Chumakov, I., 1975. Geological structure of the Mediterranean Sea floor (based on geological - geophysical data). Marine Geology, Vol. 18, Pp. 231-261.

Mantovani, E.; Albarello, D.; Tamburelli, C.; Babucci, D. and Viti, M., 1997. Plate convergence, crustal delamination, extrusion tectonics and minimization of shortening work as main controlling factors of the recent Mediterranean deformation pattern. Annali Di Geofisica, Vol. XL, No. 3, Pp. 611-643.

Marzouk, I., 1988. Study of crustal structure of Egypt deduced from deep seismic and gravity data. Ph. D. Thesis, Institute of Geophysics, University of Hamburg, Germany, P. 118.

Maerchklin, N.; El-Kelani, R.; Haberland, C.; Ryberg, T.; Scherbaum, F.; Weber, M. and DESERT 2000 Group., 2000. Seismic studies of the Arava Fault, Dead Sea rift transform, Jordan. A multi-national and interdisciplinary study. DESERT workshop-July, 2002.

Masclé, J.; Huguenot, C. and Loncke, L., 2000 a. Evidences for tectonic reactivation along the African continental margins from Egypt to Libya. African continental margins of the Mediter-

anean Sea, CIESM workshop series, Djerba, 22-25 Nov. 2000, Mascle, J. and Briand, F. (Eds)., Pp. 67-70.

Mascle, J.; Benkhelil, J.; Bellaiche, G.; Zitter, T.; Woodside, J.; Loncke, L. and Prismed II Scientific Party., 2000 b. Marine geologic evidence for a Levantine-Sinai plate, a new piece of the Mediterranean puzzle. *Geology*, Vol. 28, No. 9, Pp. 779-782.

McClusky, S.; Balassanian, S.; Barka, A.; Demir, C.; Erginativ, S.; Georgiev, I.; Gurkan, O.; Hamburger, M.; Hurst, K.; Kahle, H.-G.; Kastens, K.; Kekelidze, G.; King, R.; Kotzev, V.; Lenk, O.; Mahmoud, S.; Mishin, A.; Nadariya, M.; Ouzounis, A.; Paradissis, D.; Peter, Y.; Prilepin, M.; Reilinger, R.; Sanli, I.; Seeger, H.; Tealeb, A.; Toksöz, M. and Veis, G., 2000. Global positioning system constraints on plate kinematics and dynamics in the Eastern Mediterranean and Caucasus. *Journal of Geophysical Research*, Vol. 105, No. B3, Pp.5695-5719.

McClusky, S.; Reilinger, R.; Mahmoud, S.; Ben Sari, D. and Tealeb, A., 2003. GPS constraints on Africa (Nubia) and Arabia plate motions. *Geophysical Journal International*, Vol. 155, Pp. 126-138.

Mckenzie, D., 1970. Plate tectonic of the Mediterranean Region. *Nature*, Vol. 226., Pp. 239-243.

Mckenzie, D.; Davies, D. and Molnar, P., 1970. Plate tectonics of the Red Sea and East Africa. *Nature*, Vol. 226, Pp. 243-248.

Mckenzie, D., 1972. Active tectonics of the Mediterranean region. *Geophysical Journal of the Royal Astronomical Society*, Vol. 30, Pp. 109-185.

Mechie, J.; Weber, M.; Abu-Ayyash, K.; Ben-Avraham, Z.; El-Kelani, R. and DESERT 2000 Group., 2000. Wide-Angle seismic data reveal structure across the Jordan-Dead Sea rift (Transform). A multi-national and interdisciplinary study. DESERT workshop-July, 2002.

Menard, H., 1967. Transitional types of crust under small ocean basins. *Journal of Geophysical Research*, Vol. 72, No. 12, Pp. 3061-3073.

- Mercier, J., 1981. Extensional-compressional tectonics associated with the Aegean Arc: comparison with the Andean Cordillera of south Peru-north Bolivia. *Philosophical Transactions of the Royal Society of London, Series A, Mathematical and Physical Sciences*, Vol. 300, Pp. 337-355.
- Morelli, C., 1975. Geophysics of the Mediterranean. *Rapp. Comm. Int. Mer. Medit. Spec.*, Issue 7, Pp. 11-29.
- Morelli, C., 1978. Eastern Mediterranean: geophysical results and implications. *Tectonophysics*, Vol. 46, Pp. 333-346.
- Mueller, B.; Reinecker, J.; Heidbach, O. and Fuchs, K., 2000. The 2000 release of the world stress map, "on-line at", <http://www.world-stress-map.org/>.
- Muller, S. and Kahle, H.-G., 1993. Crust-mantle evolution, structures and dynamics of the Mediterranean-Alpine region, in *Contributions of Space Geodesy to Geodynamics: Crustal Dynamics*, *Geodyn. Ser.*, Vol. 23, Edited by Smith, D. and Turcotte, D., Pp. 249-298.
- Nafe, J. and Drake, C., 1963. Physical properties and marine sediments. In Hill, M. N., Editor, *The Sea*, Vol. 3, New York, Wiley Interscience, Pp. 794-815.
- Nettleton, L., 1954. Regional, residuals, and structures. *Geophysics*, Vol. 19, Pp. 1-22.
- Noomen, R.; Springer, T.; Ambrosius, B.; Herzberger, K.; Kuijper, D.; Mets, G.; Overgaaauw, B. and Wakker, K., 1996. Crustal deformations in the Mediterranean area computed from SLR and GPS observations. *Journal of Geodynamics*, Vol. 21, No. 1, Pp. 73-96.
- Nur, A. and Ben-Avraham, Z., 1978. The Eastern Mediterranean and the Levant: Tectonics of continental collision. *Tectonophysics*, Vol. 46, Pp. 297-311.
- Okabe, M. 1979. Analytical expression for gravity anomalies due to homogenous polyhedral bodies and translations into magnetic anomalies. *Geophysics*, Vol. 44, Pp. 730-741.

Okay, A.; Kaslilar-özcan, A.; Imren, C.; Boztepe-Güney, A.; Demirbace, E. and Kuscu, I., 2000. Active faults and evolving strike-slip basins in the Marmara Sea, northwest Turkey: a multichannel seismic reflection study. *Tectonophysics*, Vol. 321, Pp. 189-218.

Papazachos, B., 1969. Phase velocities of Rayleigh waves in Southeastern Europe and Eastern Mediterranean Sea. *Pure and Applied Geophysics*, Vol. 75, Pp. 47-55.

Papazachos, B., 1973. Distribution of seismic foci in the Mediterranean area and surrounding area and its tectonic implication. *Geophysical Journal of the Royal Astronomical Society*, Vol. 33, Pp. 421-430.

Papazachos, B. and Comninakis, P., 1978. Deep structures and tectonics of the Eastern Mediterranean. *Tectonophysics*, Vol. 46. Pp. 285-296.

Papazachos, B. and Papaioannou, A., 1999. Lithospheric boundaries and plate motions in the Cyprus area. *Tectonophysics*, Vol. 308, Pp. 193-204

Parker, R., 1972. The rapid calculation of potential field anomalies. *Geophysical Journal of the Royal Astronomical Society*, Vol. 31, Pp. 447-455.

Paul, M., 1974. The gravity effect of a homogenous polyhedron for three-dimensional bodies. *Pure and Applied Geophysics*, Vol. 112, Pp. 553-561.

Perincek, D., 1991. Possible strand of the North Anatolian fault in the Thrace Basin, Turkey-an interpretation. *American Association Petroleum Geologists Bulletin* Vol. 75, Pp. 241-257.

Peters, J. and Huson, W., 1985. The Pliny and Strabo Trenches (Eastern Mediterranean): Integration of seismic reflection data and seabeam bathymetric maps. *Marine Geology*, Vol. 64, Pp. 1-17.

Peter, Y.; Kahle, H.-G.; Cocard, M.; Veis, G.; Felekis, S. and Paradissis, D., 1998. Establishment of a continuous GPS network across the Kephallonia Fault Zone, Ionian Islands, Greece.

Tectonophysics, Vol. 294, Pp. 253-260.

Pondrelli, S.; Morelli, A.; Ekström, G.; Mazza, S.; Boschi, E. and Dziewonski, A., 2002. European-Mediterranean regional centroid-moment tensors: 1997-2000. *Physics of the Earth and Planetary Interiors*, Vol. 130, Pp. 71-101.

Piper, D. and Perissoratis, C., 2003. Quaternary neotectonics of the South Aegean arc. *Marine Geology*, Vol. 198, Pp. 259-288.

Planert, L., 2001. Untersuchung des krustenaufbaus durch onshore-offshore weitwinkelseismische Messungen im Bereich des östlichen Mittelerranen Rückens. M. Sc. Thesis, Institute of Geophysics, University of Hamburg, Germany, P. 80.

Plag, H.-P.; Ambrosius, B.; Baker, T.; Beutler, G.; Bianco, G.; Blewitt, G.; Boucher, C.; Davis, J.; Degnan, J.; Johansson, J.; Kakle, H.-G.; Kumkova, I.; Marson, I.; Mueller, S.; Pavlis, E.; Pearlman, M.; Richter, B.; Spakman, W.; Tatevian, S.; Tomasi, P.; Wilson, P. and Zebini, S., 1998. Scientific objectives of current and future WEGENER activities. *Tectonophysics*, Vol. 294, Pp. 177-223.

Rabai, S.; Philip, H.; Taboada, A., 1992. Modern tectonic stress field in the Mediterranean region: evidence for variation in stress directions at different scales. *Geophysical Journal International*, Vol. 110, Pp. 106-140.

Rabinowitz, P. and Ryan, W., 1970. Gravity anomalies and crustal shortening in the Eastern Mediterranean. *Tectonophysics*, Vol. 10, Pp. 585-608.

Reuther, C.; Ben-Avraham, Z. and Grasso, M., 1993. Origin and role of major strike-slip transfers during plate collision in the central Mediterranean. *Terra Nova*, Vol. 5, Pp. 249-257.

Reuther, C., 1990. Strike-slip generated rifting and recent tectonic stresses on the African foreland (Central Mediterranean region). *Annales Tectonica*, Vol. IV, No. 2, Pp. 120-130.

Ricou, L., 1971. Le croissant ophiolitique peri-arabe, une ceinture des nappes mises en place au

Cretace Superieur. *Revue de Geographie physique et de Geologie dynamique*. Vol. 13, Pp. 327-350.

Rihm, R.; Rosenkranz, C.; Staecker, J.; Egloff, F.; Makris, J. and Kramvis, S., 1999. Monitoring seismicity with an onshore/offshore seismic array. Symposium 005, Marine Geology and Geophysics, *Journal of Conference Abstracts*, Vol. 4, No. 1, Pp. 23-25.

Rische, M.; Endrun, B.; Meier, T. and Harjes, H., 2003. Seismogenic zones of the Hellenic Arc in the area of western and central Crete mapped by temporary local seismic networks. 63. Jahrestagung der Deutschen Geophysikalischen Gesellschaft, jena 23-28 Feb., 2003.

Robertson, A., 1990. Tectonic evolution of Cyprus. In Malpas, J., Moores, E.; Panayiotou, A. and Xenophontos, C. (Eds.), *Ophiolites: Oceanic Crustal Analogues*. Proc. Symp. "Troodos 1987" Nicosia, Cyprus, Geol. Surv. Dep. Minist. Agric. Nat. Resour., Pp. 235-250.

Robertson, A.; Kidd, R.; Ivanov, M.; Limonov, A.; Woodside, J.; Galindo-Zaldivar, J.; Nieto, L. and the Scientific Party of the 1993 "TTR-3" Cruise., 1995. Eratosthenes Seamount: collisional processes in the easternmost Mediterranean in relation to the Plio-Quaternary uplift of southern Cyprus. *Terra Nova*, Vol. 7, Pp. 254-264.

Robertson, A. and Xenophontos, C., 1993. Development of concepts concerning the Troodos ophiolite and adjacent units in Cyprus. In Prichard, H.M., Alabaster, T., Harris, N.B. and Neary, C.R. (Eds), *Magmatic processes and plate tectonics*. Geol. Soc. Spec. Publ. London, Vol., 70, Pp. 85-120.

Robertson, A., 1998. Mesozoic-Tertiary tectonic evolution of the easternmost Mediterranean Area: Integration of marine and land evidence. *Proceedings of the Ocean Drilling Program, Scientific results*, Vol. 160, Pp. 723-782.

Robinson, P.; Melson, W.; O'Hearn, T. and Schmincke, H.-U., 1983. Volcanic glass compositions of the Troodos ophiolite, Cyprus. *Geology*, Vol. 11, No. 7, Pp. 400-404.

Romberg, F., 1958. Key variables of gravity. *Geophysics*, Vol. 23, No. 4. Pp. 684-700.

- Ross, D. and Uchupi, E. 1977. Structure and sedimentary history of southeastern Mediterranean Sea-Nile Cone. American Association Petroleum Geologists Bulletin, Vol. 61, Pp. 872-902.
- Rotstein, Y. and Ben-Avraham, Z., 1985. Accretionary processes at subduction zones in the Eastern Mediterranean. Tectonophysics, Vol. 112, Pp. 551-561.
- Royden, L., 1993. The tectonic expression of slab pull at continental convergent boundaries. Tectonics, Vol. 12, Pp. 303-525.
- Ryan, W.; Stanly, D.; Hersey, J.; Fahlquist, D. and Allan, T., 1971. The tectonics and geology of the Mediterranean Sea. In: M. N. Hill (ED.), The Sea, Vol. 4, Part II, Wiley Interscience, New York, Pp. 387-492.
- Ryan, W.; Kastens, K. and Cita, M., 1982. Geological evidence concerning compressional tectonics in the eastern Mediterranean. Tectonophysics, Vol. 86, Pp. 213-242.
- Rybakov, M.; Goldshmidt, V.; Fleischer, L. and Ben-Gai, Y., 2000. 3-D gravity and magnetic interpretation for the Haifa Bay area (Israel). Journal of Applied Geophysics, Vol. 44, Issue 4, Pp. 353-367.
- Said, R., 1962. The geology of Egypt. El sevier publishing co., Amsterdam, New York, P. 377.
- Said, R., 1981. The Geological evolution of the River Nile. Springer, Berline, P. 111.
- Salamon, A.; Hofstetter, A.; Garfunkel, Z. and Ron, H., 1996. Seismicity of the Eastern Mediterranean region: Perspective from the Sinai subplate. Tectonophysics, Vol. 263, Pp. 293-305.
- Saroglu, F.; Boray, A.; Emre, ö., 1987. Active faults of Turkey (in Turkish). Mineral Research and Exploration Institute of Turkey, Unpubl. Rep. 8643, P. 399.
- Sandwell, D., 1992. Antarctic marine gravity field from high-density satellite altimetry. Geophysical Journal International, Vol. 109, Pp. 437-448.

Sandwell, D. and Smith, W., 1997a. Marine gravity anomaly from Geosat and ERS-1 satellite altimetry. *Journal of Geophysical Research*, Vol. 102, B5, Pp. 10 039-10 054.

Sandwell, D. and Smith, W., 1997 b. Exploring the ocean basins with satellite altimeter data, http://topex.ucsd.edu/marine_grav/explore_grav.html.

Sandwell, D.; Smith, W.; Smith, S. and Small, C., 1997. Measured and estimated Seafloor topography. http://topex.ucsd.edu/marine_grav/mar_grav.html.

Schembri, P., 1996. Geological history of the Mediterranean. On-line at: http://science.plym.ac.uk/departments/seed/med/Geo_Med.htm.

Sengör, A. and Yilmaz, Y., 1981. Tethyan evolution of Turkey: A plate tectonic approach. *Tectonophysics*, Vol. 75, Pp. 181-241.

Sengör, A.; Görü, N. and Saroglu, F., 1985. Strike-slip faulting and related basin formation in zones of tectonic escape: Turkey as a case study. *Soc. Ecol. Paleontol. Mineral. Spec. Publ.*, Vol. 37, Pp. 227-264.

Shepard, D., 1968. A two-dimensional interpolation function for irregularly-spaced data. In *ACM National Conference*, Pp. 517--524.

Smith, D.; Kolonkiewicz, R.; Robbins, J.; Dunn, P. and Torrence, M., 1994. Horizontal crustal motion in the central and Eastern Mediterranean inferred from satellite laser ranging measurements. *Geophysical Research Letters*, Vol. 21, No. 18, Pp. 1979-1982.

Spakman, W.; Wortel, M. and Vlaar, N., 1988. The Hellenic subduction zone: a tomographic image and its geodynamics implication. *Geophysical Research Letters*, Vol. 15, Pp. 60-63.

Stefansson, R., 1966. The use of transverse waves in focal mechanism studies. *Tectonophysics*, Vol. 3, Pp. 35-60.

- Stöckhert, B., 1999. The Hellenic subduction zone, a world site to study the mechanics of roll back. In: MASCLE J. (ed.) Mediterranean Scientific Drilling Prospectives. - CIESM Workshop, Series 6: Pp. 103-108.
- Talwani, M.; Worzel, L. and Landisman, M., 1959. Rapid gravity computation for two dimensional bodies with application to the Mendocino submarine fractures zone. *Journal of Geophysical Research*, Vol. 64, No. 1, Pp. 49-59.
- Talwani, M.; Le Pichon, X. and Ewing, M., 1965. Crustal structure of the mid-Ocean Ridges, 2. computed model from the gravity and seismic refraction data. *Journal of Geophysical Research*, Vol. 70, No. 2, Pp. 341-352.
- Taymaz, T.; Jackson, J. and McKenzie, D., 1991. Active tectonics of the north and central Aegean Sea. *Geophysical Journal International-Oxford*, Vol. 106, Pp. 433-490.
- Tealeb, A., 1989. Statistical and tectonic analysis of the Bouguer gravity field of Egypt. *J. Kuwait Uni.*, Vol. 16, Pp. 165-182.
- Ten Veen, J. and Meijer, P., 1998. Late Moicene to recent tectonic evolution of Crete (Greece): geological observations and model analysis. *Tectonophysics*, Vol. 298, Pp. 191-208.
- Telford, W.; Geldart, L. and Sheriff, R., 1990. *Applied Geophysics*, 2nd Ed., Cambridge University Press, P. 770.
- Trey, H., 1991. Weitwinkelreflexions-und refraktionsseismische Messungen im östlichen Mittelmeer/Israel. M. Sc.Thesis, Institute of Geophysics, University of Hamburg, Germany, P. 74.
- Truffert, C.; Chamot-Rooke, N.; Lallemand, S.; De Voogd, B.; Huchon, P. and Le Pichon, X., 1993. The crust of the Western Mediterranean Ridge from deep seismic data and gravity modelling. *Geophysical Journal International*, Vol. 114, Pp. 360-372.
- Udias, A., 1982. Seismicity and seismotectoinc stress filed in the Alpine-Mediterranean region. *American Geophys. Union, Geodynamics series*, Vol. 7, Pp. 75-82.

USGS, 1996, ||on-line at ||, <http://www.usgs.gov/>.

Vidal, N.; Alvarez-Marron, J. and Klaeschen, D., 2000. Internal configuration of the Levantine Basin from seismic reflection data (Eastern Mediterranean). *Earth and Planetary Science Letters*, Vol. 180, Pp. 77-89.

Vogt, P. and Higgs, P., 1969. An aeromagnetic survey of the Eastern Mediterranean Sea and its interpretation. *Earth and Planetary Science Letters*, Vol. 5, Pp. 439-448.

Wang, J., 1995. The crustal structure and geodynamics of the Eastern Mediterranean Sea derived from geophysical studies. Ph. D. Thesis, Institute of Geophysics, University of Hamburg, Germany, P. 150.

Weber, M.; Ben-Avraham, Z.; Abu-Ayyash, K.; El-Kelani, R. and DESERT 2000 Group., 2000. DESERT 2000 Group - A Multinational and Interdisciplinary project to study the Dead Sea rift/ Dead Sea transform. A multi-nat. and inter. study. DESERT workshop-July, 2002.

Wessel, P. and Smith, W., 2001. The Generic Mapping Tools: Technical Reference and Cookbook, <http://gmt.soest.hawaii.edu/>

Woodside, J., 1977. Tectonic elements and crust of the Eastern Mediterranean Sea. *Marine Geophysical Researches*, Vol. 3, Pp. 317-354.

Woodside, J.; Ivanov, M. and Shipboard Scientific participants, 1992. Geological and geophysical investigation in the Mediterranean and Black Sea. *Unesco reports in Marine science*, Vol. 56, Pp. 208-310.

Woodside, J. and Bowin, C., 1970. Gravity anomalies and inferred crustal structure in the Eastern Mediterranean Sea. *Geol. Soc. Am. Bull.*, Vol. 81, Pp. 1107-1122.

Wong, H.; Lüdmann, T.; Ulug, T. and Görür, N., 1995. The Sea of Marmara: a plate boundary sea in an escape tectonic regime. *Tectonophysics*, Vol. 244, Pp. 231-250.

Yaltirak, C.; Alpar, B. and Hüseyin, Y., 1998. Tectonic elements controlling the evolution of the Gulf of Saros (northeastern Aegean Sea, Turkey). *Tectonophysics*, Vol. 300, Pp. 227-248.

Ylmaztürk, A. and Burton, P., 1999. Earthquake source parameters as inferred from the body waveform modeling, southern Turkey. *Journal of Geodynamics*, Vol. 27, Issue 4-5, 2 March 1999. Pp. 469-499.

Youssef, M., 1968. Structural pattern of Egypt and its interpretation. *American Association of Petroleum Geologists Bulletin*, Vol. 52, No. 4, Pp. 601-614.

Deep seismic sounding experiments (DSS)

- Seismic profiles around and adjacent Dead Sea rift

A deep seismic refraction experiment, covering Sinai, and the adjacent area was performed in 1977 by through a cooperation between the Institute of Geophysics, University of Hamburg, Germany and Planetary Science, Tel Aviv University. The seismic profiles are shown in Figure 4.1 as lines [I], [II] and [III]. They run across the central and northern Sinai in various directions. Generally, Ginzburg et al. (1979 a, b and 1981) showed that the upper mantle-crust boundary is defined by a velocity of 6.6-6.7 km/s above and 7.7-8.0 km/s below.

The crustal thickness in the southern area of the Dead Sea is about 30 km, but thins southwards along the Gulf of Aqaba, where the thickness is reduced to about 22 km. The crust of NE Sinai and the central Negev is continental and covered by more than 2 km of sediments. Towards the Eastern Mediterranean Sea, the crust thins while the overlying sediments thicken considerably. Within this region, which parallels the Levant and Sinai coasts, there is a zone of depositions change within the sedimentary cover, and of crustal thinning and transition from continental to oceanic crust. This zone represents a fossil continental margin of the Arabian platform bordering the Tethys Ocean (Ginzburg, and Folkman, 1980).

In addition, in recent years as part of the DESERT 2000 Group project*, a seismic wide-angle reflection/refraction experiment covering the Jordan-Dead Sea rift transform and the adjacent area (Figure Appendix A1) has been conducted to study the crust and upper mantle, the main shear zones, and the geodynamics of the mentioned above area (e.g. DESERT 2000 Group 2000 a; DESERT 2000 Group 2000 b; Mechie et al., 2000; El-Kelani et al., 2000; Maercklin et al., 2000; and Weber et al; 2000). A brief account of the main results of these seismic experiments are summarized:

- From an analysis of the P-wave data, the seismic basement occurs at a depth of 3-4 km beneath the eastern flank of the rift in Jordan, deepens to about 7 km in the rift, and then becomes more shallow to about 6 km below the western flank in Israel and deepens westwards towards the coast (Mechie et al., 2000).

- The boundary between the upper crust (velocity of 6.1-6.4 km/s) and the lower crust (velocity about 6.7 km/s) occurs at around 20 km depth (Maercklin et al., 2000).

- The Moho depth increases from 28-29 km in the NW to 37-38 km in the SE. If at all, only a very small Moho uplift under the eastern part of the rift can be detected. The seismic image with a deep sedimentary basin, very small Moho uplift and a Pn velocity of 7.8-8.0 km/

*DESERT 2000 Group consists of several coincident geophysical (seismic, magnetotelluric and seismological) sub-projects that are performed by partners in Germany, Israel, Jordan and Palestine. The aim of the interdisciplinary and multi-scale Dead Sea Rift Transect (DESERT) project (DESERT 2000 Group) is to shed light on the question of how large shear zones work. Principal investigators are Weber, M in Germany, Ben-Avraham, Z in Israel, Abu-Ayyash, K in Jordan, and El-kelani, R in the Palestine territories.

s in the vicinity of the rift, suggests that the mantle played insignificant role in the extension process associated with the Jordan-Dead Sea rift Transform. The tectonic stability of this region was only recently (18 Ma ago) interrupted by the formation of a transform fault with a left lateral motion of about 105 km to date (DESERT 2000 Group 2000 b).

- The Dead Sea Transform (DST) is a major plate boundary separating the African and Arabian plates. It extends over 1000 km from the Red Sea rift in the south to the Taurus collision zone in the north (Weber et al; 2000). Moreover, in the area between the Dead Sea and Red Sea the DST is marked by the Arava fault which may have the potential to produce large earthquakes ($M_s \sim 7$) along some of its segments about every 200 years as shown in Figure Appendix A1 (DESERT 2000 Group 2000 a, Klinger et al., 2000).

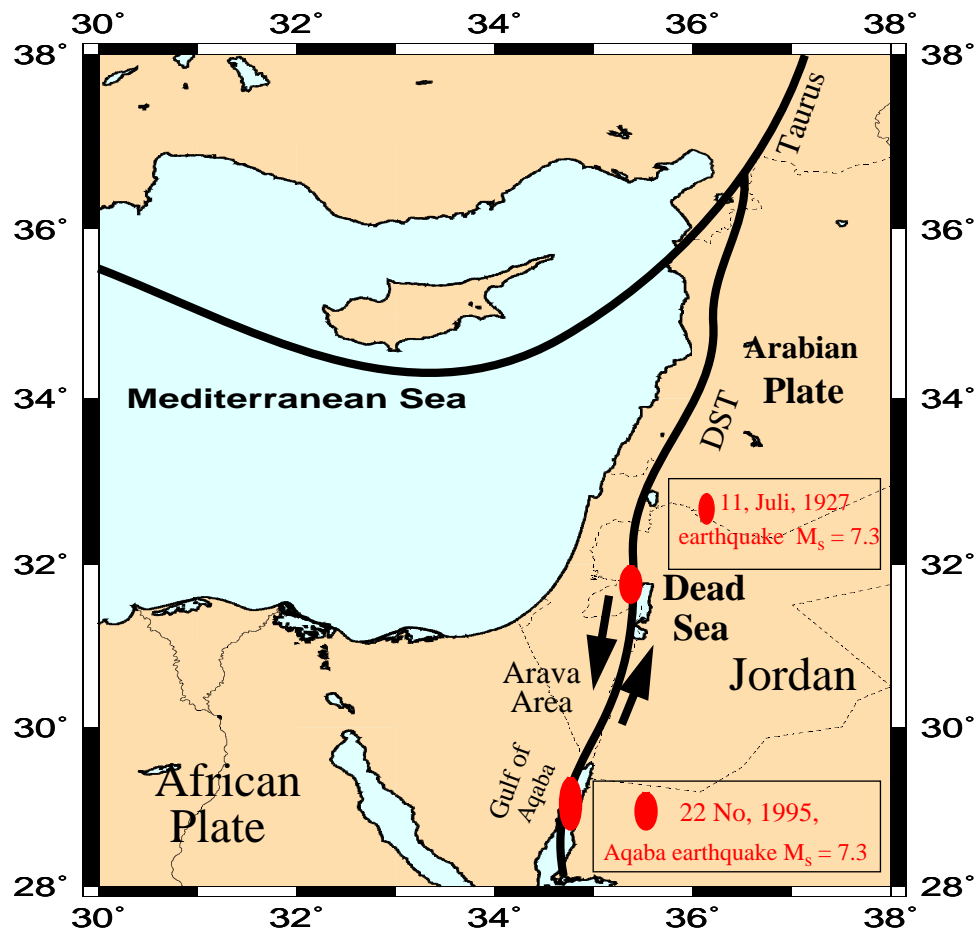


Figure Appendix [A1]: Tectonic setting of the eastern Mediterranean Sea and the Middle East. The black arrows indicate the left-lateral motion along the DST. Compiled from DESERT 2000 Group, and Klinger et al. (2000).

- Seismic profiles in the Cyprean region

The Geological survey of Cyprus has performed three deep seismic sounding profiles and numerous geophysical surveys in the Cyprean region as shown in Figure 4.1 by lines, [IV], [V] and [VI]. The results of these profiles are presented in Figures Appendix [A2] and [A3] (Wang 1995). The main features observed are as follows:

- Profile [IV] runs NE-SW crossing the Eratosthenes Seamount and terminates east of Cyprus. Below the Eratosthenes Seamount, the depth to the basement lies at about 4-5 km and a sedimentary layer with a velocity of 5.3-5.5 km/s overlies the crystalline crust. Northeast of the Seamount, sedimentary sequences exceeding 8 km thickness are identified below the Trench (Kempler, 1998).

- Profile [V] trends WNW -ESE cross the Island of Cyprus. The velocity-depth model along this profile, indicates that a layer with a velocity of 6.0-6.7 km/s outcrops on the Island (Wang, 1995). This layer is about 4-5 km thick and must be associated with the Troodos ophiolites. A very thick sedimentary sequence is identified about 60 km west of Cyprus, where the depth to the basement lies at about 12 km and an oceanic crust with a thickness less than 10 km appears to underlie the thick sediments (Robertson, 1990).

- Profile [VI] is NE-SW oriented and is situated SW of Cyprus. A thick sedimentary sequence underlain by about 8 km of oceanic crust is observed below the SW part of the profile (Figures 1 and 2). In the central part of the profile, there is a layer with a velocity of 6.0 km/s suggesting a sedimentary limestone layer. The crust below this limestone, appears to be of oceanic type. The structure in the NE part of this profile, suggests the existence of a continental crust (Figures Appendix [A2] and [A3]).

Expanding spread profiles in the Mediterranean Sea (ESP)

The two-ship refraction and reflection seismic survey profiles were performed in December, 1988, on the Mediterranean Sea (Pasiphae Cruise). Figure Appendix [A4] shows the location of the Expanding spread profiles (ESP) on the Mediterranean Sea. Accenting spread profiles which were shot parallel to major structures to avoid lateral variability, were located along the Ionian Basin, the Mediterranean Ridge and the Herodotus Abyssal Plain (De Voogd et al., 1992).

De Voogd et al. (1992) presented a summary of ESP results for the Eastern Mediterranean Sea from the Ionian Basin to the Herodotus Abyssal Plain as shown in Figure Appendix [A5]. They concluded that the thin crust “about 10 km “of the Herodotus Abyssal Plain may be either oceanic or thinned continental overlain by up to 10 km thick sediments.

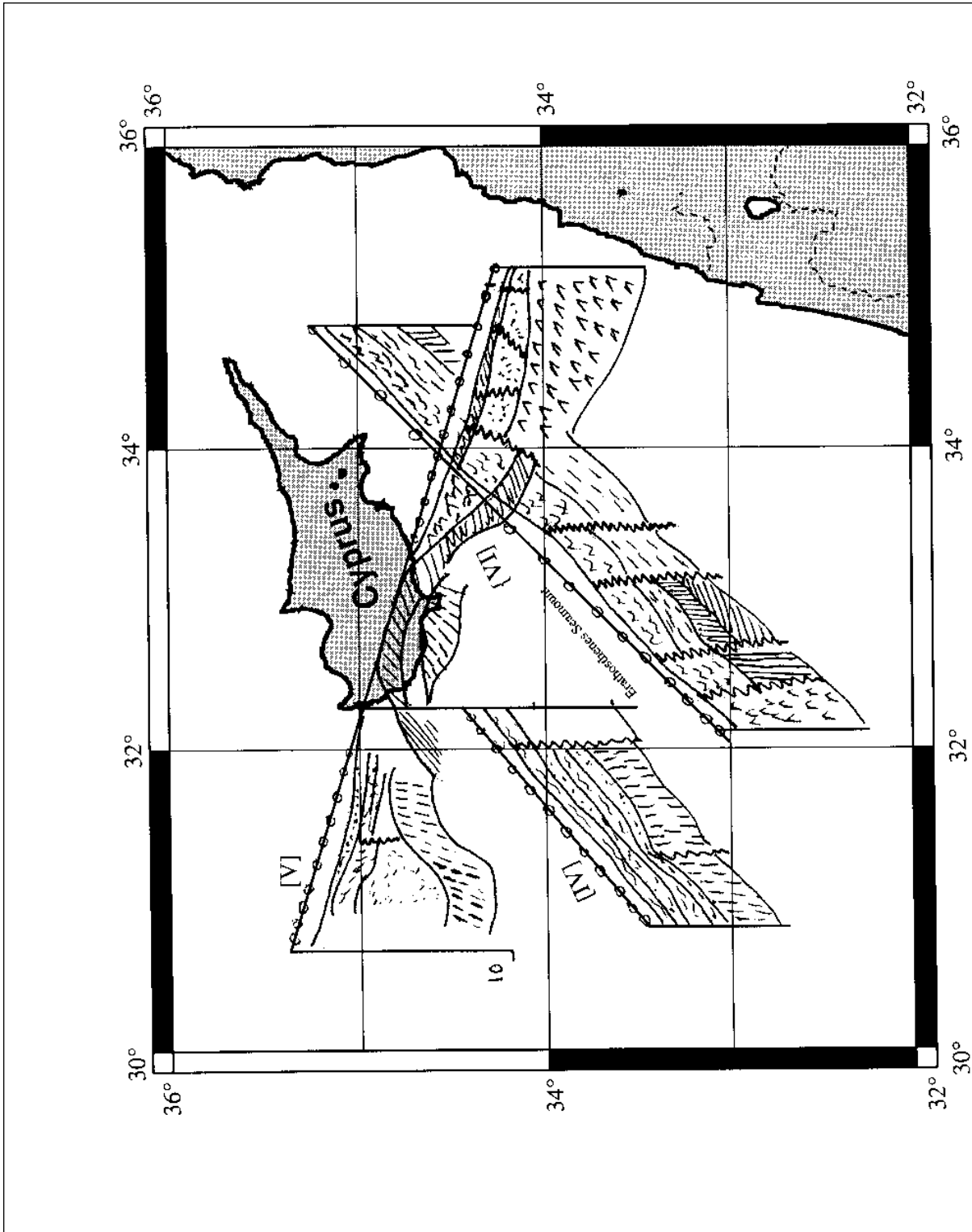


Figure Appendix [A2]: Sketch diagram shows velocity depth models of profiles [IV], [V], and [VI]. Compiled from the Geological survey of Cyprus after Wang (1995).

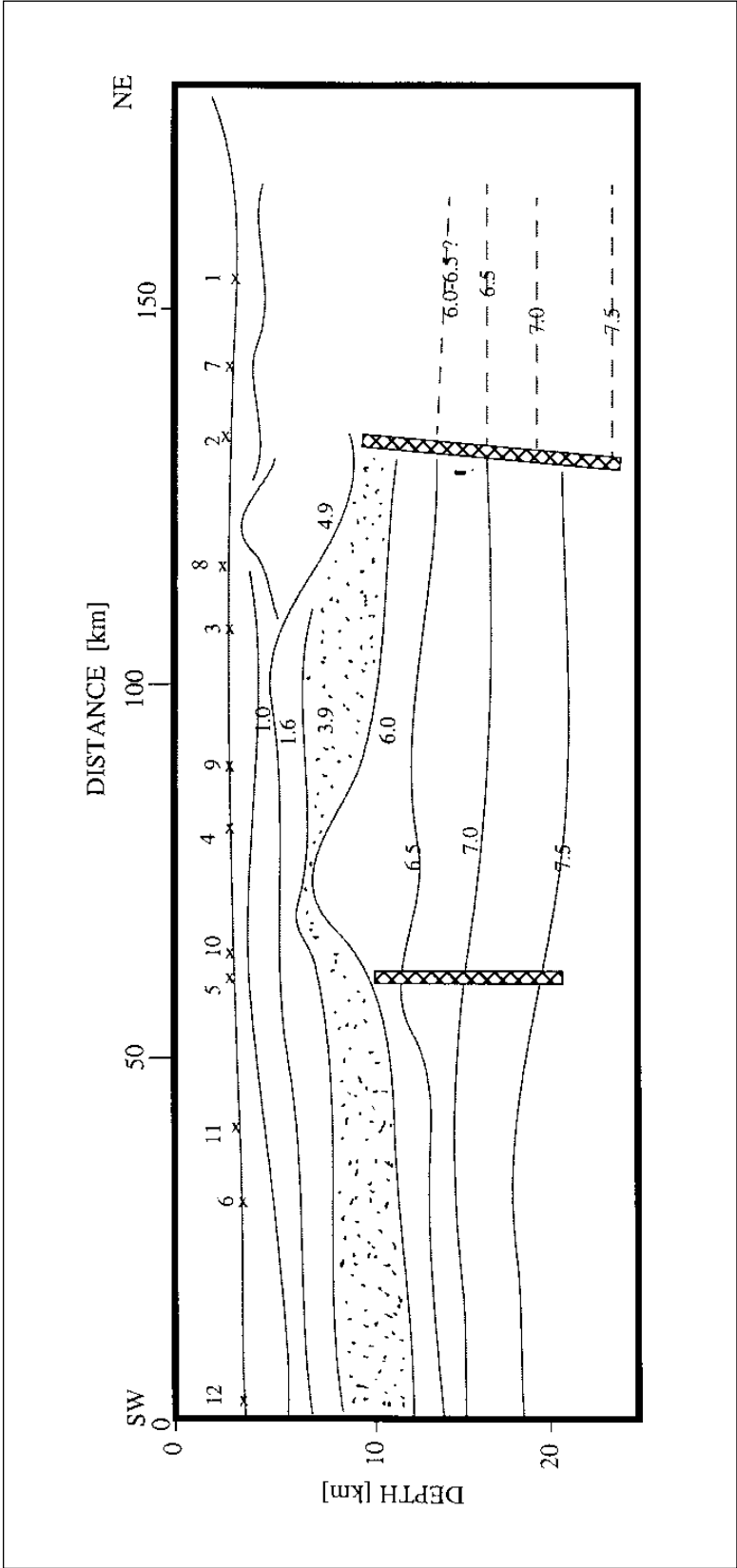


Figure Appendix [A3]: Sketch diagram shows velocity depth model of profile VI, southwest of Cyprus. Compiled from the Geological survey of Cyprus after Wang (1995).

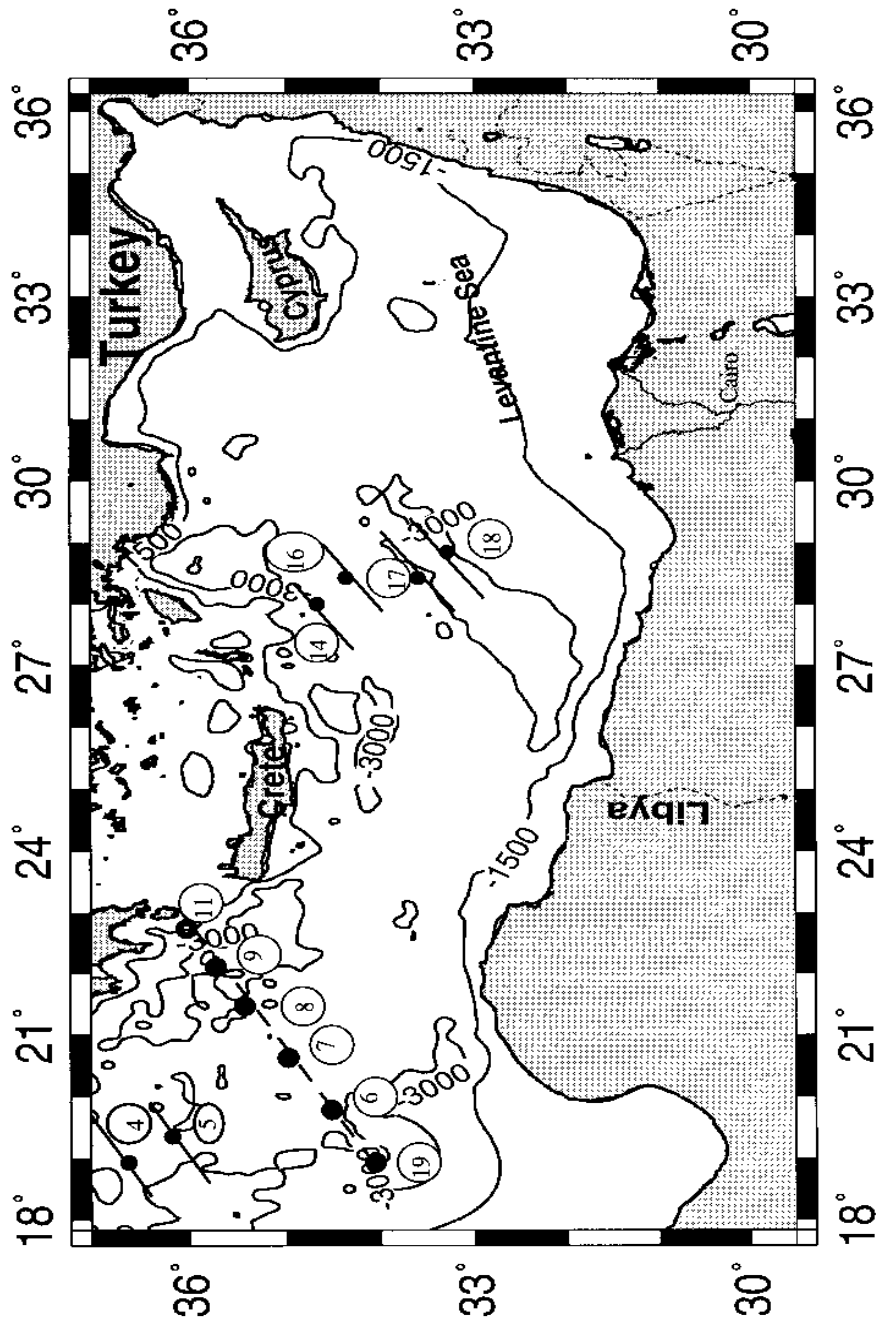


Figure Appendix [A4]: Location map of the Expanding spread profiles (ESP) recorded during the Pasiphae Cruise, black dots indicates ESP central points from where a velocity model is obtained. Compiled from De Voogd et al. (1992).

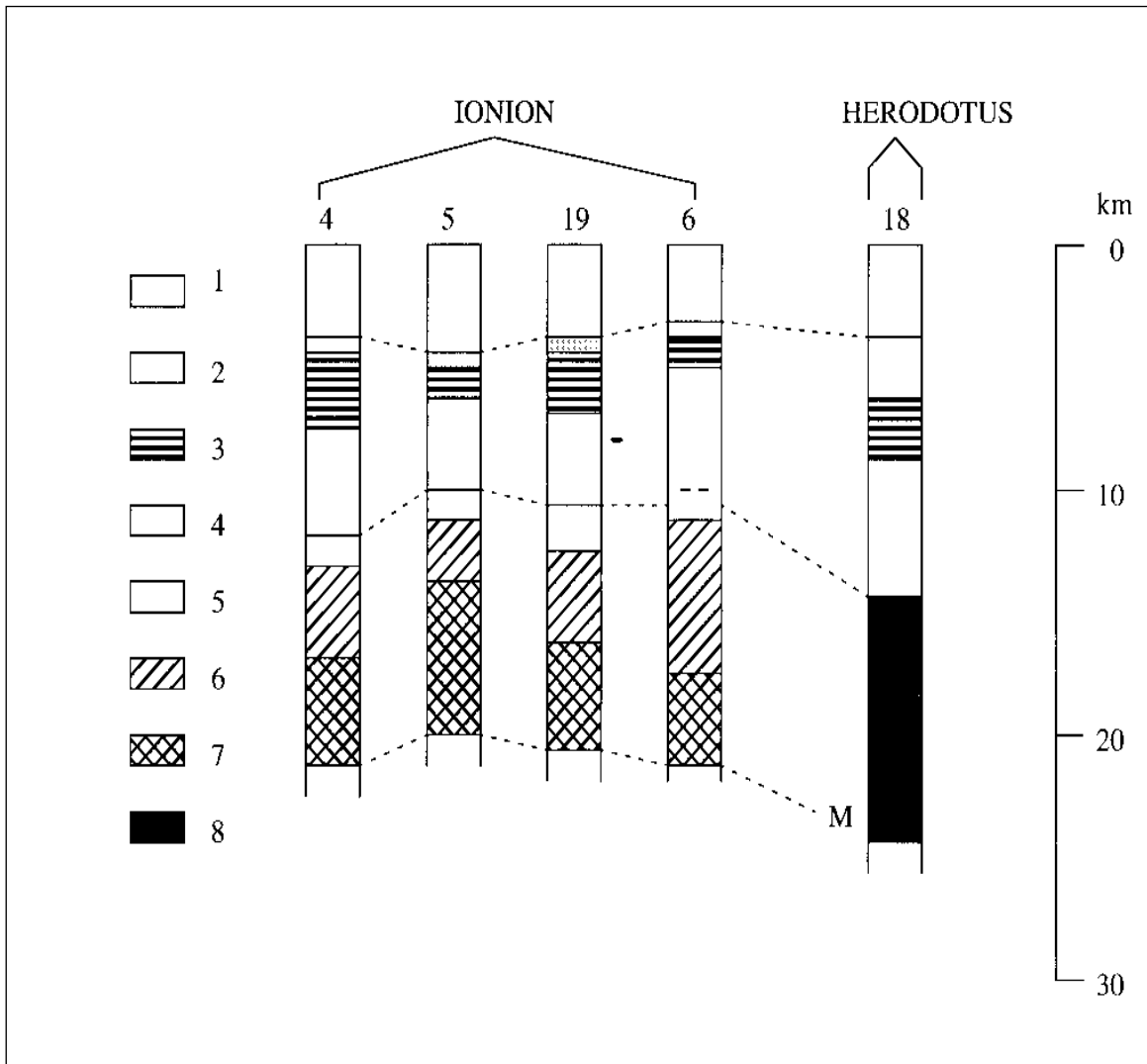


Figure Appendix [A5]: Summary of ESP results from the Ionian Basin to the Herodotus Abyssal Plain. Vertical depth scale is in km. Compiled from De Voogd et al. (1992).

1=water, 2=recent Sea-bottom sediments, 3=evaporite, 4=pre-messinian sediments, 5=oceanic layer 2a, 6=oceanic layer 2, 7=oceanic layer 3, 8=oceanic or thinned continental crust, and M=Moho

Table Appendix [B1]: Fault plane solutions data of some shocks, which occurred in the most seismically active zone of the investigated area (extracted from Harvard Seismology, CMT catalog search)

Long. (°)	Lat. (°)	Fault plane 1			Fault plane 2			M _b	F.D.	Date D/M/Y
		Strike	Dip	slip	Strike	Dip	slip			
31.69	30.72	197	40	-4	291	87	-130	4.1	10.0	14/12/87
31.89	34.47	62	48	-168	323	81	-43	4.1	32.6	27/11/96
32.04	30.17	326	40	-7	62	85	-130	4.5	10.0	22/05/92
32.10	30.18	147	62	4	55	87	152	4.7	10.0	29/03/84
31.60	30.60	326	40	-7	62	85	-130	4.8	33.0	29/04/74
32.03	34.75	147	62	4	55	87	152	4.9	33.0	10/10/96
28.24	36.73	275	52	-34	28	64	-137	4.9	33.0	05/10/99
25.84	34.02	318	60	150	63	65	33	4.9	21.6	07/10/98
35.46	36.97	321	75	171	53	81	15	4.9	10.0	28/06/98
34.81	32.38	134	56	0	44	90	146	5.0	28.0	24/08/84
32.22	30.48	147	62	4	55	87	152	5.0	24.1	02/01/87
28.01	36.44	316	54	137	75	56	44	5.0	59.5	19/06/87
35.59	30.54	197	40	-4	291	87	-130	5.1	15.0	23/04/79
30.73	36.75	131	41	125	268	58	64	5.1	122.6	11/03/91
28.12	35.66	10	33	-116	220	60	-74	5.1	53.7	09/03/98
32.68	34.42	303	42	124	80	56	63	5.1	20.0	11/08/99
26.75	35.29	61	35	-40	186	68	-119	5.2	15.0	23/07/79
24.49	32.55	326	40	-7	62	85	-130	5.2	15.0	28/06/87
28.86	35.38	24	32	-152	270	76	-61	5.2	15.0	20/11/88
28.52	35.17	341	73	177	72	87	17	5.3	33.0	18/10/91
31.48	36.17	178	30	4	84	88	120	5.4	63.0	26/04/81
28.40	34.16	67	48	-34	181	65	-133	5.4	15.0	22/07/85
26.13	34.60	245	36	-33	2	71	-122	5.4	15.0	19/03/91
27.14	36.47	315	44	173	50	85	46	5.4	151.9	12/04/96
36.00	36.28	243	39	-15	345	81	-128	5.3	15.0	22/01/97
27.70	36.97	312	46	162	54	78	46	5.5	170.0	27/09/83
27.36	31.39	154	44	89	335	46	91	5.5	10.0	28/05/98
27.94	35.18	103	46	24	356	73	133	5.6	85.0	28/11/77
24.89	34.75	358	39	131	129	62	62	5.6	65.0	19/03/83
31.48	35.79	132	64	155	234	67	29	5.7	58.6	01/06/77
32.44	35.02	239	21	140	6	77	73	5.8	15.0	23/02/95
30.63	29.74	136	42	-75	297	49	-103	5.9	22.0	12/10/92
24.89	35.02	177	63	22	76	70	151	6.0	80.0	23/05/94
32.09	34.50	48	77	170	140	80	13	6.4	23.0	09/10/96

Long. (°): longitude in degrees; Lat. (°): latitude in degrees

M_b: Body wave magnitude; F. D.: Focal depth in (kilometers)

D : day; M: month; Y: year

Table Appendix [B2]: Fault plane solutions data of some shocks, which occurred in the most seismically active zone of the investigated area (extracted from WSM).

Long. (°)	Lat. (°)	Fault plane 1			Fault plane 2			M_b	F.D.	Date D/M/Y
		Strike	Dip	slip	Strike	Dip	slip			
35.63	32.81	147	62	4	55	87	152	4.1	13	07/05/88*
25.35	34.00	347	34	157	96	77	58	4.5	33.0	22/10/2000*
33.55	34.83	147	62	4	55	87	152	4.5	49.5	07/07/86*
28.04	36.37	12	30	176	105	88	60	4.6	127.7	26/04/96*
35.50	31.90	178	30	4	84	88	120	4.7	31	25/01/85*
32.63	34.89	224	20	132	0	76	76	5.3	15.0	29/05/95*

Long. (°): longitude in degrees; Lat. (°): latitude in degrees

M_b : Body wave magnitude; F. D.: Focal depth in (kilometers)

D : day; M: month; Y: year

Focal Mechanisms

One of the most common ways of studying the seismotectonics of any particular region is the plotting of a regional stress pattern map on the basis of focal mechanisms (Kasahara, 1981). Seismologists refer to the direction of slip in an earthquake and the orientation of the fault on which it occurs as the focal mechanism solutions (e.g. Kasahara and Stevens, 1969). They use information from seismograms to calculate the focal mechanism solutions and typically display it on maps as a "beach ball" symbol. This symbol is the projection on a horizontal plane of the lower half of an imaginary, spherical shell (focal sphere) surrounding the earthquake source as illustrated in Figure Appendix C 1 part [A].

In addition, Figure Appendix C 1 part [B] shows typically four examples of the focal mechanisms solutions (after USGS, 1996). The block diagrams adjacent to each focal mechanism illustrate the two possible types of fault motion that the focal mechanism could represent. The ambiguity may sometimes be resolved by comparing the two fault-plane orientations to the alignment of small earthquakes. Moreover, the stress-field orientation at the time of rupture governs the direction of slip on the fault plane, and the beach ball also depicts this stress orientation. The minimum compressive stress direction is constrained to the gray quadrant, while the maximum compressive stress lies in the white quadrant. When studying an ensemble of fault plane solutions, one often assumes that the average orientation of the (T) axis approximates the minimum compressive stress and the average orientation of the (P) axis the maximum compressive stress. As illustrated in Figure Appendix C 1 part [B], the first three examples describe fault motion that is purely horizontal (strike slip) or vertical (normal or reverse), where as the fourth example describes the oblique-reverse mechanism illustrates that the slip may also have components of horizontal and vertical motion.

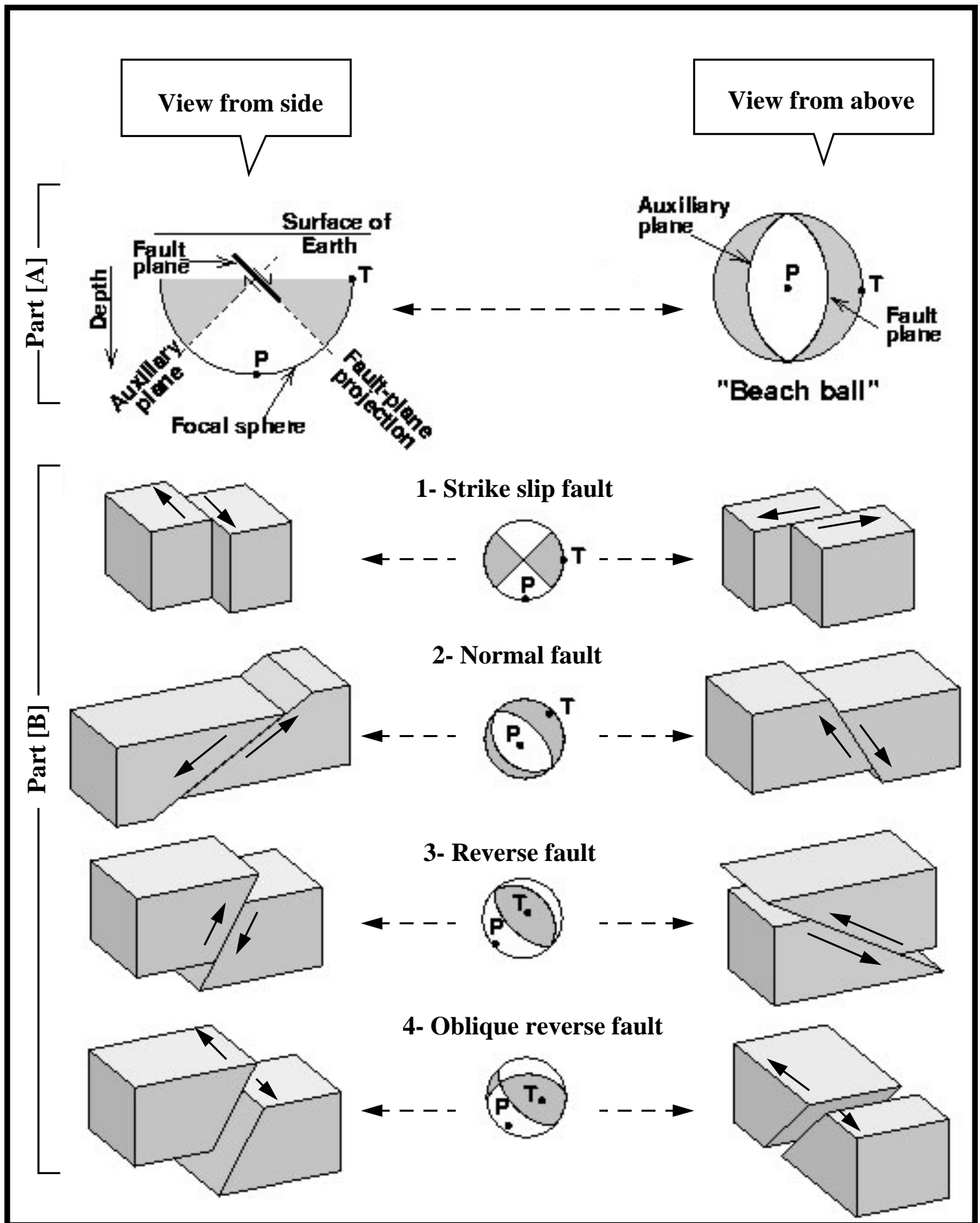


Figure Appendix [C1]: Schematic diagram of a focal mechanisms solutions. Gray and white portions represent compression and dilatation quadrants respectively. The gray quadrants contain the tension axis (T), and the white quadrants contain the pressure axis (P). (→) Arrows indicate block movements. Compiled from USGS, 1996.